

## PUBLISHER

On Behalf of Textile and Apparel Research  
Application Center

Faruk BOZDOĞAN

## EDITOR IN CHIEF

Arif Taner ÖZGÜNEY  
arif.taner.ozguney@ege.edu.tr

## ASSOCIATE EDITORS

Mehmet KÜÇÜK  
mehmet.kucuk@ege.edu.tr

Pelin SEÇİM KARAKAYA  
pelinsecim@mail.ege.edu.tr

## EDITORIAL BOARD

Aslı DEMİR

Gözde ERTEKİN

Hale KARAKAŞ

Hüseyin Aksel EREN

Pınar ÇELİK

## ENGLISH EDITING SERVICE

Mengü Noyan ÇENGEL

## SCIENTIFIC ADVISORY BOARD

Ahmet ÇAY

Andrej DEMŠAR

Arzu MARMARALI

Bojana VONČINA

Bülent ÖZİPEK

E. Perrin AKÇAKOCA KUMBASAR

Ender BULGUN

Esen ÖZDOĞAN

Hüseyin KADOĞLU

Mirela BLAGA

Nilgün ÖZDİL

Oktay PAMUK

Ozan AVİNÇ

Peter J. HAUSER

Recep EREN

Rıza ATAV

Savvas G. VASSILIADIS

Turan ATILGAN

## ABSTRACTING / INDEXING

Science Citation Index Expanded (SCIE)

Scopus

WOS

EBSCO

Ulakbim

## TYPESETTING AND PRINTING

AK-MAT Matbaacılık Yayıncılık Kır. Malz. San. Tic. Ltd. Şti  
Barbaros Mah. Refik Tulga Cd. No: 13, Bornova – İzmir  
akmatlimited@gmail.com Tel: 0 232 444 28 23  
Printed Date: 29 March, 2023

**Characterization and Antibacterial Activity of Electrospun Polyethylene oxide/Chitosan Nanofibers**  
Hanan Yunus, Emel Ceyhun Sabır, Halil İbrahim İçoğlu,  
Behzat Yıldırım, Osman Gülnaz, Mehmet Topalbekiroğlu ..... 1

**Predictive Modeling of Yarn Quality at Ring Spinning Machine using Resilient Back Propagation Neural Networks**  
Assad Farooq, Nayab Khan, Farida Irshad, Usama Nasir ..... 9

**Effect of Yarn Physical Properties on Fiber Migration and Packing Density of Cotton/Acrylic Blended Yarns**  
H. İbrahim Çelik, Gülistan Canlı ..... 15

**Investigation of the Friction Coefficients and Surface Roughness Properties of Denim Fabrics after Abrasion**  
Mine Akgun, Gizem Kara ..... 27

**Influence of Knitting Structure and Metal Wire Amount on Electromagnetic Shielding Effectiveness of Knitted Fabrics**  
Serkan Tezel, Yasemin Kavuşturan, Guy A.e. Vandenbosch,  
Vladimir Volski ..... 37

**The Effect of Fabric Structure and Ultrasonic Welding Process on the Performance of the Spunlace Surgical Gowns**  
Esra Zeynep Yıldız ..... 45

**Performance Evaluation of Newly Designed Disposable Surgical Gowns**  
Selin Hanife Eryürük, Burçak Karagüzel Kayaoğlu, Pelin Altay ..... 56

**Use of Natural and Synthetic Materials in Denim Washing Process as an Alternative to Pumice Stone**  
İsmail İvedî, Ahmet Çay ..... 68

**Investigation of Anti-Pilling Properties of Different Fabrics Applied with Polyvinylcaprolactam**  
Burcu Büyükkoru, Ali Kara ..... 77

**Linear Model Equation for Prediction and Evaluation of Surface Roughness of Plain-Woven Fabric**  
Kura Alemayehu Beyene, Nuredin Muhammed ..... 88

**The Effect of Various Textile Wastes (Human Hair, Denim and Pantyhose) on the Mechanical Properties of Composite Materials**  
Hande Sezgin ..... 95







## CONTACT

Ege Üniversitesi Tekstil ve Konfeksiyon Araştırma-Uygulama Merkezi  
35100 Bornova – İzmir, TÜRKİYE  
Tel: +90 232 311 38 89-83

[www.dergipark.gov.tr/tekstilvekonfeksiyon](http://www.dergipark.gov.tr/tekstilvekonfeksiyon)  
E-mail: [tekstilkonfeksiyon@mail.ege.edu.tr](mailto:tekstilkonfeksiyon@mail.ege.edu.tr)



# Characterization and Antibacterial Activity of Electrospun Polyethylene oxide/Chitosan Nanofibers

Hanan Yunus<sup>1</sup>  0000-0002-1704-956X  
Emel Ceyhan Sabır<sup>1</sup>  0000-0002-2385-1524  
Halil İbrahim İçoğlu<sup>2</sup>  0000-0003-0687-4721  
Behzat Yıldırım<sup>3</sup>  0000-0002-7787-0595  
Osman Gülnaz<sup>4</sup>  0000-0003-4714-7651  
Mehmet Topalbekiroğlu<sup>3</sup>  0000-0003-4345-8815

<sup>1</sup> Çukurova University / Textile Engineering Department / Adana, Türkiye

<sup>2</sup> Gaziantep University / Metallurgical and Materials Engineering Department / Gaziantep, Türkiye

<sup>3</sup> Gaziantep University / Department of Textile Engineering Department / Gaziantep, Türkiye

<sup>4</sup> Çukurova University / Science and Technology Education Department / Adana, Türkiye

**Corresponding Author:** Hanan Yunus, hanantex@gmail.com

## ABSTRACT

This study aims to characterize and evaluate polyethylene oxide (PEO) and chitosan (CS) nanofibers produced by electrospinning method. Electrospinning solutions were used at three different concentrations (1, 2, 3 wt%) with five different PEO/CS mixing ratios (30/70, 40/60, 50/50, 60/40, 100/0). FESEM, XRD and FTIR tests were applied for characterization of the nanofibers. Antibacterial activity of the nanofibers against *Staphylococcus aureus* and *Klebsiella pneumoniae* microorganisms was investigated using disk diffusion method. While 1 wt% of concentration was not suitable to obtain regular nanofibers, the nanofibers were uniform and largely free of beads at the other ones (2, 3 wt%). The average diameters of the nanofibers varied from 59 to 298 nm depending on the concentration and mixing ratio. Strong hydrogen bonds were formed between two polymers, while the crystal structure of PEO did not change significantly when mixed with chitosan. According to the study, whereas chitosan is resistant to a wide range of germs, PEO/CS nanofibers were not. The reason for this is because when chitosan is electrospun with PEO, the characteristics of the chitosan are altered by the concentrations and ratios used.

## 1. INTRODUCTION

Nanotechnology plays an important role in human life as it offers advantages in various aspects of life. On the one hand, it is able to provide new physical properties to the polymers produced with nanotechnology; on the other hand, it is characterized by a high surface area compared to its size and its application in various industrial and medical fields [1]. Electrospinning technology is considered the simplest and least expensive technique for obtaining nanofibers. This technology is based on the production of nanofibers from the desired polymer contained in the extrusion needle, using a high electric field generated by applying a positive voltage to the polymer material, at the tip of the needle, and a negative voltage to the collector plate [2].

The need to preserve nature leads mankind to constantly seek natural alternatives and use them in various aspects of their lives. This has led them to use natural polymers such as chitosan (CS), which is obtained by the deacetylation process of chitin found in the shells of marine animals and fungi [3]. Chitosan is characterized by the presence of amine groups in its molecular structure, which are positively charged when chitosan is dissolved in weak or concentrated acids and thus is able to interact with other groups found in other compounds to obtain various mixtures in the form of films, gels, molecules or nanofibers [4]. Chitosan is characterized by its biocompatibility and biodegradability, in addition to its large presence in nature, which allows it to be easily obtained and applied in various

**To cite this article:** Yunus H, Sabır EC, İçoğlu Hİ, Yıldırım B, Gülnaz O, Topalbekiroğlu M. 2023. Characterization and antibacterial activity of electrospun polyethylene oxide/chitosan nanofibers. *Tekstil ve Konfeksiyon* 33(1), 1-8.

fields [5]. Because of the high viscosity of chitosan, it is very difficult to obtain it in the form of nanofibers by electrospinning method, so it must be mixed with other materials that help reduce its viscosity and facilitate the process of electrostatic spinning. Among the materials, there is polyethylene oxide (PEO), which is a non-toxic, water-soluble, synthetic polymer and stable in acidic media. It is characterized by biocompatibility and it becomes capable of being an electrospun nanofiber [6].

In a study by Singh, PEO was used to reduce the interlocking chitosan chains and obtain nanofibers. In this study, PEO/CS different mixing ratios and different concentrations of acetic acid were used. The study showed that increasing the acetic acid concentration and PEO content helped to obtain nanofibers with a larger diameter and a smaller number of beads [7]. To determine the effect of deacetylation degree of chitosan on its adhesion properties in mucous membranes, nanofibers were formed from the mixture of PEO/CS with different deacetylation degree of chitosan. It was found that the degree of deacetylation plays an important role in changing the physicochemical properties of chitosan. The higher the deacetylation degree of chitosan, the greater the stability of nanofibers in aqueous media and the degree of adhesion to mucous membranes increases [8]. In another study, the anti-inflammatory teicoplanin was coated with PEO/CS nanofibers, and this material showed a higher ability to resist bacteria when coated with PEO/CS nanofibers than when not coated, and the concentration of 4% teicoplanin was the best in resisting bacteria [9]. PEO/CS nanofibers were also used as a supporting membrane to which metal-organic frameworks-5 (MOF-5) nanoparticles were added, and they were used as effective filters to clean the air from PM<sub>2.5</sub> (particulate matters  $\leq 2.5 \mu\text{m}$ ), which are harmful to the lungs and cause cancer [10]. In another study, the PEO/CS nanofibers showed resistance to *S. aureus* but no resistance to e.coli except when phenolic was added to the PEO/CS nanofibers [11]. Pomegranate peel extract solution was added to the PEO/CS mixture and showed antibacterial resistance against e.coli [12].

There have been many studies that have looked at the method of producing PEO/CS nanofibers with good specifications. Some studies discussed the effect of the type of solvent and the addition of sodium chloride on the morphology of PEO/CS nanofibers [13], other studies discussed the different mixing ratios and concentrations of the chitosan and PEO mixture [14, 15], and there were many studies about the applications of PEO/CS nanofibers as filters [16] and antibacterial membranes [17], as well as their role in controlling some diseases caused by bacteria infecting plants [18].

There was limited studies on the effect of the solution concentrations below 4 wt% and the CS ratios below 50 wt% on morphological and structural properties of PEO/CS

electrospun nanofibers. In this study, eletrospun PEO/CS nanofibers were produced by using electrospinning solutions at three different concentrations (1, 2, 3 wt%) with five different PEO/CS mixing ratios (30/70, 40/60, 50/50, 60/40, 100/0). Before electrospinning process, viscosity, surface tension and electrical conductivity of the solutions were measured. Morphology, chemical bonds and crystal structure of the nanofibers were investigated by using FESEM, FTIR and XRD, respectively. Lastly, the resistance of the nanofibers to some types of bacteria were tested.

## 2. MATERIAL AND METHOD

### 2.1 Material

In this study, two polymers (CS and PEO) were used. Low molecular weight CS (Mw: 50-190 kDa), and medium molecular weight PEO (Mw: 900 kDa) obtained from Sigma-Aldrich, were dissolved with (50 wt%) acetic acid by magnetic stirring for 24 h at room temperature. The electrospinning solutions were obtained by mixing of CS and PEO solutions at three different PEO/CS concentrations with five different mixing ratios by stirring at room temperature for 5 h (Table 1).

**Table 1.** The PEO/CS electrospinning solutions

Solution concentration (wt%)	PEO/CS ratio (wt/wt)
1	30/70-40/60-50/50-60/40-100/0
2	30/70-40/60-50/50-60/40-100/0
3	30/70-40/60-50/50-60/40-100/0

### 2.2 Nanofiber Production

Electrospinning method was used to produce PEO/CS nanofibers. The electrospinning setup with two variable DC high voltage power supplies (+50 kV and -50 kV), consisted of a syringe with needle, a syringe pump and a flat plate collector. While the needle was connected to the positive voltage supply, the collector plate was connected to a negative voltage supply. The applied voltage, solution flow rate, tip to collector distance (TCD), and needle inner diameter were kept constant as 25 kV, 15  $\mu\text{L}/\text{min}$ , 20 cm, and 0.8 mm, respectively. During the electrospinning process, the ambient temperature and relative humidity were also constant at 30 °C and 50%, respectively.

### 2.3 Characterization

Viscosity, surface tension and electrical conductivity of PEO/CS electrospinning solutions were determined using Brookfield DV-III Ultra Rheometer, Attention Theta optical tensiometer and Orion 4 Star Plus meter, respectively. These measurements were made under standard laboratory conditions at  $23 \pm 2$  °C of ambient temperature and  $45 \pm 5$  % of relative humidity. FTIR spectra were recorded in a frequency range of 4000-500  $\text{cm}^{-1}$  with a resolution of 4

cm<sup>-1</sup>. The Jasco FTIR 6800 was used. QUANTA FEG 650 scanning electron microscope (FESEM), was used to show the morphologies of the nanofibrous mats. The samples were coated with gold at 15 kV for 90 s before observing the fiber morphologies. Depending on the density of the nanofiber sample, between 20 and 40 nanofibers were randomly selected to determine the average diameters of the PEO/CS nanofibers. The Image J program was used to measure diameters of the nanofibers. A PANalytical X-ray diffractometer (model EMPYREAN XRD) was used for XRD measurements, with CuK $\alpha$  radiation ( $\lambda$ : 0.154059 nm) accelerated at a voltage and current of 45 kV and 40 mA, respectively. XRD patterns were recorded from 10° to 90° 2 $\theta$  with a step size of 0.013°. Statistical analyzes were performed using SPSS statistical program (latest trial version) to investigate the relationship between nanofiber diameters at different mixing ratios and different concentrations. ANOVA tests were used and the results are considered significant at  $p \leq 0.05$ . The antibacterial activity of the PEO/CS nanofiber samples against the microorganisms *Staphylococcus aureus* ATCC25923 as Gram positive organism and *Klebsiella pneumoniae* ATCC43816 as Gram negative organism was investigated using the disk diffusion method. Two types of bacteria *S. aureus* and *K. pneumoniae* were distributed with sterile cotton swabs on the surface of Petri dishes filled with Mueller Hinton agar (LAB039, A Neogen company). Before spreading the bacteria in the Petri dishes, two types of bacteria were suspended in saline (0.85% wv<sup>-1</sup>) the day before the test to prepare them for the test. Samples containing only pure PEO nanofibers were used as control sample. After the different PEO/CS nanofiber samples were added to the Petri dishes with two types of bacteria, they were incubated at 37°C for 24h in the bacteriological incubator (Binder). In order to easily apply this assay,

PEO/CS nanofibers were collected onto a nylon layer and these nylon layers loaded with PEO/CS nanofibers were cut as samples with the dimensions as 1×1 cm<sup>2</sup>.

### 3. RESULTS AND DISCUSSION

#### 3.1 Solution Characterization

The surface tension, viscosity, and electrical conductivity values of PEO/CS electrospinning solutions at different concentrations and mixing ratios were measured and given in Table 2.

According to Table 2, slight changes in the surface tension values of the solutions can be observed, but these changes did not follow a certain rule. The highest value was reached at sample PEO/CS: 30/70-2%, while the lowest value was at the sample of PEO/CS:50/50-3% with values 37.99, 36.43, respectively. However, significant changes occurred in the viscosity values with the increase in CS ratio, as well as with the increase in concentration of the solutions. The highest value of viscosity was obtained for the sample of PEO/CS:30/70-3%. Similarly, the cationic nature of chitosan causes the electrical conductivity of a PEO/CS mixture to increase by increasing the CS ratio and by increasing solution concentration [19, 20], so that the highest value of conductivity was also obtained for the sample of PEO/CS:30/70-3%. The high viscosity of this sample makes it difficult to increase the solution concentration to higher values, which makes it impossible to obtain nanofibers by electrospinning, so the concentration and CS ratio were not exceeded to higher values than in the sample of PEO/CS: 30/70-3%.

**Table 2.** The surface tension, viscosity and electrical conductivity of PEO/CS electrospinning solutions

PEO/CS solution concentration (wt%)	PEO/CS ratio (wt/wt)	Surface tension (mN/m)	Viscosity (cP)	Electrical conductivity ( $\mu$ S/cm)
1	30/70	36.84	121	860
	40/60	36.84	115	816
	50/50	37.04	112	783
	60/40	36.91	108	758
	100/0	36.76	54	730
2	30/70	37.99	947	1142
	40/60	36.93	895	1033
	50/50	36.62	713	945
	60/40	36.89	553	854
	100/0	36.62	401	702
3	30/70	37.45	4692	1463
	40/60	36.83	4613	1294
	50/50	36.43	4463	1151
	60/40	36.81	3630	986
	100/0	36.61	1695	675

### 3.2 FTIR Analysis of PEO/CS Nanofibers

Due to the steady increase in chitosan ratio at each concentration in the PEO/CS polymeric combination, analyzing all samples will reveal minor differences in the test. Thus it was preferable to chose two samples with the same concentration and leave it at that (2 wt percent). One sample containing the highest ratio of CS (70%) while the other containing chitosan free- pure PEO sample. To determine the effect of the incorporation of CS into the polymer blend with PEO. Figure 1 shows the relationship between the wavenumber of the functional groups present in both samples PEO/CS:30/70-2% and PEO 2% with the peak intensities of these groups.

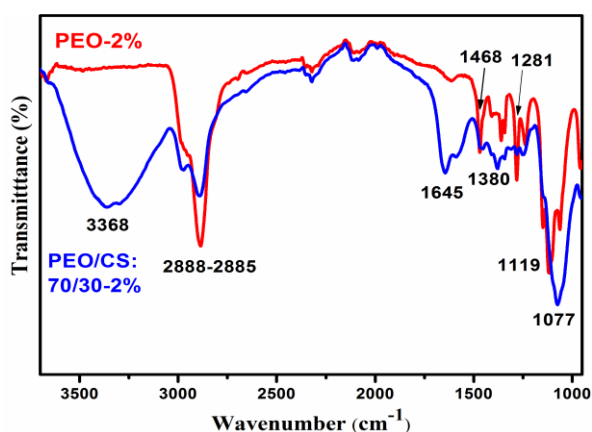


Figure 1. The FTIR spectra of PEO 2% and PEO/CS: 30/70-2%

A broad range from 3100  $\text{cm}^{-1}$  to 3600  $\text{cm}^{-1}$  can be observed in the sample PEO/CS:30/70-2%, indicating the formation of hydrogen bonds between the CS and PEO. A peak appears at the wavenumber 3368.07  $\text{cm}^{-1}$  which is due to the OH stretching vibration of the polysaccharide. While at the same broad range in the pure PEO 2% sample, no peak or extended bond is seen, indicating the presence of hydrogen bonds, confirming that hydrogen bonds were formed only when CS entered the PEO sample [7, 9, 21]. In PEO/CS nanofibers, the peaks at 2887.88, 1453.10, 1281.47, 1077.05  $\text{cm}^{-1}$  indicate the stretching of aliphatic C-H, pending of C-H, stretching vibration of C-OH and stretching vibration of C-O groups in glycoside bond of

polysaccharide structure of chitosan, respectively. Whereas these groups were observed in PEO sample at wavenumbers of 2884.99, 1468.53, 1281.47, 1063.55  $\text{cm}^{-1}$ , respectively [7-9, 21]. In the PEO/CS sample, pending of secondary amine group NH and stretching of CN group can be observed at wave numbers 1645.95 and 1379.82  $\text{cm}^{-1}$ , respectively [7, 8]. A peak at 1119.48  $\text{cm}^{-1}$  is seen, indicating the presence of the C-O-C group in the PEO sample [9, 21].

### 3.3 XRD Analysis of PEO/Chitosan Nanofibers

The highest CS ratio (70 wt%) was chosen for XRD analysis to see obvious differences on the crystalline structures according to neat PEO nanofibers at each concentration of 1, 2, 3 wt% (Figure 2). In PEO 1% sample, peaks were observed at angles 78.23°, 64.90°, 44.55°, while in PEO/CS:30/70-1% they were at angles 78.60°, 65.25°, 45.25° (Figure 2a). Similarly, peaks in PEO 2% appear at angles 78.39°, 64.72°, and 44.49°, while in PEO/CS:30/70-2% they were at angles 78.39°, 65.68°, and 45.24° (Figure 2b). Peaks also appear in PEO 3% at angles 77.88°, 64.90°, 44.90°, while in PEO/CS:30/70-3% they were at angles 78.95°, 65.25°, 44.90° (Figure 2c).

From the previous results, besides the fact that the incorporation of chitosan, even at its highest percentage, that there was a large congruence in the angles of refraction. However, as a result of the amorphous chitosan structure there was a decrease in the height of the peaks, so it can be said that chitosan had no effect on the crystal structure of PEO, also increasing the concentration of the polymer mixture from 1 wt% to 3 wt% did not lead to any significant effect on the crystal structure of the samples [7, 11, 22]. According to the results, the introduction of chitosan in the PEO sample did not lead to any significant change in the crystal structure, with a slight decrease in the peaks.

### 3.4 Morphological Analyses

By applying FESEM analysis to each of the samples, the average diameters of PEO/CS nanofibers were calculated according to different mixing ratios and concentrations (Table 3).

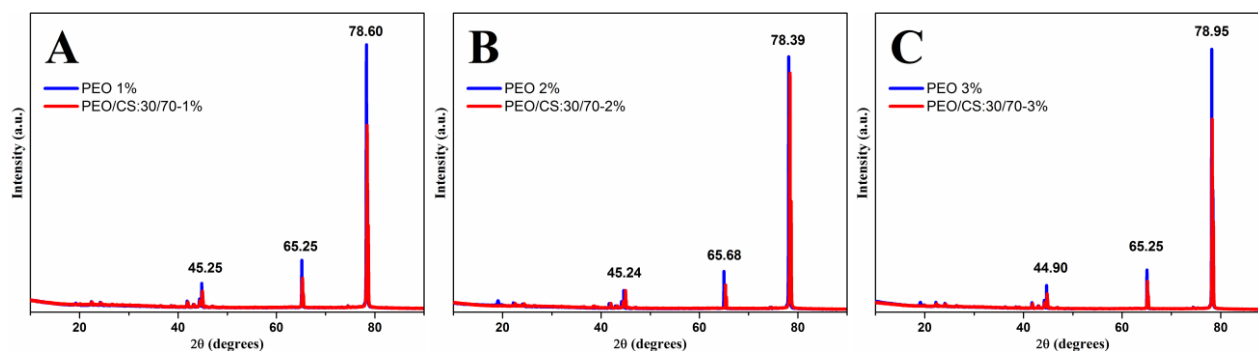


Figure 2. XRD analysis for PEO 1% and PEO/CS:30/70-1% nanofibers (A), PEO 2% and PEO/CS:30/70-2% nanofibers (B), PEO 3% and PEO/CS:30/70-3% nanofibers (C)

**Table 3.** PEO/CS average nanofiber diameters [nm] according to different mixing ratios and concentrations

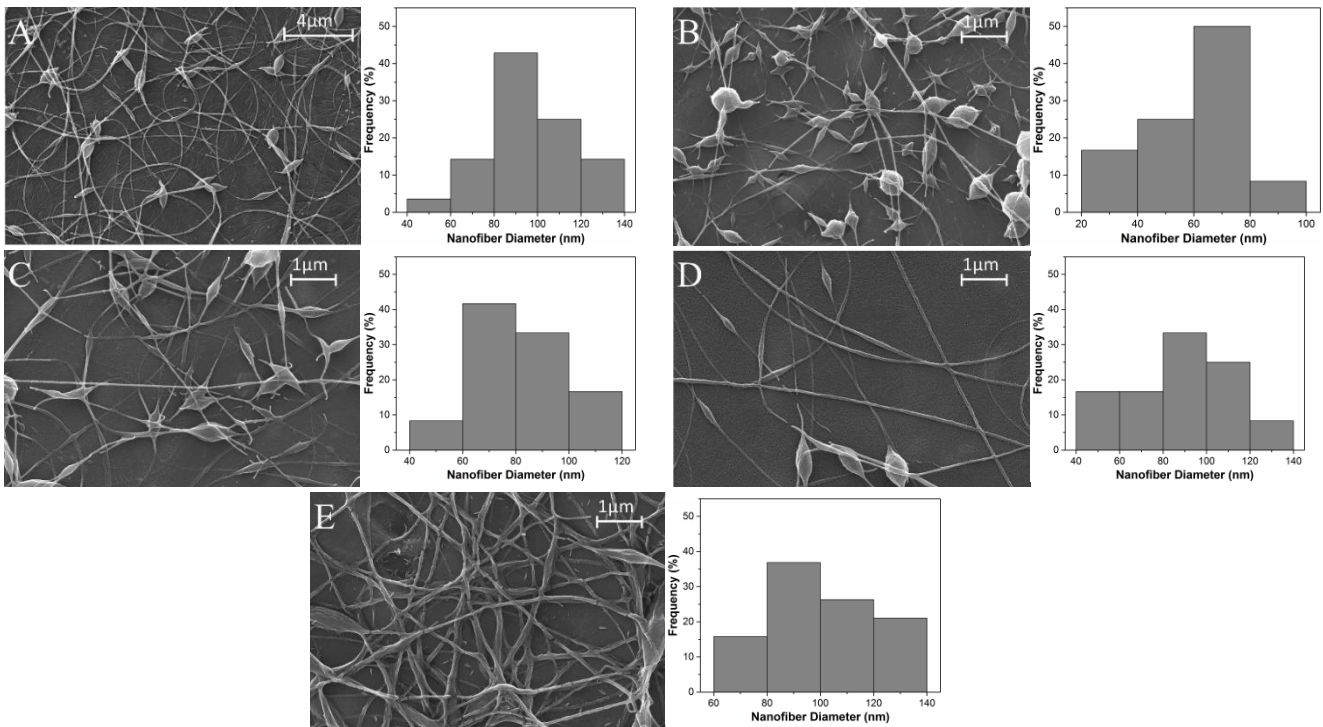
PEO/CS concentration (wt%)	PEO/CS (wt/wt)				
	30/70	40/60	50/50	60/40	100/0
1	59 ± 14	82 ± 17	89 ± 21	102 ± 18	97 ± 19
2	137 ± 16	164 ± 28	191 ± 49	208 ± 56	225 ± 46
3	138 ± 24	166 ± 26	216 ± 31	222 ± 30	298 ± 48

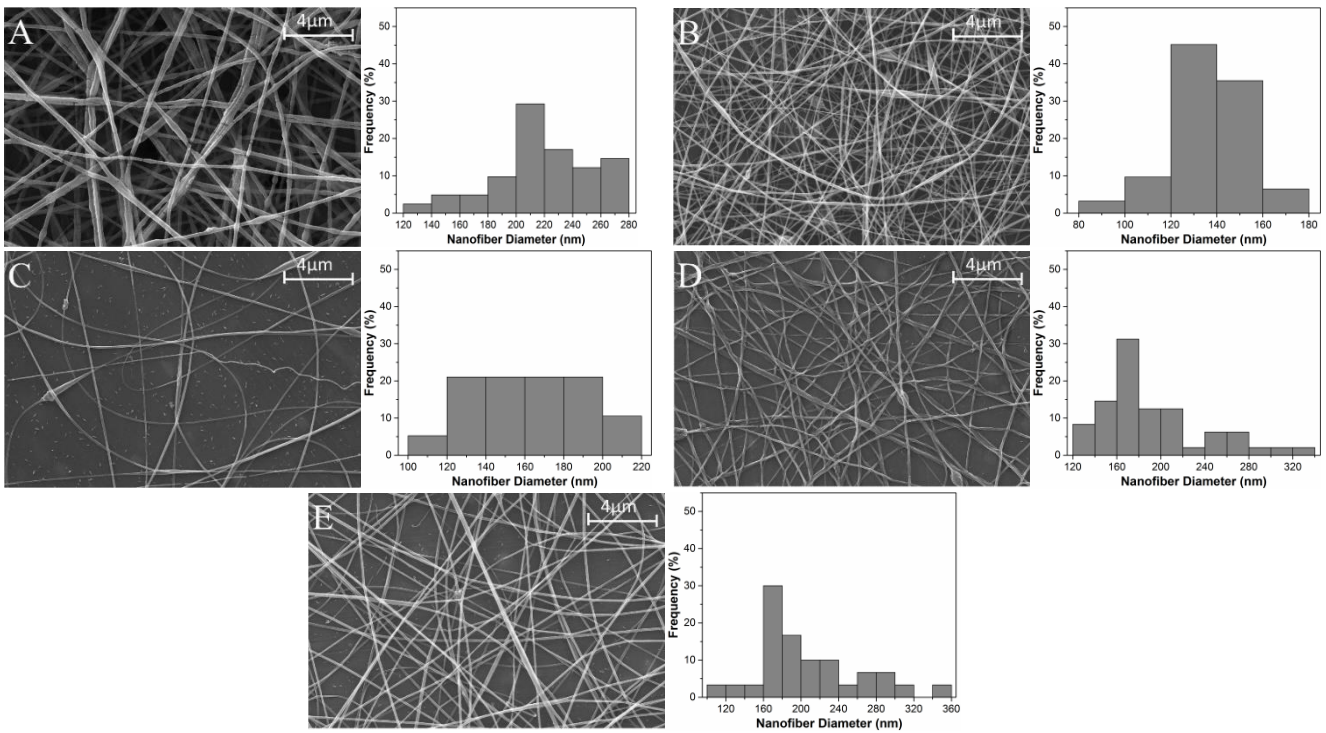
The average diameters of the nanofibers increase with the increase of the concentration of the solution, which was statistically significant ( $p < 0.05$ ). Since the increase in the concentration of the solutions is accompanied by an increase in its viscosity, fibers with a thicker diameter and fewer beads can be obtained.

The chitosan-free PEO sample should theoretically have a larger diameter than any other sample containing chitosan, but the concentration of 1 wt% was very low viscosity, which made it difficult to form nanofibers by electrospinning, so PEO 1% nanofibers appeared with small diameters filled with beads (Figure 3). For all of the concentrations, the diameters of PEO/CS nanofibers decreased with the increase of the ratio of chitosan. Although the presence of chitosan contributes to the high viscosity of the solution, this must be accompanied by an increase in the diameters of the nanofibers. However, the strong hydrogen bonds that chitosan forms with other

polymers, in addition to its cationic nature, which increases the electrical conductivity of the solution, makes the diameters of the fibers decrease even if the viscosity of the solution increases [7, 11]. While the relationship between average diameter and mixing ratio is not statistically significant for 1 wt% ( $p > 0.05$ ), it is significant for 2 wt% and 3 wt% ( $p < 0.05$ ).

As can be seen in (Figure 3), the 1 wt% of concentration was completely unsuitable for obtaining regular, bead-free nanofibers. The chitosan-free PEO nanofibers showed full of beads. The introduction of chitosan helped to improve the viscosity of the solution, but the beads still occurred, so the fibers resulting from the 1 wt% concentration cannot be considered as regular nanofibers. The PEO/CS:60/40 ratio can be considered the best in terms of small number of beads, but the nanofibers were like flat strips. Figure 4 shows FESEM images of the nanofibers at 2 wt% of concentrations.

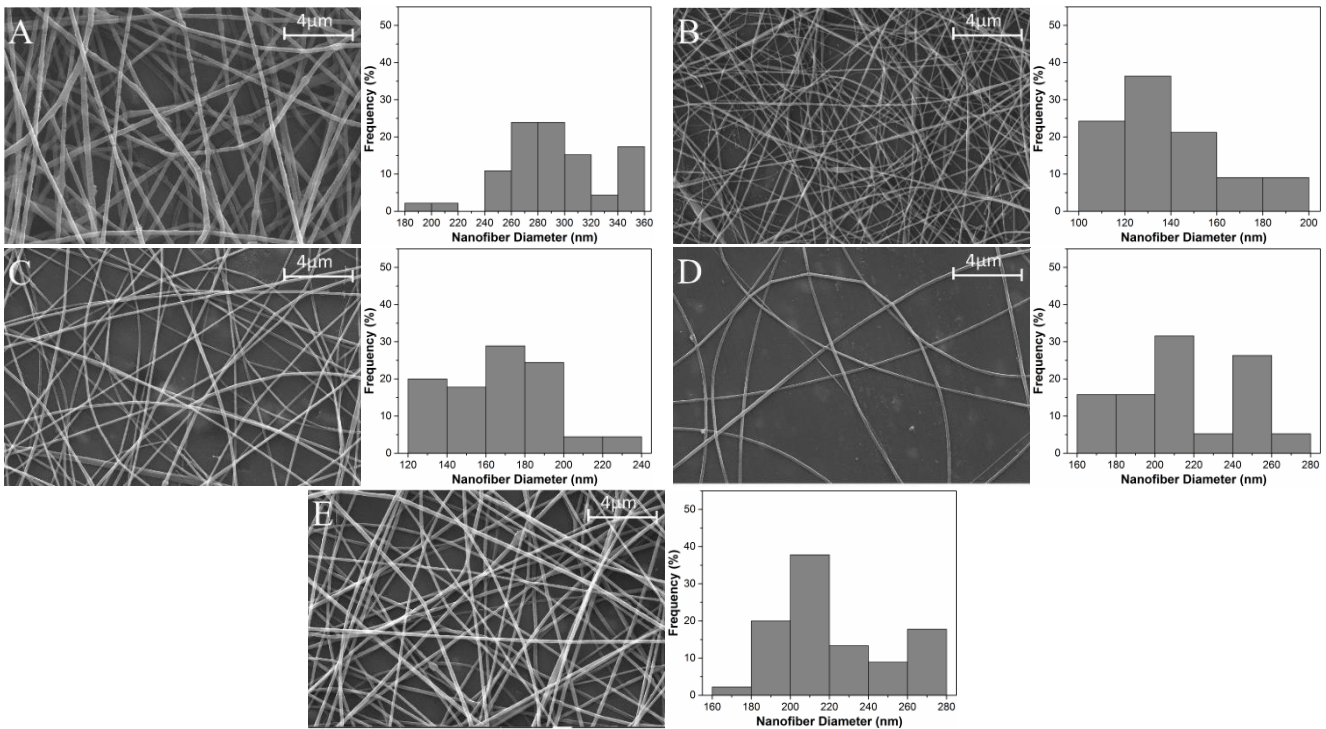
**Figure 3.** The electrospun nanofibers at concentration of 1 wt%: PEO/CS:100/0 (A), PEO/CS:30/70 (B), PEO/CS:40/60 (C), PEO/CS:50/50 (D), PEO/CS:60/40 (E)



**Figure 4.** The electrospun nanofibers at concentration of 2 wt%: PEO/CS:100/0 (A), PEO/CS:30/70 (B), PEO/CS:40/60 (C), PEO/CS:50/50 (D), PEO/CS:60/40 (E)

The nanofibers at concentration of 2 wt% were produced as more uniform and regular and bead-free. The nanofibers containing chitosan at different ratios compared to the neat PEO nanofibers have a more regular shape. When the histogram graphs of nanofibers were examined, the

nanofiber diameter distribution of the PEO/CS:30/70 was more uniform than the others (Figure 4). FESEM images of PEO/CS nanofibers at 3 wt% of concentration were given in Figure 5.



**Figure 5.** The electrospun nanofibers at concentration of 3 wt%: PEO/CS:100/0 (A), PEO/CS:30/70 (B), PEO/CS:40/60 (C), PEO/CS:50/50 (D), PEO/CS:60/40 (E)



The nanofibers at concentration of 3 wt% were generally produced more uniformly and regularly than those of 1 wt% and 2 wt%. Similarly, the diameter distributions of the nanofibers at 3 wt% are more regular for all mixing ratios. Neat PEO nanofibers showed a wider range of nanofiber diameter distribution. The nanofibers at the highest CS ratio at 3 wt% of concentration were more regular and uniform.

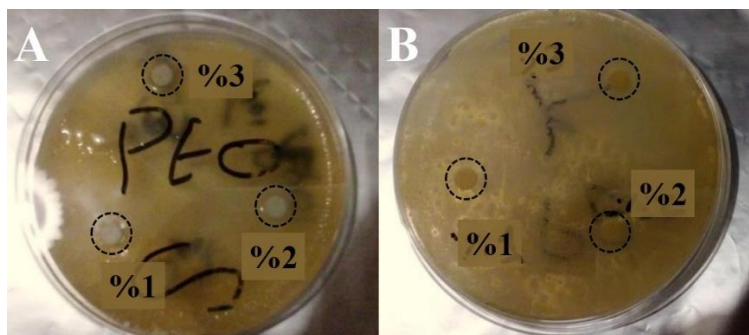
### 3.5 Evaluation of Antibacterial Activity

Antibacterial activity of PEO and PEO/CS samples, against *S. aureus* and *K. pneumoniae* was given in Figure 6 and Figure 7, respectively. PEO sample was applied disk diffusion method for the determination of its antibacterial properties. Three disks were placed on agar and PEO prepared in different concentrations (1, 2 and 3 wt%) were poured onto the disk as a solution using a needle. As Figure 6 shows, two types of bacteria completely surrounded the disks and areas of inhibition were not formed [23].

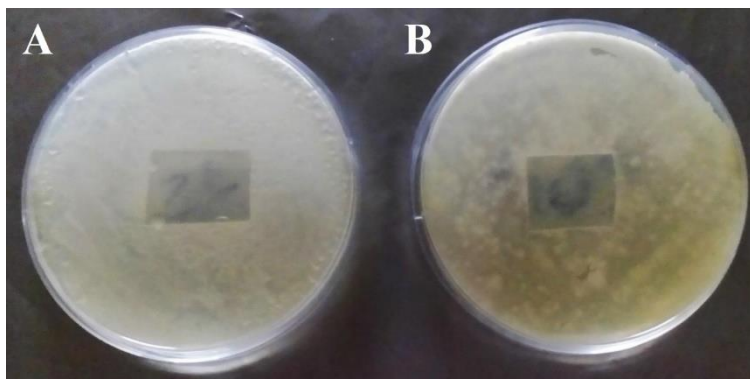
The PEO/CS nanofiber samples with different mixing ratios and concentrations showed no inhibition zone against *S. aureus* or *K. pneumoniae* bacteria in the surrounding area of PEO/CS samples. The nylon layer loaded with PEO/CS nanofibers appeared as a transparent area within the agar, with no space between it and the bacteria. Thus, it can be said that despite the antibacterial properties of chitosan as a cationic polymer, the process of electrospinning with other

polymers prevented the occurrence of these properties because the PEO molecules were able to surround the chitosan molecules in the process of electrospinning and prevent the occurrence of the antibacterial properties [12]. At the same time, other studies indicate that the antibacterial property of chitosan does not occur continuously and is closely related to its physical properties, especially its molecular weight [24]. Therefore, this study tested the highest concentrations and the highest proportions of chitosan that can be obtained from this low molecular weight of chitosan in the form of nanofibers via electrospinning technique.

At all the high concentrations and proportions of chitosan, the PEO molecules were able to prevent the occurrence of the antibacterial property of chitosan. Therefore, it is difficult to use these fibers in an application that depends on the antibacterial properties of chitosan, such as wound dressing or medical tissues, without adding other materials with antibacterial properties to support the property of chitosan. However, due to the uniformity of the fibers resulting from the concentrations (2, 3 wt%) and their absence of beads, it is recommended to use them as packaging fibers for different materials such as medicines, fertilizers or in the field of filtration. The identical results were seen in all tested samples, so just antibacterial tests of PEO/CS:30/70-3% sample was given as an example (Figure 7).



**Figure 6.** Antibacterial activity for PEO solution against *S. aureus* (A) and *K. pneumoniae* (B)



**Figure 7.** Antibacterial activity of PEO/CS:30/70-3% sample against *S. aureus* (A) and *K. pneumoniae* (B)

## 4. CONCLUSION

In this study, nanofibers were produced from a mixture of low molecular weight chitosan and medium molecular weight PEO at different concentrations and mixing ratios by electrospinning method. Increasing of CS ratio and solution concentration caused to increase both viscosity and electrical conductivity of the solutions. While 1 wt% of concentration was not suitable to obtain regular nanofibers, the other concentrations are better to obtain more regular, uniform and bead-free nanofibers. The sample of PEO/CS:60/40 at 3 wt% has the largest diameter and the least amount of beads among CS containing nanofibers. The average diameters of the nanofibers increased with the increase of the concentration of the solution, which was statistically significant ( $p < 0.05$ ). The average diameters of

PEO/CS nanofibers decreased with the increase of chitosan ratio at all concentrations. CS caused to increase of H bonds intensity of PEO nanofibers. Existence of CS in the PEO nanofibers did not lead to any significant change in the crystal structure. There was no antibacterial activity of the PEO/CS nanofibers to two types of bacteria *S. aureus* and *K. pneumoniae*. PEO/CS nanofibers can be used as packaging fibers for different materials such as medicines, fertilizers or in the field of filtration due to their small diameters, uniform and bead-free nanofiber formation.


## Acknowledgement


This study was supported by the Scientific Research Projects Unit of Çukurova University (Project code: FDK-2019-11674).


## REFERENCES


1. Cengiz Çalılıoğlu F. 2013. The production of nanofiber by roller electrospinning method. *Tekstil ve Mühendis* 20(91), 35-49.
2. Göktepe F, Mülayim BB. 2015. Nanofiber yarn production methods by electrospinning. *Tekstil ve Mühendis* 22(99), 51-67.
3. Antonino RSCMQ, Fook BRDL, Lima EPN, Lima RJS, Fook MVL, Covas CAP, Rached RIF, Lima VAO. 2017. Preparation and characterization of chitosan obtained from shells of shrimp. *Marine Drugs* 15(141), 1-12.
4. Ayodele O, Okoronkwo AE, Oluwasina OO, Abe TO. 2018. Utilization of blue crab shells for the synthesis of chitosan nanoparticles and their characterization, *Songklanakarin Journal of Science and Technology* 40(5), 1043-1047.
5. Sandeep A, Sangameshwar K, Mukesh G, Chandarktan R, Avinash D. 2013. A brief overview on chitosan applications. *Indo American Journal of Pharmaceutical Research* 3(12), 1564-1574.
6. Hung L, Nagapudi K, Apkarian R, Chaikof E, 2001. Engineered collagen-PEO nanofibers and fabrics. *Journal of Biomaterials Science, Polymer Edition* 12(9), 979-993.
7. Singh Y, Dasgupta S, Nayar S, Bhaskar R. 2020. Optimization of electrospinning process & parameters for producing defect-free chitosan/polyethylene oxide nanofibers for bone tissue engineering. *Journal of Biomaterials Science, Polymer Edition* 31(6), 1-23.
8. Stie M, Catke J, Wan F, Chronakis I, Jascobsn J, Nielsen H. 2020. Swelling of mucoadhesive electrospun chitosan/polyethylene oxide nanofibers facilitates adhesion to the sublingual mucosa. *Carbohydrate Polymers* 242, 1-29.
9. Amiri N, Ajami S, Shahroodi A, Jannatabadi N, Darbab S, Bazzaz B, Pishavar E, Kalalinia F, Movaffagh J. 2020. Teicoplanin-loaded chitosan-PEO nanofibers for local antibiotic delivery and wound healing. *International Journal of Biological Macromolecules* 162, 645-656.
10. Pan W, Wang J, Sun X, Wang X, Jian J, Zhang Z, Hao Qu C, Zelong Y, Feng G. 2020. Ultra uniform metal-organic framework-5 loading along electrospun chitosan/polyethylene oxide membrane fibers for efficient PM2.5 removal. *Journal of Cleaner Production* 291, 1-29.
11. Kuntzler S, Costa J, Morais M. 2018. Development of electrospun nanofibers containing chitosan/PEO blend and phenolic compounds with antibacterial activity. *International Journal of Biological Macromolecules* 117, 800-806.
12. Surendhiran D, Li C, Cui H, Lin L. 2020. Fabrication of high stability active nanofibers encapsulated with pomegranate peel extract using chitosan/PEO for meat preservation. *Food Packaging and Shelf Life* 23, 1-9.
13. Martinova L, Lubosova D. 2008. Electrospun chitosan based nano fibers. *Tekstil ve Konfeksiyon* 12(2), 22-79.
14. Lemma SM, Bossard F, Rinaudo M. 2016. Preparation of pure and stable chitosan nanofibers by electrospinning in the presence of poly ethylene oxide. *International Journal of Molecular Sciences* 17, 1-16.
15. Bizarria MTM, Davila MA, Mei LHI. 2014. Non woven nano fiber chitosan/PEO membranes obtained by electro spinning. *Brazilian Journal of Chemical Engineering* 31(1), 57-68.
16. Min LL, Yuan ZH, Zhong LB, Liu Q, Wu RX, Zheng YM. 2014. Preparation of chitosan based electrospun nanofiber membrane and its adsorptive removal of arsenate from aqueous solution. *Chemical Engineering Journal* 267, 132-141.
17. Rieger KA, Schiffman JD. 2014. Electrospinning an essential oil: cinnamaldehyde enhances the antimicrobial efficacy of chitosan/Poly(Ethylene Oxide) nanofibers. *Carbohydrat Polymers* 113, 561-568.
18. Noruzi M. 2016. Electrospun nanofibers in agriculture and the food industry: A review. *Society of Chemical Industry* 10, 1-16.
19. Koosha M, Mirzadeh H. 2015. Electrospinning, mechanical properties, and cell behavior study of chitosan/PVA nanofibers, *Society For Biomaterials* 103(9), 3081-3093.
20. Paipitaka K, Pornprac T, Mongkantalang P, Techitdheera CW, Pecharapaa W. 2011. Characterization of PVA-chitosan nanofibers prepared by electrospinning. *Science Direct* 8, 101-105.
21. Aliabadi M, Irani M, Ismaeili J, Piri H, Parnian MJ. 2013. Electrospun Nanofiber Membrane of PEO/Chitosan for the Adsorption of Nickel, Cadmium, Lead And Copper Ions From Aqueous Solution. *Chemical Engineering Journal* 220, 237-243.
22. An J, Zhang H, Zhang J, Zhao Y, Yuan X. 2009. Preparation and antibacterial activity of electrospun chitosan/poly(ethylene oxide) membranes containing silver nanoparticles, *Colloid and Polymer Science* 287(12), 1425-1434.
23. Gatti J, Smithgall M, Paranjape S, Rolles R, Parajope M. 2013. Using electrospun poly(ethylene-oxide) nanofibers for improved retention and efficacy of bacteriolytic antibiotics. *Biomedical Microdevices* 15(5), 887-93.
24. Benhabiles MS, Salah R, Lounici H, Drouiche N, Goosen MFA, Mameri N. 2012. Antibacterial activity of chitin, chitosan and its oligomers prepared from shrimp shell waste. *Food Hydrocolloids* 29, 48-56.

# Predictive Modeling of Yarn Quality at Ring Spinning Machine using Resilient Back Propagation Neural Networks

Assad Farooq  0000-0003-4532-4431

Nayab Khan  0000-0001-7844-3272

Farida Irshad  0000-0002-2881-3172

Usama Nasir 

<sup>1</sup>Department of Fibre and Textile Technology, University of Agriculture, Faisalabad, Pakistan

**Corresponding Author:** Assad Farooq, assadfarooq@uaf.edu.pk

## ABSTRACT

The final attenuation and twisting of fiber take place at ring spinning machine and hence its optimized performance is very crucial in terms of yarn quality. Drafting at ring spinning machine has a decisive effect on quality. There exist many influencing parameters in the spinning geometry that have to be optimized for manufacturing of quality yarn. The present research work was carried out to develop the Artificial neural networks (ANN) based prediction model for the polyester/cotton blended ring spun yarns by using these influencing parameters as inputs. ANN prediction model was developed using resilient backpropagation algorithm. Yarn quality parameters like yarn evenness, hairiness and tensile parameters were predicted. The low mean absolute error values for the yarn quality parameters proved that it is possible to predict the yarn quality on the basis of spinning geometry for cotton/polyester blended ring spun yarns using Resilient Back Propagation Neural Networks.

## 1. INTRODUCTION

Ring spinning hold the top position among other spinning processes due to its excellent quality, high count range and flexibility of processing variety of materials. Draft zone is the heart of heading spinning machine. The quality of drafting procedure is directly associated with the quality of the yarn produced. During the movement of the fibres in the drafting zone the fibres have to change their speed from a lower level to a higher level so that the draft can be accomplished. However, this acceleration can be smooth or can be abrupt. The smooth acceleration of the fibres indicates that drafting process is being performed with minimum variations. On the other hand, abrupt acceleration can cause the high number of imperfections in the yarn. In

this backdrop the drafting force must be kept as uniform as possible by overcoming the cohesive friction among the fibers. The acceleration of fibers inside the drafting zone is influenced by the cohesion between the fibers, the draft zone settings, amount of draft and the processing speeds. The draft quality as well as the ultimate yarn quality is the combined effect of the interaction of these influencing variables with the fibrous material. The optimization of draft zone settings using different modeling and optimization techniques has been the topic of research in last few decades [1-8]. Similar researches had been carried out for the rotor spun yarns [9, 10]. The aim of the presented research is to optimize these technological parameters for optimal yarn quality.

**To cite this article:** Farooq A, Khan N, Irshad F, Nasir U. 2023. Predictive Modeling of Yarn Quality at Ring Spinning Machine using Resilient Back Propagation Neural Networks. *Tekstil ve Konfeksiyon* 33(1), 9-14.

## ARTICLE HISTORY

Received: 06.04.2021

Accepted: 07.07.2022

## KEYWORDS

Ring Spinning, Artificial Neural Networks, Resilient Back Propagation Neural Networks, Draft zone settings, Yarn Quality

By changing the total draft of ring frame, the yarn count range can be altered. However, the same yarn count can be manufactured by changing the amount of draft. This can be done by changing the hank roving along with changing the amount of draft to produce the same yarn count. However, it does not mean that characteristics of the yarn produced at various draft settings even having the same count would be same. This implies that influence of the amount of draft cannot be ignored at any stage of yarn formation, as it plays a key role in deciding the quality parameters of ring spun yarn.

Top arm pressure is one of the significant draft zone setting at ring spinning machine and greatly influence the quality and performance of drafting. As the top arm pressure increased the fibre friction field increases, which lead to better control over the fibre flow in the drafting zone, but if the top arm pressure is too high it can obstruct the drafting process. Similarly, a lower top arm pressure is associated with poor fibre control. Hence, the amount of pressure exerted depends upon types of raw material and its volume and other process parameters and therefore, must be optimized accordingly [11-13].

Another vital drafting parameter is the apron spacing. In the main drafting zone, the top aprons are forced by a spring pressure against the lower aprons. The distance between the top and bottom apron is known as apron spacing and is set by the "spacer". The intensity of fibre clamping, and thus fibre guidance, depend upon the size of the spacer. Spacers exert major influence during drafting process, which can be exhibited from yarn evenness. Similarly, spacers are also associated with end breakages at ring spinning machine thus influencing the yarn production. Artificial neural network (ANN) is a powerful tool to model and simulate the non-linear processes where a large number of influencing variables are involved. The artificial neural networks are capable of understanding the complex relationship that exist between the input and output variable and can make accurate and precise prediction on the basis of the provided experimental data. The artificial neural networks have been applied to various areas of the textile and yarn spinning in past [14-17]. In this research work, keeping in view the power of ANN to predict the output parameters using the experimental data of input parameters, ANNs have been selected in order to establish a

quantitative relationship of yarn properties and ring machine variables. The present research study will be useful for textile researchers as a tool for further investigation and optimization the quality of ring spun yarn by adjusting the different parameters of ring spinning machine.

## 2. MATERIAL AND METHOD

The presented research work was conducted on Polyester / Cotton blended yarns having blend ratio of (52:48). Both possibilities of producing PC blended yarns, i.e. blending of PES with carded cotton slivers and blending of PES with combed cotton slivers were taken into consideration. After processing from the blow room and card the slivers of 70 grains/yards were produced for both cotton and polyester. For carded yarns the card slivers were blended at draw frame. The second passage was autolevelling draw frame. The resulted sliver were fed to roving frame and different hank rovings as mentioned in the table 1 were manufactured.

For the preparation of combed yarns, the polyester slivers were drafted at a pre-drawing passage at Draw frame while cotton is fed to the Lap former (UNI-LAP) after pre-drawing. Then the combing was performed and 14% waste (noil) was extracted at this stage. Then the combed cotton slivers were blended with the pre-drawn polyester slivers for two draw frame passages to produce the slivers of 70 grains/yard. The drawing slivers were fed to roving machine to produce the desired rovings.

The produced hank rovings were subjected to yarn manufacturing at the miniature ring spinning as per following plan.

As four different counts were produced from three different kinds of hank rovings, therefore, the amount of draft in each case is different. The said situation for the 30S is depicted in the following figure1.

The yarn samples were tested under Standard atmospheric conditions (20±2°C and 65% RH). Yarn unevenness U%, yarn imperfections and hairiness were measured using the Uster Evenness tester UT-3. The tensile strength parameters were determined by using the different strength testers for single yarn and yarn skiens.

**Table 1** Experimental Plan

Material	Roving Hank	Yarn Count	Top arm pressure	Spacer	Spindle Speed
H <sub>1</sub> = (carded)	0.8	C <sub>1</sub> = 20 <sup>s</sup>	P <sub>1</sub> = 14 lb	S <sub>1</sub> = 2.00mm	14500 rpm
		C <sub>2</sub> = 22 <sup>s</sup>	P <sub>2</sub> = 16 lb	S <sub>2</sub> = 2.5mm	16000 rpm
H <sub>2</sub> = (combed)	1.0	C <sub>3</sub> = 26 <sup>s</sup>	P <sub>3</sub> = 18 lb	S <sub>3</sub> = 3.5mm	17000 rpm
		C <sub>4</sub> = 30 <sup>s</sup>		S <sub>4</sub> = 4.00mm	18000 rpm
	1.2				

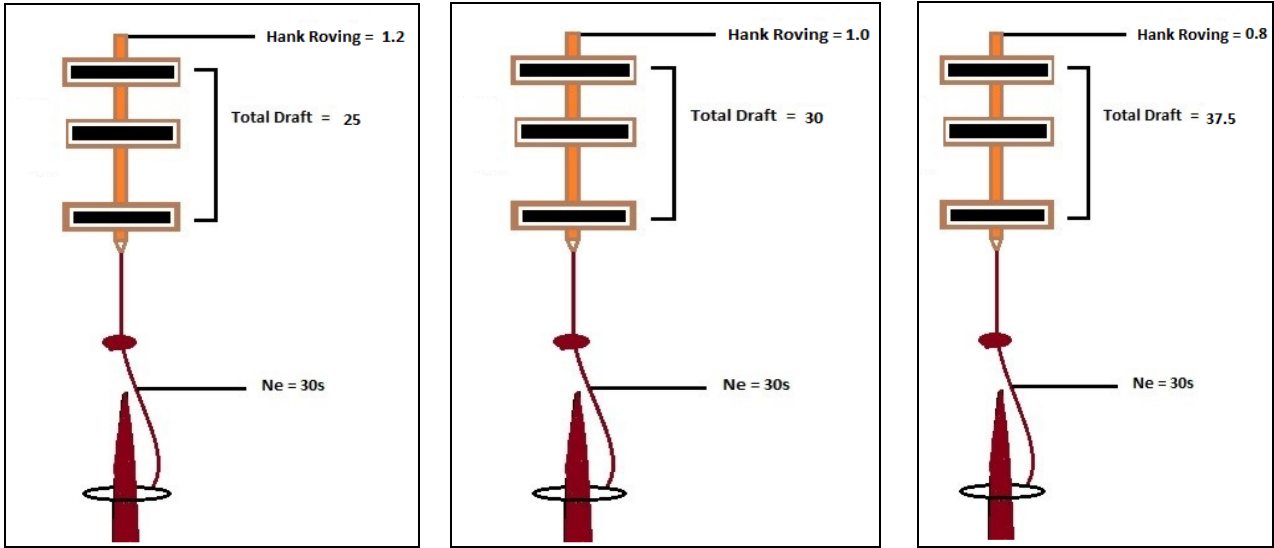


Figure 1. Draft settings for experimental phase

### Artificial Neural Networks Modeling and Simulation

In order to train the artificial neural networks for the present research work, a Graphic User Interface (GUI) is programmed using Matlab software.

The precision in modeling of artificial neural networks is of prime importance which can only be achieved with correct input selection and correct choice of network parameters and training algorithm. The most commonly used training algorithm for predictive modeling is backpropagation. However, it has the problems like getting stuck in local minima and overfitting. By using the resilient backpropagation algorithm, the shortcomings of backpropagation can be compensated. In resilient backpropagation the sign of derivatives is used to find out the increase or decrease in weights whereas the magnitude of weights is updated by a separate value. Backpropagation being the conventional gradient descent method uses the partial derivatives. The magnitude of these partial derivatives is too small and hence the possibility of getting stuck in the local minima is higher. Moreover, it takes long time for training [18-22].

The weights are updated in backpropagation by using the following terms

$$\Delta w_{ij}(t) = \alpha * x_i(t) * \delta_j(t)$$

Where

$\Delta w$  = Weight Change

$\alpha$  = Learning Rate

$\delta$  = Error Gradient

$x_i(t)$  = Inputs propagation back at time step t.

However, individual delta  $\Delta_{ij}$  are calculated for each connection to determine the direction & size of the weight update.

$$\Delta_{ij}(t) = n^t \times \Delta_{ij}^{(t-1)}, \quad \text{if } \frac{\partial E^{(t-1)}}{\partial W_{ij}} \times \frac{\partial E^t}{\partial W_{ij}} > 0$$

$$\Delta_{ij}(t) = n^{-t} \times \Delta_{ij}^{(t-1)}, \quad \text{if } \frac{\partial E^{(t-1)}}{\partial W_{ij}} \times \frac{\partial E^t}{\partial W_{ij}} < 0$$

$$\Delta_{ij}^{(t-1)}, \quad \text{else}$$

Where

An evolution of  $\Delta_{ij}$  (updated value) takes place during the learning process, which is determined by the sign of error

gradient of the  $\frac{\partial E^{(t-1)}}{\partial W_{ij}}$  last cycle and error gradient of  $\frac{\partial E^{(t-1)}}{\partial W_{ij}}$  current cycle.

The commonly used method for testing the performance of artificial neural networks on the unseen data is 'Hold out Method'. This implies that 90% of data is used for training while randomly selected 10% data is used for the testing of the performance of trained networks. Another method is the cross-validation technique in which the data is divided into 10 subsets and the network is trained 10 times using one of the subsets for testing while remaining 9 for the training. The mean absolute error in each case was calculated and mean absolute error was determined by taking the average of 10 values the law mean absolute error values resulted from cross validation ensure the good generalization ability of the train network [23]. After validation, the post-processed data was de-normalized to get the original values from the normalized data.

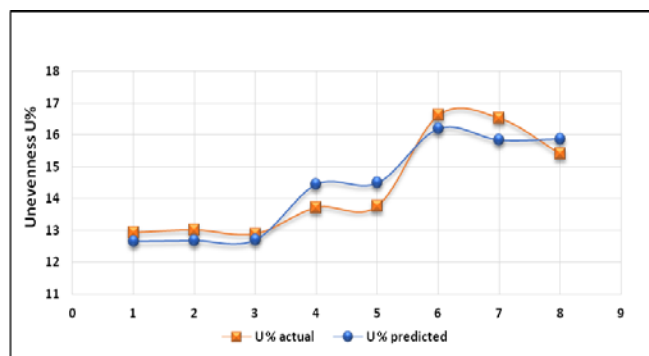
### 3. RESULTS AND DISCUSSION

#### Yarn Unevenness (U%):

The data regarding yarn unevenness is used for neural network training under the below mentioned parameters in the table 2. The accuracy in the prediction of the trained network is presented in the following figure 2. Mean absolute error on the test set as given in term of yarn unevenness values is 0.479. The little difference between the experimental and predicted values shows the aptness for the neural networks.

**Table 2.** Neural Network Training Parameters for Yarn Unevenness (U%)

Network Parameters Values	NN_ Unevenness
Number of Neurons in Input Layer	8
Number of Neurons in First Hidden Layer	7
Number of Neurons in Second Hidden Layer	8
Number of Neurons in Output Layer	1
Learning Rate	0.06
Momentum	0.7
Number of Epochs	2000
Stopping Error	0.001



**Figure 2.** Test Set Performance of U%

The three levels in the figure 2 shows that the values of all blends were included in the unseen data used for the testing and simulation of the trained neural network for yarn unevenness (U%). The cross validation was also applied to the data which shows the results of 0.39 and 0.57 for 10% and 20% cross validations respectively.

#### Yarn Lea Strength:

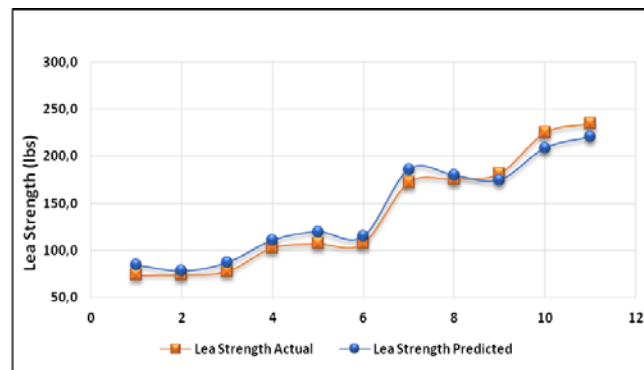
The data relating to yarn lea strength is subjected to neural network training using the following training parameters mentioned in the table 3. It is worth to mention here that the network structure used for the training of the blended yarns is complex in comparison with that of used for cotton. This is because of more number of materials used and presence of more complex relationships among the influencing parameters.

The accuracy of the prediction of trained network is showed in the following figure 3. The four levels of yarn lea

strength shows that for the unseen data set all four materials; PES/CO 70:30, 50:50, 30:70 and 100:0 were used to observe the performance of the trained neural network. Mean absolute error on the test set as given in term of lea strength values is 9.84. The slight difference in the actual and predicted values indicates the suitability for the neural networks. 8.43 lbs and 10.15lbs mean absolute error was observed in case of 10% and 20% cross validation respectively.

**Table 3.** Neural Network Training Parameters for Yarn Lea Strength

Network Parameters Values	NN_Lea Strength
Number of Neurons in Input Layer	8
Number of Neurons in First Hidden Layer	7
Number of Neurons in Second Hidden Layer	6
Number of Neurons in Output Layer	1
Learning Rate	0.01
Momentum	0.6
Number of Epochs	2000
Stopping Error	0.001



**Figure 3** Test Set Performance for Yarn Lea Strength

#### Yarn Single End Strength

The data pertaining to SES is subjected to the neural network training using the training parameters written in the table 4. The prediction accuracy of the trained network using the hold out method is depicted in the following Figure 4. Mean absolute error on the test set as given in term of SES values is 9.12. The Cross-validation analysis, i.e. 10%, 20% cross validations, is conducted on the data and the mean absolute error in terms of SES values is 8.3 and 13.7 is reported respectively. The little difference between the experimental and predicted values indicates the goodness of fit for the neural networks.

**Table 4.** Neural Network Training Parameters for Yarn Single End Strength

Network Parameters Values	Values
Number of Neurons in Input Layer	8

Number of Neurons in First Hidden Layer	7
Number of Neurons in Second Hidden Layer	5
Number of Neurons in Output Layer	1
Learning Rate	0.08
Momentum	0.3
Number of Epochs	2000
Stopping Error	0.001

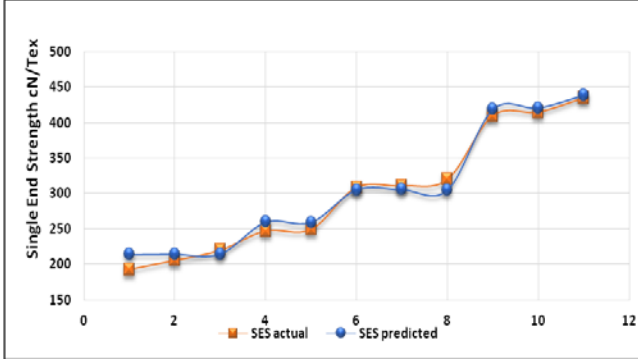


Figure 4. Test Performance for SES

#### Yarn Elongation:

The data relating to the yarn elongation is subjected to neural network training using the training parameters mentioned in the table 5. The accuracy in the prediction of the trained network is demonstrated in the figure 5. Mean absolute error in the test set as given in term of yarn elongation values is 0.24. The minute differences between the experimental and estimated values illustrate the fitness for the neural networks. The cross validation was also applied to the data which shows the results of 0.29 and 0.42 for 10% and 20% cross validations respectively.

Table 5. Neural Network Training Parameters for Yarn Elongation

Network Parameters Values	Values
Number of Neurons in Input Layer	8
Number of Neurons in First Hidden Layer	5
Number of Neurons in Second Hidden Layer	3
Number of Neurons in Output Layer	1
Learning Rate	0.02
Momentum	0.5
Number of Epochs	2000
Stopping Error	0.001

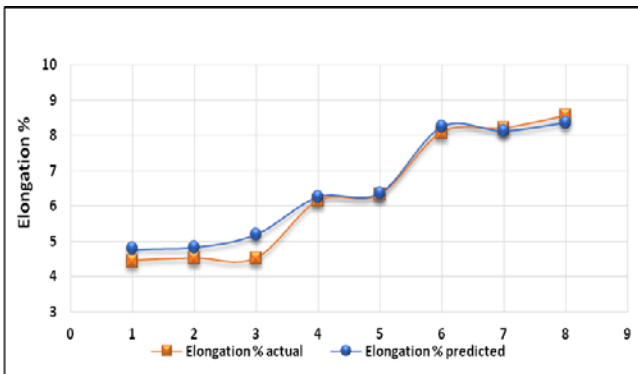


Figure 5 Test Performance for Elongation %

#### Yarn Hairiness:

The data regarding yarn hairiness is used for neural network training under the network parameters mentioned in the following table 6. In comparison with other yarn characteristics, the network structure for yarn hairiness is complex, because of the dependance of yarn hairiness on different material parameters.

Table 6 Neural Network Training Parameters for Yarn Hairiness

Network Parameters Values	Values
Number of Neurons in Input Layer	8
Number of Neurons in First Hidden Layer	8
Number of Neurons in Second Hidden Layer	7
Number of Neurons in Output Layer	1
Learning Rate	0.05
Momentum	0.3
Number of Epochs	2000
Stopping Error	0.001

The prediction accuracy of the trained network is portrayed in the figure 6. Mean absolute error in the test set as given in term of yarn hairiness values is 0.44. The difference between the experimental and predicted values depicts the aptness for the neural networks.

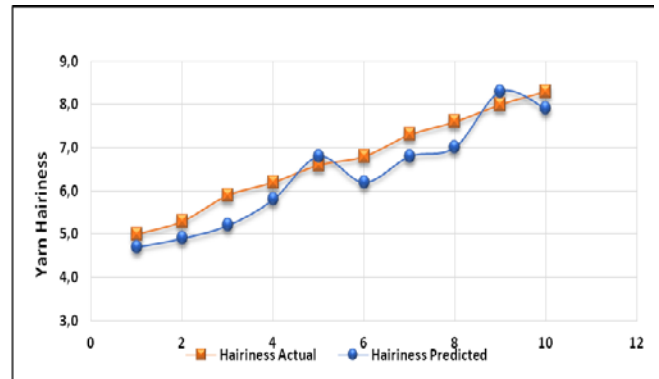


Figure 6 Test Performance for Hairiness

The 10% cross validation results in the MAE of 0.48 while 20% cross validation results in MAE of 0.69 expressed in terms of yarn hairiness H value. However, here that the prediction accuracy is not as good as with the other yarn quality characteristics. This is due to the fact that yarn hairiness is not entirely dependent on the ring spinning parameters. The fiber control during the spinning is one of the major factors influencing the yarn hairiness, however, fibre characteristics are also very important in case of yarn hairiness.

#### 4. CONCLUSION

The influence of yarn count, spacer size and top arm pressure and draft settings on the quality of ring spun cotton carded as well as combed yarn was studied. In each case, the optimum conditions within the industrially acceptable

limits of the process were established. The data of yarn quality thus obtained was used to train the artificial neural networks. The trained neural networks were tested using hold out method and cross validation methods.

The results showed that neural networks have accurately predicted the cotton yarn quality, both with carded and combed rovings. Higher degree of prediction accuracy was found while predicting the all the vital characteristics like,

yarn lea strength, single end strength and yarn unevenness. However, the prediction accuracy in case of IPI is relatively low which is mainly attributed to the amount of neps present in the rovings. In this backdrop it can be concluded that artificial neural networks have proved success for predicting the yarn properties using ring spinning frame settings as input.

## REFERENCES


1. Ishtiaque, S, Rengasamy, R,Ghosh, A. 2004. Optimization of Ring Frame Process Parameters for Better Yam Quality and Production. *Indian Journal of Fibre & Textile Research* 29(2), 190-195.
2. Majumdar, P K,Majumdar, A. 2004. Predicting the Breaking Elongation of Ring Spun Cotton Yarns Using Mathematical, Statistical, and Artificial Neural Network Models. *Textile Research Journal* 74(7), 652-55.
3. Üreyen, M E,Gürkan, P. 2008. Comparison of Artificial Neural Network and Linear Regression Models for Prediction of Ring Spun Yarn Properties. I. Prediction of Yarn Tensile Properties. *Fibers and Polymers* 9(1), 87-91.
4. Üreyen, M. E., & Gürkan, P. 2008. Comparison of Artificial Neural Network and Linear Regression Models for Prediction of Ring Spun Yarn Properties. II. Prediction of Yarn Hairiness and Unevenness. *Fibers and Polymers* 9(1), 92-96.
5. Moghassem, A. Fallahpour, A,Shanbeh, M. 2012. An Intelligent Model to Predict Breaking Strength of Rotor Spun Yarns Using Gene Expression Programming. *Journal of Engineered Fibers and Fabrics* 7(2), 155892501200700202.
6. Feng, J, Xu, B G,Tao, X M. 2013. Systematic Investigation and Optimization of Fine Cotton Yarns Produced in a Modified Ring Spinning System Using Statistical Methods. *Textile Research Journal* 83(3), 238-48.
7. Malik, S A, Farooq, A, Gereke, T,Cherif, C. 2016. Prediction of Blended Yarn Evenness and Tensile Properties by Using Artificial Neural Network and Multiple Linear Regression. *Autex Research Journal* 16(2), 43-50.
8. Khurshid, F, Aslam, S, Ali, U, Abbas, A, Hamdani, T A,Hussain, F. 2018. Optimization of Break Draft, Pin Spacer and Rubber Cots Hardness to Enhance the Quality of Ring Spun Yarn Using Factorial Design. *Journal of Engineered Fibers and Fabrics* 13(2), 155892501801300209.
9. Demiryürek, O,Koç, E. 2009. Predicting the Unevenness of Polyester/Viscose Blended Open-End Rotor Spun Yarns Using Artificial Neural Network and Statistical Models. *Fibers and Polymers* 10(2), 237-45.
10. Demiryürek, O,Koç, E. 2009. The Mechanism and/or Prediction of the Breaking Elongation of Polyester/Viscose Blended Open-End Rotor Spun Yarns. *Fibers and Polymers* 10(5), 694-702.
11. Ishtiaque, S M, Das, A,Niyogi, R. 2006. Optimization of Fiber Friction, Top Arm Pressure and Roller Setting at Various Drafting Stages. *Textile Research Journal* 76(12), 913-21.
12. Ghane, M, Semnani, D, Saghafi, R,Beigzadeh, H. 2008. Optimization of Top Roller Diameter of Ring Machine to Enhance Yarn Evenness by Using Artificial Intelligence. *Indian Journal of Fibre & Textile Research* 33(4), 365-370.
13. Malik, S, Mengal, N, Saleemi, S,Abbasi, S. 2013. Blended Yarn Analysis: Part II—Influence of Twist Multiplier and Back Roller Cot Hardness on Mass Variation, Hairiness, and Physical Properties of 15 Tex Pes/Co-Blended Ring-Spun Yarn. *Journal of Natural Fibers* 10(3), 271-81.
14. Veit, D. 2001. Adjustment of False Twist Texturing Machines Using Evolution Strategy and Neural Networks, Ph.D. Dissertation, Rheinisch-WesTechnical University of Aachen, Germany.
15. Mac, T. 2007. Methodology for determining fiber blend and yarn properties based on the individual components, Ph.D. Dissertation, Rheinisch-Westfälische Technische Hochschule Aachen, Germany.
16. Farooq, A,Cherif, C. 2008. Use of Artificial Neural Networks for Determining the Leveling Action Point at the Auto-Leveling Draw Frame. *Textile Research Journal* 78(6), 502-09.
17. Murrells, C M, Tao, X M, Xu, B G,Cheng, K P S. 2009. An Artificial Neural Network Model for the Prediction of Spirality of Fully Relaxed Single Jersey Fabrics. *Textile Research Journal* 79(3), 227-34.
18. Dutta, M, Chatterjee, A,Rakshit, A. 2006. Intelligent Phase Correction in Automatic Digital Ac Bridges by Resilient Backpropagation Neural Network. *Measurement* 39(10), 884-91.
19. Saini, L M. 2008. Peak Load Forecasting Using Bayesian Regularization, Resilient and Adaptive Backpropagation Learning Based Artificial Neural Networks. *Electric Power Systems Research* 78(7), 1302-10.
20. Chen, C-S,Su, S-L. 2010. *Resilient Back-Propagation Neural Network for Approximation 2-D Gdop, Proceedings of the International Technical Multi Conference of Engineers and Computer Scientists, Chengdu, China.* Citeseer, 900904.
21. Naoum, R S, Abid, N A,Al-Sultani, Z N. 2012. An Enhanced Resilient Backpropagation Artificial Neural Network for Intrusion Detection System. *International Journal of Computer Science and Network Security (IJCSNS)* 12(3), 11.
22. Pani, A K,Mohanta, H K. 2015. Online Monitoring and Control of Particle Size in the Grinding Process Using Least Square Support Vector Regression and Resilient Back Propagation Neural Network. *ISA transactions* 56, 206-21.
23. Gonzalez Viejo, C, Torrico, D D, Dunshea, F R,Fuentes, S. 2019. Development of Artificial Neural Network Models to Assess Beer Acceptability Based on Sensory Properties Using a Robotic Pourer: A Comparative Model Approach to Achieve an Artificial Intelligence System. *Beverages* 5(2), 33.





# Effect of Yarn Physical Properties on Fiber Migration and Packing Density of Cotton/Acrylic Blended Yarns

H. İbrahim Çelik  0000-0002-1145-6471

Gülistan Canlı  0009-0006-5320-659X

Gaziantep University, Faculty of Engineering, Textile Engineering Department, Gaziantep, Türkiye

**Corresponding Author:** H.İbrahim Çelik, hcelik@gantep.edu.tr

## ABSTRACT

In the scope of the study, the effect of fiber blending ratio, yarn count and twist factor on fiber migration, packing density and diameter of the cotton/acrylic blended yarns were investigated. The yarn samples with 75/25%, 50/50%, 40/60% cotton/acrylic blending ratios were produced with three different yarn numbers; 20/1 Ne, 24/1 Ne, 30/1 Ne and three twist factors; 3.5 ae, 4 ae, 4.5 ae. Thus, totally 27 yarn samples were obtained. The yarn cross-sectional samples were sliced with microtome. The image frames of yarn cross-sections were acquired via digital microscope. The yarn packing density was calculated by using image processing algorithm and the fiber migration was determined via cross-section images. The results were evaluated statistically. When the results of the study were examined, it was seen that the yarn blend ratio, twist factor and yarn count have a significant effect on the yarn packing density and diameter properties. According to fiber migration analyze results, it was revealed that the acrylic fiber distributed toward the yarn surface with (+) sign index values and cotton fiber distributed to core of the yarn with (-) sign index values for all yarn counts and twist factors of 40/60 and 50/50 cotton/acrylic blend ratios.

## 1. INTRODUCTION

The blended yarns are produced by combining two or more different fiber components in order to benefit their advantages and strength in the same final product. Since synthetic and natural fibers have different mechanical, chemical and comfort characteristics, they are blended within the same yarn structure according to the required yarn properties. The distribution and uniformity of the fibers in the blended yarns cross-sections are important for determining the structural, functional, mechanical and visual properties of the products. The outer fibers tend to show more tension as they travel a longer distance during the ring yarn production. However, the fibers in the yarn center have a lower tension because they follow a straighter path. The outer fibers try to move to the inner region because they tend to have low density, while the inner fibers tend to have the opposite direction. The tendency of

the fibers to displace during yarn formation is called fiber migration. In other words, variations of the fiber placement in the yarn can be defined as fiber migration. The two most important parameters to be considered in terms of cohesion and rigidity are yarn twist and fiber migration [1-8]. The packing density that is the maximum amount of fiber in yarn cross-section is also very significant parameter because it determines the characteristics of the yarn such as feeling, dyeing, thermal conductivity and bulkiness. [5]. Properties of the fibers such as elasticity, rigidity, length, fineness and strength have considerable influence on yarn properties. The rigidity and cohesion properties of the fibers are significant in the spinning and twisting process. It has been stated that as the twist factor becomes higher, yarns will have a stiffer structure because of holding fibers more tightly. It has been mentioned that the covering ability is reduced due to the decrease in the yarn diameter [9-14].

**To cite this article:** Çelik Hİ, Canlı G. 2023. Effect of yarn physical properties on fiber migration and packing density of cotton/ acrylic blended yarns. *Tekstil ve Konfeksiyon*. 33(1), 15-26.

## ARTICLE HISTORY

Received: 27.04.2021

Accepted: 15.09.2022

## KEYWORDS

Fiber migration, yarn packing density, yarn diameter, blended yarn, image processing

The relationship between yarn structure and yarn properties has been investigated with many different previous studies. In the literature it was stated that the yarn hairiness has major effect on packing density of a yarn. The increase in hairiness leads to the increase in inter-fiber distance. As the hairiness increases, yarn diameter also increases which decreases the packing density of yarn [15, 16]. If the number of twists on the yarn structure is high, it ensures that the fibers are held firmly. Since the pores in fibrous assemblies determines displacement of a fiber-air interface with a fiber-liquid interface in a capillary system, the liquid transfer through the fiber assemblies is restricted with high twist level due to less pores between fibers. So, high twisted yarns are often preferred where good water resistance and less is desired. The twist factor has important effect on yarn diameter and softness. So, it can be stated that the twist factor affects the structural and appearance properties of the yarn. Wearing properties (abrasion and pilling) are improved with the increase in the twist factor. Raising the level of twist helps to endure abrasion since the fibers cannot be easily pulled out of the yarn [15-20]. The fiber intensity incorporated into the yarn structure determines the yarn structural integrity. The higher fiber intensity leads to higher fiber cohesion and increased yarn strength [18].

Most of the previous studies about the effect of yarn physical properties on structural properties have focused on yarn samples with single fiber type [21-30]. Especially, the fiber migration characteristics have been analyzed mostly for single fiber types. Furthermore, the distribution of cotton and acrylic fibers in yarn cross-section have not been investigated yet. Since each fiber component demonstrate different behavior during their individual movements in spinning process, the distribution of the fiber component in yarn cross-section and fiber clustering characteristics

changes according to the fiber type. So, this study was conducted to analyze the fiber distribution attribute for different cotton/acrylic blend ratios. The effects of yarn twist factor and linear density on fiber distribution characteristics were also investigated. Thus, the relationship between yarn physical properties (fiber blending ratio, yarn count and twist factor) and fiber distribution attributes (fiber migration, yarn packing density and yarn diameter) was revealed.

## 2. MATERIAL AND METHOD

### 2.1 Material

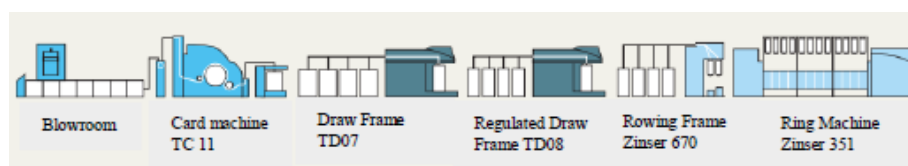
For the purpose of the study, ring spun yarns were produced with 3 different cotton/acrylic blend ratios and 3 different twist factors of each yarn count. The blend ratios were determined as 75/25%, 50/50%, 40/60% cotton/acrylic. Sample yarns were blended as fibers in the blowroom line. The twist factors were determined as  $\alpha_c=3.5, 4, 4.5$  and the yarn counts were chosen as Ne 20/1, 24/1, 30/1. Thus, totally 27 yarn samples were produced by using conventional ring spinning machine (Zinser 351). The fiber properties used in yarn production are submitted in Table 1. The physical properties of yarn samples are given in Table 2.

All yarn samples were tested with Uster Tester 5-S800. The test device adjustment was determined as speed ( $v$ ) = 5000 mm/min, measurement length ( $L_h$ ) = 500mm, pre-tension ( $F_v$ ) = 12.3 cN/tex. The tests were performed on sample coils. For each yarn property, 10 measurement were taken from each sample.

In the scope of the study, production was performed on the machine park shown in Figure 1. Yarns were produced via blowroom blend. The brand of blowroom, card machine, draw frame and regulated draw machine is Trützschler. The roving frame and ring machine brand is Zinser.

**Table 1.** Fiber properties

Fiber Properties	Cotton (American)	Acrylic (Dralon)
Fiber Fineness (dtex)	2.05	1.3 ± 0.2
Fiber Length (mm)	28.72	37
Strength	30.6 g/tex	26 cN/tex
Breaking Elongation (%)	5.10	23 ± 5 %
U.I.	81.8	-
SFI	8.4	2.4
CG	30-1	898
Reflectance	76.6	Bright
Moisture (%)	6.6	-



**Figure 1.** Ring spinning production line

Table 2. Yarn physical properties

	Blend Ratio % (Cotton/Acrylic)	Ne	Twist Factor, $\alpha_e$	U%	CVm %	Thin -50%	Thick +50%	Neps +200%	H.	Strng. (cN/tex)	Elong. (%)
1	40/60	30/1	3.5 $\alpha_e$	11.99	15.53	16.30	268.80	580.00	8.86	13.18	8.80
2	40/60	30/1	4.0 $\alpha_e$	12.13	15.59	11.30	303.80	665.00	7.86	12.59	7.31
3	40/60	30/1	4.5 $\alpha_e$	11.96	15.33	10.00	245.00	617.50	7.02	13.86	7.74
4	40/60	24/1	3.5 $\alpha_e$	10.99	14.08	1.30	176.30	246.30	9.19	13.69	8.62
5	40/60	24/1	4.0 $\alpha_e$	10.50	13.45	1.30	120.00	227.50	8.36	13.70	8.62
6	40/60	24/1	4.5 $\alpha_e$	10.91	13.95	1.30	121.30	232.50	10.62	12.38	8.98
7	40/60	20/1	3.5 $\alpha_e$	9.86	12.57	0.00	58.80	168.80	9.58	14.62	9.31
8	40/60	20/1	4.0 $\alpha_e$	9.72	12.47	0.00	78.80	206.30	8.48	14.50	9.00
9	40/60	20/1	4.5 $\alpha_e$	9.92	12.67	2.50	91.30	211.30	10.74	13.10	9.70
10	50/50	30/1	3.5 $\alpha_e$	11.20	14.35	2.50	168.80	372.50	8.29	5.77	13.32
11	50/50	30/1	4.0 $\alpha_e$	11.07	14.12	2.50	146.30	385.00	7.19	13.45	6.85
12	50/50	30/1	4.5 $\alpha_e$	12.01	15.40	8.80	278.80	518.80	6.66	13.69	7.29
13	50/50	24/1	3.5 $\alpha_e$	10.14	12.92	1.30	88.80	202.50	7.30	13.90	7.55
14	50/50	24/1	4.0 $\alpha_e$	9.90	12.67	0.00	95.00	142.50	8.29	13.39	7.47
15	50/50	24/1	4.5 $\alpha_e$	10.05	12.82	0.00	100.00	148.80	10.35	13.16	7.62
16	50/50	20/1	3.5 $\alpha_e$	9.40	12.00	0.00	38.80	135.00	9.64	13.63	7.70
17	50/50	20/1	4.0 $\alpha_e$	9.29	11.83	0.00	47.50	132.50	8.14	14.88	8.17
18	50/50	20/1	4.5 $\alpha_e$	9.14	11.65	0.00	46.30	168.80	7.74	15.84	8.95
19	75/25	30/1	3.5 $\alpha_e$	13.12	17.03	12.50	475.00	738.80	8.95	9.99	5.68
20	75/25	30/1	4.0 $\alpha_e$	13.52	17.41	11.30	470.00	792.50	8.13	13.30	6.50
21	75/25	30/1	4.5 $\alpha_e$	13.42	17.31	23.80	515.00	833.80	7.18	14.03	6.28
22	75/25	24/1	3.5 $\alpha_e$	12.21	15.64	2.50	258.80	283.80	9.19	12.35	5.93
23	75/25	24/1	4.0 $\alpha_e$	11.74	15.15	1.30	260.00	262.50	8.91	13.40	6.27
24	75/25	24/1	4.5 $\alpha_e$	12.05	15.48	2.50	271.30	246.30	7.90	14.97	6.58
25	75/25	20/1	3.5 $\alpha_e$	11.61	14.83	0.00	157.50	165.00	10.56	11.58	6.10
26	75/25	20/1	4.0 $\alpha_e$	10.65	13.63	0.00	96.30	142.50	9.16	14.66	7.30
27	75/25	20/1	4.5 $\alpha_e$	11.22	14.39	0.00	160.00	203.80	7.83	15.60	7.64

## 2.2 Method

### 2.2.1. Fiber Migration

The distribution of fibers in the yarn cross-section has significant effect on yarn physical and performance properties. In order to determine the visual, mechanical and structural properties of the blended yarns, the fiber distribution and the fiber blend irregularity in the cross-section are evaluated as vital parameters. Mathematical models were proposed to analyze the radial pattern in packing density [31] and fiber distribution irregularity [27]. Most common method used for the fiber distribution analysis for blended yarns is Hamilton Fiber Migration Index [27]. *Hamilton Migration Method (HMM)* analyzes the fiber distribution and orientation in yarn cross-section and explains it as an index. This index is predicated on the specific first moments of the fibers around the center of the yarn cross-section. The migration index is attributed to specific first moments of a constituent about the center of yarn cross-section and relates the moment ( $FMa$ ) corresponding to the actual distribution of moments that are three hypothetical distributions; uniform distribution

( $FM\mu$ ), maximum inward migration ( $FMI$ ) and maximum outward migration ( $FM O$ ) respectively. Therefore, it can be said that the fiber migration index is an explanation of whether the migration is outward or inward.

In accordance with HMM, first of all, the digital image of yarn cross-section is divided into 5 equal parts as shown in Figure 2. The different fibers in the mixture are identified by a separate letter. In this study, “a” was used for acrylic and “c” was used for cotton [8].

$a_i$  : Acrylic fibers quantity

$c_i$  : Cotton fibers quantity

$i$  : Sectional ring number

For all rings, the quantity of the fibers in the mixture are counted separately [8].

Because the densities of the acrylic and cotton fibers are different, the fiber cross-section areas are not the same with the same linear densities [8]. So, the ratio of fiber numbers for each layer is converted into ratio of the fiber volume by means of Equation (1):

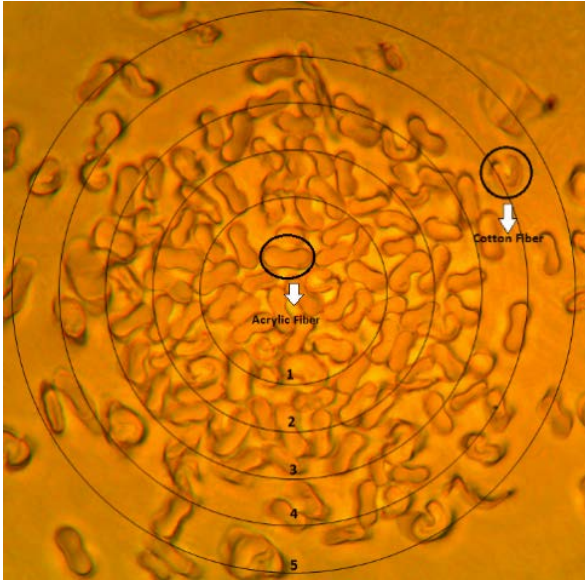


Figure 2. Dividing the yarn cross-section into 5 equal areas

$$C = \frac{VA}{VC} = \frac{TA \cdot \rho_C}{TC \cdot \rho_A} \quad (1)$$

Where;

$V_A$  = the volume of acrylic fibers,

$V_C$  = the volume of cotton fibers,

$T_A$  = the linear density of the acrylic fiber (dtex)

$T_C$  = the linear density of the cotton fiber (dtex)

$\rho_A$  = the density of the acrylic fiber ( $g/cm^3$ ),

$\rho_C$  = the density of the cotton fiber ( $g/cm^3$ ),

$C$  = ratio between the volume of the acrylic fibers and cotton fibers.

The relative volume of the acrylic fibers,  $a'_i$ , is calculated by multiplying the number of acrylic fiber ( $a_i$ ) with coefficient C. Similarly, the relative volume of cotton fibers,  $c'_i$ , is determined by multiplying the number of cotton fibers ( $c_i$ ) with coefficient C. The relative volume of fibers at each layer,  $t'_i$ , is the sum of  $a'_i$  and  $c'_i$ .

The actual moment ( $FM_a$ ) and uniform moment ( $FM_u$ ) of acrylic fiber distribution in the yarn cross section is calculated with Equation (2) and Equation (3) respectively.

$$FM_a = (-2a'_1) + (-1a'_2) + (0a'_3) + (1a'_4) + (2a'_5) \quad (2)$$

$$FM_u = \frac{A}{T[2(t'_5 - t'_1) + (t'_4 - t'_2)]} \quad (3)$$

$$A = \sum a'_i \quad T = \sum t'_i$$

Where,

If  $FM_a < FM_u$ , the acrylic fibers are prior to transfer inward.

Then the fiber migration index ( $M_{in}$ ) is calculated with following Equation (4).

$$M_{in} = \frac{FM_a - FM_u}{FM_u - FM_i} \times 100\% \quad (4)$$

If  $FM_a > FM_u$ , the acrylic fibers are prior to transfer outward. The fiber migration index ( $M_{out}$ ) is calculated with following Equation (5).

$$M_{out} = \frac{FM_a - FM_u}{FM_o - FM_u} \times 100\% \quad (5)$$

Where;

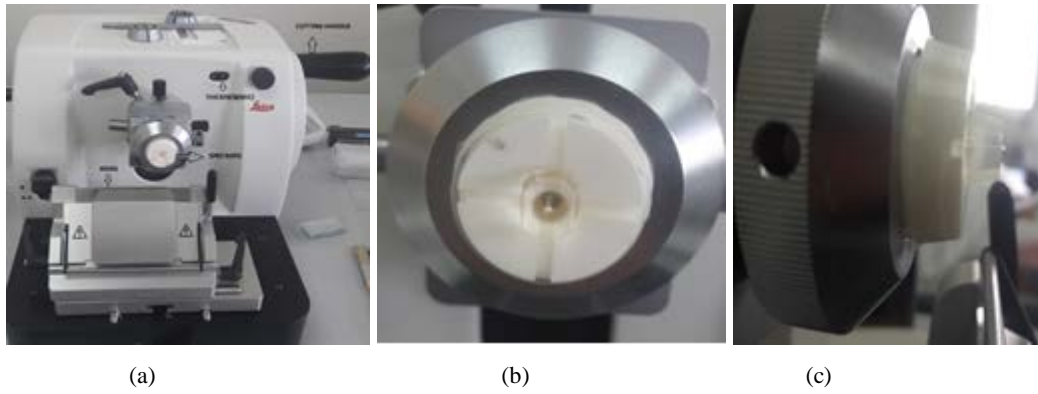
$FM_o$  is the maximum possible outward migration of the component and  $FM_i$  is the maximum possible inward migration.

The fiber migration index (M) has values between -100% and +100%. When the fiber migration index (M) takes a negative sign, it indicates that the fiber component migrates to inner layer. On the other hand, the positive sign of the fiber migration index value indicates that the fiber component migrates to the outer layer [27]. When the fiber migration index value is zero, it can be said that the fibers are uniformly distributed within the yarn cross-section. In this case, uniform and balanced distribution of fiber components on the core and the surface is obtained [6].

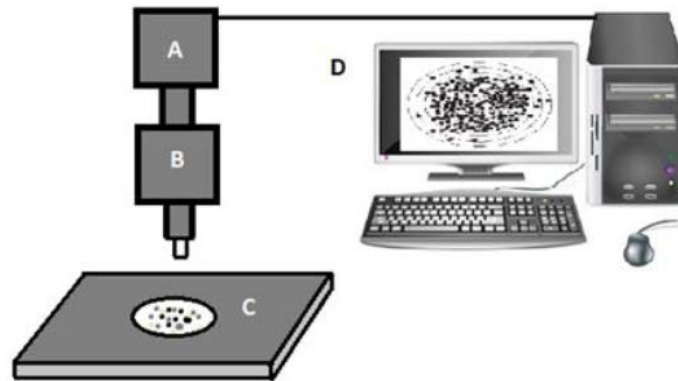
In order to analyze the fiber migration index, the cross-section views of the yarn samples were taken under microscope. For this aim, the yarn cross-section slices were obtained with microtome device (Figure 3). Each yarn sample was inserted through a special mold and fixed by using solidification resin. The yarn molds were placed into a mold holder to fix them on the microtome device. For each sample, 10 slices were taken via microtome with an optimum section thickness value of  $16\mu m$ . An image processing system that consists of digital microscope camera, computer and image processing software was constructed as given in Figure 4. After the slices were taken at the specified thickness, they were analyzed under a microscope and yarn cross-section image frames were acquired. The migration rings (Figure 2) were inserted precisely on the yarn cross-section image frame by using MATLAB Image processing toolbox and the fibers were counted manually in each ring.

## 2.2.2. Yarn Diameter

In this study, yarn diameter was measured by using Uster Tester 5-S800. The Uster Tester 5 is a modular laboratory system, which measures the yarn diameter, density and roundness with optical sensor. The system also determines yarn evenness based on 0.3 mm and 8 mm measuring zone. Short-term diameter variations were measured with 0.3 mm zones. The Uster Tester 5 uses two parallel light beams creating double illumination on the yarn to measure these parameters optically in a two-dimensional environment at a high degree of sensitivity and precision [32].



**Figure 3.** Microtome and yarn sample mold views; (a) Microtome (b) yarn sample mold front view (c) yarn sample mold side view

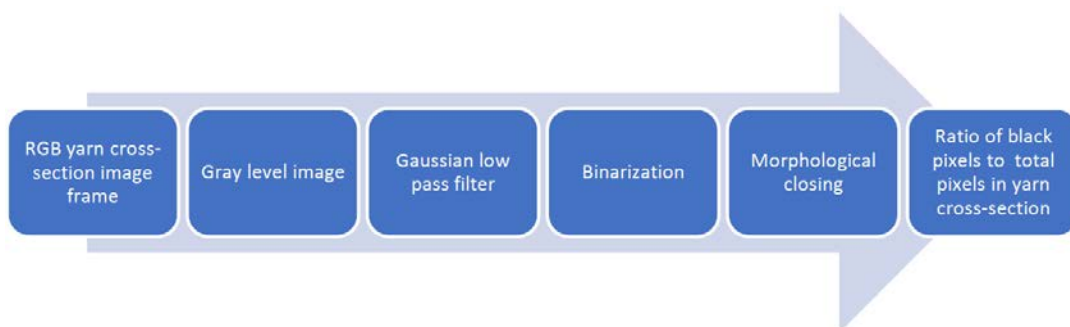


**Figure 4.** Schematic diagram of the image-processing system (A) Camera (Leica DM1000), (B) Optical microscope, (C) Yarn cross-section sample, (D) Computer

### 2.2.3. Yarn Packing Density

Packing density is accepted as an important feature for yarn structure because it has a significant effect on many properties such as yarn feel, thermal conductivity, bulkiness, dyeability etc. Besides this, it has been seen that the amount of maximum yarn that can be wound on a package is also affected [15]. Packing density was calculated by the ratio of total area of fibres in a given zone to the total area of zone in the yarn cross-section. The yarn packing density can be determined by using three different methods; direct method, secant method and tracer fiber method. In this study, direct method was used.

The yarn packing density was determined by using image processing method that has also been proposed by Kılıç M. et al. [25]. For this aim, the cross-section image frames of the yarn samples acquired by using the system in Figure 4 were also used for yarn packing density analysis. Cross-sectional images were processed with the algorithm that is prepared in MATLAB environment. The flow chart of the developed image processing algorithm was given in Figure 5. In yarn cross-section view, the space between fibers was detected in accordance with the light intensity differences between fibers and spaces.



**Figure 5.** Yarn packing density algorithm

The size adjustments were made on the yarn cross-section image frames. The image frame in RGB (Figure 6.a) form was converted to gray level. The noise removing operation was achieved by using Gaussian filter. The Gaussian filter was used for image smoothing as low-pass filter. Then, the image frame was converted to binary form (Figure 6.b) via Otsu's thresholding technique. In order to determine the yarn packing density exactly, morphological closing was applied to fill in the spaces in fiber lines (Figure 6.c). Closing is the name given to the morphological operation of dilation followed by erosion with the same structuring element. The yarn total cross-section area is calculated by selecting the maximum axis of the binary image size as the diameter of the yarn (Figure 6.c). Finally, the ratio of total black pixels to total pixels in yarn cross-section area was calculated as yarn packing density.

### 3. RESULT AND DISCUSSION

#### 3.1. Fiber Migration Results

In the yarn samples consist of two different fiber mixture, the migration index takes the same value for each fiber component but in the opposite sign. Therefore, the sum of the migration index of the two fibers is equal to zero. In case of yarns consisting of more than two fibers, calculating the migration index is not as simple as mentioned, but it is calculated in a more complex way [8]. As the number of fiber components increases, since the number of equations will increase, more difficult and complex calculation must be made for each fiber type separately. In accordance with HMM calculation, the migration index of cotton and acrylic fibers were given in Table 3. For each yarn sample, 10 migration index calculation were performed and average migration index value was presented.

The migration index and direction in term of (-) and (+) signs of both acrylic and cotton fibers was presented according to yarn count and twist factor groups in Figure 7(a) and Figure 7(b) respectively. Migration values of acrylic and cotton fiber components are given separately for each sample. The (-) sign in the values (Table 3) indicates that the fiber is oriented towards the yarn core. Migration values with (+) sign (Table 3) indicate that the fiber is oriented towards the yarn surface. When the results were analyzed according to the blend ratio, it can be clearly seen that the acrylic fiber distributed toward the yarn surface with (+) sign index values and cotton fiber distributed to core of the yarn with (-) sign index values for all yarn counts and twist factors of 40/60 and 50/50 cotton/acrylic blend ratios. According to the theoretical and experimental findings, it was proved that the fibers with higher Young's modulus move toward the inner side of the yarn structure. So, the mass percentage of the fibers with lower Young's modulus increases on the external side of the yarn structure [1,5,27]. Since the acrylic fiber have lower Young's modulus than that of cotton, the acrylic fibers located to the

surface of the yarn and the cotton placed on the core. This result coincidence with the previous studies submitted by Ryklin D. and Silich T. [1] and Najar S.S. et al. [5]. This situation is different for 75/25 cotton/acrylic blended yarns. The acrylic fiber placed to the core of the yarn and the cotton fiber placed to the outer side of the yarn cross-section for 75/25 cotton/acrylic yarn samples for all counts and twist factors. This result was attributed to the fact that the cotton fiber occupies the larger part of the yarn cross-section and also cotton fiber component have higher length than acrylic fiber (Table 1). When the general trend of acrylic migration index with respect to the cotton blend ratio is investigated, it can be said that as the acrylic ratio increases, the cotton fibers migrate to the core and the acrylic fiber migrates to the outward of the yarn cross section. According to the yarn linear density, as the yarn becomes thicker, the migration indexes of components increase in all mixtures. This obtained result coincides with experimental and theoretical findings of the study achieved by Zheng, S.M. et al. [27]. It was proved that the migration index values are larger with courser yarns [27].

Table 3. Fiber migration index (M) values (%)

Cotton/Acrylic Blend Ratio (%)	Twist Factor (ae)	Yarn Count (Ne)	M (Acrylic)	M (Cotton)		
40/60	3.5	30/1	7	-7		
		24/1	9	-9		
		20/1	10	-10		
	4	4	30/1	8	-8	
			24/1	10	-10	
			20/1	8	-8	
		4.5	4.5	30/1	10	-10
				24/1	11	-11
				20/1	12	-12
	50/50	3.5	30/1	4	-4	
			24/1	6	-6	
			20/1	7	-7	
4		4	30/1	6	-6	
			24/1	7	-7	
			20/1	9	-9	
		4.5	4.5	30/1	7	-7
				24/1	8	-8
				20/1	9	-9
75/25		3.5	30/1	-10	10	
			24/1	-11	11	
			20/1	-12	12	
	4	4	30/1	-11	11	
			24/1	-12	12	
			20/1	-14	14	
		4.5	4.5	30/1	-12	12
				24/1	-13	13
				20/1	-14	14

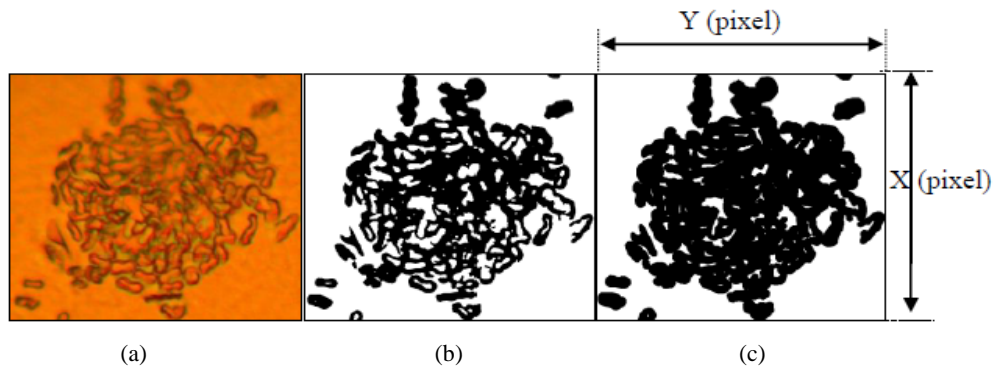


Figure 6. Packing density MATLAB views of yarn cross-sections, (a) Microscope view, (b) Binary view, (c) Closing morphological view

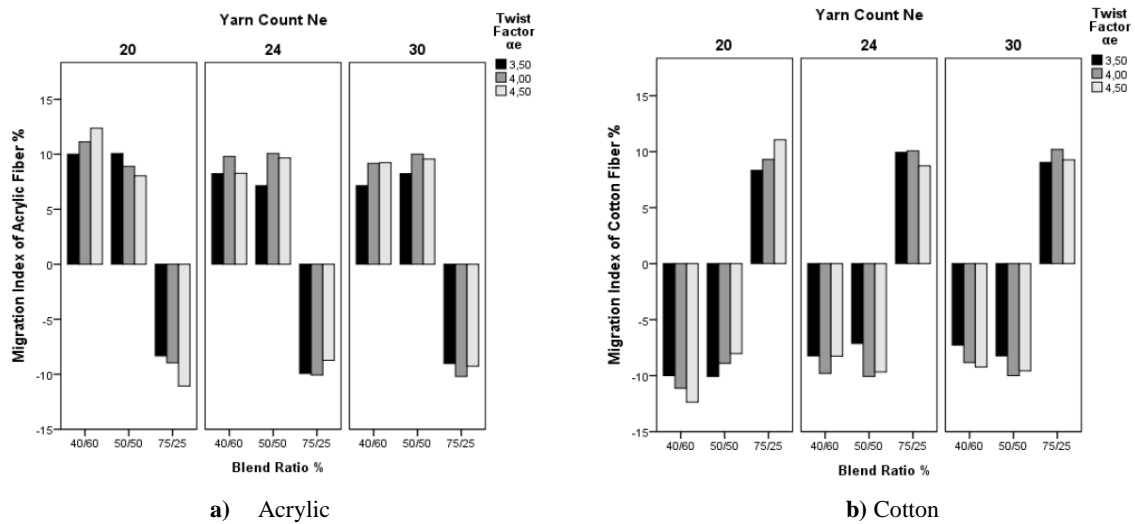


Figure 7. Fiber Migration Index (%) values representation

Since the migration index values of the both fiber components differ only for their signs, ANOVA is made for only one component in order to determine the significance of the independent components; yarn count, twist factor and blend ratio. In this study, univariate analysis of variance test was used for ANOVA. According to ANOVA results in Table 4, among three yarn physical properties, only the fiber blend ratio has statistically significant (Sig = 0.000) effect at 95% confidence interval on fiber migration values.

Tukey multiple comparison test was applied to compare the acrylic migration values of the blend ratios (Table 5).

According to the results of Tukey analysis, it is seen that there is a significant difference between the values 75/25 blend ratio and other two blend ratios of 40/60 and 50/50. However, there is no difference between the acrylic migration values of the yarn samples with 40/60 and 50/50 blend ratios. The lowest acrylic migration value was obtained with 75/25 blend ratio, while the highest acrylic migration value was obtained with 50/50 blend ratio. As observed from the subsets, the acrylic fiber positioned to the core of the yarn cross-section with 75/25 cotton/acrylic blend ratio and they are placed to the outer surface of the yarn structure with 50/50 and 40/60 cotton/acrylic blend ratios.

Table 4. Acrylic fibers migration ANOVA result

Tests of Between-Subjects Effects							
Acrylic Migration							
Dependent Variable:	Source	Type III Sum of Squares	df	Mean Square	F	Sig.	Partial Eta Squared
	Blend Ratio	63566.430	2	31783.215	862.894	.000	.688
	Twist Factor	71.207	2	35.604	.967	.381	.002
	Yarn Count	125.267	2	62.633	1.700	.183	.004
	Error	28840.467	783	36.833			
	Total	100822.000	810				
	Corrected Total	93459.822	809				

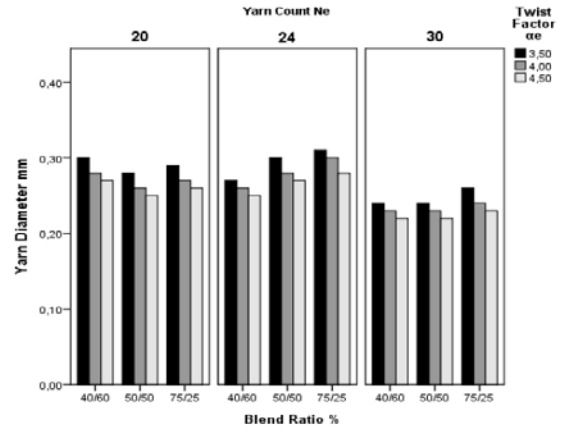
a. R Squared = .691 (Adjusted R Squared = .681)

**Table 5.** Tukey multiple comparison test of blend ratio on acrylic fiber migration

Blend Ratio %, (Cotton/Acrylic)	N	Subset	
		1	2
75/25	270	-9.51	
50/50	270		9.07
40/60	270		9.48

### 3.2. Yarn Diameter Results

The fibers are considered as the main factor in the yarn structure. More efficient estimation of the fabric properties is achieved by knowing the volume of fibers in the yarn formation. One of the parameters used in the analysis of fabric structural properties such as width, cover and comfort is the yarn diameter. The cover factor of the fabric can cause a large change even with a small change in the diameter of the yarns. As the twist factor increases, the yarn diameter decreases. Similarly, when the yarn count in Ne increases, that means the finer yarns, the yarn diameter decreases [12]. The yarn diameter measurements that were achieved with Uster Tester 5 are given in Table 6.

**Figure 8.** Yarn diameter values**Table 6.** Yarn diameter values

	Blend Ratio % (Cotton/Acrylic)	Yarn Count, Ne	Twist Factor, $\alpha_c$	Diameter (mm)
1	40/60	30/1	3.5	0.24
2	40/60	30/1	4	0.23
3	40/60	30/1	4.5	0.22
4	40/60	24/1	3.5	0.27
5	40/60	24/1	4	0.26
6	40/60	24/1	4.5	0.25
7	40/60	20/1	3.5	0.30
8	40/60	20/1	4	0.28
9	40/60	20/1	4.5	0.27
10	50/50	30/1	3.5	0.24
11	50/50	30/1	4	0.23
12	50/50	30/1	4.5	0.22
13	50/50	24/1	3.5	0.28
14	50/50	24/1	4	0.26
15	50/50	24/1	4.5	0.25
16	50/50	20/1	3.5	0.30
17	50/50	20/1	4	0.28
18	50/50	20/1	4.5	0.27
19	75/25	30/1	3.5	0.26
20	75/25	30/1	4	0.24
21	75/25	30/1	4.5	0.23
22	75/25	24/1	3.5	0.29
23	75/25	24/1	4	0.27
24	75/25	24/1	4.5	0.26
25	75/25	20/1	3.5	0.31
26	75/25	20/1	4	0.30
27	75/25	20/1	4.5	0.28



The diameters of the samples were compared according to the blend ratio, yarn count and twist factor in Figure 8. When the yarn sample diameters were analyzed according to yarn count, it is seen that with 40/60 cotton/acrylic blend ratio, yarn diameter value increases as the yarn gets courser. However, similar consistency was not obtained with other blend ratios; 50/50 and 75/25 cotton/acrylic. As observed from Figure 8, the yarn diameter increases from Ne 20/1 to Ne 24/1 and it decreases from Ne 24/1 to Ne 30/1. When all the yarn samples are investigated, it can be observed that the yarn diameter decreases as the twist factor increases in the same blend ratio. For the yarn samples with 24 Ne count, the yarn diameter increases with the increase of cotton fiber content for all twist factor values.

According to the variance analysis of yarn diameter results (Table 7), all yarn physical parameters; yarn count (Sig = 0.000), twist factor (Sig = 0.000) and blend ratio (Sig = 0.000) have significant effect on the yarn diameter results in 95% confidence interval. When F values are examined, it is seen that the highest effect comes from yarn count (F = 185.444). Other two parameters; blend ratio and twist factor have fewer effects on the yarn diameter than yarn count.

Tukey multiple comparison tests were applied to compare the yarn diameter values of the blend ratio, twist factor and yarn count groups. According to the Tukey analysis results for blend ratio (Table 8), it is seen that there is a significant difference between 75/25 blend ratio and other blend ratio groups. However, it is seen that there is no difference between the yarn diameter values of the yarn samples with the blend ratio of 40/60 and 50/50. The lowest yarn diameter values were obtained in the blend ratio of 40/60, while the highest yarn diameter values were obtained in the blend ratio of 75/25. According to Table 8, it can be analyzed that the yarn diameter increases, as the cotton ratio of yarn content increases.

According to Tukey table given in Table 9, there is a significant difference between the yarn diameter values of the yarn samples with the twist factors;  $\alpha_e = 3.5$ ,  $\alpha_e = 4$  and  $\alpha_e = 4.5$ . The lowest yarn diameter value was obtained with  $\alpha_e = 4.5$ , and the highest yarn diameter was obtained in  $\alpha_e = 3.5$ . Also, it is seen that the yarn diameter values decrease as the twist factor increases. This finding can be explained by the fact that the twist effect has a higher radial force and thus results in a more compact and stiffer yarn structure.

**Table 7.** Yarn diameter ANOVA result

Tests of Between-Subjects Effects						
Dependent Variable:	Diameter					
Source	Type IV Sum of Squares	df	Mean Square	F	Sig.	Partial Eta Squared
Blend Ratio	.003	2	.002	17.444	.000	.392
Twist Factor	.011	2	.005	52.778	.000	.662
Yarn Count	.037	2	.019	<b>185.444</b>	<b>.000</b>	.873
Error	.005	54	.000			
Total	5.659	81				
Corrected Total	.057	80				

a. R Squared = .906 (Adjusted R Squared = .861)

**Table 8.** Tukey multiple comparison test of blend ratio on yarn diameter

Blend Ratio % (Cotton/Acrylic)	N	Subset	
		1	2
40/60	270	.2578	
50/50	270	.2589	
75/25	270		.2722

**Table 9.** Tukey multiple comparison test of twist factor on yarn diameter

Twist Factor $\alpha_e$	N	Subset		
		1	2	3
4.5	270	.2500		
4.0	270		.2611	
3.5	270			.2778

**Table 10.** Tukey multiple comparison test of yarn count on yarn diameter

Yarn Count Ne	N	Subset		
		1	2	3
30	270	.2356		
24	270		.2656	
20	270			.2878

The diameter differences between yarn count groups were analyzed according to Tukey multiple comparison test (Table 10). It was obtained that there is a significant difference between the yarn diameter values of each yarn count. It is also seen that the yarn diameter value increases as the yarn count decreases that means courser yarns. This situation is expected because of yarn structure. When the yarn count decreases (gets courser), the higher number of fibers will be inserted in unit length and so greater yarn diameter will be obtained.

### 3.3. Yarn Packing Density Results

Table 11 shows the packing density values of the yarn samples. The yarn packing density were analyzed according to blend ratio, twist factor and yarn count in Figure 9. When all yarn samples were examined, it was clearly seen that the packaging density increase with increase in the twist factor. Similar relationship between twist factor and packing density was also revealed by Taheri M. et al. [10]. It was stated that for a given yarn count, assuming the yarn cross-section is negligible, higher twist factor cause higher pressure from the surface to internal fibers, which results in a more packed cross-section and hence higher packing density [10]. According to the comparison of the yarn samples in terms of blend ratio, it can be revealed that yarn packing density generally increases as the cotton content increases. This finding can be attributed to the cross-section shape of cotton and acrylic fibers. The kidney shaped cotton fiber allows higher compression and packing in a unit area than that of dog bone shaped acrylic fiber. The study on the effect of constituent fibers on yarn packing density has also been investigated by Sinha et al. [30]. They

also found a similar result and proved that cross-section shape and other factors deciding the compatibility of blend constituents influence the degree of packing.

It was stated that the mixing of non-circular fibers with circular fibers is likely to disrupt the uniformity in the distribution of the masses and thus affect the packing of the fibers. The study [30] revealed that non circular cross section of PVA cause hindrance in close packing.

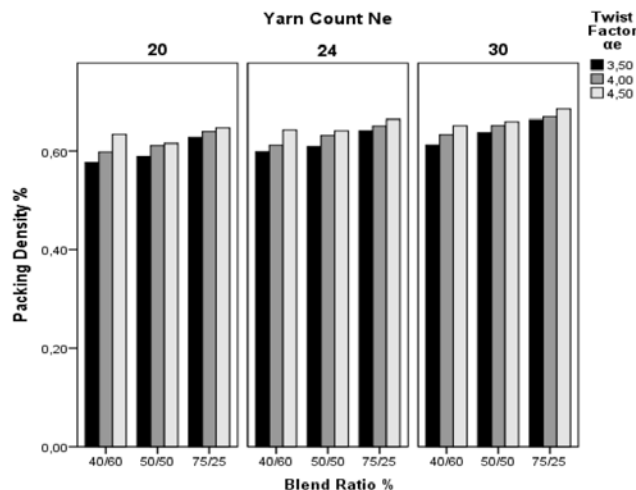


Figure 9. Packing density of yarn samples

According to the variance analysis (Table 12); all independent parameters; yarn count (Sig = 0.000), twist factor (Sig = 0.000) and blend ratio (Sig = 0.000) have significant effect on the yarn packing density values within 95% confidence interval. When F values are examined, it is seen that the maximum effect was obtained with blend ratio (F = 17.840).

Table 11. Packing density values of yarn samples according to fiber blend ratio

40/60 % Cotton/Acrylic								
	3.5 $\alpha_e$			4 $\alpha_e$			4.5 $\alpha_e$	
30/1	24/1	20/1	30/1	24/1	20/1	30/1	24/1	20/1
0.61	0.60	0.58	0.63	0.61	0.60	0.65	0.64	0.63
50/50 % Cotton/Acrylic								
	3.5 $\alpha_e$			4 $\alpha_e$			4.5 $\alpha_e$	
30/1	24/1	20/1	30/1	24/1	20/1	30/1	24/1	20/1
0.64	0.61	0.59	0.65	0.63	0.61	0.66	0.64	0.62
75/25 % Cotton/Acrylic								
	3.5 $\alpha_e$			4 $\alpha_e$			4.5 $\alpha_e$	
30/1	24/1	20/1	30/1	24/1	20/1	30/1	24/1	20/1
0.66	0.64	0.63	0.67	0.65	0.64	0.69	0.66	0.65

Table 12. Yarn packing density ANOVA result

Tests of Between-Subjects Effects							
Dependent Variable:	Packing Density						
Source	Type IV Sum of Squares	df	Mean Square	F	Sig.	Partial Eta Squared	
Blend Ratio	.195	2	.098	17.840	.000	.044	
Twist Factor	.136	2	.068	12.400	.000	.031	
Yarn Count	.176	2	.088	16.040	.000	.039	
Error	4.284	783	.005				
Total	329.189	810					
Corrected Total	4.820	809					

a. R Squared = .111 (Adjusted R Squared = .082)

According to the comparison analysis in terms of blend ratio groups (Table 13), it is seen that there is a significant difference between the packing density values of 75/25 blend ratio and other two blend ratios of 40/60 and 50/50 cotton/acrylic. There is no difference between the yarn packing density values of the yarn samples with the blend ratio of 40/60 and 50/50 cotton/acrylic. The lowest yarn packing density value was obtained in the blend ratio of 40/60 cotton/acrylic, while the highest yarn packing density value was obtained in the blend ratio of 75/25 cotton/acrylic. As proved from Table 13, higher cotton ratio leads to greater packing density in yarn cross-section.

**Table 13.** Tukey multiple comparison test of blend ratio on packing density

Blend Ratio % (Cotton/Acrylic)	N	Subset	
		1	2
40/60	270	.6173	
50/50	270	.6271	
75/25	270		.6540

**Table 14.** Tukey multiple comparison test of twist factor on packing density

Twist Factor $\alpha_e$	N	Subset		
		1	2	3
3.5	270	.6170		
4.0	270		.6328	
4.5	270			.6487

**Table 15.** Tukey multiple comparison test of yarn count on packing density

Yarn Count Ne	N	Subset		
		1	2	3
20	270	.6512		
24	270		.6321	
30	270			.6151

The packing density values were statistically compared in terms of yarn count in Table 15. According to the Tukey table (Table 15), there is a significant difference between the yarn packing density values of each yarn count. There is a direct proportion between packing density and yarn count, so it can be said that as the yarn gets finer, the yarn packing density decreases vice versa. This result is similar to the previous studies performed by [10,13,24,27,28]. According to both theoretical and experimental measurements, it was found out that the courser yarns signify that they have more fibers in their cross sections and so the total compressive load acting on the yarn leading to increased packing density [13].

#### 4. CONCLUSION

The most important challenge of the study is revealing effect of yarn physical properties such as yarn count, blend ratio and twist factor on yarn packing density, diameter and fiber migration properties for blend yarn. This study proposes a detailed analysis for yarn samples consists of two fiber components.

According to the Tukey comparison for twist factor groups (Table 14), there is a significant difference between the yarn packing density values of all twist factor groups. It can be clearly seen that there is a direct proportion between packing density and twist factor. So, yarn packing density values increases as the twist factor increases. This result was attributed to the fact that the level of transverse pressure is influenced by the level of twist [30]. According to finding by Jiang et al. [13], the fibers are distributed in a less scattered way with increased twist factor, and this makes the whole yarn structure more compact.

In 40/60 and 50/50 cotton/acrylic blend ratios, the cotton fibers placed toward the inner part of the yarn and acrylic placed toward the yarn surface. In the blend ratio of 75/25 cotton/acrylic, acrylic fibers move toward the inner part of the yarn and cotton fiber locates toward the yarn surface. It was proved that the blend ratio has significant effect on fiber migration property. It was revealed that the yarn structure can be designed according to the migration property of corresponding blend ratio. For example, the colored fiber constituent can be placed to the outer side and the gray fiber can be positioned in the core. On the other hand, the fiber with soft hand touch and higher moisture regain can be distributed to the outer surface and the stiffer and stronger fiber constituent can be located to the inner side of the yarn cross-section.

It was revealed that three of yarn independent parameters; blend ratio, twist factor and yarn count have significant effect on yarn diameter. The most prominence property among all independent parameters was determined as yarn count. As it is expected from the spinning technology, the

yarn diameter decreases with the increase in yarn count (finer yarns). It was observed that the cotton content in the yarn structure leads to higher yarn diameters for finer counts. Since the higher twist factor causes higher radial force on the yarn structure, the diameter of the yarn decreases with increased twist factors.

Direct proportion between cotton content and yarn packing density was determined. As, the cotton ratio increases, the yarn packing density value also increases. The higher twist factor leads to higher packing density. This result can be attributed to the higher radial forces caused by the higher twist factor and hence the higher compression effect on the

fibers. There is an inverse proportion between yarn count and packing density. As the yarn count increases i.e., the yarn becomes finer, packing density decreases. It was found out that the courser yarns include higher amount of fiber in their cross sections and so the higher compressive load acting on the yarn leading to increased packing density.

### Acknowledgement

This study is a project supported by Gaziantep University Scientific Research Projects Management Unit. The project number is MF.ALT.18.06.

### REFERENCES

1. Ryklin D, Silich T. 2014. Investigation of fibers migration in cotton/polypropylene blended yarn. *Materials Science* 20(3), 301-305.
2. Lin Q, Oxenham W, Yu C. 2012. Sstudy on the blend irregularity in blended yarns. *The Journal of The Textile Institute* 103(1), 28-33.
3. Xu B, Ma J. 2010. Radial distribution of fibers in compact-spun flax-cotton blended yarns. *Fibers & Textiles in Eastern Europe* 18, 24-27.
4. Basal G, Oxenham W. 2006. Comparison of properties and structures of compact and conventional spun yarns, *Textile Research Journal* 76(7), 567-575.
5. Najar SS, Armani M, Hasani H. 2003. Analysis of blend irregularities and fiber migration index of wool/acrylic blended worsted yarns by using an image-analysis technique. *The Journal of The Textile Institute* 94(3-4), 177-185.
6. Sengupta AK, Gomber SP, Singh VP. 1997. Studies on fiber migration in blended yarns. *Indian Journal of Fibre & Textile Research* 2, 103-105.
7. Chao NPC. 1963. Blending cotton and polyester fibers-effect of processing methods on fiber distribution and yarn properties, Georgia Tech University Library, 09.11.2018 [https://smartech.gatech.edu/bitstream/handle/1853/8480/chao\\_nelson\\_p\\_196312\\_ms\\_129637.pdf](https://smartech.gatech.edu/bitstream/handle/1853/8480/chao_nelson_p_196312_ms_129637.pdf)
8. Hamilton JB. 1958. The radial distribution of fibers in blended yarns, *Journal of the Textile Institute Transactions* 49(9), 411-423.
9. Křemenáková D, Krupincová G, Nováková J. 2015. Image analysis for description of structural parameters of textile, Technical University of Liberec Research Centre Textile. 2(3), 1-6. <https://www.researchgate.net/publication/260300596> 29.03.2018.
10. Taheri M, Vadood M, Johari MS. 2013. Investigating the effect of yarn count and twist factor on the packing density and wicking height of lyocell ingspun yarns. *Fibers and Polymers* 14 (9), 1548-1555.
11. Gharahaghaji AA, Zargar EN, Ghane M, Hossaini A. 2010. Cluster-spun yarn – A new concept in composite yarn spinning. *Textile Research Journal* 80(1), 19-24.
12. Mounir J, Faouzi S, Msahli S. 2007. Evaluation of real yarn diameter. *The Indian Textile Journal*. 3(12), 31-37.
13. Jiang XY, Hu L, Cheng KPS. 2005. Determining the cross-sectional packing density of rotor spun yarns. *Textile Research Journal* 75(3), 233-239.
14. Grishanov SA, Lomov SV, Harwood RJ, Cassidy T, Farrer C. 1997. The simulation of the geometry of two-component yarns. Part I: the mechanics of strand compression: simulating yarn cross-section shape. *The Journal of The Textile Institute* 88(2), 118-131.
15. Balasubramanian N. 2014. Yarn diameter, specific volume & packing density. *The Indian Textile Journal* 8(11), 1-28.
16. Hussain U, Sarwar A, Shafqat AR, Muzaffar M, Iqbal M, Zahra N, Hussain T. 2014. Effect of spinning variables on packing density of cotton yarn. *Indian Journal of Fiber & Textile Research* 39, 434-436.
17. Kilic M, Okur A. 2011. The properties of cotton-tencel and cotton-promodal blended yarns spun in different spinning systems. *Textile Research Journal* 81(2), 156–172.
18. Ishtiaque SM, Das A, Vishnoi P. 2011. Influence of process parameters on packing density of open-end and core-sheath friction spun yarns. *Indian Journal of Fiber & Textile Research* 36, 152-157.
19. Kumar A, Ishtiaque SM, Salhotra KR. 2006. Study of effect of spinning process variables on the packing density of ring, rotor and air-jet yarns using taguchi method. *AUTEX Research Journal* 6(3), 122-135.
20. Matsuo T, Matsumoto T. 2004. Structure and properties of MVS yarns in comparison with ring yarns and open-end rotor spun yarns. *Textile Research Journal* 74(9), 819-826.
21. Ghosh A, Raihan M. 2015. Effect of fiber blend ratios on yarn properties. *International Journal of Scientific Engineering and Technology* 4(4), 243-246.
22. Harwood RJ, Grishanov SA, Lomov SV, Cassidy T. 1997. Modelling of two-component yarns. Part I: the compressibility of yarns. *The Journal of The Textile Institute*, 88(4), 373-384.
23. Kuang, X., Hu, Y., Yang, J., & Yu, C. (2015). Application of finite mixture model in cotton fiber length probability distribution. *The Journal of The Textile Institute* 106(2), 146-151.
24. Zou Z, Zheng S, Cheng L, Xi B, Yao J. 2014. Effect of some variables on the fiber packing pattern in a yarn cross-section for vortex spun yarn. *Fibers & Textiles in Eastern Europe* 2(104), 40-46.
25. Kilic M, Buyukbayraktar RB, Kilic GB, Aydin S, Eski N. 2014. Comparing the packing densities of yarns spun by ring, compact and vortex spinning systems using image analysis method. *Indian Journal of Fibre & Textile Research* 39, 351-357.
26. Kumar A, Ishtiaque SM, Das A. 2012. Impact of yarn extension on packing density of ring spun yarn. *Fibers and Polymers* 13(8), 1071-1078.
27. Zheng SM, Zou ZY, Shen W, Cheng LD. 2012. A study of the fiber distribution in yarn cross section for vortex-spun yarn. *Textile Research Journal* 82(15), 1579–1586.
28. Yilmaz D, Goktepe F, Goktepe O. 2007. Packing density of compact yarns. *Textile Research Journal* 77(9), 661-667.
29. Tyagi GK, Kaushik RCD. 2000. Radial packing density and related properties of polyester DREF-3 yarns. *Indian Journal of Fiber & Textile Research* 25, 20-24.
30. Sinha SK, Kumar P, Ghosh S. 2016. A study on the packing density of structurally modified ring spun yarn. *Fibers and Polymers* 17(11), 1898-1907.
31. Neckar B, Ishtiaque SM, Svehlova L. 1988. Rotor yarn structure by cross-sectional microtomy. *Textile Research Journal* 79, 625–632 (1988).
32. Uster Tester 5 - S800 Application Report (2009). The Measurement of the yarn diameter, density and shape of yarns.

# Investigation of the Friction Coefficients and Surface Roughness Properties of Denim Fabrics after Abrasion

Gizem Kara<sup>1</sup>  0000-0001-5202-8863

Mine Akgün<sup>2</sup>  0000-0002-6415-7782

<sup>1</sup> Almaxtex Tekstil Sanayi ve Ticaret A.Ş., Bursa, Türkiye

<sup>2</sup> Bursa Uludağ University, Engineering Faculty, Department of Textile Engineering, Bursa, Türkiye

**Corresponding Author:** Mine Akgün, akgunm@uludag.edu.tr

## ABSTRACT

The abrasion behavior of denim fabrics could be affected by fabric surface properties (surface friction coefficient and roughness) depending on fabric structural parameters. This work aimed to investigate the friction coefficients and surface roughness properties of denim fabrics woven with different structural parameters after abrasion. In general, while the abrasion process reduced the fabric friction coefficients during the initial abrasion cycles, the surface's friction coefficient increased as the number of abrasion cycles increased. However, due to the increased abrasion cycles, there was a steady decline in the roughness values of the fabric surfaces. Denim fabrics were woven with a 3/1 twill weave pattern. When the effect of the fabric structural parameters on fabric friction coefficient and roughness values were evaluated, the yarn count (Nm), yarn density, and fabric cover factor showed negative correlation coefficients. In contrast, the thickness, unit weight, and bulk density of fabric showed positive correlation coefficients.

## 1. INTRODUCTION

Denim fabrics are conventionally woven with a 3/1 twill weave structure using 100% cotton yarns. While indigo-dyed cotton yarns are used in the warp yarns that make up the fabric structure, the weft yarns consist of undyed cotton yarns. As a result of denim fabrics woven with dyed warp yarns and undyed weft yarns using warp-faced twill weave structure, fabrics' front and back surfaces appear in different colors [1]. In addition, denim fabrics are woven in 2/2 twill or plain weave structures [2, 3]. Denim structures can be produced with yarns containing polyester, polyamide, and elastane to have ergonomically designed and the desired performance properties. [3, 4].

Surface roughness plays an important role in fabric handling properties. Fabric surfaces are not exactly smooth; they have geometric roughness at specific intervals according to their structural properties. Periodic variations

of the fabric surface resulted from the regular crossings of the yarns in the weave structure. Each of the yarns intersecting with each other causes geometric roughness. The large repeating units in the structure form rough textures, while the smaller ones form fine textures. [5, 6].

The friction force is the force that resists moving relatively to each other between two materials' opposing surfaces. Frictional properties of fabrics are essential for determining roughness degree, smoothness, or other tactile properties. Moreover, fabric friction property is necessary for determining fabric features such as abrasion and wear. Fabric structures with a low friction coefficient are generally smooth. These fabric structures indicate little frictional resistance to movement applied to their surface. Some studies assume that fabric's low friction coefficient is less affected by the mechanical effects resulting of low abrasion [7-11].

**To cite this article:** Kara G, Akgun M. 2023. Investigation of the friction coefficients and surface roughness properties of denim fabrics after abrasion. *Tekstil ve Konfeksiyon* 33(1), 27-36.

## ARTICLE HISTORY

Received: 17.08.2021

Accepted: 20.09.2022

## KEYWORDS

Denim fabric, friction coefficient, surface roughness, structural properties

---

Friction properties of fabrics vary according to fiber content variations, yarn properties, fabric structure, and finishing processes [12]. In polyester blends made with cotton and viscose fibers, it was found that the friction force increased as the cellulose ratio increased in the blend [9]. Due to the variation of fabric surfaces, the friction resistance of fabrics is not always linearly proportional. A study on the effect of weave structure on the friction coefficient of cotton fabric surfaces found that the highest friction coefficient values were obtained in plain fabrics, and the lowest friction coefficient values were obtained in twill fabrics. Regarding the effect of weave structure on the friction coefficient of plain, twill, and satin weaves, it was concluded that the open contact area was the essential factor in fabric's frictional characteristics. [13-15]. Structurally, the yarn crowns and fiber ends that are formed as a result of the yarn intersections on the fabric surface affect the fabric smoothness [16] and friction properties [17-20].

The balance of the fabric surface depends on the position of warp and weft yarns. In determining the surface characteristics of the fabric, yarn crimp values are significant, as well as the yarn densities and yarn counts. Yarn crimps are influenced by the yarn count, yarn density, and weave structure. If the crimp values of the warp and weft yarns are close to each other, the fabric appearance is more or less stable. When the yarn crimp values are quite different, an irregular fabric surface is formed where one of the yarn systems is dominant [5]. In the study carried out by Ukponmwan [21], it was observed that the systematic increase in yarn settlings changed the yarn crimps (surface boundaries) and thus the fabric smoothness, provided that the yarn counts were constant [18, 20]. When the yarn settlements are systematically increased in woven fabric constructions, for example, the friction resistance against movement on the fabric surface systematically increases in the case of an increase in weft yarn density. As a result, it was obtained that the friction on the weft-faced surface is greater than the friction on the warp-faced surface. This result is due to the "knuckle effect" [11] as a result of the high level of crimps in the warp yarns, although there is a reduction in the spacing between the weft yarns due to the increase in the weft density [17-20]. Although a systematic increase in fabric structures (such as the number of yarns in cm) increases frictional resistance, it makes the fabric surface smoother. This result is due to the tightening of the yarn settlements and the reduction of the peak heights of the yarns during yarn intersections. As the yarn thickness increases (yarn diameter increases), the friction resistance and surface roughness increase too. This result is due to the increase in the mechanical intersection heights of the yarn crowns [22, 23].

There are studies investigating the effects of abrasion on various mechanical performance properties of fabrics [24, 25]. In a study examining the effects of abrasion on tensile and tear strength properties of newly developed structural

denim fabrics [24], it was stated that the tensile strength properties of abraded large structural pattern denim fabrics were generally lower compared to small structural pattern and conventional denim fabrics. In addition, it was stated that the tensile and tear strength properties of all denim fabrics generally decreased as the abrasion cycles were increased [24].

In a study investigating the effects of abrasion on the strength, elasticity, and recovery properties of stretch-denim fabrics stated that the comfort related to body movement and the shape retention properties of the stretch-denim fabrics were affected by abrasion. In addition, it was stated that the fabric structure with a higher level of elastane content resulted in a more significant loss of shape-retention properties due to abrasion [25].

Due to wearing, using, washing, and cleaning, abrasion damage occurs on the fabric structures. In addition to causing a loss of performance durability, such as strength in fabric structures, abrasion also affects properties such as fabric appearance, wearing comfort, and comfort durability [25].

The extent to which abrasion affects the friction coefficients and fabric surface roughness of denim fabrics in terms of appearance and wearing comfort, especially in denim structures with a high usage lifetime in terms of durability, should be considered as a design parameter. For this purpose, it was investigated to what extent the fabric structural parameters and abrasion cycles affect the tribological properties of denim fabric structures, such as friction coefficients and fabric surface roughness.

This study aimed to investigate the effect of surface roughness and friction coefficient values of denim fabrics woven with different structural properties on abrasion behaviors. Fabrics were abraded at different abrasion cycles. The friction coefficients and surface roughness values of the fabrics after each abrasion cycle were tested. The effects of abrasion cycles on the friction coefficients and roughness values of the fabric surfaces were evaluated depending on the fabric structural parameters. From the results, the effects of fabric structural parameters on abrasion, which should be taken into consideration in determining the structural parameters suitable for fabric usage performance in denim fabric designs, were analyzed.

## 2. MATERIAL AND METHOD

### 2.1 Material

The denim fabrics used in the experimental study were woven with 100 % cotton open-end indigo dyed warp yarns and with undyed open-end weft yarns containing 97 % cotton - 3% elastane. Fabrics were woven with a 3/1 twill weave structure. The structural properties of denim fabrics are given in Table 1.

Table 1. Fabric structural properties

Fabric Code	Yarn Count [Nm]		Yarn Density [thread/cm]		Yarn Crimp [%]		Cover Factor			Fabric Thickness [mm]	Fabric Unit Weight [g/m <sup>2</sup> ]	Fabric Bulk Density [g/cm <sup>3</sup> ]
	Warp	Weft	Warp	Weft	Warp	Weft	Warp [K <sub>wa</sub> ]	Weft [K <sub>we</sub> ]	Fabric [K <sub>f</sub> ]			
F1	14	12	26	18	18	19	22.93	17.15	26.04	0.78	423.5	0.54
F2	14	17	30	20	17	30	26.46	16.01	27.34	0.73	412.1	0.56
F3	14	18	29	20	15	28	25.58	15.56	26.92	0.75	411.5	0.55
F4	14	18	31	19	20	18	27.34	14.78	27.69	0.76	388.6	0.51
F5	20	25	39	22	10	40	28.78	14.52	28.38	0.68	342.0	0.50
F6	22	33	37	22	10	40	26.03	12.64	26.92	0.55	284.0	0.52

## 2.2 Method

### Measurement of thickness and unit weight of the fabric

The thickness and unit weight of fabrics were measured according to ASTM D1777-96 (2007) [26] and ASTM D3776 (2011) [27], respectively.

### Calculation of fabric bulk density

Fabric bulk density (FBD) was calculated according to Equation (1) [28, 29]:

$$FBD \text{ (g/cm}^3\text{)} = \frac{\text{Fabric unit weight (g/cm}^2\text{)}}{\text{Fabric thickness (cm)}} \quad (1)$$

### Calculation of fabric cover factor

Warp cover factor ( $K_{wa}$ ) and weft cover factor ( $K_{we}$ ) were calculated to Equations (2) and (3) [30]:

$$K_{wa} = \frac{3,3 \times n_1}{\sqrt{Nm_1}} \quad (2)$$

$$K_{we} = \frac{3,3 \times n_2}{\sqrt{Nm_2}} \quad (3)$$

where,  $n_1$  and  $n_2$  are warp and weft yarn density (thread/cm);  $Nm_1$  and  $Nm_2$  are warp and weft yarn count in Nm (metric count; length in meters of 1 g of yarn), respectively.

Calculation of fabric cover factor ( $K_f$ ) is presented by Equation (4) [30-32]:

$$K_f = K_{wa} + K_{we} - \frac{K_{wa} \times K_{we}}{28} \quad (4)$$

where 'f' stands for fabric, 'wa' stands for warp, and 'we' stands for weft.

### Abrasion test

The abrasion tests of the fabrics were carried out under the load of 12 kPa, in the Nu-Martindale abrasion test device, by the standard of ASTM D 4966 [33], and four different abrasion cycles (2500, 5000, 10000, and 50000) were applied. Since denim fabrics were generally designed as structures with long-term use resistance and, simultaneously,

considering the properties such as the high fabric unit weight of the denim samples used in the experimental study, it was aimed to obtain a higher abrasion effect. Therefore, the fabric samples were tested under a 12 kPa abrasive load.

However, to obtain a measurement length of at least 50 mm for roughness and friction, the locations of standard abrasive wool fabric and denim fabric samples were changed in the test device. Standard abrasive wool fabric was used on the upper face (the face with 38 mm diameter) of the motion plate, while denim fabric under test was mounted on the stable plate (the face with 140 mm diameter). Surface friction and roughness values were measured after each abrasion cycle, and the same fabric samples were used in the continuing abrasion cycles.

### Friction coefficient test

The ratio of friction force (F) to normal force (N) between two surfaces is defined as the friction coefficient ( $\mu=F/N$ ). Static friction coefficient ( $\mu_s$ ) is the ratio between the maximum value of the friction force and the normal force, and kinetic (dynamic) friction coefficient ( $\mu_k$ ) is the ratio between the friction force and the normal force in motion. In general, the static friction coefficient is higher than the kinetic friction coefficient for the same material. According to the adhesion theory, when the friction behavior of two surfaces is investigated microscopically, contact is occurred on touching roughs between two surfaces when a force is applied to two surfaces that touch each other. Strong asperities must be eliminated to overcome the object's frictional force and slip from the surface. The smaller the actual contact area (the sum of the asperities), the less load required for the slip to occur, and the friction coefficient will decrease accordingly [7].

The static ( $\mu_s$ ) and kinetic ( $\mu_k$ ) friction coefficients used to evaluate the friction characteristics of the fabrics were measured according to ASTM D1894 [34] standard on a Labthink Param MXD-02 friction coefficient test device (Figure 1). Static and kinetic friction coefficients of the denim samples were measured by fabric-to-fabric (i.e., denim fabric-to-abrasive wool fabric) friction by using standard abrasive wool fabric (ASTM D 4966) [33]. The

denim fabric sample under test was mounted on the sled (mass of sled: 200 g), and the standard abrasive wool fabric was mounted on the moving plate (the test speed: 150 mm/min; the measurement length: 150 mm) of the coefficient tester. Friction measurements of fabric samples were made in warp and weft directions, three measurements were recorded in each fabric direction, and mean values were calculated.



**Figure 1.** Friction coefficient tester (Labthink Param MXD-02)

### Surface roughness test

Surface roughness values of denim samples were measured by a roughness tester (Accrettech Surfcom 130A) (Figure 2). Surface roughness values were recorded according to ISO 4287-1997 standard [35]. The measurement was performed in a steady-state without causing any further tension on the sample. Three roughness measurements were made in each direction (warp and weft) with the selected measurement parameters of 50 mm evaluation length (0.8 mm cut-off value) and 1.5 mm/s measurement speed. Three measurements were recorded in each fabric direction, and mean values were calculated.



**Figure 2.** Surface roughness tester (Surfcom 130 A)

The arithmetic average height ( $R_a$ ) parameter was measured to characterize the surface roughness properties of denim fabrics. Arithmetical average height is defined as the average absolute deviation of the roughness irregularities from the mean line in the evaluation length [36].

### Correlation coefficient analysis

The effects of fabric structural parameters (yarn count, yarn density, yarn crimp, yarn cover factor, fabric thickness, fabric unit weight, fabric bulk density, and fabric cover factor) on fabric friction coefficient and surface roughness to abrasion were investigated by correlation analysis.

The correlation coefficients (r-value) higher than 0.3 were considered related but with a weak relationship, and the correlation coefficients higher than 0.6 were considered to have moderate to strong relationship levels [37,38]. The correlation coefficient analysis results (r-value) are given in Tables 2 - 4.

### Microscopic Analysis

Optical microscopic photographs of original (non-abraded) and 50000 cycles fabric samples, taken under a microscope coupled to a digital camera, were presented (15 times magnified) to observe the fabric surface appearance after the abrasion process according to the different constructional parameters.

## 3. RESULTS AND DISCUSSION

### 3.1 Friction coefficients of fabrics

In Figures 3 and 4, the changes in the friction coefficients of denim fabrics in warp and weft directions depending on the abrasion cycles were presented. In Fig. 3, it was observed that as the number of abrasion cycles increases, the  $\mu_s$  values of surface increase in the overall fabrics except for the F1 fabric. This increase appeared to occur in an almost linear form due to abrasion in F5 and F6. When the structural properties of F5 and F6 fabrics were examined (Table 1), it was observed that they have low fabric unit weight, low fabric thickness, and low fabric bulk density values. Also, in the F5 and F6 fabrics, the weft crimp values were significantly higher than that of the other fabric structures. Unlike other fabrics, the  $\mu_s$  values of the F1 fabric, which had the highest fabric unit weight, decreased as the number of abrasion cycles increased, and it increased after 10000 abrasion cycles. When the changes in the  $\mu_k$  values of the warp direction were examined, it was found that generally, in all fabrics (except for F3 fabric), there was a decrease in the  $\mu_k$  with the increasing number of abrasion cycles, and a significant increase occurred after about 10000 abrasion cycles.

When the warp direction friction behaviors of the fabrics in Fig.3 were examined, it could be observed that the tendencies of abrasion-related changes in the  $\mu_s$  and  $\mu_k$  were different from each other. It was observed that the deformation, which occurred on the surface (such as the fiber ends pulled out of the yarn structure in the fabric surface) of the fabric after the abrasion, increased the  $\mu_s$  values (which occurs because of the resistant effect between the two surfaces during the start of the first movement) of the fabric surface, while it decreased the  $\mu_k$  values obtained after the process started. It was seen that the decrease in the  $\mu_k$  values might occur by the deformation of the twill diagonals due to the abrasion effect. And also, the fiber ends that were pulled through the yarn to the fabric surface after abrasion would decrease the  $\mu_k$ , as they filled the gaps between twill diagonals within the fabric structure.



When the weft direction friction behaviors of the fabrics in Fig.4 were examined, it was observed that the  $\mu_s$  and  $\mu_k$  values decreased as the number of abrasion cycles increased at 10000 abrasion cycles. However, they increased after almost 10000 abrasion cycles. It was found that the diagonal peaks originating from the 3/1 twill weave structure forming the denim fabrics deformed due to the abrasion, and the friction coefficients decreased in the initial abrasion cycles. However, due to the continued abrasion process, it was found that the fiber piles and deformation on the fabric surface could have caused the increased friction coefficient between the two friction surfaces.

Correlation analysis between the fabric structural properties and friction coefficients was presented in Tables 2 and 3 depending on the different abrasion cycles in warp and weft directions.

In Tables 2 and 3, it could be seen that there was a negative correlation between yarn count and fabric friction coefficient values. This result showed that as the yarn count increased (in Nm), in other words, as the yarn fineness increased, the friction coefficient values decreased. When the effects of the yarn densities on the fabric friction coefficients were examined, the correlation between them was found to be negative. This result showed that as the yarn densities increased, the friction coefficients of the denim fabrics decreased.

When the effects of yarn crimps in the fabric structure on the friction coefficient of the fabric surface were examined, it was seen that the crimp effect of the yarns created a negative correlation in the weft direction while creating a positive correlation in the warp direction. This result showed that; as the crimps on the warp yarn increased, the values of the friction coefficients in the warp direction also increased; on the other hand, as the crimps on the weft yarn

increased, the values of the friction coefficients in the weft direction decreased. This effect of the yarn crimps on the fabric friction coefficient values was because of their having a warp-dominant surface due to the 3/1 twill weave structure of the denim fabrics used in this study, and the increase in the friction coefficient in the warp direction with the rise in the amount of the crimps on the warp yarns, which were dominant on the fabric surface.

In Tables 2 and 3, it was observed that there was a negative correlation between the warp cover factor and the fabric friction coefficient in the warp direction. At the same time, there was a positive correlation between the weft cover factor and the fabric friction coefficient in the weft direction. Here, as the warp cover factor increased, the warp direction friction coefficient decreased. This result showed that as the warp direction cover factors of the warp-faced fabric surfaces (3/1 twill) increased, the friction coefficients of these surfaces would decrease. When the cover factor values of the weft yarns increased, their weft direction friction coefficient would also increase. This result was thought to be due to the fact that factors that increase the cover factor of the weft yarn system (such as increased weft density or increased thickness of the weft yarn) caused an increase in the distance between the diagonals formed by the twill structure on the warp faced fabric. Thus, the increase in the distance between the diagonals originating from the twill structure on the fabric surface also increases the friction coefficients in the weft direction. In denim structures, it was observed that the warp yarn cover factors' having higher values gave favorable results in reducing the friction coefficient in the warp direction. It could be also stated that keeping the weft yarn cover factor at low levels might be appropriate to reduce the friction coefficient in the weft direction. However, it was observed that negative correlation coefficients were obtained in both warp and weft directions between the fabric cover factor values and fabric friction coefficients.

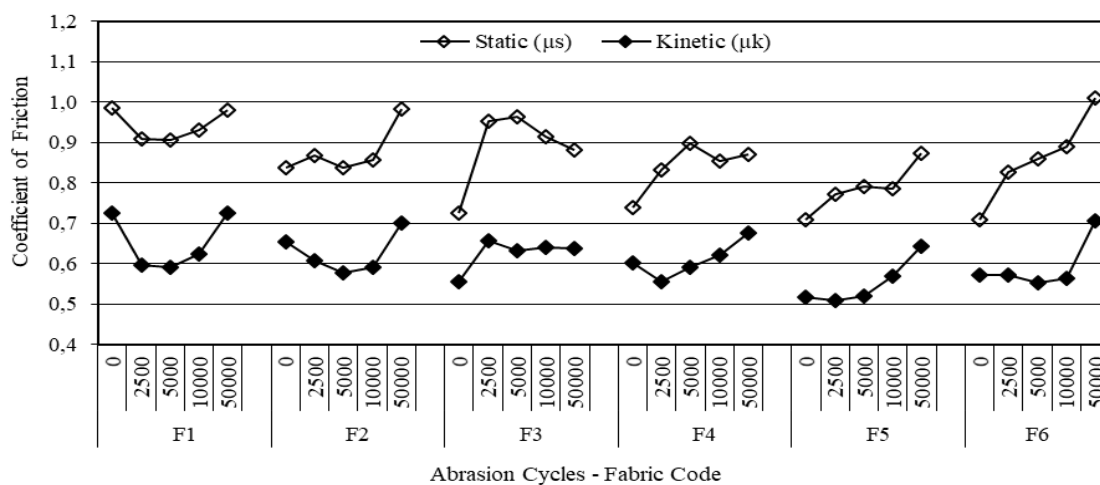


Figure 3. Change of fabric friction coefficient values in the warp direction

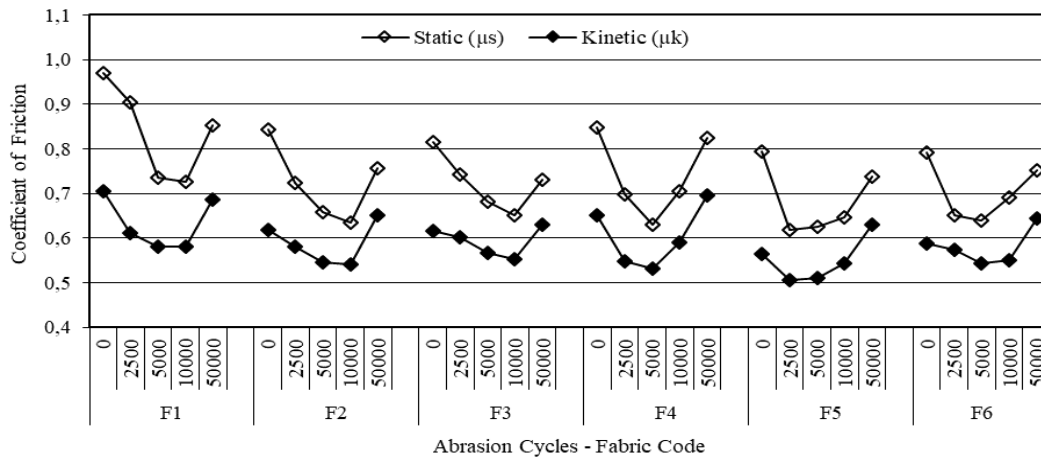


Figure 4. Change of fabric friction coefficient values in the weft direction

Table 2. Correlation coefficients between the fabric structural properties and friction coefficients in the warp direction

Coefficient of Friction	Abrasion Cycle	Warp Yarn Count	Warp Yarn Density	Warp Yarn Crimp	Warp Cover Factor	Fabric Thickness	Fabric Unit Weight	Fabric Bulk Density	Fabric Cover Factor
$\mu_s$	0	-0.53	-0.73	0.54	-0.78	0.54	0.62	0.54	-0.69
	2500	-0.65	-0.85	0.56	-0.78	0.41	0.58	0.75	-0.80
	5000	-0.75	-0.91	0.64	-0.81	0.42	0.61	0.61	-0.60
	10000	-0.77	-0.95	0.66	-0.84	0.67	0.77	0.67	-0.80
	50000	0.21	-0.13	-0.11	-0.55	-0.41	-0.20	0.41	-0.61
$\mu_k$	0	-0.57	-0.77	0.67	-0.78	0.48	0.58	0.57	-0.72
	2500	-0.58	-0.72	0.66	-0.62	0.63	0.55	0.83	-0.66
	5000	-0.79	-0.66	0.67	-0.62	0.76	0.71	0.63	-0.62
	10000	-0.75	-0.95	0.79	-0.86	0.59	0.70	0.65	-0.82
	50000	-0.05	-0.35	0.29	-0.63	-0.09	0.02	0.29	-0.64

Table 3. Correlation coefficients between the fabric structural properties and friction coefficients in the weft direction

Coefficient of Friction	Abrasion Cycle	Weft Yarn Count	Weft Yarn Density	Weft Yarn Crimp	Weft Cover Factor	Fabric Thickness	Fabric Unit Weight	Fabric Bulk Density	Fabric Cover Factor
$\mu_s$	0	-0.77	-0.87	-0.75	0.79	0.63	0.64	0.58	-0.69
	2500	-0.64	-0.75	-0.60	0.76	0.57	0.56	0.65	-0.48
	5000	-0.58	-0.66	-0.49	0.68	0.41	0.54	0.61	-0.93
	10000	-0.22	-0.61	-0.63	0.52	0.43	0.48	0.69	-0.67
	50000	-0.57	-0.81	-0.81	0.48	0.50	0.40	-0.01	-0.47
$\mu_k$	0	-0.78	-0.96	-0.90	0.72	0.67	0.67	0.39	-0.72
	2500	-0.45	-0.69	-0.70	0.60	0.30	0.47	0.67	-0.80
	5000	-0.53	-0.66	-0.53	0.56	0.37	0.53	0.68	-0.96
	10000	-0.50	-0.81	-0.87	0.31	0.45	0.40	0.63	-0.57
	50000	-0.51	-0.77	-0.83	0.35	0.46	0.36	-0.03	-0.33

In Tables 2 and 3, it was observed that there was a positive correlation between the fabric thickness and the fabric friction coefficient in the warp and weft directions. In other words, the fabric friction coefficients increased as the fabric thickness increased. Because the diagonal peak heights would also increase as the fabric thickness increase in the twill fabric structures, the difference in height between the peak and the valley points of the fabric surface increased the friction coefficient between the two surfaces. Similar to fabric thickness, fabric unit weight and fabric bulk density was found to be positively correlated with the friction coefficients in the warp and weft directions. The friction

coefficient of the fabric surfaces increased together with the increase in the fabric unit weight and fabric bulk density.

In Tables 2 and 3, it was observed that the correlation between fabric structural properties and the friction coefficients of the fabrics was remarkable up to 50000 abrasion cycles. Especially, it was observed that the fabric structural properties did not significantly affect the fabric friction coefficients in warp direction at 50000 abrasion cycles. It was seen that the correlation coefficients between the structural parameters and the friction coefficients were low in warp direction at 50000 abrasion cycles. This result

was because the warp-faced denim fabric surfaces were subjected to abrasion.

### 3.2 Surface roughness of fabrics

In Fig.5, the changes in arithmetic average roughness values ( $R_a$ ) of denim fabrics depending on the abrasion were presented. It was observed that when the abrasion cycle increased, the roughness values in the warp and weft direction of the fabrics decreased. In Fig.5, it was also shown that the roughness values in the weft direction of the fabrics were higher than the roughness values in the warp direction. This result could be due to the 3/1 twill weave structure of the denim fabrics. During the roughness measurement in the warp direction, the stylus probe of the roughness measurement device moves on the warp yarn floating since it carries out the measurement on a warp yarn dominant surface. During the measurement of roughness in the weft direction, while the stylus probe of the instrument moves in the direction of the weft, it carries out its

movements in the cross direction on each of the three floating yarn crowns of the warp yarn dominant surface. Therefore, since the measurement device moved in the weft direction and passed over each of the warp yarns one by one, it was considered that the indentation-protrusion zones between the yarns increased the roughness of the surface.

Regression equations and  $R^2$  values of the changes in surface roughness of fabric samples after abrasion cycles were given in Figure 5. In Fig. 5, when the slopes of the changes in the surface roughness values that vary depending on the abrasion were examined, it was observed that the change in the warp direction roughness values was greater than in the weft direction. This result was because of the high deformation of the abraded warp yarn surface at the fabric surface where the warp yarns dominate due to the 3/1 twill structure. Experimental results showed that surface roughness values of denim fabrics decreased as abrasion cycles increased.

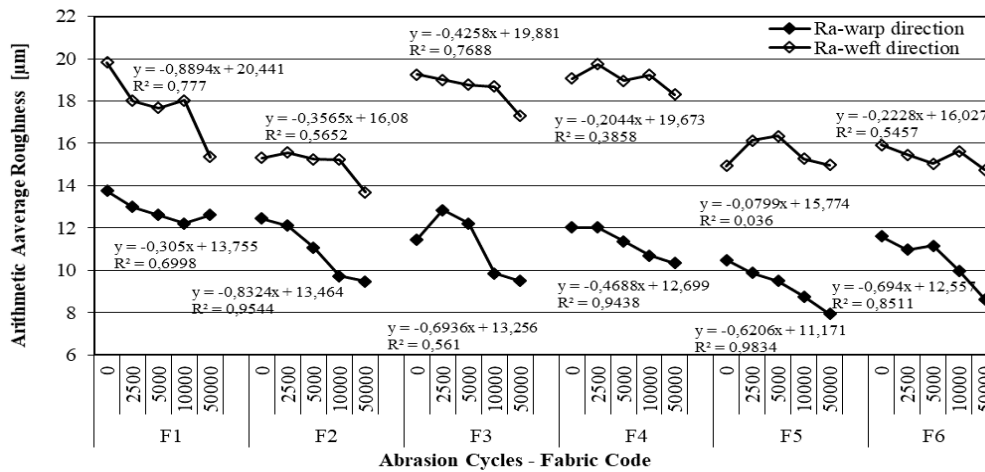


Figure 5. Change of fabric surface roughness values in warp and weft direction

Table 4. Correlation coefficients between the fabric structural properties and surface roughness

Surface Roughness	Abrasion Cycle	Yarn Count	Yarn Density	Yarn Crimp	Warp Cover Factor	Fabric Thickness	Fabric Unit Weight	Fabric Bulk Density	Fabric Cover Factor
Warp Direction	0	-0.32	-0.61	0.46	-0.81	0.34	0.30	0.65	-0.77
	2500	-0.84	-0.97	0.76	-0.78	0.66	0.78	0.72	-0.75
	5000	-0.61	-0.87	0.59	-0.89	0.44	0.55	0.57	-0.90
	10000	-0.45	-0.71	0.61	-0.83	0.42	0.41	0.49	-0.79
	50000	-0.69	-0.87	0.77	-0.82	0.66	0.68	0.43	-0.74
Weft Direction	0	-0.58	-0.72	0.73	-0.64	0.60	0.51	0.06	-0.59
	2500	-0.64	-0.55	0.69	-0.20	0.68	0.54	-0.06	-0.15
	5000	-0.62	-0.52	0.59	-0.17	0.71	0.56	-0.05	-0.11
	10000	-0.64	-0.63	0.66	-0.36	0.62	0.53	0.06	-0.34
	50000	-0.42	-0.31	0.35	-0.01	0.41	0.30	-0.09	-0.02

---

In Table 4, the correlation between the yarn properties constituting the denim fabrics and the surface roughness ( $Ra$ ) depending on different abrasion cycles was presented. It was observed that there was a negative correlation between the yarn counts and the roughness values of the fabric surface. As the yarn count was increased (in Nm), in other words, as the yarn became finer, the roughness values of the fabric surface decreased. When the correlation between yarn densities and fabric surface roughness was examined, it would be seen that there was a negative correlation between the yarn densities and the surface roughness values of the fabrics. As the yarn densities forming the fabric increased, the roughness values of the fabric surface decreased. A positive correlation was observed between the yarn crimps in the fabric structure and the roughness values of the fabrics, and the surface roughness increased as the yarn crimp increased.

The literature stated that the fabric surface roughness decreased with increasing yarn density. This result could be due to the positioning of the yarns within the fabric structure. An increase in yarn density decreased the gaps between the yarn peaks, decreasing surface roughness [39-41].

In Table 4, when the values of cover factor and the roughness values in warp and weft directions of fabrics were examined, a negative correlation was observed between them. This result indicates that when the cover factors were increased, the roughness values of the fabric surface would be reduced. Also it was seen that the correlation coefficients between cover factor and roughness values in the warp direction were higher than in the weft direction. This could be result the fabrics where the warp yarns dominate, due to the 3/1 twill structure. In general, it was observed that there was a positive correlation between the fabric thickness, fabric unit weight, fabric bulk density, and fabric surface roughness values. When the thickness, unit weight, and bulk density values of fabrics were increased, the surface roughness values of the fabrics were increased.

Digital photographs of all fabric samples (F1 – F6) were presented in Figure 6 to consider the abrasion effect on the fabric surface appearance.

#### 4. CONCLUSION

This study investigated the abrasion behaviors of denim fabrics woven with different structural parameters and the relation between surface friction coefficients and surface roughness values of fabrics depending on these parameters.

While the abrasion process reduced the friction coefficients of the fabrics during the initial abrasion cycles, the surface's friction coefficient increased as the number of abrasion cycles increased. The changes occurring in the friction coefficient due to abrasion showed different tendencies for the warp and weft directions of the fabrics. However, due to the increased number of abrasion cycles, there was a steady decline in the roughness values of the fabric surfaces.

Denim fabrics were woven with a 3/1 twill weave pattern. When the effect of the fabric structural parameters on fabric friction coefficient and roughness values were evaluated, the yarn count (Nm), yarn density, and fabric cover factor showed negative correlation coefficients. In contrast, the thickness, unit weight, and bulk density of fabric showed positive correlation coefficients.

Results showed that the highest friction coefficient and roughness values were in fabrics woven with thick yarn and low yarn density values. And also the maximum variation on the fabric surface in terms of friction coefficient and roughness due to abrasion was in these types of fabrics. However, even though the non-abraded states of the fabrics woven with fine yarn and high density values have low roughness and friction coefficients, it was determined that the variations in surface roughness and friction coefficients of these structures were high with increasing abrasion cycles.

The extent to which abrasion affects the friction coefficients and fabric surface roughness of denim fabrics in terms of appearance and wearing comfort, especially in denim structures with a high usage lifetime in terms of durability, should be considered as a design parameter.

Due to the fact that the abrasion effect on the fabric surface could be measured precisely and objectively with the friction coefficient and surface roughness measurements; it could be envisaged that the friction coefficient and surface roughness parameters might be the parameters to be considered in the stages of determining the appropriate structural parameters in the fabric design process and determining various performance properties in the production and usage process.

#### Acknowledgement

This study is a part of the MSc thesis titled "Investigation of Relations between Constructional Parameters and Some Surface Properties in Denim Fabrics Woven with Different Fiber Contents" by Gizem Kara.

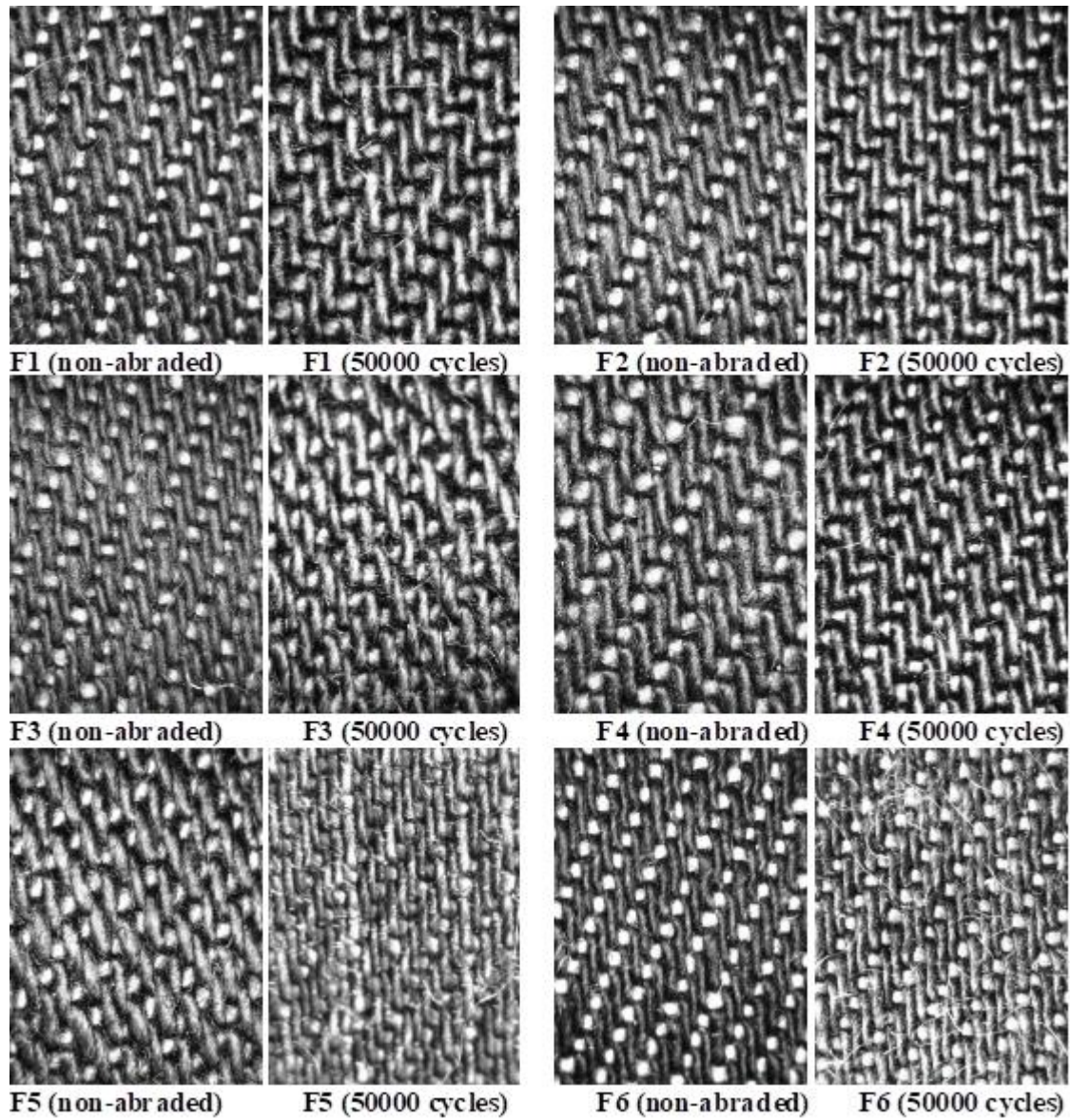


Figure 6. Digital photographs of all fabric samples

## REFERENCES

1. Korkmaz İB. 2009. Denim kumaş imalatı ve üzerine uygulanan işlemler (Master's thesis). Haliç Üniversitesi, Sosyal Bölümler Enstitüsü, Tekstil ve Moda Tasarımı Anasanat Dalı, Tekstil ve Moda Tasarımı Programı, İstanbul, p. 108.
2. Çakır N. 2010. Kot pantolon üretiminde bitim işlemlerinin ve farklı denim kumaşların fit üzerine etkileri (Master's thesis). Pamukkale Üniversitesi, Fen Bilimleri Enstitüsü, Tekstil Mühendisliği Anabilim Dalı, Denizli, p. 99.
3. Tarhan M. 2005. Eskitme yöntemlerinin denim mamullerinin performans özelliklerine etkisi (Master's thesis). Dokuz Eylül Üniversitesi, Fen Bilimleri Enstitüsü, Tekstil Mühendisliği Ana Bilim Dalı, İzmir, p. 120.
4. Toksöz M, Mezarcıöz S. 2013. Application of special washing processes to denim fabrics. *Çukurova University Journal of the Faculty of Engineering and Architecture* 28(2), 141-147.
5. Vassiliadis SG, Provatidis CG. 2004. Structural characterization of textile fabrics using surface roughness data. *International Journal of Clothing Science and Technology* 16(5), 445-457.
6. Xin JH, Lam CC. 2005. Investigation of texture effect on visual colour difference evaluation. *Color Research and Application* 30(5), 341-347.
7. Balcı G, Sülar V. 2009. Yarn friction properties: Importance and test methods. *Tekstil ve Mühendis* 16(74), 6-15.
8. Budinski KG. 2007. Guide to friction, wear and erosion testing. ASTM Stock Number: MNL56, ASTM International, 95.
9. Das A, Kothari VK, Vandana N. 2005. A study on frictional characteristics of woven fabrics. *AUTEX Research Journal* 5(3), 133-140.
10. Ajayi JO. 1992a. Fabric smoothness. friction and handle. *Textile Research Journal* 62(1), 52-59.
11. Ajayi JO. 1992b. Effects of fabric structure on frictional properties. *Textile Research Journal* 62(2), 87-93.
12. Hearle JWS, Husain AKMM. 1971. Studies in needled fabrics. Part VIII: The effect of friction on the processing and properties of needle-bonded fabrics. *The Journal of The Textile Institute* 62, 83-107.

13. Stülar V, Öner E, Okur A. 2013. Roughness and frictional properties of cotton and polyester woven fabrics. *Indian Journal of Fibre & Textile Research* 38, 349-356.
14. Wilson D. 1963. A study of fabric-on-fabric dynamic friction. *Journal of the Textile Institute Transactions* 54(4), T143-T155.
15. Ohsawa M, Namiki S. 1979. Anisotropy of static friction of plain-woven filament fabrics. *Journal of the Textile Machinery Society of Japan* 32, T40.
16. Stockbridge HCW, Kenchington KWL, Corkindale KG, Greenlands J. 1957. The subjective assessment of the roughness of fabrics. *Journal of the Textile Institute Transactions* 48(1), T26-T34.
17. Thornedike GH, Varley L. 1961. Measurement of the coefficient of friction between samples of the same cloth. *Journal of the Textile Institute Proceedings* 52(6), 255-271.
18. Ohsawa M, Namiki S, Kodaka H. 1969. Relationship between fabric balance and surface friction of plain woven fabrics. *Journal of the Textile Machinery Society of Japan* 15, 98-105.
19. Thomas TR. 1999. Rough surfaces (2<sup>nd</sup> ed.), Imperial College Press, London.
20. Zurek W, Jankowiak D, Frydrych I. 1985. Surface frictional resistance of fabrics woven from filament yarns. *Textile Research Journal* 55(2), 113-121.
21. Ukponmwan JO. 1987. Appraisal of woven fabric quality. *Textile Research Journal* 57(5), 283-298.
22. Ajayi JO, Elder HM. 1997. Effects of surface geometry on fabric friction. *JTEVA* 25, 182-188.
23. Militký J. 2005. Fabric roughness characterization. Technical University of Liberec. Czech Republic, ITSAPT Summer School, September, [http://centrum.tul.cz/centrum/itsapt/Summer2005/files/militky\\_3.pdf](http://centrum.tul.cz/centrum/itsapt/Summer2005/files/militky_3.pdf) - (07.07.2009)
24. Bilisik K, Yolacan G. 2011. Tensile and tearing properties of newly developed structural denim fabrics after abrasion. *Fibres & Textiles in Eastern Europe* 19(5), 54-59.
25. Shaw VP, Mukhopadhyay A. 2022. Impact of abrasion on strength, elasticity and elastic recovery properties of stretch-denim fabric. *International Journal of Clothing Science and Technology* 34(2), 241-261.
26. ASTM D1777-96. 2007. Test method for thickness of textile materials.
27. ASTM D3776. 2011. Standard test methods for mass per unit area (weight) of fabric.
28. Hsieh YL. 1995. Liquid transport in fabric structures. *Textile Research Journal* 65(5), 299-307.
29. Hsieh YL, Cram LA. 1998. Enzymatic hydrolysis to improve wetting and absorbency of polyester fabrics. *Textile Research Journal* 68(5), 311-319.
30. Peirce FT. 1937. The geometry of cloth structure. *The Journal of The Textile Institute Transactions* 28(3), T45-T96.
31. Seyam AM. 2002. The structural design of woven fabrics: theory and practice. *The Textile Institute, Textile Progress* 31, 11-19.
32. Hearle JWS, Grosberg P, Backer S. 1969. Structural mechanics of fibers, yarns and fabrics. Wiley-Interscience, New York, USA.
33. ASTM D 4966-12. 2012. Standard test method for abrasion resistance of textile fabrics.
34. ASTM D1894-14. 2014. Standard test method for static and kinetic coefficients of friction of plastic film and sheeting.
35. ISO 4287-1997. 2005. Geometrical product specification (GPS) - Surface texture: profile method – terms, definitions and surface texture parameters.
36. Gadelmawla ES, Koura MM, Maksoud TMA, Elewa IM, Soliman HH. 2002. Roughness parameters, *Journal of Materials Processing Technology* 123(1), 133-145.
37. Mansor A, Ghani SA, Yahya MF. 2016. Knitted fabric parameters in relation to comfort properties. *American Journal of Materials Science* 6(6), 147-151.
38. Mukaka MM. 2012. A guide to appropriate use of correlation coefficient in medical research. *Malawi Medical Journal* 24(3), 69-71.
39. Akgun M, Becerir B, Alpay HR. 2012. The effect of fabric constructional parameters on percentage reflectance and surface roughness of polyester fabrics. *Textile Research Journal* 82(7), 700-707.
40. Akgun M. 2014. Assessment of the surface roughness of cotton fabrics through different yarn and fabric structural properties. *Fibers and Polymers* 15, 405-413.
41. Akgun M. 2015. Assessment of the effect of fabric constructional parameters on surface roughness of wool fabrics. *The Journal of The Textile Institute* 106(8), 845-852.

# Influence of Knitting Structure and Metal Wire Amount on Electromagnetic Shielding Effectiveness of Knitted Fabrics

Serkan TEZEL<sup>1</sup>  0000-0003-4078-8210

Yasemin KAVUŞTURAN<sup>1</sup>  0000-0002-9919-564X

Guy A. E. VANDENBOSCH<sup>2</sup>  0000-0002-5878-3285

Vladimir VOLSKİ<sup>2</sup>  0000-0002-4423-0401

<sup>1</sup>Bursa Uludag University, Faculty of Engineering, Department of Textile Engineering, Bursa, Türkiye

<sup>2</sup>KU Leuven / Department of Electrical Engineering, Leuven, Belgium

**Corresponding Author:** Serkan Tezel, serkantezel@uludag.edu.tr

## ABSTRACT

In this study, the influence of knitting structure and metal wire amount on the electromagnetic shielding effectiveness (EMSE) of knitted fabrics were investigated comparatively. Single jersey, single pique, weft locknit, and cross miss fabrics involving stainless steel or copper wires were produced on a flat knitting machine. In order to measure the EMSE, a free space measurement method was used in an anechoic chamber because of its high reproducibility and accuracy. The variance analysis results of the EMSE values showed that knitting structure, metal wire type, metal wire amount, and incident wave frequency is highly significant. It was observed that fabrics with tuck and miss loop structures had higher EMSE values than single jersey fabrics. Also, single pique fabrics had higher EMSE than single jersey fabrics that contain twice as much metal wire. It indicates that the knitting structure has a great effect on EMSE rather than the amount of the conductive material.

## 1. INTRODUCTION

The proliferation of electricity demand, ever-advancing technologies such as AM and FM radio, television, cordless and mobile phones, base station transmitters, wireless networks, cordless baby monitors, garage door openers, global positioning systems, microwave ovens, radar, etc. and changes in social behavior have dramatically increased our exposure to electromagnetic radiation (EMR), or electromagnetic fields (EMF) in the last two decades. Therefore, everyone is exposed to a complex mix of weak electric and magnetic fields, both at home and at work[1]. While the health impacts of this form of radiation are inconclusive[2–4], many people are concerned about how long-term exposure to excessive EMR may impact human health and nature. As a result, a need to develop textile products that implement electromagnetic shielding has occurred[5].

The electromagnetic shielding effectiveness (EMSE) of a shielding material is related to the residual traveling energy after applying the shield. The residual energy is the energy

that is neither reflected nor absorbed by the shield, but that emerges out of the shielding material[6]. EMSE can be measured with different methods as reported by the standards [7–10].

Conductive fabrics have been used to shield electromagnetic fields in the defense, electrical, and electronic industries[6]. Metallic coated yarns, metal wires, metallic fibers, conductive polymers, or composite yarns are used for producing electromagnetic shielding textile materials. Electromagnetic shielding fabrics are produced via various types of fabric production techniques, including knitting, weaving, or nonwoven. Conductive fabric reinforced composites and conductive material coated fabrics are also used as electromagnetic shielding textile materials. [11].

There have been some researches about the EMSE properties of knitted fabrics in literature. Researchers used the free space measurement technique, the shielded box shielding efficiency measurement technique, and the coaxial transmission line technique. Palamutçu et al.[12]

## ARTICLE HISTORY

Received: 17.09.2021

Accepted: 13.10.2022

## KEYWORDS

Electromagnetic Shielding Effectiveness, Conductive Yarn, Knitted Fabric, Anechoic Chamber, Free Space Measurement Technique

**To cite this article:** Tezel S, Kavuşturan Y, Vandenbosch GA, Volski V. 2023. Influence of Knitting Structure and Metal Wire Amount on Electromagnetic Shielding Effectiveness of Knitted Fabrics. *Tekstil ve Konfeksiyon* 33(1), 37-44.

designed a new setup to measure EMSE based on the free space technique. They investigated the EMSE of four kinds of single jersey knitted fabrics (860 - 960 MHz, 1.750 - 1.850 GHz). Çeken et al.[13–15] and Kayacan[16] also designed an EMSE setup based on the free space technique as well. In their study, they investigated the EMSE of knitted fabrics (750 MHz - 3 GHz) under room conditions. Çeken et al. investigated the EMSE of plain, rib, full cardigan, plain knitted fabrics with one and two miss stitch rows [13], cross-miss 1x1 plain knit, single pique, interlock, double pique [14] and six types of knitted fabrics with their backside covered with conductive yarns [15]. Kayacan [16] also investigated the EMSE of single jersey and interlock knitted fabrics before and after washing cycles. Ciesielska-Wróbel and Grabowska[17] examined the EMSE of three kinds of knitted fabric samples, namely single -left-right stitch, double - a sleeve type - left-right stitch, and double - left-right stitch - layer exchange. The EMSE values were measured for the electric field (30 Hz - 6 GHz) and for the magnetic field (10 Hz - 1 GHz) using isotropic E-field and H-field probes. Özkan studied the antimicrobial and EMSE properties of metal composite single jersey[18] and 1x1 rib fabrics[19, 20]. EMSE of samples was measured according to the free space test method (0.8 - 5.2 GHz). Tezel et al.[11] investigated the EMSE with both the coaxial transmission line (100 MHz - 1.5 GHz) and free space measurement (1 GHz - 18 GHz) techniques on single jersey fabrics. Mühl and Obelenski[21] investigated the EMSE of jersey fabrics which consist of cotton yarns including silver coated polyamide fibers and warp-knitted fabrics produced with a weft lapping technique. A shielded box shielding efficiency measurement set-up (800 MHz - 3 GHz) was used to measure the EMSE. Stegmaier et al.[22] designed a shielded box EMSE test device. The researchers measured the EMSE of knitted fabrics including silver coated filaments (250 MHz - 3 GHz). Perumalraj and Dasaradan[23] examined the EMSE of rib, interlock, and single jersey samples produced with Cu wire/cotton fiber core yarns. They used shielded box shielding efficiency measurement method (800 MHz - 3 GHz). Örtlek et al.[24] examined the EMSE of pique, plain (E28), and double-knit structures (E18) with the shielded box shielding efficiency measurement method (30 MHz - 9.93 GHz). Apart from the studies performed with the free space measurement technique[11–20] and the shielded box shielding efficiency measurement technique[21–24], there are also studies on EMSE of knitted fabrics performed with the coaxial transmission line technique[11, 25–44]. Knitted fabrics give different EMSE values for each frequency when measured with different measurement techniques and / or different polarizations[11]. In other words, the results of the coaxial transmission line technique are not directly comparable with shielded box and free space measurement techniques.

The main point of EMSE measurement is to minimize the electromagnetic noise caused by electrical devices, mobile phones, base stations, and Wi-Fi transmitters. In other words,

the electromagnetic noise caused by the environment affects the test accuracy. In this study the free space measurement technique by using an anechoic chamber was preferred for the EMSE measurements because of its high reproducibility and accuracy[45–48]. Therefore, the noise caused by the environment was eliminated. In addition to this, a mathematical-based software solution to remove the contribution due to scattering, namely the time-gating technique was applied. As a result of using a professional EMSE test operation system, we could able to measure the EMSE results with high accuracy.

In this study the effects of the knitting structure and metal wire amount on the EMSE of knitted fabrics comparatively. Therefore, four knitting fabric structures (single jersey, single pique, weft locknit, cross miss) were produced. For the comparison of metal wire amount and knitting structures, single jersey fabrics were knitted with three different amounts of stainless steel (SS) and copper (Cu) wires.

## 2. MATERIAL AND METHOD

### 2.1 Material

A hollow spindle twisting machine was used to produce conductive composite yarns (CCYs). Same machine settings were applied for all productions. In order to investigate the metal wire type effects, AISI 316L type 50  $\mu\text{m}$  SS and 50  $\mu\text{m}$  Cu conductive metal wires were doubled with Ne 60/2 count cotton yarns (Co). The linear resistance of SS and Cu wires were 400  $\Omega/\text{m}$  and 14  $\Omega/\text{m}$  respectively. In Table 1, linear density of the Co and CCYs are given.

Single jersey, single pique (lacoste), weft locknit and cross miss knitting structures were produced to investigate the influence of plain, tuck and miss loop structures on the EMSE of the knitted fabrics. While single jersey fabrics have only loop structure, single pique fabrics have loop and tuck structures. Both, weft locknit and cross miss fabrics have loop and miss loop structures. In Figure 1, the knitting structures and schematic views of the fabrics that were investigated in the study are given.

Fabrics were knitted with the same machine settings on an E12 Stoll CMS 411.6 flat knitting machine. Tezel et al.[49] reported that while spandex yarn usage improves the residual extension properties of the knitted fabrics with CCYs, they do not have an effect on the EMSE of the fabrics. In this respect, for having better fabric quality, three yarns and a 70 denier spandex yarn (EL) were not wrapped, but they were fed together during the knitting process. Each single jersey, single pique, weft locknit and cross miss fabric sample was produced with one CCY, two cotton yarns, and a spandex yarn. In order to understand the metal wire amount effects on EMSE, Single Jersey fabrics involving a spandex yarn were also produced with 3 different composite yarn amounts. In Table 2, yarn composition and fabrics' dimensional properties are given.



## 2.2 Method

The fabrics were subjected to dry-relaxation. The samples were laid on a flat and smooth surface and kept in atmospheric conditions for one week ( $20\pm 2^{\circ}\text{C}$  and  $65\pm 4\%$  relative humidity). The fabric properties were measured according to ISO 7211-2 (course and wale per cm) and ISO 3801 (fabric weight) standards. The yarn loop length values were determined by using a Hatra-like tester. The test was conducted as suggested in the literature [50, 51]. Loop length values of the single pique and weft locknit fabrics that have

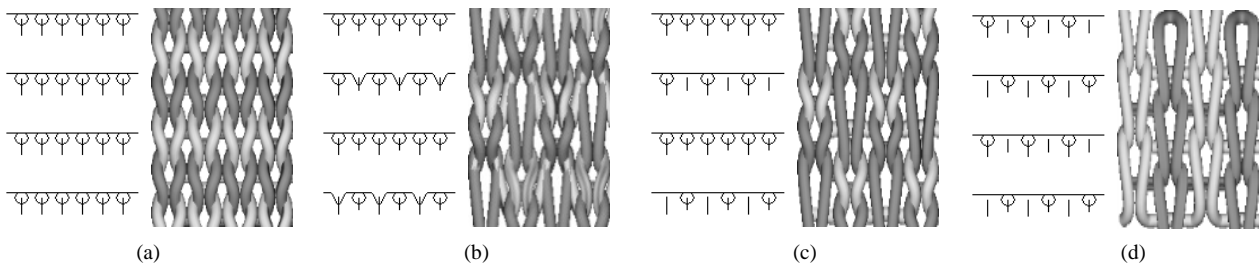
different knitting structures for alternating courses such as knit and tuck or miss loop structures were also measured and calculated separately for each alternating course.

### EMSE Measurements

EMSE measurements were conducted in an anechoic chamber by using the free space measurement technique because of its high reproducibility and accuracy [45–48]. Measurements were performed at 200 different frequencies (1 GHz–18 GHz) with 85 MHz intervals by positioning two horn type directive antennas (Figure 2).

**Table 1.** Linear density of the cotton yarn and CCYs

Yarn Composition			Linear Density	
Metal Wire		Cotton Yarn	Ne	Nm
50 $\mu\text{m}$ SS	+	Ne 60/2 Co	Ne 17,28	Nm 29,26
50 $\mu\text{m}$ Cu	+	Ne 60/2 Co	Ne 15,30	Nm 25,91
-	+	Ne 60/2 Co	Ne 30,76	Nm 52,08

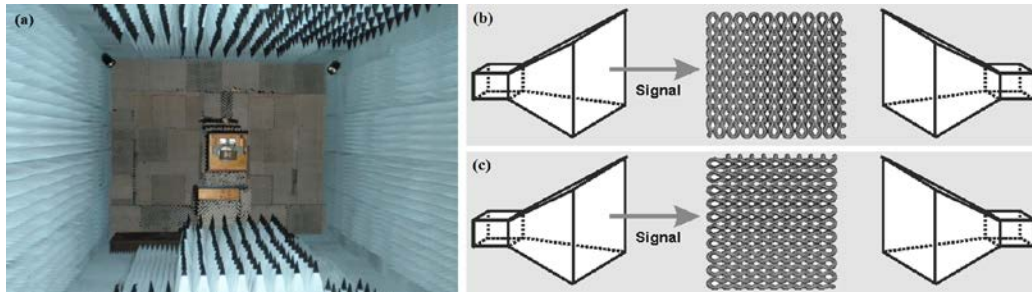


**Figure 1.** Knitting notations and schematic views of the fabric samples, (a) Single Jersey, (b) Single Pique, (c) Weft Locknit, (d) Cross Miss

**Table 2.** Yarn composition and dimensional properties of the fabrics

Knit Structure	Fabric Code	Yarn Composition	Courses per cm	Wales per cm	Stitches per $\text{cm}^2$	Weight ( $\text{g}/\text{m}^2$ )	Loop Length (mm)
Single Jersey	RL-CO	(Ne60/2Co)+(Ne60/2Co)+(Ne60/2Co)+70DenEL	13,7	8,9	121,9	358,2	4,76
	RL-SS	(50 $\mu\text{m}$ SS+Ne60/2Co)+(Ne60/2Co)+(Ne60/2Co)+70DenEL	14,0	7,9	110,6	381,3	4,68
	RL-SSx2	(50 $\mu\text{m}$ SS+Ne60/2Co)+(50 $\mu\text{m}$ SS+Ne60/2Co)+(Ne60/2Co)+70DenEL	15,7	6,1	95,8	416,7	4,69
	RL-SSx3	(50 $\mu\text{m}$ SS+Ne60/2Co)+(50 $\mu\text{m}$ SS+Ne60/2Co)+(50 $\mu\text{m}$ SS+Ne60/2Co)+70DenEL	15,0	5,8	87,0	444,6	4,65
	RL-CU	(50 $\mu\text{m}$ Cu+Ne60/2Co)+(Ne60/2Co)+(Ne60/2Co)+70DenEL	13,2	8,4	110,9	432,6	4,71
	RL-CUx2	(50 $\mu\text{m}$ Cu+Ne60/2Co)+(50 $\mu\text{m}$ Cu+Ne60/2Co)+(Ne60/2Co)+70DenEL	13,7	7,8	106,9	515,6	4,71
	RL-CUx3	(50 $\mu\text{m}$ Cu+Ne60/2Co)+(50 $\mu\text{m}$ Cu+Ne60/2Co)+(50 $\mu\text{m}$ Cu+Ne60/2Co)+70DenEL	15,0	6,7	100,5	564,9	4,65
Single Pique	PIQ-CO	(Ne60/2Co)+(Ne60/2Co)+(Ne60/2Co)+70DenEL	22,3	7,3	162,8	392,6	Knit:4,51 Tuck:4,15
	PIQ-SS	(50 $\mu\text{m}$ SS+Ne60/2Co)+(Ne60/2Co)+(Ne60/2Co)+70DenEL	22,3	5,9	131,6	392,0	Knit:4,38 Tuck:4,08
	PIQ-CU	(50 $\mu\text{m}$ Cu+Ne60/2Co)+(Ne60/2Co)+(Ne60/2Co)+70DenEL	21,7	6,6	143,2	485,3	Knit:4,43 Tuck:4,15
Weft Locknit	MIS-CO	(Ne60/2Co)+(Ne60/2Co)+(Ne60/2Co)+70DenEL	17,7	9,0	159,3	389,7	Knit:4,78 Miss:3,37
	MIS-SS	(50 $\mu\text{m}$ SS+Ne60/2Co)+(Ne60/2Co)+(Ne60/2Co)+70DenEL	18,3	7,1	129,9	424,1	Knit:4,68 Miss:3,32
	MIS-CU	(50 $\mu\text{m}$ Cu+Ne60/2Co)+(Ne60/2Co)+(Ne60/2Co)+70DenEL	18,0	8,0	144,0	471,6	Knit:4,72 Miss:3,33
Cross Miss	MISS-CO	(Ne60/2Co)+(Ne60/2Co)+(Ne60/2Co)+70DenEL	19,3	10,6	204,6	413,4	3,51
	MISS-SS	(50 $\mu\text{m}$ SS+Ne60/2Co)+(Ne60/2Co)+(Ne60/2Co)+70DenEL	23,3	8,2	191,1	468,2	3,04
	MISS-CU	(50 $\mu\text{m}$ Cu+Ne60/2Co)+(Ne60/2Co)+(Ne60/2Co)+70DenEL	23,3	8,8	205,0	500,1	3,42

Co: cotton yarn, SS: stainless steel wire, Cu: copper wire, EL: spandex yarn



**Figure 2.** Free space measurement: (a) anechoic chamber, illustration of fabric positions: horn antennas and the fabric sample, in (b) horizontal, and (c) vertical direction.

A dedicated mathematical algorithm was applied to remove the contribution due to scattering. More information can be found in [11, 45–48, 52]. EMSE properties of fabrics were measured in both horizontal, and vertical directions (Figure 2) related to the electric field polarization of the antennas. The test was repeated three times for each direction. However, the EMSE test of horizontal positioned cross miss knitted fabric with SS wire (MISS-SS) could not be performed because of an insufficient sample size. EMSE is defined as the ratio of the field before and after applying the shield. EMSE is logarithmically expressed in decibels (dB). The percentage of electromagnetic shielding efficiency (%) represents the material's ability to block waves in terms of percentage. EMSE [dB] is converted into percentage of electromagnetic shielding (%) using the Equation (1) as in [53]:

$$\text{Percentage of electromagnetic shielding (\%)} = 100 - \frac{100}{10^{EMSE/10}} \quad (1)$$

In order to show the significance of the knitting structure or the amount of metal and the frequency on the EMSE of horizontally positioned knitted fabrics with SS and Cu wire content, a two factor completely randomized ANOVA analysis was carried out with a significance level of %5. “Student Newman Keuls” (SNK) method was used to compare the means for a rejected hypothesis. The levels of the treatment were noted in accordance with the mean values. The levels with the same letters indicate insignificant differences.

### 3. RESULTS AND DISCUSSION

Consistent with former studies [11, 21, 24, 38], the free space measurement technique EMSE results indicate that the knitted fabrics with CCYs that are investigated in the study have an EMSE ability in the main direction where the conductive materials are running. It was found that all horizontally positioned knitted fabrics with metal wire have 14 dB or more EMSE in the frequency range from 1 GHz to 3 GHz, 10 dB, or more EMSE up to 6.695 GHz and 5 dB or more EMSE up to 11.710 GHz (Figure 3). Vertically positioned fabrics and 100% cotton fabrics did not show any EMSE.

The resistance of the knitted fabrics involving conductive materials differs according to the direction of the measurement procedure [54]. In weft knitted fabrics, the

conductive material runs in the horizontal direction by forming loops. For this reason, weft-knitted fabrics have very low resistance in the horizontal direction. The resistance of the fabric in the vertical direction is higher than in the horizontal direction. The resistance in the vertical direction is realized by the contact of the conductive material with each other. If the fabric contains both the conductive material and insulating material (for instance in this study we have both metal wires and cotton yarns), the resistance in the vertical direction will be very high because of the limited contact points. Since the contact points are excessive in fabrics produced with pure conductive threads/wires, conductivity is also high in the vertical direction. The contact resistance property of the conductive material (Silver coated PA, Cu wire, SS wire, etc.) and the tightness of the fabric structure also affect the resistance in the vertical direction. Thus, course per cm values directly affect the EMSE values whereas wales per cm values have limited effect on the EMSE.

#### 3.1. The Effect of Knitting Structure on the EMSE of Fabrics

Figure 3 shows the EMSE test results for the horizontally positioned diverse knit structures that are investigated in the study. Test results reveal that single pique fabrics have the highest EMSE values, and single jersey fabrics have the lowest EMSE values. 100% cotton fabrics (RL-CO, PIQ-CO, MIS-CO, and MISS-CO) do not have any EMSE ability.

According to variance analysis, the effect of knitting structure and frequency is highly significant and SNK tests showed that each fabric have different EMSE for each frequency value.

While single pique fabrics have the highest EMSE values, cross miss fabrics have higher EMSE values than weft locknit fabrics and single jersey fabrics have the lowest EMSE values according to SNK test results (Table 3). There are two criteria that affect the EMSE of the knitted fabric mainly resistance of the fabric and the apertures in the fabric. Liu et al. [55, 56] produced knitted fabrics with tuck and miss loop structures as well as RL fabrics. They demonstrated that, the fabrics with miss loops had lower resistance values than RL fabrics, while the fabrics with tuck loops had the lowest resistance values. In addition to this, Basyigit et al. [57, 58] also showed that aperture shape

and the aperture length/width ratio in the conductive material are effective on the EMSE values. The tuck and miss loop structures reduce the gaps between the metal wires in the fabric structure, also with the help of increasing the course density. This is also consistent with former studies [14, 24].

### 3.2. The Effect of Metal Wire Amount on the EMSE of Fabrics

EMSE test results showed that single jersey fabrics involving three CCYs have the highest EMSE values and single jersey fabrics involving one CCY have the lowest EMSE values, as expected (Figure 4).

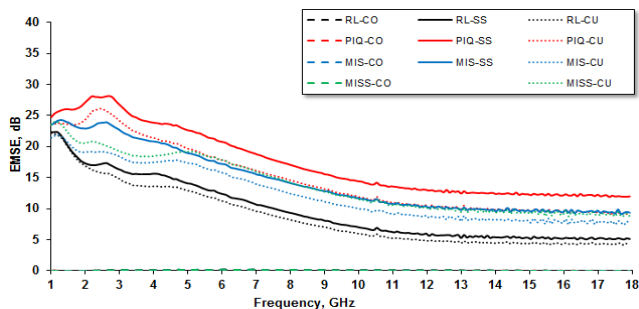


Figure 3. EMSE test results of diverse knit structures

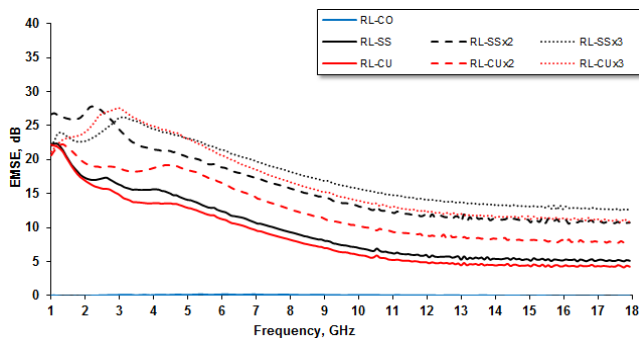


Figure 4. EMSE results of single jersey knitted fabrics with diverse metal wire amounts

Table 3. SNK ranking for the EMSE of diverse knitting structures with SS and Cu wire content

Knitting Structure	EMSE (1 GHz - 18 GHz)
RL	9.12903 a
MIS	13.33747 b
MISS	13.79144 c
PIQ	16.03103 d

\*Lower cases indicate significant differences between the values.

Table 4. SNK ranking for the EMSE of single jersey fabrics with diverse metal wire amounts

Metal Wire	EMSE (1 GHz - 18 GHz)
RL-CO	0.02998 a
RL-CU	8.60867 b
RL-SS	9.64939 c
RL-CUx2	12.66529 d
RL-SSx2	15.95900 e
RL-CUx3	16.72949 f

Variance analysis results of the EMSE values indicate that the metal wire type and the amount is highly significant in single jersey knitted fabrics as well as the frequency.

The fabrics with SS wire have higher EMSE values than the fabrics with Cu wire (Table 4). This is also consistent with the former study of Tezel et al.[11] Resistance of the conductive metal wire affects the EMSE of the fabric. It is clear that, the decrease in the loop length value leads to a decrease in the resistance. However, with the decrease of the loop length value, the deformation of the metal wire increases. This deformation increases the resistance [23, 59]. The Cu wires used in this study have a resistance value of 14  $\Omega$ /m, and the SS wires have a resistance of 400  $\Omega$ /m. However, the fabrics with SS wire have higher EMSE values than the fabrics with Cu wire (for the same knitting structures). Thus, it is thought that the increase in the resistance caused by the deformation is much higher for Cu wires than SS wires. 100% cotton fabrics did not show any EMSE. SNK test results also reveal that fabrics involving three CCYs have the highest EMSE values. Fabrics involving two CCYs and one cotton yarn have higher EMSE values than fabrics involving one CCY and two cotton yarns. For instance, while RL-SS have 9,65 dB EMSE, RL-SSx2 fabrics have 15,96 dB EMSE and RL-SSx3 fabrics have 17,73 dB EMSE. This result is very interesting and unexpected: the EMSE values of the fabrics containing 3 times more metal wires are not as high as expected.

### 3.3. The Effect of Knitting Structure and Metal Wire Amount on the EMSE of Fabrics

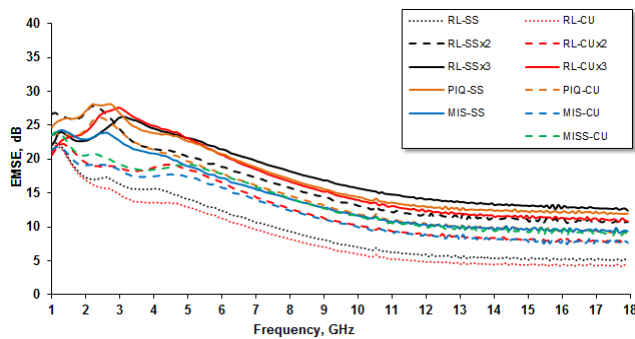
Figure 5 shows the EMSE test results of the horizontally positioned knitted fabrics with diverse knitting structures and metal wire amounts that are investigated in the study. Single jersey fabrics with three CCYs involving SS wire have the highest EMSE values, and single jersey fabrics with one CCY involving Cu wire have the lowest EMSE values.

\*Lower cases indicate significant differences between the values.

**Table 5.** SNK ranking for the EMSE of fabrics with diverse knitting structures and metal wire amounts

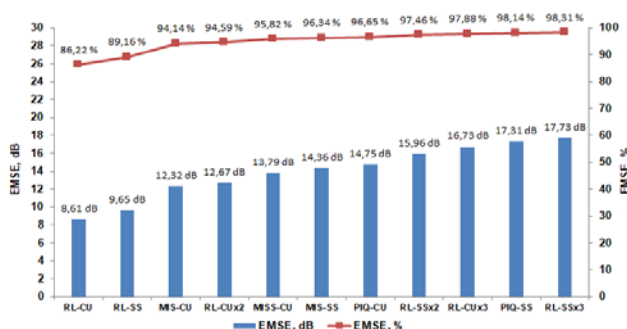
Fabric Code	EMSE (1 GHz - 18 GHz)
RL-CU	8,61 a
RL-SS	9,65 b
MIS-CU	12,32 c
RL-CUx2	12,67 d
MISS-CU	13,79 e
MIS-SS	14,36 f
PIQ-CU	14,75 g
RL-SSx2	15,96 h
RL-CUx3	16,73 i
PIQ-SS	17,31 j
RL-SSx3	17,73 k

\*Lower cases indicate significant differences between the values.



**Figure 5.** EMSE of the fabrics with diverse knitting structure and metal wire amounts

According to variance analysis the wave frequency and fabric type highly affect the EMSE results. Single jersey fabrics with three CCYs involving SS wire have the highest EMSE values (Table 5). Single pique knitted fabrics involving SS wire have the second highest EMSE values. For a better understanding, EMSE values (dB) of the fabrics and percentage of electromagnetic shielding (%) are shown in Figure 6.



**Figure 6.** Comparison of EMSE values (dB) and percentage of electromagnetic shielding (%) of the fabrics according to SNK test results

#### 4. CONCLUSION

In this study, the influence of knitting structure and metal wire amount on the EMSE of knitted fabrics via the free space measurement technique were investigated comparatively.

The parameters affecting the EMSE can be summarised as follows:

- Course per cm value
- Loop length value
- Increase in the resistance caused by the deformation of the metal wire
- Resistance change caused by the knitting structure and the metal wire amount
- Change in the aperture shape and the aperture length/width ratio caused by the knitting structure and the metal wire amount

The primary result of this study is that knitted fabrics with CCYs have an EMSE ability in the main direction in which the metal wires are running. Weft knitted fabrics have very low resistance in the horizontal direction due to the conductive material running in the horizontal direction by forming loops. The resistance in the vertical direction is realized by the contact of the conductive material with each other. In this study, we have both metal wires and cotton yarns in the fabric structure. EMSE results show that the knitted fabrics are not conductive in the vertical direction indicating that course per cm values directly affect the EMSE values whereas wales per cm values have limited effect on the EMSE.

Variance analysis for the EMSE indicate that the effect of knitting structure, metal wire type, metal wire amount, and incident wave frequency is highly significant. Also, the fabrics with SS wire have higher EMSE values than fabrics with Cu wire for all knitting structure types. The Cu wires have lower resistance value than the SS wires. However,

the results showed that the fabrics with SS wire have higher EMSE values than the fabrics with Cu wire for the same knitting structures. This might be due to the higher increase in the resistance caused by the deformation of Cu wires than SS wires.

EMSE values increase as the metal wire amount in the fabric increases, as expected. However, it was also found that EMSE values do not increase as much as the metal wire amount in the fabric increases as it was expected. The resistance of the fabric and the apertures in the fabric affect the EMSE of the knitted fabric. Therefore, both the metal wire amount and knitting structure change the resistance of the fabric and the apertures in the fabric structure, resulting in the change of the EMSE values. EMSE test results of diverse knit structures show that fabrics with tuck and miss loop structures have higher EMSE values than single jersey fabrics. While single pique fabrics with tuck loop structures have the highest EMSE values, cross miss and weft locknit fabrics, that both have miss loop structures, have higher EMSE values than single jersey fabrics. Since cross miss fabrics have more miss loop structures, they have higher EMSE values than weft locknit fabrics.

In our study, single jersey fabrics with three CCYs involving SS wire (RL-SSx3) have the highest EMSE values (17,73 dB), and single pique knitted fabrics also involving SS wire (PIQ-SS) have the second highest EMSE values (17,31 dB). Although RL-SSx3 fabrics have three times as much SS wires as PIQ-SS single pique fabrics, the difference in EMSE between these two fabrics is not as high as it was expected. Although RL-SSx2 Single Jersey

fabrics have twice as much SS wires as PIQ-SS single pique fabrics, they have lower (15,96 dB) EMSE values than PIQ-SS single pique fabrics. This result can be considered as the most interesting and the most important result of the study. The study shows that the knitting structure has a great impact on the EMSE of knitted fabrics. It can be concluded that single pique knitted fabrics involving SS wire combine a high EMSE with a lower production cost.

The aim of this research is to investigate the influence of the basic knitting structure and the metal wire amount on the electromagnetic shielding effectiveness of knitted fabrics experimentally. A detailed study on observing the complex knitting structures' EMSE properties via experimental investigations and/or full-wave electromagnetic modelling of the fabrics is recommended as follow-up research.

### Acknowledgement

The work of Serkan Tezel was supported by The Scientific and Technological Research Council of Türkiye (TUBITAK-BİDEB 2214). This study is a part of the PhD thesis of the first author. The authors would like to thank Yeşim Tekstil Co., Türkiye, for their support during knitting operations, Sarkuysan Elektrolitik Bakır Co., Türkiye for providing copper wires, and Mebiteks Tekstil Co., Türkiye, for providing stainless steel wires and for their support during the yarn doubling operations.

### REFERENCES

1. Who Team, 2016, World Health Organization - Electromagnetic Fields, What are the Electromagnetic Fields, Retrieved from <http://www.who.int/peh-emf/about/WhatisEMF/en/index1.html>
2. Samaras T, Leitgeb N, Auvinen An, Danker-Hopf H, Hansson Mild K, Mattsson MO, Norppa H, Rubin GJ, Scarfi MR, Schüz J, Sienkiewicz Z, Zeni O. 2015. Potential health effects of exposure to electromagnetic fields (EMF). European Commission SCENIHR (Scientific Committee on Emerging and Newly Identified Health Risks). DOI: 10.2772/75635
3. Phillips JL, Singh NP, Lai H. 2009. Electromagnetic fields and DNA damage. *Pathophysiology* 16(2-3), 79-88.
4. Kim JH, Lee JK, Kim HG, Kim KB, Kim HR. 2019. Possible effects of radiofrequency electromagnetic field exposure on central TEKSTİL ve KONFEKSİYON Vol(Issue), Year Page number nerve system. *Biomolecules and Therapeutics* 27(3), 265-275.
5. Das A, Kothari VK, Kothari A, Kumar A, Tuli S. 2009. Effect of various parameters on electromagnetic shielding effectiveness of textile fabrics. *Indian Journal of Fibre & Textile Research* 34, 144-148.
6. Cheng KB, Lee ML, Ramakrishna S, Ueng TH. 2001. Electromagnetic Shielding Effectiveness of Stainless Steel/Polyester Woven Fabrics. *Textile Research Journal* 71(1), 42-49.
7. IEEE-STD 299-1997. IEEE Standard Method for Measuring the Effectiveness of Electromagnetic Shielding Enclosures.
8. ASTM D4935-10. Standard Test Method for Measuring the Electromagnetic Shielding Effectiveness of Planar Materials.
9. TS EN 50147-1. 2005. Anechoic chambers - Part 1: Shield attenuation measurement.
10. MIL-STD-285-1956: Method of Attenuation Measurement for Enclosures, Electromagnetic Shielding, for Electronic Test Purposes.
11. Tezel S, Kavuşturan Y, Vandembosch GA, Volski V. 2014. Comparison of Electromagnetic Shielding Effectiveness of Conductive Single Jersey Fabrics with Coaxial Transmission Line and Free Space Measurement Techniques. *Textile Research Journal* 84(5), 461-476.
12. Palamutçu S, Özek A, Karpuz C, Dağ N. 2010. Electrically Conductive Surfaces and Their Electromagnetic Shielding Efficiency Measurements. *Tekstil ve Konfeksiyon* 20(3), 199-207.
13. Çeken F, Kayacan Ö, Özkurt A, Uğurlu ŞŞ. 2011. The Electromagnetic Shielding Properties of Copper and Stainless Steel Knitted Fabrics. *Tekstil* 60(7), 321-328.
14. Çeken F, Kayacan Ö, Özkurt A, Uğurlu ŞŞ. 2012. The Electromagnetic Shielding Properties of Some Conductive Knitted Fabrics Produced on Single or Double Needle Bed of a Flat Knitting Machine. *Journal of the Textile Institute* 103(9), 968-979.
15. Çeken F, Pamuk G, Kayacan O, Özkurt A, Uğurlu ŞŞ. 2012. Electromagnetic Shielding Properties of Plain Knitted Fabrics Containing Conductive Yarns. *Journal of Engineered Fibers and Fabrics* 7(4), 81-87.
16. Kayacan Ö. 2014. The Effect of Washing Processes on The Electromagnetic Shielding of Knitted Fabrics. *Tekstil ve Konfeksiyon* 24(4), 356-362.
17. Ciesielska-Wróbel I, Grabowska K. 2012. Estimation of the EMR Shielding Effectiveness of Knit Structures. *Fibres & Textiles in Eastern Europe* 20(2), 53-60.

18. Özkan İ. 2019. Investigation on antimicrobial activity and electromagnetic shielding effectiveness of metal composite single jersey fabrics. *Journal of Engineered Fibers and Fabrics* 14, 1-11.
19. Özkan İ. 2020. Investigation of the technical and physical properties of metal composite 1×1 rib knitted fabrics. *Industria Textila* 71(01), 41-49.
20. Özkan İ. 2020. Investigation on The Electromagnetic Shielding Performance of Copper Plate and Copper Composite Fabrics: A Comparative Study. *Tekstil ve Konfeksiyon* 30(2), 156-162.
21. Mühl T, Obelenski B. 2004. Knitted and Warp-Knitted Fabrics Offering Electromagnetic Shielding. *Melliand Textilberichte* 7-8, 587-588, Melliand English E88.
22. Stegmaier T, Schmeer-Lioe G, Abele H, Planck H. 2008. Shielding Effect of Textiles Against Electromagnetic Waves - New High-Frequency Test Device. *Technical Textiles* 51(3), 128.
23. Perumalraj R, Dasaradan BS. 2009. Electromagnetic Shielding Effectiveness of Copper Core Yarn Knitted Fabrics. *Indian Journal of Fibre & Textile Research* 34, 149-154.
24. Örtlek HG, Alpyildiz T, Kilic G. 2013. Determination of electromagnetic shielding performance of hybrid yarn knitted fabrics with anechoic chamber method. *Textile Research Journal* 83(1), 90-99.
25. Cheng KB. 2000. Production and Electromagnetic Shielding Effectiveness of the Knitted Stainless Steel/Polyester Fabrics. *Journal of Textile Engineering The Textile Machinery Society of Japan* 46(2), 42-52.
26. Bedeloğlu A. 2013. Electrical, electromagnetic shielding, and some physical properties of hybrid yarn-based knitted fabrics. *Journal of the Textile Institute* 104(11), 1247-1257.
27. Eren S, Ulcay Y. 2015. Production of Bi-Component Polyester Fibres for EMR (Electromagnetic Radiation) Protection and Examining EMR Shielding Characteristics. *Tekstil ve Konfeksiyon* 25(2), 140-147.
28. Celen R, Ulcay Y. 2019. Investigating electromagnetic shielding effectiveness of knitted fabrics made by barium titanate/polyester bicomponent yarn. *Journal of Engineered Fibers and Fabrics* 14, 1-9.
29. Tunakova V, Tunak M, Bajzik V, Ocheretna L, Arabuli S, Kyzymchuk O, Vlasenko V. 2020. Hybrid knitted fabric for electromagnetic radiation shielding. *Journal of Engineered Fibers and Fabrics* 15, 1-9.
30. Mohammadi Mofarah H, Shaikhzadeh Najar S, Mohammad Etrati S. 2019. Investigating the electromagnetic shielding effectiveness of copper/cotton full Milano and 1 × 1 rib weft-knitted fabrics. *Journal of the Textile Institute* 110(6), 891-900.
31. Huang CH, Lin JH, Yang RB, Lin CW, Lou CW. 2012. Metal/PET Composite Knitted Fabrics and Composites: Structural Design and Electromagnetic Shielding Effectiveness. *Journal of Electronic Materials* 41(8), 2267-2273.
32. Yu ZC, Zhang JF, Lou CW, He HL, Chen AP, Lin JH. 2015. Determination of electromagnetic shielding and antibacterial properties of multifunctional warp-knitted fabrics. *Journal of the Textile Institute* 106(11), 1203-1211.
33. Cheng KB, Lee KC, Ueng TH, Mou KJ. 2002. Electrical and impact properties of the hybrid knitted inlaid fabric reinforced polypropylene composites. *Composites Part A - Applied Science And Manufacturing* 33(9), 1219-1226.
34. Jagatheesan K, Ramasamy A, Das A, Basu A. 2018. Electromagnetic shielding effectiveness of carbon/stainless steel/polypropylene hybrid yarn-based knitted fabrics and their composites *Journal of the Textile Institute* 109(11), 1445-1457.
35. Sancak E, Akalin M, Usta İ, Yuksek M, Özen MS. 2018. The Effects of Fabric and Conductive Wire Properties on Electromagnetic Shielding Effectiveness and Surface Resistivity of Interlock Knitted Fabrics. *Fibers and Polymers* 19(4), 843-853.
36. Lin JH, Lou CW, Liu HH. 2007. Process and Anti-Electrostatic Properties of Knitted Fabrics Made from Hybrid Staple/Metallic-Core Spun Yarn. *Journal of Advanced Materials* 39(1), 11-16.
37. Palanisamy S, Tunakova V, Militky J. 2018. Fiber-based structures for electromagnetic shielding – comparison of different materials and textile structures. *Textile Research Journal* 88(147), 1992-2012.
38. Volski V, Vandenbosch GA. 2009. Full-wave electromagnetic modelling of fabrics and composites. *Composites Science and Technology* 69(2), 161-168.
39. Soyaslan D, Göktepe Ö, Çömlekçi S. 2010. Determination of electromagnetic shielding performance of plain knitting and 1X1 rib structures with coaxial test fixture relating to ASTM D4935. *Journal of the Textile Institute* 101(10), 890-897.10
40. Örtlek HG, Kılıç G, Okyay G, Bilgin S. 2011. Electromagnetic Shielding Characteristics of Different Fabrics Knitted From Yarns Containing Stainless Steel Wire. *Industria Textila* 62(6), 304-308.
41. Örtlek HG, Güneşoğlu C, Okyay G, Okyay G., Türkoğlu Y. 2012. Investigation of Electromagnetic Shielding and Comfort Properties of Single Jersey Fabrics Knitted From Hybrid Yarns Containing Metal Wire. *Tekstil ve Konfeksiyon* 22(2), 90-101.
42. Rajendrakumar K, Thilagavathi G. 2013. A Study on The Effect of Construction Parameters of Metallic Wire/Core Spun Yarn Based Knitted Fabrics on Electromagnetic Shielding. *Journal of Industrial Textiles* 42(4), 400-416.
43. Lin JH, Huang YT, Li TT, Lin, CM., Lou CW. 2016. Manufacture technique and performance evaluation of electromagnetic shielding / far-infrared elastic warp-knitted composite fabrics. *Journal of the Textile Institute* 107(4), 493-503.
44. Turksöy HG, Bilgin S. 2016. Electromagnetic shielding effectiveness of spacer knitted hybrid fabrics. *Industria Textila* 67(5), 297-301.
45. Chiumento A. 2010. Modeling of Shielding Textiles (M.Sc. thesis). Retrieved from <https://www.politesi.polimi.it/handle/10589/11282>
46. Håkansson E, Amiet A, Kaynak A. 2007. Dielectric Characterization of Conducting Textiles Using Free Space Transmission Measurements: Accuracy and Methods for Improvement. *Synthetic Metals* 157(24), 1054-1063.
47. Marvin AC, Dawson L, Flintoft ID, Dawson JF. 2009. A Method for the Measurement of Shielding Effectiveness of Planar Samples Requiring No Sample Edge Preparation or Contact. *IEEE Transactions on Electromagnetic Compatibility* 51(2), 255-262.
48. Volski V, Aerts W, Vasylychenko A, Vandenbosch GA. 2006, June. Analysis of Composite Textiles Filled with Arbitrarily Oriented Conducting Fibres Using a Periodic Model for Crossed Strips. In: 11th International Conference on Mathematical Methods in Electromagnetic Theory (58-63). Kharkiv, Ukraine
49. Tezel S, Kavuşturan Y, Vandenbosch GA. 2013, May. Effect of Spandex Yarn on Electromagnetic Shielding Effectiveness of Double Jersey Knitted Fabrics. In: 14th National & 1st International Recent Developments, Textile Technology and Chemistry Symposium (112-13). Bursa, Türkiye.
50. Smirfitt JA. 1965. Worst 1x1 Rib Fabrics Part I Dimensional Properties. *Journal of the Textile Institute Transactions* 56(5), 248-256.
51. Munden DL. 1960. Dimensional Stability of Plain Knit Fabrics. *Journal of the Textile Institute Proceedings* 51(4), 200-209.
52. Volski V, Vandenbosch GA, Vasylychenko A. 2011. A Dedicated Technique to Measure Shielding Effectiveness of Textiles Using A Two Horn Antenna Set-Up. *Journal of the Textile Institute* 102(2), 164-171.
53. Wan C, Jiao Y, Li X, Tian W, Li J, Wu Y. 2020. Multi-dimensional and level-by-level assembly strategy for constructing flexible and sandwich-type nanoheterostructures for high-performance electromagnetic interference shielding. *Nanoscale* 12(5), 3308-3316.
54. Tokarska M, Orpel M. 2019. Study of anisotropic electrical resistance of knitted fabrics. *Textile Research Journal* 89(6), 1073-1083.
55. Liu S, Liu Y, Li L. 2019. The impact of different proportions of knitting elements on the resistive properties of conductive fabrics. *Textile Research Journal* 89(5), 881-890.

- 
56. Liu S, Yang C, Zhao Y, Tao XM, Tong J, Li L. 2016. The impact of float stitches on the resistance of conductive knitted structures. *Textile Research Journal* 86(14), 1455-1473.
57. Basyigit IB, Dogan H, Helhel S. 2019. The effect of aperture shape, angle of incidence and polarization on shielding effectiveness of metallic enclosures. *Journal of Microwave Power and Electromagnetic Energy* 53(2), 115-127.
58. Basyigit IB, Tosun PD, Ozen S, Helhel, S. 2011, August. An affect of the aperture length to aperture width ratio on broadband shielding effectiveness. In: 2011 30th URSI General Assembly and Scientific Symposium (1-4). İstanbul, Türkiye.
59. Bedeloglu A, Sunter N, Yildirim B, Bozkurt Y. 2012. Bending and tensile properties of cotton/metal wire complex yarns produced for electromagnetic shielding and conductivity applications. *Journal of the Textile Institute* 103(12), 1304-1311.



# The Effect of Fabric Structure and Ultrasonic Welding Process on the Performance of the Spunlace Surgical Gowns

Esra Zeynep Yıldız 0000-0001-6143-8768

Ege University/ Emel Akin Vocational Training School/ Ege University Emel Akin Vocational Training School 35100 Izmir/TURKEY

**Corresponding Author:** Esra Zeynep Yıldız, esra.zeynep.yildiz@ege.edu.tr

## ABSTRACT

This study investigates the effects of fabric properties and ultrasonic welding on the performance of surgical gowns. For this purpose, eight spunlace fabrics with different structural properties were provided. 100% polyester, 100% viscose, and their blends were used as test materials. First, the fabrics' thickness, breaking force, elongation at break, air permeability, drape behavior, and surface friction properties were investigated. Then the fabrics were sewn with the ultrasonic sewing machine. Afterward, the sewn fabrics' seam strength, air permeability, and drape behavior were tested. The results were statistically evaluated. A detailed comparison was made based on the data obtained. The higher the polyester content in the fabric, the higher the fabric strength, seam strength, and air permeability. However, viscose-rich fabrics have a softer feel and are easier to drape compared to polyester fabrics. Moreover, the sewing process leads to a reduction in the air permeability of the fabrics.

## 1. INTRODUCTION

Surgical gowns are the most important part of the surgical clothing system that covers a large part of the body. They have been used for more than a century by doctors and nurses, as protective clothing in the operating room to prevent the transmission of bacteria from patients to surgical staff, thereby reducing the incidence of hospital-acquired infections. In addition to providing protection, it also affects the comfort level of the healthcare personnel and, thus the success of the surgery [1].

The clothing comfort of surgical gowns is an important parameter for the surgical team, which often has to wear the surgical gown for several hours while performing complicated operations in the operating room.

Surgical gowns must have some protective properties. They must be resistant to penetration by blood and other body fluids, depending on their intended use. They should be designed considering liquid repellency, liquid impermeability, air

permeability, and similar properties in mind. They should be tear, puncture, and abrasion-resistant. They should not generate dust or flies or allow them to pass through. They should be soft and flexible, lightweight, and should not cause discomfort during use [1]. They should repel liquids but ventilate the surgeon's extreme body heat. And all of this must be achieved in a cost-effective manner [2].

Surgical gowns are classified as "disposable/single-use" or "reusable/multi-use/multiple." Disposable surgical gowns and drapes are usually made from nonwoven alone or in combination with materials that provide greater protection against liquid penetration (e.g., plastic films). Nonwoven fabrics are made from various forms of natural fibers (wood pulp, cotton) and synthetic fibers (polyester, polyolefin) that can be adjusted to desired properties by specific fiber types, bonding processes, and fabric finishes. There are a variety of nonwoven fabrics of all types, including hydroentangled, bonded, stitched, and laminated

**To cite this article:** Yıldız EZ. 2023. The Effect of Fabric Structure and Ultrasonic Welding Process on the Performance of the Spunlace Surgical Gowns. *Tekstil ve Konfeksiyon*, 33(1), 45-55.

## ARTICLE HISTORY

Received: 23.11.2021

Accepted: 26.05.2022

## KEYWORDS

Surgical gown, nonwoven fabric, spunlace, ultrasonic welding, seam strength, performance



---

nonwovens, which vary in quality depending on the manufacturer's intended use [3, 4]. Nonwoven fabrics are preferred for surgical gowns due to their low cost, lightweight, durability, breathability, low hairiness, and disposability [5]. Moreover, nonwoven fabrics can prevent almost all possible strike-through of blood and body fluids.

It is well known that cellulose-based garments also provide the best fit on human skin. For this reason, spunlace fabric is the most preferred nonwoven structure due to its softness and surface properties.

Spunlace nonwoven fabric, also known as hydroentangled nonwoven fabric, is produced using high-pressure water jets to entangle loose assemblies of fibers and impart strength to the final nonwoven fabric [6]. The essential steps in the production of hydroentangled spunlace nonwoven fabric include [7]: Formation of the precursor web, web entanglement through water jet application, dewatering, drying of the web, and winding.

Hydroentangled fabrics are often used in medical applications due to their relatively high absorbency. Another important criterion for the large-scale use of hydroentangled fabrics in medical applications is the absence of a binder in the fabric, which allows the fabric to be sterilized at high temperatures [7]. Since no binder is required for its production, it also provides a high degree of softness, a flexible handle, a high drape, and volume. These fabrics exhibit good physical and mechanical properties and are therefore considered a promising alternative fabric for the apparel sector. It is reported that the flexural rigidity and surface properties of spunlace fabrics are superior to those of other nonwovens, while the structural rigidity is comparable to these products. Due to these properties, spunlace fabrics are used as bacteria-proof garments, cleanroom garments, wet wipes, and interlinings [8].

The most common and conventional method of joining these functional garments is sewing with needle and thread. However, conventional seams have small needle holes, and the perforations caused by a conventional seam compromise the integrity and performance of the garment [9]. Ultrasonic sewing is preferred over other conventional sewing methods in the manufacture of nonwoven-based products. The main reason is that the structure of nonwoven fabrics is more suitable for ultrasonic sewing [10].

Ultrasonic is defined as sound waves that cannot be heard by the human ear or at frequencies above about 20 kHz. The ultrasonic bonding mechanism is a physical process that uses mechanical vibrations to soften or melt a thermoplastic material at the joint line [11, 12]. It is an advanced technique for joining synthetic materials and blends to produce continuous and impermeable seams. Fabrics may be 100% synthetic (thermoplastic) or blends with up to 40% natural fiber content [13]. This process can be used to weld materials such as nylon, polyester, polyethylene, polypropylene, urethanes, and

polyvinylchloride producing continuous, smooth, durable, and impermeable seams. Welding takes place as a result of the high-frequency mechanical motion of the vibrating horn and compression between the horn and the anvil [14].

Ultrasonic welding has the advantage of low energy consumption, eliminating the costs associated with the needles and threads as in conventional sewing methods. Worldwide usage of welding is still increasing, and its use is expected to grow further due to its economic advantages, as well as environmentally friendly, fast, and clean process conditions. Moreover, variable seam widths and welding of several layers can be achieved and the needle holes in conventional stitched seams are eliminated in the ultrasonic welding method [14].

The mechanical, physical, and comfort properties of spunlace fabrics have been investigated by various researchers. Zhou and Zhang (2012) compared the absorbency rate, water-vapor transmission rate, and diffusion area in a solution of three different polyester/viscose spunlaced nonwoven fabrics [15]. Jain et al. (2019) studied the effect of fiber type, mass per unit area, and the number of cycles on the compressional and recovery behavior of spunlace fabrics [8]. Maiti et al. (2020) investigated the effects of the type of fiber, blend ratio, and process parameters like jet pressure on air permeability, mass per unit area, thickness, liquid absorbency time, liquid absorptive capacity, and tensile strength [16].

The effects of ultrasonic welding parameters on the performance of nonwoven fabrics have been studied by various researchers. Kayar (2014) discussed the ultrasonic seam strength and elongation at the break of thermally bonded nonwoven fabrics. Also, the effects of fiber type, fabric area density, and roller type on the tensile properties of nonwovens were reported [10]. Seram and Cabon (2013) investigated the possibility of constructing different types of seams for apparel using ultrasonic technology [17]. Jevnik et al. (2017) studied the effects of ultrasonic welding parameters on bond strength, seam, and thickness of the inner part of sports shoes [11]. Boz and Küçük (2021) analyzed the performance of ultrasonic welding in terms of air permeability, water resistance, and bursting strength. For this purpose, nonwoven fabrics with different production methods and masses were compared [18]. Yildiz et al. (2017) investigated the seam tensile properties of ultrasonically bonded nonwoven fabrics and studied the effects of the fabric type, roller type, and sewing speed on the seam tensile properties of the samples [19]. Eryürük et al. (2017) analyzed the bond strength and permeability properties of ultrasonically welded nonwoven fabrics and compare them with traditional sewing techniques [14]. Nguyen et al. (2020) considered the influence of the roller type on the formation of welding joints and their mechanical properties, different roller profiles were designed, fabricated, and tested [20].

This study investigates the effects of fabric properties and ultrasonic welding on the performance of surgical gowns. For this purpose, spunlace fabrics with different materials, blend ratios and masses, commonly used for surgical gowns, are investigated for their mechanical properties and comfort properties before and after ultrasonic welding.

## 2. MATERIAL AND METHOD

### 2.1 Material

Eight spunlace fabrics with different materials, blend ratios (100% polyester, 100% viscose, and their blends), and masses, commonly used for manufacturing surgical gowns, were used to investigate the performance, as listed in Table 1.

Spunlace nonwoven samples were supplied from Mogul Tekstil. The fabrics were produced from polyester (PES) with a fineness of 1.5 denier and a fiber length of 38 mm, and viscose (CV) with a fineness of 1.5 denier and a fiber

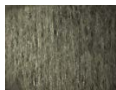





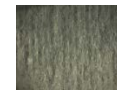
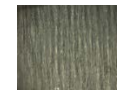








length of 38 mm. All specimens were produced in parallel directions and had the same flat pattern.

### 2.2 Method

Fabrics were sewn using Pfaff 8310 Seamsonic ultrasonic sewing machine (Figure 1a), and ultrasonic sewing was performed using 4 mm pointed engraving roller (Figure 1b). The amplitude and the distance between the horn and the roller were kept constant. The specimens were joined at a speed of 20 dm/min in the machine direction (MD) and cross direction (CD). CD refers to the widthwise of the machine, while MD refers to the lengthwise direction of the produced fabric [21]. The sewn fabric images were given in Figure 2.

As mentioned above, the ultrasonic sewing machine can join fabrics made of 100% synthetics (thermoplastic) or blended fabrics with up to 40% natural fiber content. For this reason, ultrasonic sewing was not applied to fabrics S4, S5, and S6.

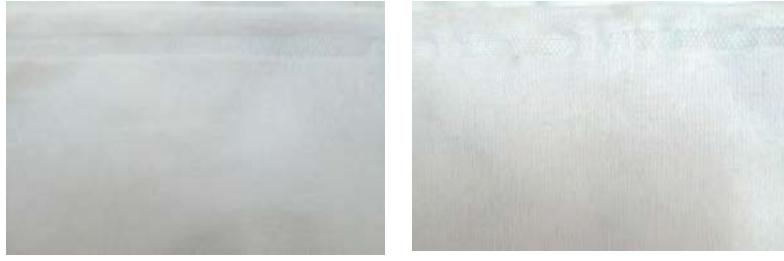
**Table 1.** Properties of spunlace fabrics

	<i>S1</i>	<i>S2</i>	<i>S3</i>	<i>S4</i>	<i>S5</i>	<i>S6</i>	<i>S7</i>	<i>S8</i>
<b>Material</b>	100% PES	70% PES - 30% CV	50% PES - 50% CV	30% PES - 70% CV	100% CV	100% CV	100% PES	100% PES
<b>Fabric weight (g/m<sup>2</sup>)</b>	50	50	50	50	50	70	70	100
<b>Thickness (mm)</b>	37,20	49,00	37,60	40,80	36,00	41,80	49,80	63,60
<b>Microscopic images (machine direction)<sup>a</sup></b>								
<b>Microscopic images (cross direction)<sup>a</sup></b>								

Note: <sup>a</sup> Images of the fabrics were taken at 6.4× magnification using a Leica light microscope



**Figure 1.** (a) Pfaff 8310 Seamsonic Ultrasonic Sewing Machine, (b) The roller



**Figure 2.** The images of sewn samples (S7) (a) parallel to MD, (b) vertical to MD

The thickness, breaking strength, air permeability, drape behavior, and surface friction properties of the unsewn fabrics and the seam strength, air permeability, and drape behavior of the sewn fabrics were tested. The specimens with and without seams were conditioned for 24 hours under standard atmosphere conditions ( $20^{\circ}\text{C} \pm 2^{\circ}\text{C}$  temperature,  $65\% \pm 4\%$  RH) before testing.

The thickness values were measured with the SDL ATLAS Digital Thickness Gauge according to TS 7128 EN ISO 5084 standard. Breaking force and elongation at break tests were performed using a Zwick Roell ZO10 tensile tester in accordance with the standard TS EN ISO 13934-1. The test speed was 100 mm/min, and the gauge length was 20 mm. Specimens were tested in the machine and the cross directions for each fabric type. Seam strength tests were performed in accordance with the standard ISO 13935-2 using a Zwick ZO10 tester. The fabrics were cut to a size of  $350 \times 100$  mm, then folded and ultrasonically bonded from 1 cm of the fabric edge. The speed of the instrument was set at 50 mm/min. Air permeability was measured using the FX3300 tester according to TS EN ISO 9237 standard. The air pressure during the tests was 100 Pa, and the test area was  $20 \text{ cm}^2$ . Ten measurements were taken for each specimen.

The fabric drapability test was performed using the Cusick Drape Tester according to TS EN ISO 9073-9. In the drape test, a circular specimen is held concentrically between two smaller horizontal discs and allowed to fold under its weight. A light is shined from underneath the specimen,

and the shadow cast by the fabric is observed [22]. The draped image of the mounted fabric sample is captured by a digital camera mounted above the drape meter. The captured image is transferred to a computer, and the area is calculated in pixel values by the software. The drape coefficient was calculated according to Equation (1). Three measurements were taken for each specimen. The air permeability and drape coefficient of the specimens with seams were measured, as shown in Figure 3.

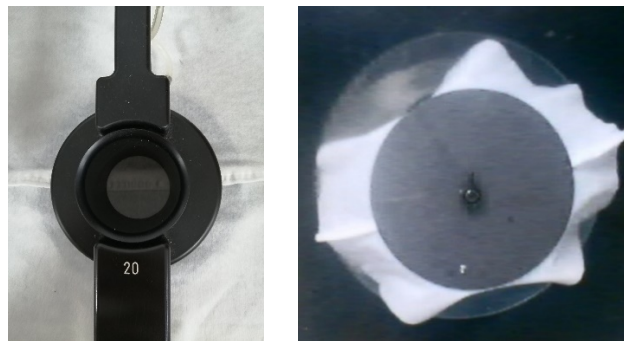
The surface friction properties of the investigated fabrics were measured using the FricTorq instrument with three repetitions and indicated as “friction coefficient ( $\mu_{kin}$ )”. FricTorq is based on a method for measuring the coefficient of friction of the fabrics using a rotational principle and thus measures the torque [23-25].

The statistical software SPSS was used to analyze the test results. ANOVA and Student-Newman-Keuls tests were performed to determine whether the effect of material type, blend ratio, and weight on the measured properties was statistically significant at the 95% confidence level ( $p < 0,05$ ).

### 3. RESULTS AND DISCUSSION

The statistical results in terms of p-values are shown in Table 2. For the Student-Newman-Keuls test, the mean values are indicated by letters. All values marked with the same letter are not significantly different (“a” represents the lowest value and “f” the highest value).

$$\text{Drape Coefficient (\%)} = \frac{\text{Area under the draped sample} - \text{Area of supported disk}}{\text{Area of the specimen} - \text{Area of supported disk}} \times 100 \quad (1)$$



**Figure 3.** The measurement of welded specimens (a) The air permeability measurement (b) The drape coefficient measurement

**Table 2.** Statistical analysis results

Parameters		p-value	Value	Parameters		p-value	Value		
<b>Breaking force - MD</b>	S5	0,000*	53,7597 a	<b>Breaking force - CD</b>	S5	0,000*	15,3800 a		
	S4		69,6367 ab		S4		17,0633 a		
	S3		84,7433 b		S3		20,1100 a		
	S2		85,6467 b		S2		27,2733 b		
	S6		120,9567 c		S6		32,0667 bc		
	S1		152,5900 d		S7		36,1967 c		
	S7		219,6333 e		S1		38,2600 c		
	S8		513,0867 f		S8		76,8200 d		
<b>Elongation at break - MD</b>	5	0,000*	15,5867 a	<b>Elongation at break - CD</b>	6	0,000*	54,7633 a		
	6		18,3100 a		4		57,3000 a		
	4		22,0167 b		5		58,0867 a		
	8		26,1700 c		3		84,3300 b		
	3		27,3633 c		2		85,8067 b		
	2		35,8200 d		8		90,6200 bc		
	1		44,2567 e		7		102,1200 c		
	7		46,3633 e		1		104,1733 c		
<b>Air permeability - fabric</b>	8	0,000*	715,20 a	<b>Drape coefficient</b>	4	0,000*	22,9699 a		
	6		751,80 a		5		23,5526 a		
	7		1174,00 b		3		32,4105 b		
	5		1464,00 c		2		34,2138 bc		
	4		1668,00 d		1		34,8256 bc		
	3		1742,00 d		6		35,4638 bc		
	1		1840,00 e		7		36,4096 c		
	2		1990,00 f		8		46,6210 d		
<b>Drape coefficient – sewn parallel to MD</b>	3	0,000*	34,88 a	<b>Drape coefficient - sewn parallel to CD</b>	3	0,000*	27,80 a		
	2		36,06 ab		2		29,89 b		
	1		37,70 b		1		30,09 b		
	7		38,04 b		7		31,30 b		
	8		47,90 c		8		42,24 c		
<b>Seam strength – sewn parallel to MD</b>	3	0,000*	22,5100 a	<b>Seam strength - sewn parallel to CD</b>	3	0,000*	26,9900 a		
	2		30,6167 b		2		45,1600 b		
	1		45,1500 c		1		56,3200 c		
	7		59,7267 d		7		99,8900 d		
	8		114,7467 e		8		142,7400 e		
<b>Coefficient of friction</b>	6	0,000*	0,3834 a	<b>Air permeability - sewn samples</b>	8	0,000*	514,40 a		
	4		0,4190 ab		7		992,80 b		
	5		0,4209 ab		3		1224,00 c		
	8		0,4455 b		2		1306,00 c		
	3		0,4998 c		1		1450,00 d		
	7		0,5055 c		*Statistically significant (p<0,05).				
	2		0,5264 c						
	1		0,5355 c						

**3.1 Breaking Force and Elongation at Break**

The average breaking force values against the blend ratio in the machine and the cross directions of the fabric specimens are shown in Figure 4.

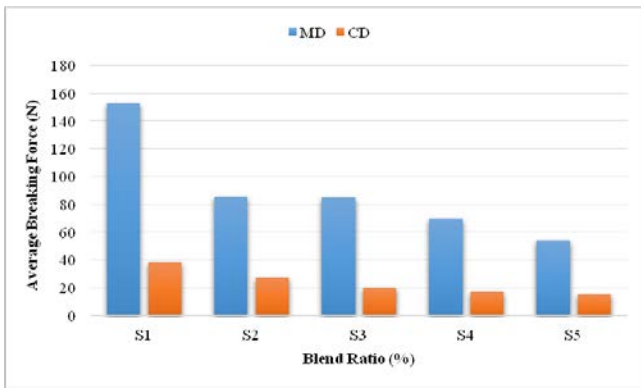
The breaking force of MD is always higher than that of CD for all samples, and the difference between the values is statistically significant (p=0,000). It agrees with earlier work by other researchers [26-28]. This is because the fabrics are composed of staple fibers and the fibers are aligned in MD so because of less number of fibers in the cross direction region, the developed fabric exhibited lower tensile strength in CD [29]. Also, Zhao et al. (2020) found that this is a typical effect caused by the carding process, in which most of the fibers are laid parallel at MD [30].

Moreover, it is also noticeable that the fabric strength increases in both directions as the blend ratio of polyester

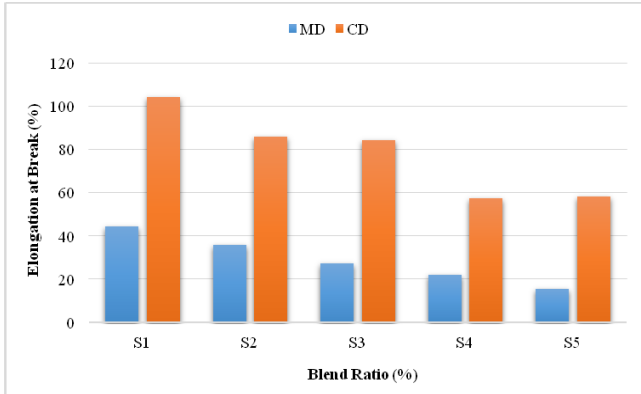
fibers increases in the range of 0 to 100%. On the contrary, as the proportion of viscose fibers increases, the fabric strength decreases. This is due to the higher breaking strength of polyester fibers compared to viscose fibers used in sample preparation.

The effects of the blend ratio on the elongation at break are shown in Figure 5. The figure clearly shows that the elongation at break is higher for CD than for MD, and the difference between the values is statistically significant (p=0,000). Since the webs were laid in parallel, the low elongation in MD and the higher elongation in CD are due to the predominant orientation of the MD fiber segment orientations in the parallel-laid web [31]. The figure also shows that the elongation at break increases with increasing polyester fiber content in both directions.

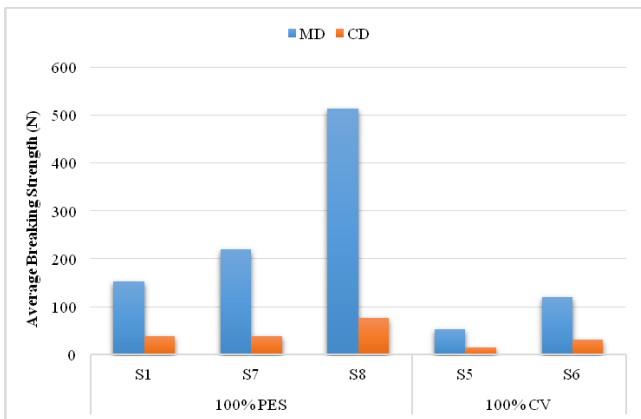
The effects of fabric weight on the breaking force and elongation at break are shown in Figures 6 and 7.



**Figure 4.** Effect of blend ratio on breaking force in machine and cross directions



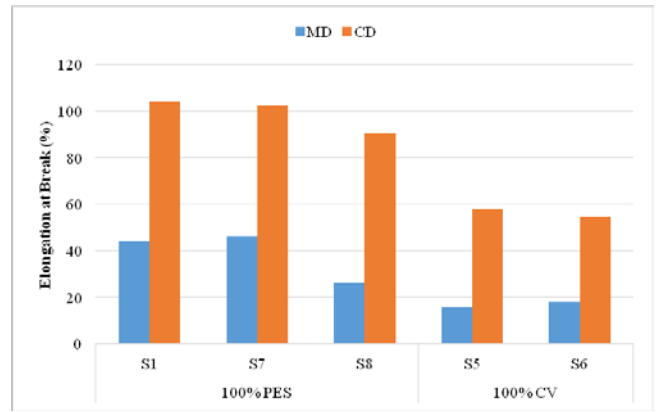
**Figure 5.** Effect of blend ratio on elongation at break in machine and cross directions



**Figure 6.** Effect of fabric weight on breaking force in machine and cross directions

Figure 6 shows that the breaking force values increase with increasing fabric weight for both fiber types. Polyester-containing fabrics have higher values than viscose-containing fabrics for the same weight. Moreover, the breaking force values in MD are always higher than those of CD for all samples, as explained above.

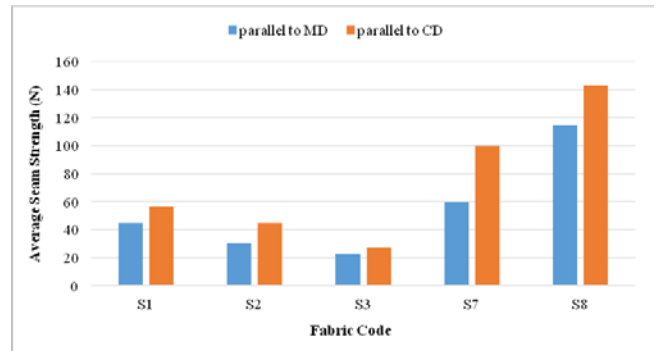
As shown in Figure 7, the elongation at break in MD increases as the weight increases from 50 to 70 g/m<sup>2</sup>. However, as it increases further from 70 to 100 g/m<sup>2</sup>, it begins to decrease. For CD, the elongation at break decreases with increasing weight.



**Figure 7.** Effect of fabric weight on elongation at break in machine and cross directions

### 3.2 Seam Strength

The average seam strength values in the machine and the cross directions of the fabric samples are shown in Figure 8.



**Figure 8.** Effects of blend ratio and fabric weight on seam strength

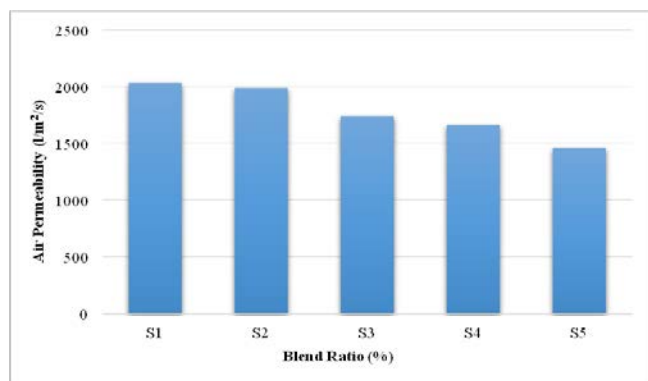
As shown in Figure 8, the highest seam strength value is measured at S8 and the lowest at S3 in both directions. The analysis shows that there is a statistically significant difference between the seam strength of fabrics. The seam strength of fabrics increases as the ratio of polyester in a blend increases, indicating that polyester-rich fabrics have a more durable structure than viscose-rich fabrics. It can also be noted that seam strength is directly proportional to the fabric weight in both directions. That is, the heavier the fabric, the greater the seam strength. A higher fabric weight provides more resistance to seam breakage, resulting in higher seam strength.

In general, seam strength is higher for specimens sewn parallel to the cross direction than for specimens sewn parallel to the machine direction. The term seam parallel to the machine and cross directions refers to the condition that the seam is formed in the corresponding direction and the load is applied perpendicular to the seam line. The extensibility of nonwoven fabrics is lower in the MD and higher in the CD. Since the extensibility is higher in the

CD, the seam zone reaches the elongation limit in a shorter time and results in lower strength values.

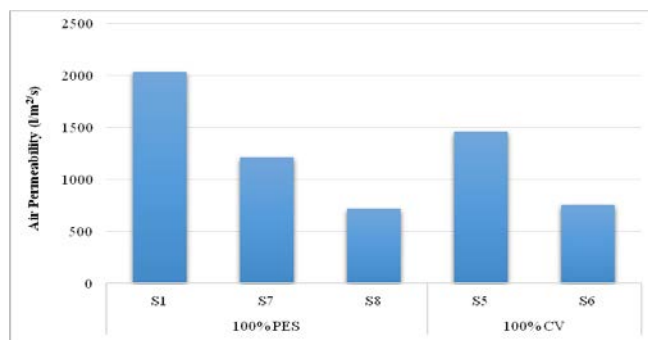
### 3.3 Air Permeability

Air permeability is a measure of the airflow that can be maintained through a material at a specified pressure. It provides information about the breathability and comfort of the fabric [32]. The effects of blend ratio and fabric weight on the air permeability of unsewn samples are shown in Figures 9 and 10.



**Figure 9.** Effect of blend ratio on air permeability of unsewn samples

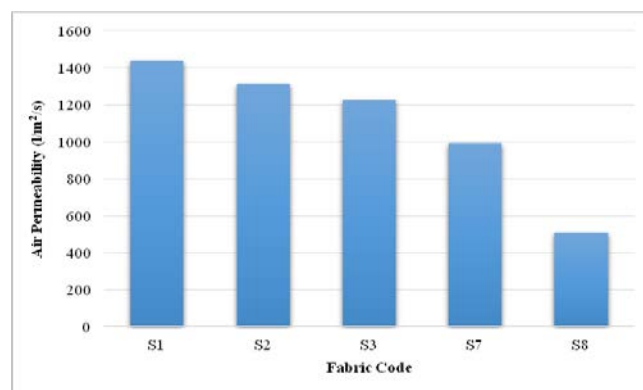
Increasing the polyester content leads to an increase in the air permeability of spunlace samples, while the trend is reversed for viscose-rich fabrics. Polyester-containing fabrics have higher values than those with viscose for the same weight (Figure 9). This phenomenon can be attributed to the crimp factor of the fibers, as found by Maiti et al. (2021). It can be concluded that polyester fibers with higher crimp, compared to 100% viscose fibers, result in more voluminous webs, thus increasing air permeability [33]. Moreover, due to the high bending rigidity and low packing density of polyester, viscose-rich fabrics also have a more compact structure than polyester fabrics with the same density [34].



**Figure 10.** Effect of fabric weight on air permeability of unsewn samples

As shown in Figure 10, the air permeability of polyester or viscose nonwoven fabrics decreases with increasing weight. As the weight increases, the number of pores increases with the number of fibers, while the pore size decreases. A higher number of fibers leads to an increase in thickness.

Higher fabric thickness and the greater number of fibers per unit area provide more resistance to airflow, which in turn leads to a decrease in air permeability as the weight of the fabric increases [34-36]. As noted by Zhao et al. (2020), when the weight of the spunlace fabric decreases, the fiber web is thinner, and the pores between the fibers are larger, resulting in high air permeability [37]. This is also consistent with the results of Midha and Mukhopadhyay (2005), and Maduna (2018) [38-39]. As a result, lower air permeability with higher fabric weight makes the garment uncomfortable [36].



**Figure 11.** Effects of blend ratio and fabric weight on air permeability of sewn samples

According to Figures 9-11, the comparison of the sewn and unsewn samples shows that ultrasonic sewing has a significant effect on the air permeability values and reduces the air permeability of the samples compared to the unsewn samples, as indicated by Daukantiene and Vadeike (2018) [40]. The reason for this is the increase in fabric thickness in the seam area. As mentioned in the literature, air permeability decreases with increasing thickness, weight, and fabric density. Thus, the ultrasonic sewing method increases the thickness of the seam area, resulting in lower air permeability.

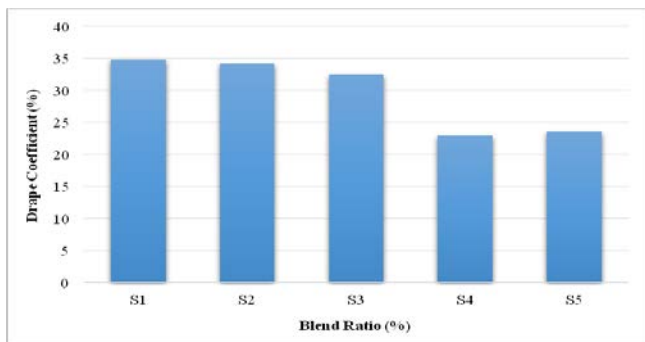
### 3.4 Drape Behavior

Drape is an important component of the esthetic appearance of a garment and plays a critical role in the comfort and fit of the garment [11]. Drape behavior is determined by the drape coefficient. The drape coefficient is the ratio between the projected area of the fabric sample and its undraped area, from which the area of the supporting disk is derived. The higher the drape coefficient, the lower the drapability of the fabric and the stiffer the fabric [41, 42].

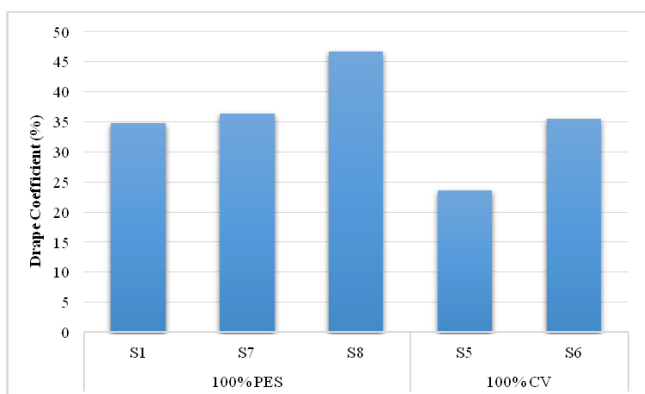
The effects of blend ratio and fabric weight on the drape behavior of unsewn samples are shown in Figures 12 and 13.

As shown in Figure 12, the drape coefficient of the fabrics increased with the increase in the ratio of polyester in a blend, indicating that polyester-rich fabrics have a stiffer structure than viscose-rich fabrics. This can be explained by

the high bending rigidity of polyester fibers compared to viscose fibers.



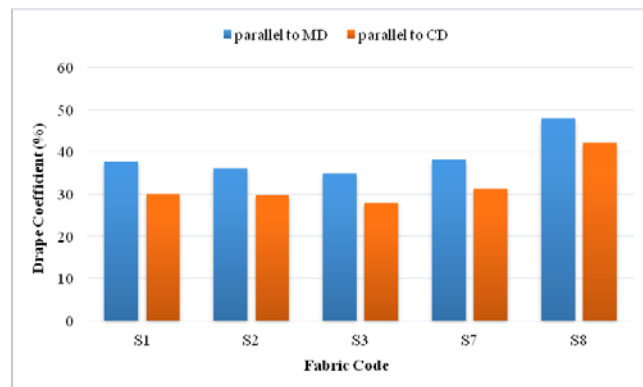
**Figure 12.** Effect of blend ratio on drape coefficient of unsewn samples



**Figure 13.** Effect of fabric weight on drape coefficient of unsewn samples

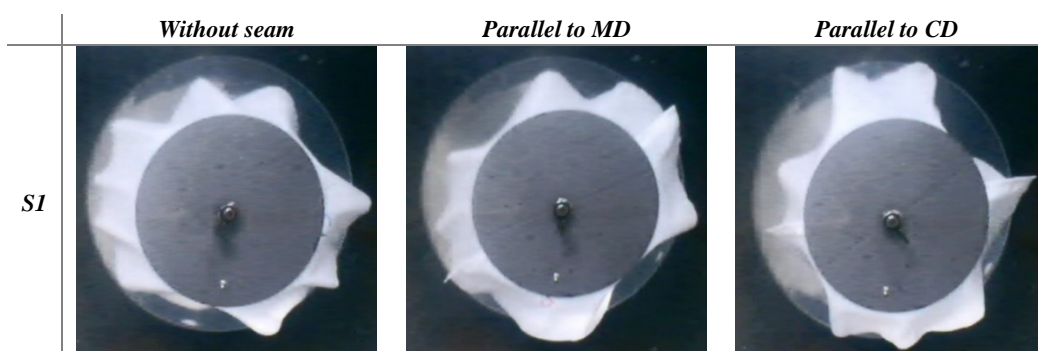
As shown in Figure 13, the drape coefficient value of polyester and viscose nonwoven fabrics increases with increasing weight. This is due to the rise in fabric tightness, as stated by Eryürük et al. (2019) [43].

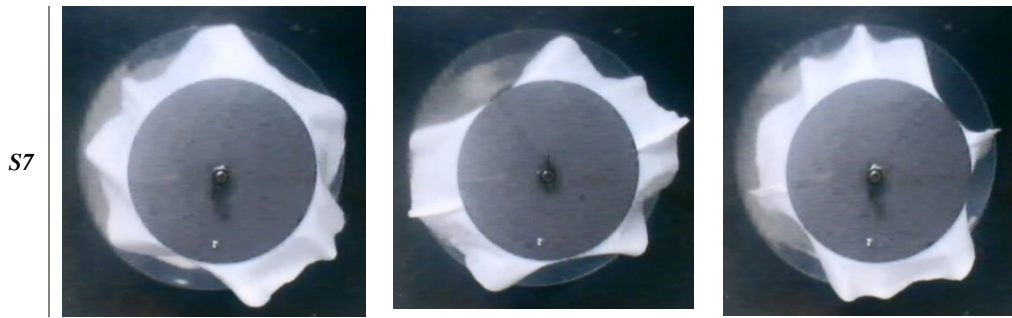
To investigate the effects of sewing and sewing direction, the fabric samples were sewn parallel and perpendicular to the machine direction. The effects of blend ratio and fabric weight on the drape coefficient of the sewn pieces are shown in Figure 14. Also, Figure 15 shows the comparison between drape coefficients of draped samples with and without seams.



**Figure 14.** Effects of blend ratio and fabric weight on drape coefficient of sewn samples

While the highest drape coefficient results were obtained for the seams parallel to MD, the values for the unsewn fabrics were lower than MD and above CD. A sewn fabric is not a single piece of fabric but consists of two joined pieces of the same fabric. Due to the greater mass concentration in the seam area, sewing leads to an increase in fabric stiffness [11, 44]. As a result, sewing operations increase the drape coefficient of fabrics. This means that sewing operations lead to a reduction in the drape of fabrics.



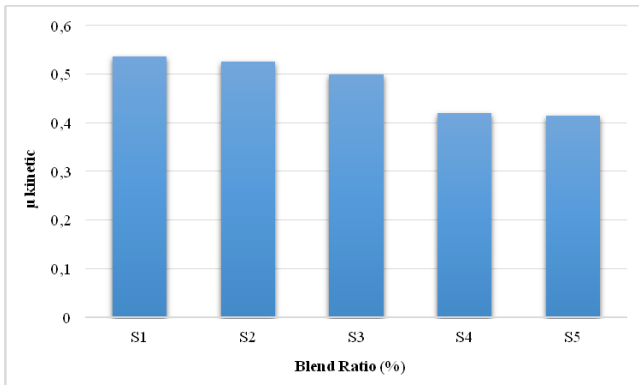


**Figure 15.** The comparison between drupe coefficients of draped samples with and without seams

Moreover, the drupe coefficient of the samples sewn parallel to MD is higher than the drupe coefficient of the fabrics sewn parallel to CD. This is because the fibers are more aligned and more tightly entangled in the machine direction. This restricts the movement of fibers in the machine direction, resulting in a higher drupe coefficient in this direction.

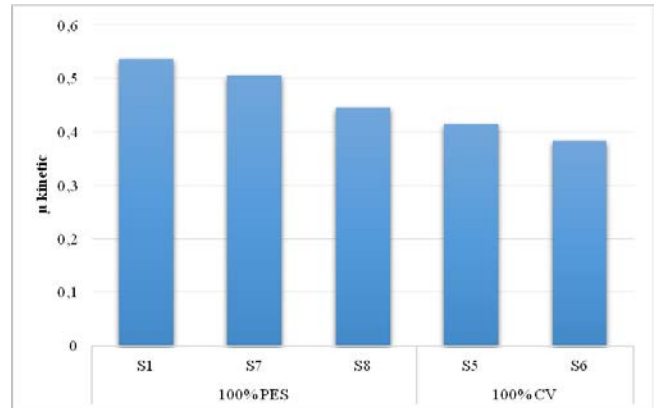
### 3.5 Coefficient of Friction

The physical properties of fabrics directly affect the handling properties of the garments made from them. Therefore, fabrics with a lower coefficient of kinetic friction have better handling properties [45]. The coefficient of friction results against the blend ratio is shown in Figure 16.



**Figure 16.** Effect of blend ratio on coefficient of kinetic friction

According to the test results shown in Figure 16, the kinetic friction coefficients of blended fabrics with higher viscose content are lower than those of fabrics with higher polyester fiber content. It can be concluded that viscose fabrics have a softer handle when compared to polyester fabrics.



**Figure 17.** Effect of fabric weight on coefficient of kinetic friction

As can be seen from Figure 17, it is found that the coefficient of friction values decreases with increasing weight. As stated by Babaarslan and Avcioglu Kalebek, this can be explained by the fact that the fibers are not uniformly distributed in the low-weight specimens [46]. The test results show that, with increasing weight, the fiber orientation of the nonwovens becomes more stable, and nonwoven fabrics with a more stable structure have a lower coefficient of friction. This result shows that viscose-containing fabrics and heavier fabrics have smoother surfaces and provide a softer feel.

## 4. CONCLUSION

This study investigates the effects of fabric properties and ultrasonic welding on the performance of disposable surgical gowns. For this purpose, eight spunlace fabrics with different structural properties (material and weight) were provided. First, the thickness, breaking force, elongation at break, air permeability, drupe behavior, and surface friction properties of the fabrics were investigated. Then the fabrics were sewn with the ultrasonic sewing machine and the seam strength, air permeability, and drupe behavior of the sewn fabrics were tested. The main results of these analyses are summarized below.

- Specimens cut in the machine direction are significantly stronger and less extensible than specimens cut in the cross direction because of the predominance of fiber orientation in that direction.



- The fabric strength and the seam strength increase in both directions as the blend ratio of polyester fibers and the weight of the fabric increase.
- The higher the polyester content in the fabric, the higher the fabric strength, seam strength, and air permeability. However, polyester-rich fabrics have a stiffer structure than viscose-rich fabrics, and viscose-rich fabrics have a softer handle and are more drapeable compared to polyester-rich fabrics.
- Sewing operations result in a reduction in air permeability of fabrics as fabric thickness increases in the seam area.
- Heavier fabrics are stronger, more durable, have a smoother surface, and provide a softer feel.

Nevertheless, their air permeability values are lower, which can worsen the comfort properties.

- It is recommended to use heavy polyester fabrics in areas where strength is more important, and viscose-containing fabrics in areas where handling is important.


## REFERENCES

- Atay Y, Pamuk O, Boyacı B, Yıldız EZ, Göksel T, Metin DY, Gül S, Devrim G, Topbaş Ö. 2021. A new approach to surgical gowns. In A. Agrawal (Ed.), *Healthcare Access*. IntechOpen, 1-17.
- May-Plumlee T, Pittman A. 2002. Surgical gown requirements capture: A Design Analysis case study *Journal of Textile and Apparel, Technology and Management* 2, 1-10.
- Rutala WA, Weber DJ. 2001. A review of single-use and reusable gowns and drapes in health care. *Infection Control and Hospital Epidemiology* 4, 248-257.
- Abreu MJ, Silva ME, Schacher L, Adolphe D. 2003. Designing surgical clothing and drapes according to the new technical standards. *International Journal of Clothing Science and Technology* 1, 69-74.
- Eryürük SH, Karagüzel Kayaoğlu B, Altay P. 2018. Thermal comfort properties of nonwoven fabrics used in surgical gowns. *IOP Conf. Series: Materials Science and Engineering*, 459, 1-6.
- Wang H, Zhu J, Jin X, Wu H. 2013. A study on the entanglement and high-strength mechanism of spunlaced nonwoven fabric of hydrophilic Pet fibers. *Journal of Engineered Fibers and Fabrics* 8(4), 60-67.
- Chellamani KP, Vignesh Balaji RS, Veerasubramanian D. 2013. Medical textiles: The spunlace process and its application possibilities for hygiene textiles. *Journal of Academia and Industrial Research* 1(12), 735-739.
- Jain RK, Sinha SK, Das A. 2019. Compression characteristics of spunlace nonwoven fabric. *Indian Journal of Fibre & Textile Research* 44, 39-44.
- Jana P. 2011. Assembling technologies for functional garments - An overview. *Indian Journal of Fibre & Textile Research* 36, 380-387.
- Kayar M. 2014. Analysis of ultrasonic seam tensile properties of thermal bonded nonwoven fabrics. *Journal of Engineered Fibers and Fabrics* 9(3), 8-18.
- Jevsnik S, Zunic-Lojen D. 2007. Drape behaviour of seamed fabrics. *Fibers and Polymers* 8(5), 550-557.
- Şevkan Macit A., Tiber B. 2022. Evaluation of some physical performance properties of ultrasonic seaming, conventional seaming and sealing adhesive tape on waterproof polyester knitted fabrics with polyurethane. *Textile Research Journal* 92(3-4), 498-510.
- Shi W, Little T. 2000. Mechanisms of ultrasonic joining of textile materials. *International Journal of Clothing Science and Technology* 12(5), 331-350.
- Eryürük SH, Karagüzel Kayaoğlu B, Kalaoğlu F. 2017. A study on ultrasonic welding of nonwovens used for surgical gowns. *International Journal of Clothing Science and Technology* 29(4), 539-552.
- Zhou Z, Zhang R. 2012. Effect of polyester and viscose content on the performance of spunlaced nonwoven dressings. *Advanced Materials Research* 627, 293-297.
- Maiti S, Bele VS, Basu SK. 2020. Effect of material properties and process parameters on properties of hydroentangled nonwoven fabrics. *The Journal of the Textile Institute* 112(6), 914-920.
- Seram N, Cabon D. 2013. Investigating the possibility of constructing different seam types for clothing using ultrasonic. *International Journal of Clothing Science and Technology* 25(2), 90-98.
- Boz S, Küçük M. 2021. The analysis of the ultrasonic welding performance for the medical protective clothing. *Tekstil ve Konfeksiyon* 31(1), 53-62.
- Yıldız EZ, Pamuk O, Boz S. 2017. An investigation on the seam tensile properties of ultrasonically bonded nonwoven fabrics. *Industria Textila* 68(2), 126-130.
- Nguyen T, Thanh LQ, Loc NH, Huu MN, Van AN. 2020. Effects of different roller profiles on the microstructure and peel strength of the ultrasonic welding joints of nonwoven fabrics. *Applied Sciences* 10(12), 1-12.
- Gürkan Ünal P. 2018. The effect of laying direction on the characteristics of nonwoven fabrics. *European Journal of Engineering and Applied Sciences* 1(2), 59-62.
- Süpüren Mengüç G, Özgüney AT, Dalbaşı ES, Özdil N. 2019. A comparative study on handle properties of bamboo and cotton fabrics. *Industria Textila* 70(3), 278-284.
- Özçelik Kayseri G, Özdil N, Süpüren Mengüç G. 2012. Sensorial comfort of textile materials. In H.Y. Jeon (Ed.), *Woven Fabrics*. Croatia: InTech, 235-266.
- Lima M, Hes L, Vasconcelos R, Martins J. 2005. Friction-accessing fabric friction with a novel fabric surface tester. *Autex Research Journal* 5(4), 194-201.
- Silva LF, Seabra E, Lima M, Vasconcelos R, Alves J, Guise C, Martins D. 2010, July. A successful partnership for the development of a laboratory friction testing apparatus: A project review. *International Conference on Engineering Education Proceedings*, Gliwice, Poland.

- 
26. Zheng H, Seyam AM, Shiffler D. 2003. The impact of input energy on the performance of hydroentangled nonwoven fabrics. *International Nonwovens Journal* 34-44.
27. Wang H, Zhu J, Jin X, Wu H. 2013. A study on the entanglement and high-strength mechanism of spunlaced nonwoven fabric of hydrophilic PET fibers. *Journal of Engineered Fibers and Fabrics* 8(4), 60-67.
28. Niedziela M, Szaśiadek M, Woźniak W. 2022. Pore size, shape and orientation analysis with respect to tensile tests in nonwoven spunlace textiles using image processing. *The Journal of the Textile Institute Advance online publication*. [DOI: 10.1080/00405000.2022.2046302]
29. Cheema SM, Shah T, Anand SC, Soin N. 2018. Development and characterisation of nonwoven fabrics for apparel applications. *Vlakna a Textil* 8(3), 1-7.
30. Zhao Y, Chen R, Ni R, Liu H, Li J, Huang C. 2020. Fabrication and characterization of a novel facial mask substrates based on thermoplastic polyester elastomer fibers. *The Journal of the Textile Institute* 111(8), 1231-1237.
31. Ahmad F, Tausif M, Hassan MZ, Ahmad S, Malik MH. 2018. Mechanical and comfort properties of hydroentangled nonwovens from comber noil. *Journal of Industrial Textiles* 47(8), 2014-2028.
32. Behera BK, Arora H. 2009. Surgical gown: A critical review. *Journal of Industrial Textiles* 38(3), 205-231.
33. Maiti S, Bele VS, Basu SK. 2021. Effect of material properties and process parameters on properties of hydroentangled nonwoven fabrics. *The Journal of the Textile Institute* 112(6), 914-920.
34. Çiñçik E, Koç E. 2012. An analysis on air permeability of polyester/viscose blended needle-punched nonwovens. *Textile Research Journal* 82(5), 430-442.
35. Debnath S, Madhusoothanan M. 2010. Thermal insulation, compression and air permeability of polyester needle-punched nonwoven. *Indian Journal of Fibre & Textile Research* 35, 38-44.
36. Midha VK, Dakuri A, Midha V. 2012. Studies on the properties of nonwoven surgical gowns. *Journal of Industrial Textiles* 43(2), 174-190.
37. Zhao Y, Chen R, Ni R, Liu H, Li J, Huang C. 2020. Fabrication and characterization of a novel facial mask substrates based on thermoplastic polyester elastomer fibers, *The Journal of the Textile Institute* 111(8), 1231-1237.
38. Midha VK, Mukhopadhyay A. 2005. Bulk and physical properties of needle-punched nonwoven fabric. *Indian Journal of Fibre & Textile Research* 30, 218-229.
39. Maduna L. 2018. Development of spunlaced nonwoven filters from PAN, PPS and PI fibres for industrial use (Doctoral dissertation). Nelson Mandela University, South Africa.
40. Daukantiene V, Vadeike G. 2018. Evaluation of the air permeability of elastic knitted fabrics and their assemblies. *International Journal of Clothing Science and Technology* 30(6), 839-853.
41. Li Y, Dai XQ. 2006. Fabrics. *Biomechanical Engineering of Textiles and Clothing* 199-222.
42. Matusiak M. 2017. Influence of the structural parameters of woven fabrics on their drapeability. *Fibres & Textiles in Eastern Europe* 25 1(121), 56-64.
43. Eryürük SH, Kuşun Bahadır S, Sarçam C, Kalaoglu F. 2019. The effects of finishing processes on the dynamic drape of wool fabrics. *International Journal of Clothing Science and Technology* 31(2), 195-206.
44. Sharma KR, Behera BK, Roedel H, Schwnk A. 2005. Effect of sewing and fusing of interlining on drape behaviour of suiting fabrics. *International Journal of Clothing Science and Technology* 17(2), 75-90.
45. Yüksekaya ME, Celep G, Doğan G, Tercan M, Urhan B. 2016. A comparative study of physical properties of yarns and fabrics produced from virgin and recycled fibers. *Journal of Engineered Fibers and Fabrics* 11(2), 68-76.
46. Babaarslan O, Avcioğlu Kalebek N. 2010. Effect of weight and applied force on the friction coefficient of the spunbond nonwoven fabrics. *Fibers and Polymers* 11(2), 277-284.

# Performance Evaluation of Newly Designed Disposable Surgical Gowns

Selin Hanife Eryürük<sup>1</sup>  0000-0002-9576-3101

Burçak Karagüzel Kayaoğlu<sup>1</sup>  0000-0002-1974-9615

Pelin Altay<sup>1</sup>  0000-0001-7888-9477

<sup>1</sup>Textile Engineering Department, Faculty of Textile Technologies and Design, Istanbul Technical University, Istanbul, Türkiye

**Corresponding Author:** Selin Hanife ERYÜRÜK, eryuruk@itu.edu.tr

## ABSTRACT

Surgical gowns are used as protective clothing in operating room for medical personnel and patients to minimize the transmission of viruses and pathogens, and are designed to serve as a barrier against non-sterile area and to reduce the risk of infections. In this study, since disposable gowns provide better barrier effect compared to reusable ones, surgical gowns designed using nonwoven fabric and membrane-nonwoven combination were investigated in terms of their performance characteristics and thermal comfort properties. Functional properties of produced disposable surgical gowns such as tensile strength, tear strength, resistance to water penetration, air permeability, thermal properties, water vapor permeability and water vapor resistance were tested and statistically evaluated. Results show that SMS fabrics have higher tear strength than that of PP and PE fabrics, and welding method provides higher seam strength than that of ultrasonic one. Membrane reinforcement was found to be required for both PP and SMS fabrics, especially in areas that may be exposed to fluid passage. SMS fabrics have higher air permeability values than that of PP fabrics leading to improved comfort of the wearer. Membrane reinforcement caused an increase in thermal conductivity, thermal resistance, thermal diffusion, thermal absorption and water vapor resistance values. Considering the performance and comfort requirements of the wearer, SMS nonwoven fabric, and membrane reinforcement in areas where there is a possibility of exposure to body fluids was the most suitable model.

## 1. INTRODUCTION

Surgical gowns are used in the operating room to prevent transfer of microorganisms and body fluids from medical personnel to patient and also from patient to personnel. These gowns should be impervious to blood, liquids, and other infectious material. Current surgical gowns can be categorized as either reusable or disposable. The disposable surgical gowns are generally produced from nonwoven fabric. They should provide protection against body liquids and microorganisms with adequate level of comfort. Triple layer fabrics are generally used for surgical gown to meet desired requirements. Triple layer covers an outer layer resisting abrasion and tearing, middle layer providing barrier resistance to fluid penetration, soft bottom layer improving

comfort. However, surgical gown usually has a chemical finish to further protective properties, and most likely areas to be exposed to body fluids should be reinforced with an extra layer. However, medical personnel feel less comfortable when wearing reinforced gown due to the less heat transfer leading to more sweating [1-6].

Thermal comfort is a critical product requirement, especially for prolonged operations. Thermophysiological comfort is associated with thermal balance of the human body and the body internal temperature must be kept constant at 37 °C. Any minor deficiency of comfort may have an adverse effect on the quality of work and safety. Even 5 °C changes in body temperature may result in fatal consequences such as hypothermia or hyperthermia [7].

**To cite this article:** Eryürük SH, Karagüzel Kayaoğlu B, Altay P. 2023. Performance Evaluation of Newly Designed Disposable Surgical Gowns. *Tekstil ve Konfeksiyon* 33(1), 56-67.

## ARTICLE HISTORY

Received: 05.08.2021

Accepted: 21.10.2022

## KEYWORDS

Protective textile, surgical gown, thermal comfort, water vapour permeability

---

Since thermophysiological comfort is directly related to human physiology, its analysis is of great importance in textile applications, where there is an interaction between the textile material and human body. Therefore, the comfort of the person is a vital factor in evaluating the performance of the garment, as well as its protective performance. Thermophysiological clothing comfort depends on the heat and moisture transport properties of the garment that provide the body's heat balance [8-9]. In the literature, parameters affecting thermophysiological comfort are given as personal features, environmental features and clothing features [10-17]. Major clothing properties affecting thermal comfort include thermal conductivity, water vapor permeability, air permeability and water impermeability [2]. In addition, surgical gowns should allow freedom of movement, be lightweight and have adequate tensile strength.

To date, there is limited number of studies on the thermal comfort properties of nonwoven surgical gowns [18-22]. Pamuk et al. evaluated thermal comfort properties of different disposable surgical gowns (Spunlace normal, Spunlace reinforced and SMS normal) using the thermal manikin [18]. Woo et al. developed a theoretical model that provides thermal conductivity estimation for nonwoven fabrics. They measured the thermal conductivity of various nonwoven barrier fabrics for the designed model [19]. Issa et al. analyzed some of the thermal properties of disposable surgical gowns before and after different sterilization methods by evaluating the effects of sterilization on thermal comfort [20]. They concluded that disposable materials (laminated, nonwoven, PE) used in the hospital are affected by the sterilization process. Bogdan et al. examined the thermal insulation of modern materials used in the production of medical clothing and the thermal comfort properties of surgical clothing [21]. They stated that medical clothes made of modern materials lead to the risk of thermal stress. Aslan et al. investigated the comfort and microbial protection performances of two types of disposable and two types of reusable surgical gowns [22]. They found that the microfiber polyester woven gown has good thermal comfort performance.

The aim of this paper is to present comprehensive research to design a surgical gown considering the constructional and technological requirements of wearer. Three different types of polypropylene-based nonwoven fabric (a spunbond, a spunbond/meltblown/spunbond and a polyethylene coated nonwoven fabric) with different unit weights were used for surgical gown design. Differently from current literature, the regions that may be exposed to fluid passage were determined and their resistance to fluid transmission was improved by membrane integration. Secondly, nonwoven fabrics and nonwoven-membrane combinations were joined using new welding techniques including ultrasonic and hot air welding method. The performance of nonwoven fabrics and nonwoven-membrane combinations were extensively investigated in

terms of thermal comfort, water vapor permeability, water permeability resistance, air permeability, and tensile strength. The findings of this study will provide a number of practical implications for designing a surgical gown considering wearer's comfort as well as protection.

## 2. MATERIALS AND METHODS

### 2.1 Material

Since disposable gowns provide better barrier effect compared to reusable gowns, surgical gowns produced using polypropylene-based nonwoven fabrics were investigated. The nonwoven fabrics used in this study were supplied from Mogul Tekstil (Turkey), which is a key supplier of meltblown and meltblown/spunbond fabrics globally. Since fabric unit weight is one of the most important factors determining thermal comfort [23], three different types of polypropylene-based nonwoven fabric with different unit weights were used for surgical gown design. Polyurethane membrane (85 g/m<sup>2</sup>) was used as a reinforcement for resistance to fluid transmission and integrated to nonwoven fabrics. The nonwoven fabrics used are as following:

1. 100% polypropylene based spunbond nonwoven fabric (PP)
2. 100% polypropylene based spunbond/meltblown/spunbond nonwoven fabric (SMS)
3. Polyethylene coated 100% polypropylene based spunbond nonwoven fabric (PE-coated nonwoven)

The technical properties of the fabrics were given in Table 1.

### 2.2 Methods

#### Production of the samples

Ultrasonic and hot air welding methods were used for the production of surgical gown. High frequency vibrations are used to bond two or more material layers in the ultrasonic welding method by means of a rapid heat increase inside the material. Ultrasonic welding machine parameters have a critical importance on the joint strength of fabric layers. Teksmak ultrasonic welding machine was used at a pressure of 2.2 bar, 2 m/min and 10 mm distance. Pfaff hot air welding sewing machine was used as an alternative method to the ultrasonic one in the regions where liquid impermeability is required and cannot be joined with ultrasonic welding method. Pfaff hot air welding sewing machine parameters are used as 355 °C temperature, 3 m/min velocity and 3.3 bar pressure. The parameters were kept constant for all samples.

**Table 1.** Properties of nonwoven fabrics used in this study

Sample codes	Mass per unit area (g/cm <sup>2</sup> )	Thickness (mm)
SMS 35	35	0.33
SMS 50	50	0.37
SMS 60	60	0.42
SMS 80	80	0.45
SMS 90	90	0.50
PP 30	30	0.28
PP 50	50	0.38
PP 60	60	0.44
PP 70	70	0.48
PP 80	80	0.51
PP105	105	0.61
PP110	110	0.63
PE-coated nonwoven	35	0.15
PE-coated nonwoven	80	0.28
PE-coated nonwoven	100	0.38

In order to improve the resistance to fluid transmission, polyurethane membrane (85 g/m<sup>2</sup>) was used as a reinforcement and integrated to nonwoven fabrics. PE-coated nonwoven fabric covers an absorbent inner layer made from spunbond and an outer layer made from a polyethylene material with a barrier effect against bacteria and fluid transmission. Since it is impervious to water, no membrane reinforcement is required for this type of fabrics. For this reason, membrane integration was only applied for PP and SMS fabrics. Two nonwoven fabrics were joined at the side seams using ultrasonic welding while hot air welding was used to join membrane-nonwoven combinations.

#### Performance evaluation of the samples

All nonwoven samples were tested for tensile and tear strength, water permeability resistance (hydrostatic pressure tester), air permeability tests. Tensile and tear strength tests were carried out using Titan James Heal Universal Strength Tester in accordance with the standard of TS EN ISO 13934-1 and TS EN ISO 13937-2, respectively. The hydrostatic pressure tester (M023B) was used to evaluate the seam's resistance to water penetration and resistance of the samples to water penetration according to TS 257

EN 20811 and ISO 811:2018, respectively. Air permeability test was carried out using Prowhite air permeability tester according to the standards of TS 391 EN ISO 9237. Seam strength of the samples was measured for both ultrasonic and hot air welding techniques using Titan James Heal Universal Strength Tester according to the standard of TS 1619-2 EN ISO 13935-2.

Nonwoven samples (SMS, PP and PE coated fabrics) and nonwoven samples reinforced with membrane (SMS + Membrane and PP + Membrane fabric) were evaluated in terms of thermal comfort properties, water vapor permeability and water vapor resistance. Thermal properties of the samples including thermal conductivity ( $\lambda$ ), thermal absorptivity (b), thermal diffusion (a), thermal resistance (R) were measured by using Alambeta device according to standard of TS EN ISO 11092. Water vapor permeability and water vapour resistance of the samples were tested using Permetest tester (Skin model) according to TS EN ISO 11092.

Relative thermal comfort index (RTCI) of the samples was calculated to evaluate their capability to ensure comfort for winter clothing using the following formula [24]:

$$RTCI = \sum_{i=1}^n \left( a_{xi} * \frac{Xi - XiminIG}{Xi} \right) + \sum_{j=1}^m \left( a_{zj} * \frac{Zjmax - Zj}{ZjmaxIG} \right)$$

**RTCI** – Relative thermal comfort index

**Xi** – The value of i<sup>th</sup> parameter, which results in an improvement of thermal comfort when increased, where i = 1, 2, ..., n,

**ximinIG** – minimum value of i<sup>th</sup> parameter needed to ensure thermal comfort,

$z_j$  – the value of  $j$ th parameter, which results in a deterioration in thermal comfort when increased, where  $j = 1, 2, \dots, m$ ,  
 $z_{jmaxIG}$  – maximum value of  $j$ th parameter, which is acceptable from the point of view of thermal comfort

Experimental design for all tests has been given in Table 2. All tests have been repeated for five times and the average was taken as a result.

**Table 2.** Experimental design of all tests

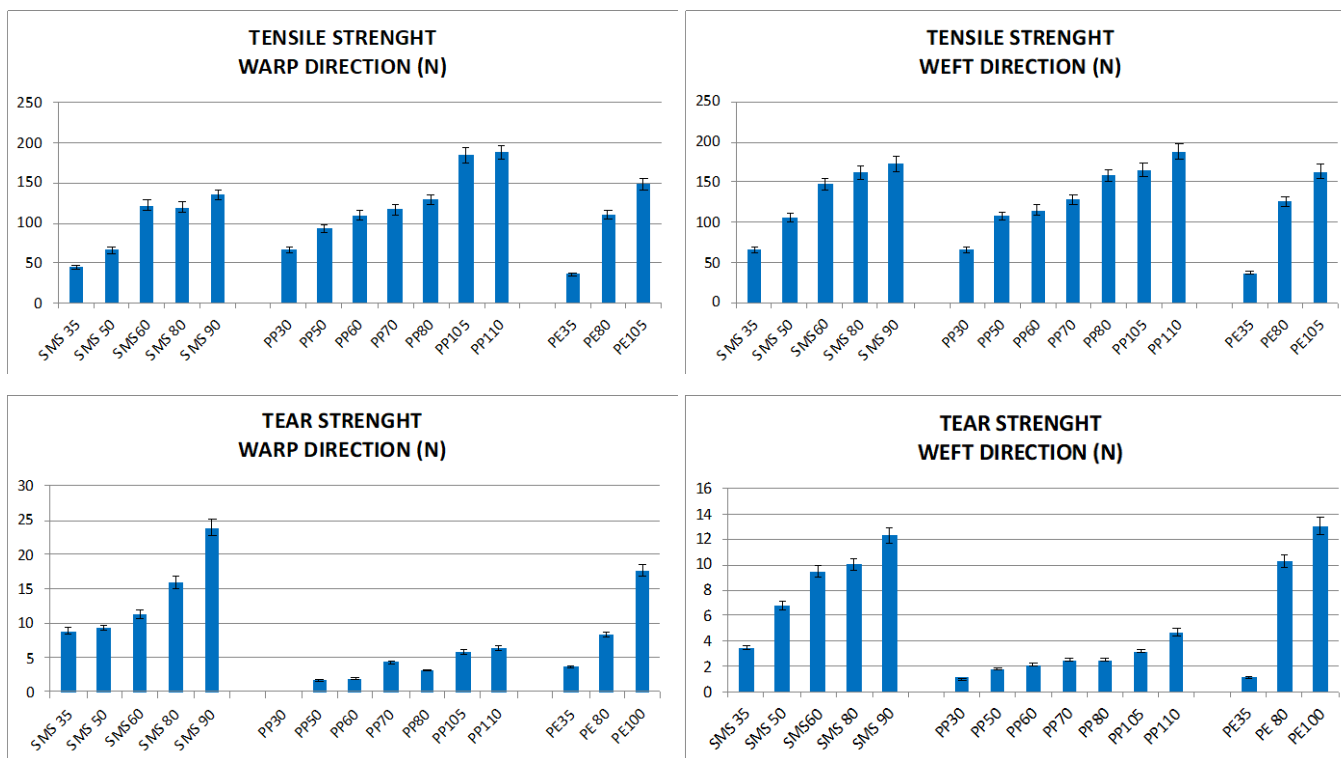
Independent variables for all tests			
Tear Strength	Seam strength	Thermal comfort tests, water vapor permeability	Air permeability, Water permeability resistance
SMS (in all unit weights)	Hot air welding method	SMS (in all unit weights) SMS (in all unit weights) + membrane	SMS (in all unit weights)
PP (in all unit weights)	Ultrasonic welding	PP (in all unit weights) PP (in all unit weights) + membrane	PP (in all unit weights)
PE-coated nonwoven (in all unit weights)		PE-coated nonwoven (in all unit weights)	PE-coated nonwoven (in all unit weights)

### 3. RESULTS AND DISCUSSIONS

#### 3.1 Evaluation of tensile, tear and seam strength

The tensile and tear strength of nonwoven fabrics are presented in Figure 1. It is seen that tensile strength of nonwoven fabrics for both direction was quite high and suitable for use as a surgical gown [25]. Tear strength along warp direction was found to be higher than weft direction. In addition, SMS fabrics were observed to have higher tear strength than polypropylene and PE-coated nonwoven fabrics.

Seam strength of the samples was evaluated for both ultrasonic and hot air welding techniques. Table 3&4 show the seam strength of the samples for ultrasonic and hot air welding method, respectively. From Table 3, it is seen that samples sewed by ultrasonic method exhibited very high seam strength while some of them ruptured without allowing seam to open. Welding method was applied for fusing the membrane and nonwoven samples to each other. Table 4 shows that higher seam strength was obtained for welding method as compared to ultrasonic one.



**Figure 1.** Tensile and tear strength of nonwoven fabrics

### 3.2 Evaluation of thermal properties

Thermal properties of the nonwoven (SMS, PP, PE-coated nonwoven fabric) and combined membrane-nonwoven samples (SMS+membrane, PP+membrane) were assessed in terms of thermal conductivity, thermal resistance, thermal absorption and thermal diffusion. Thermal results of nonwoven samples were presented in Figure 2, 3, 4 and 5.

Thermal conductivity is an important factor affecting heat transfer from the body to the garment. Thermal conductivity is the amount of heat transferred from the

unit thickness of the material to the unit surface area under steady state conditions and when the heat transfer is only dependent on the temperature difference. The higher the thermal conductivity, the faster the heat transfer from the skin to the fabric, resulting in colder feeling [7, 9]. As shown in Figure 2, thermal conductivity of the samples is in the range of 27-43 mW/m.K. Combined membrane-nonwoven samples (SMS+membrane, PP+ membrane) have higher thermal conductivity as compared to SMS and PP samples without membrane. Heat conduction increases with increase in mass per unit area.

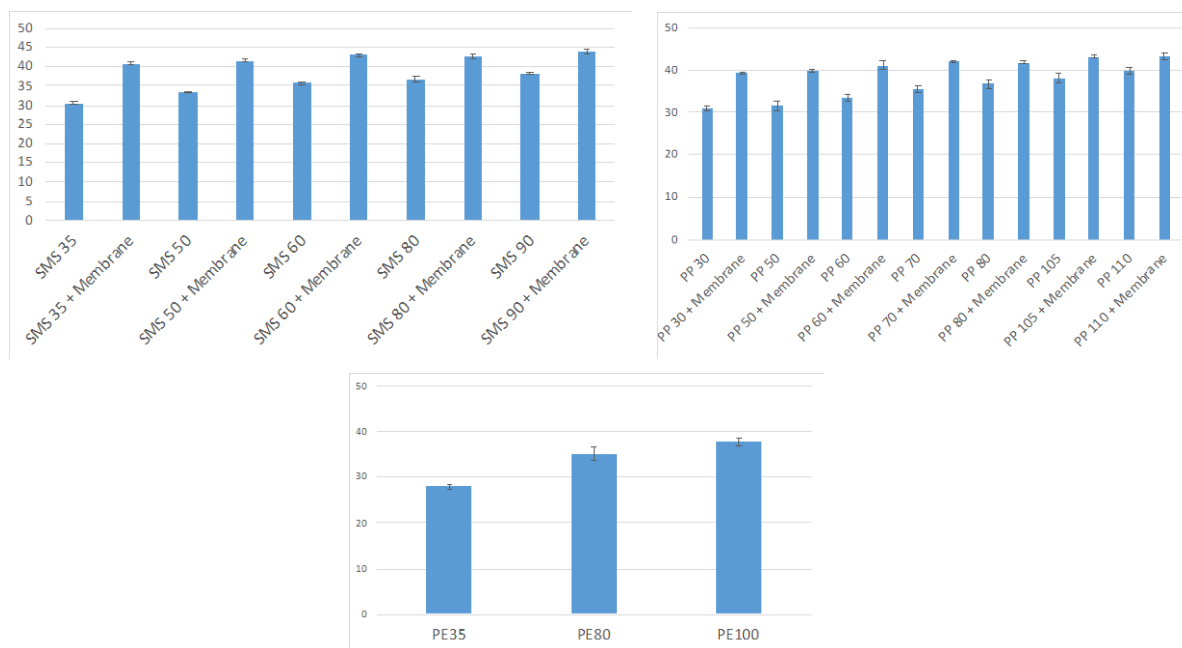


Figure 2. Thermal conductivity of the samples in (mW/m.K)

Table 3. Seam strength for ultrasonic welding method

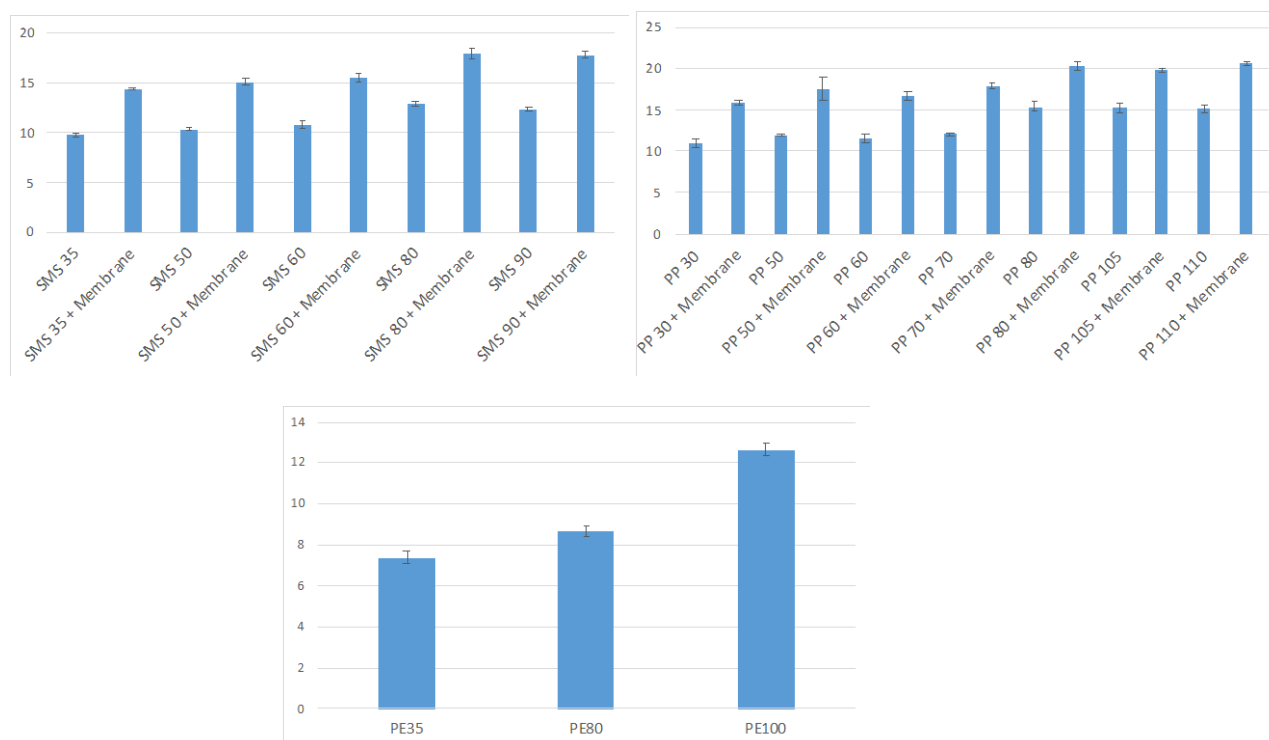
Sample	WARP		WEFT			
	FORCE AT SEAM OPENING OF 6 MM		UNSEAMED WEFT		SEAMED	
	Mean	Std deviaton	Mean	Std deviation	Mean	Std deviation
SMS 35	74.87	24.91	105.92	12.74	83.85	18.33
SMS 50	BREAKDOWN		148.91	14.56	66.39	15.75
SMS60	77.5	6.65	>200		98.69	6.76
SMS 80	85.2	2.04	>200		104.3	4.3
SMS 90	105.25	3.64	>200		114.97	3.47
PP30	76.35	3.89	91.58	3.31	81.17	6.14
PP50	87.46	17.56	157.42	12.87	159.06	14.4
PP60	119.5	6.42	169.94	8.25	128.17	10.12
PP70	166.44	18.03	>200		193.63	5.54
PP80	157.9	14.57	>200		>200	
PP105	BREAKDOWN		>200		145.83	27.3
PP110	BREAKDOWN		>200		145.34	32.37
PE 35	100.53	22	>200		116.82	17.51
PE100	154.43	18.33	>200		116.84	25.98
PE105	BREAKDOWN		>200		175.21	10.06

**Table 4.** Seam strength for hot air welding method

Sample	FORCE AT SEAM OPENING OF 6 MM		UNSEAMED WEFT		SEAMED	
	Mean	Std deviaton	Mean	Std deviation	Mean	Std deviation
SMS 35	BREAKDOWN	NA	140.04	10.39	>200	
SMS 50	142.2	BREAKDOWN	162.33	18.37	184.92	19.34
SMS60	169.65	33.87	>200		>200	
SMS 80	>200		>200		>200	
SMS 90	>200		>200		>200	
PP30	>200		>200		>200	
PP50	>200		>200		>200	
PP60	>200		>200		>200	
PP70	>200		>200		>200	
PP80	>200		>200		>200	
PP105	>200		>200		>200	
PP110	>200		>200		>200	

Thermal comfort is greatly dependent on the insulating properties of clothing. Thermal resistance determines thermal insulation property of a textile material. Since the thermal insulation is to insulate the body against the heat loss by trapping the heat into the air spaces inside the garment, an increase in thermal insulation reduces the comfort of medical clothes. Thermal resistance is related to thickness and thermal conductivity coefficient. By adding a membrane to the garment, the thickness of the fabric

increases leading to an increase in the thermal insulation/resistance properties of the fabrics. Thermal resistance is observed to increase with increase in mass per unit area, which could be due to the increased quantity of enclosed air. The minimum thermal insulation values were obtained as 9.80, 10.98, 7.38  $W^{-1}.K. m^2 \times 10^{-3}$  for SMS 35, PP 30 and PE 35, respectively (Figure 3). It is thought that with the increase in thermal resistance value, the feeling of comfort is adversely affected.



**Figure 3.** Thermal resistance of the samples ( $W^{-1}.K. m^2 \times 10^{-3}$ )



Thermal diffusivity is the rate of the heat transfer of a material. The higher the thermal diffusivity, the faster the heat dissipation [7, 9]. It is seen from Figure 4 that membrane caused an increase in thermal diffusion of fabrics. The higher thermal diffusion is mainly related to bulky structure of the fabric due to air entrapped inside its structure. The thermal diffusion value of the fabrics increases up to a certain mass per unit area, and then it begins to decrease. This could be attributed to the formation of very tight structure with reduced air gap inside the fabric due to the increased mass per unit area. For polypropylene fabrics, thermal diffusion of nonwoven fabrics with a unit weight higher than 80 gr/m<sup>2</sup> and membrane reinforced ones with a unit weight higher than 70 gr/m<sup>2</sup> are observed to decrease. This leads to increased thermal stress of the body of wearer and uncomfortable microclimate. For SMS nonwoven fabrics, thermal diffusion showed a reduction in fabrics with a unit weight greater than 50 g/m<sup>2</sup>, while no significant changes were observed in membrane-integrated ones with a unit weight above 50 g/m.

Thermal absorptivity can be defined as the sensation of warmth and coolness during wearing and depends on the skin contact area of the fabric surface. If the contact area between the fabric and the skin is increased, the thermal absorbance value increases, leading to cooler feeling. Fabrics with low thermal absorptivity give a warm feeling while those with high thermal absorptivity give a cold feeling. As shown in Figure 5, polypropylene fabrics with a unit weight of 70 g/m<sup>2</sup> and higher have higher thermal absorptivity as compared to other PP fabrics. In PP fabrics with a unit weight of 60 g/m<sup>2</sup> and higher,

membrane integration caused to decrease thermal absorptivity. In SMS fabrics, thermal absorptivity was not significantly affected by unit weight and membrane reinforcement. SMS 80 has a maximum thermal absorptivity value of 204.04 W.s<sup>1/2</sup>/m<sup>2</sup>.K. In PE-coated fabrics, the increase in unit weight from 80 to 100 g/m<sup>2</sup> caused a decrease in thermal absorptivity value. Fabrics such as PE 80, PP 105, PP 110, SMS 80, SMS 60 and SMS 90 have higher thermal absorptivity (150 W.s<sup>1/2</sup>/m<sup>2</sup>.K and higher), giving a more comfortable feeling to wearer. It is seen that thermal absorption values did not change proportionally to weight or thickness of the nonwoven samples, which may be caused by the large variation/non-uniformity in the surface smoothness/roughness of the fabrics. Because the surface property of a fabric (roughness/smoothness) greatly affects this sensation (thermal absorptivity), which is related to the contact area between the fabric and the skin [26-28]. Nonwoven fabrics have non-homogeneous structure because they have uneven thickness caused by the uneven spread of fiber. In order to alleviate this constraint, all the tests have been repeated for five times from different areas of the nonwoven samples.

### 3.3 Water vapour permeability results

Water vapour permeability, one of the most important factors determining wearer comfort, is the ability of a fabric to allow moisture vapor to pass through it. Lower water vapour permeability values reduce the moisture transport through the fabric, resulted in increased vapour resistance. The higher the water vapour resistance, the lower the 'breathability' of the fabric.

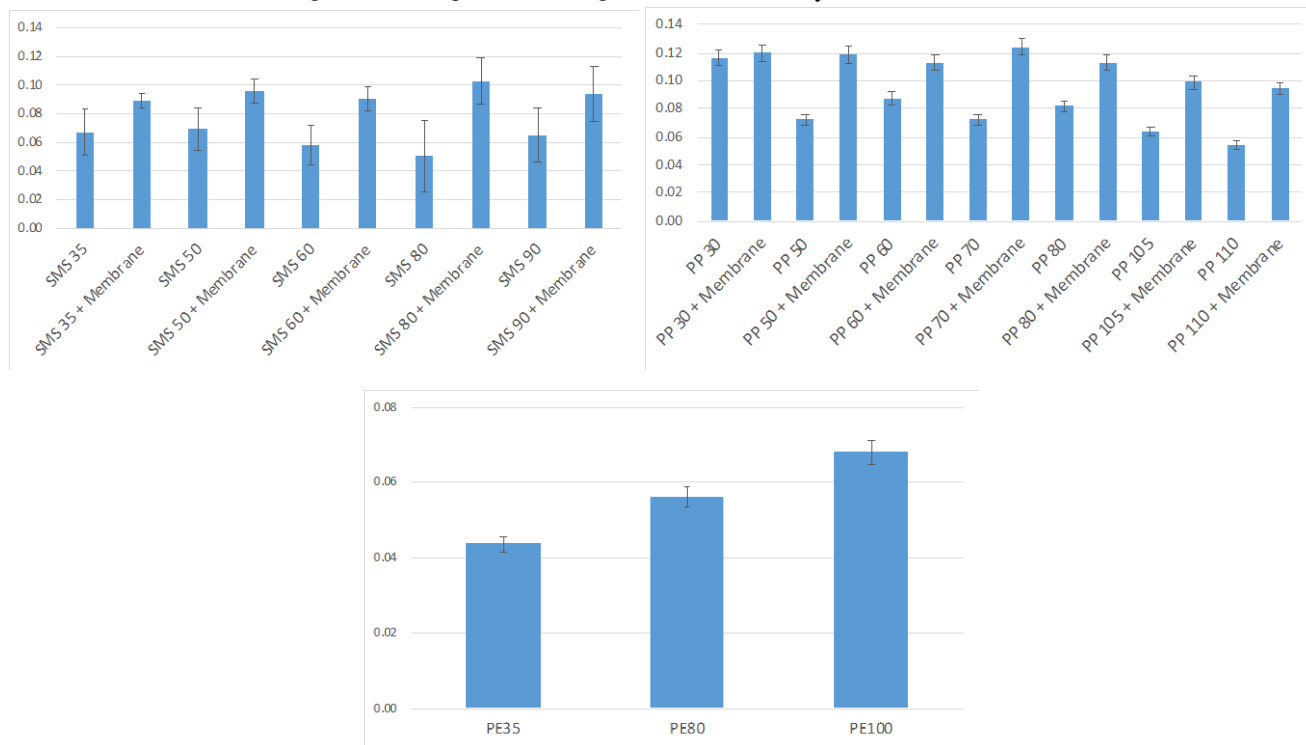
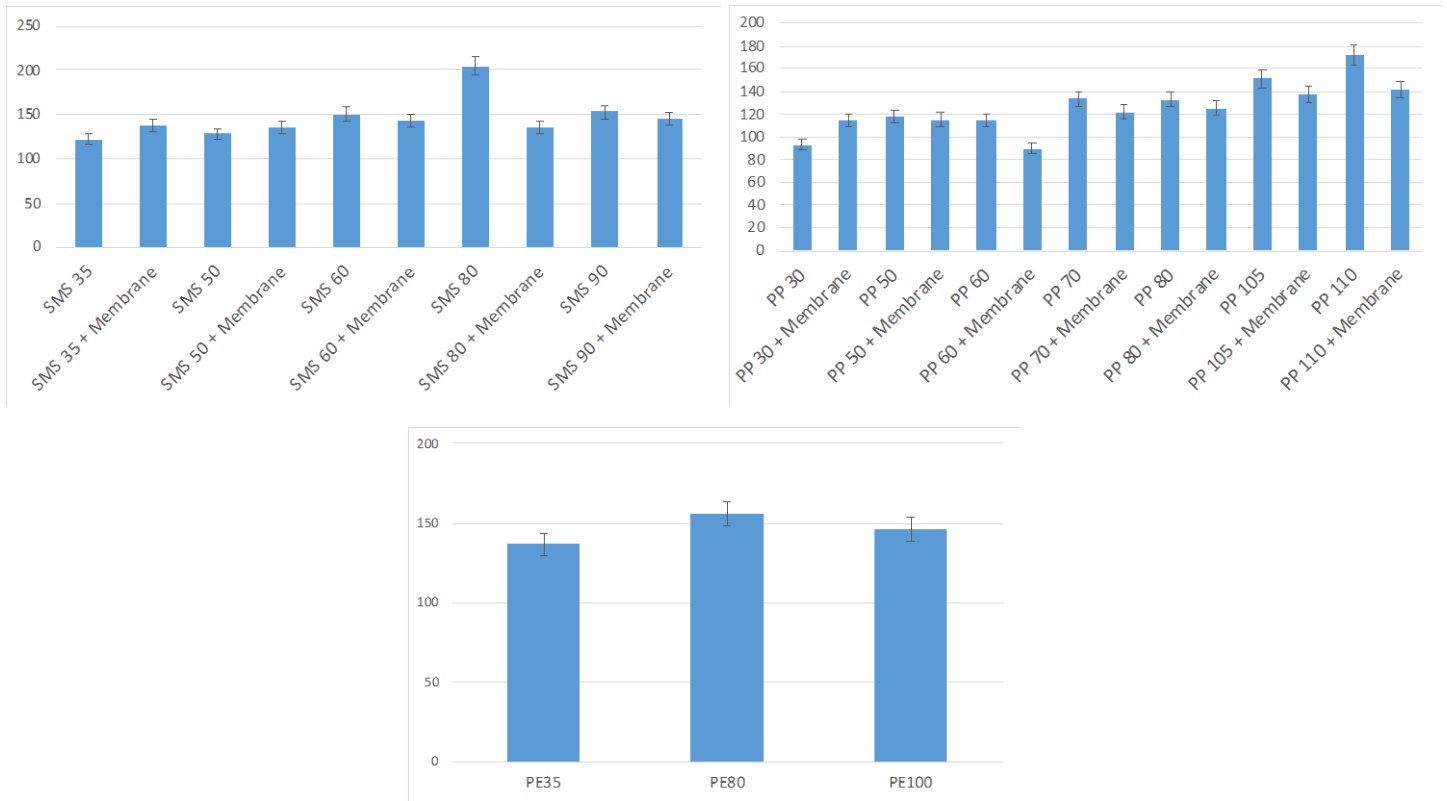


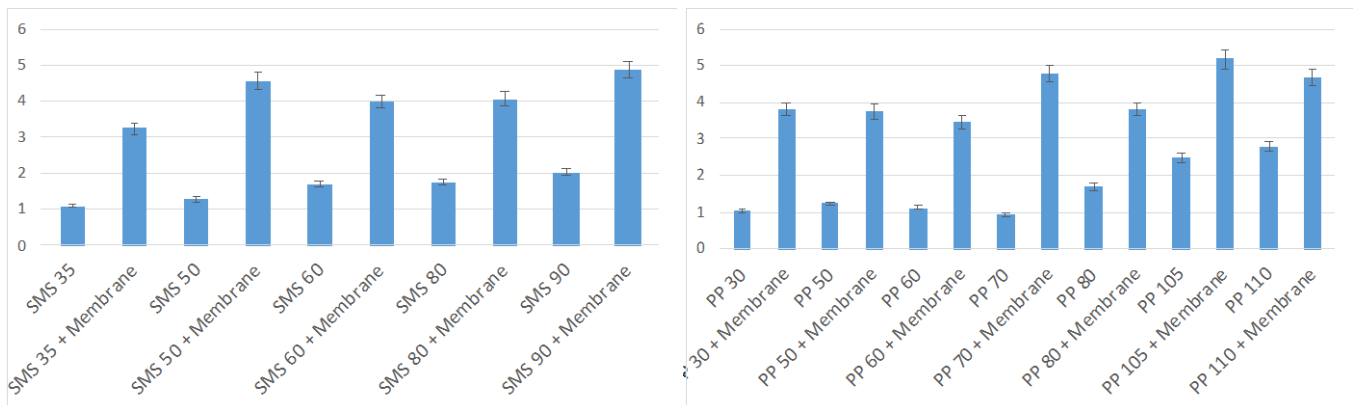
Figure 4. Thermal diffusivity of the samples (mm<sup>2</sup>/s)



**Figure 5.** Thermal absorption of the samples ( $W.s^{1/2}/m^2.K$ )

Water vapor resistance also affects the comfort feeling in determining the comfort level of a fabric. High water vapor resistance reduces the excretion of sweat in the body, which causes moisture to accumulate on the skin, creating an uncomfortable feeling. Figure 6 and 7 show the RET values (water vapour resistance) and relative water vapour permeability of nonwoven and combined membrane-nonwoven fabrics, respectively. SMS 90, PP 105 and PP 110 fabrics were found to have higher Ret values among non-membrane fabrics. Increase in Ret value, which means high resistance to moisture transfer, reduced water vapour

permeability and impaired comfort, was clearly observed with the addition of membrane. All SMS and PP samples have a RET value lower than  $6.0 Pa \cdot m^2/W$ , indicating that they are extremely breathable and comfortable at higher activity rate [2]. Results revealed that SMS 35, 50, 60, 80, 90 and PP 30, 50, 60, 70, 80, 105 fabrics have a water vapour permeability value higher than 70% and greater comfort for wearers. No meaningful result was obtained for PE-coated samples, which could be attributed to the high water vapour resistance owing to the coated structure.



**Figure 6.** Water vapour resistance (RET) of the samples ( $Pa \cdot m^2/W$ )

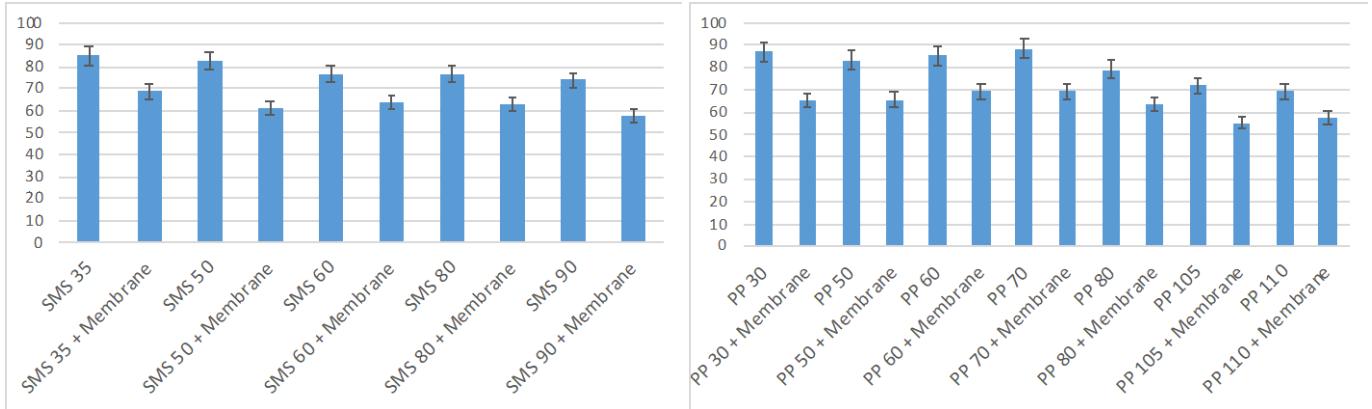


Figure 7. Relative water vapour permeability of the samples (%)

### 3.4 Air permeability results

Air permeability is a feature that increases the comfort properties of garments in terms of breathability of fabrics. Figure 8 shows the air permeability of non-membrane fabrics since the membrane-integrated ones have an air permeability of zero. It is observed that SMS 35, 50 and PP 105 samples are found to have higher air permeability than others. Since SMS spunbond consists of two layers of spunbond, which sandwich a layer of meltblown, its air permeability decreased with an increase in mass per unit area. However, in polypropylene samples, air permeability increased with increasing mass per unit area due to the increased surface porosity. The air permeability of PE-

coated fabrics was found to be zero due to the PE coating, leading to uncomfortable feeling for the wearer.

### 3.5 Water permeability resistance (hyrostatic pressure test)

Resistance of samples against water penetration was measured from both their back and front side under hydrostatic pressure. The mean of the pressures recorded for the specimens are shown in Figure 9 and 10. Water permeability resistance of the front and back sides of the fabrics is found to be very low in polypropylene fabrics. This indicates that SMS fabrics would be a better choice for protection as compared to polypropylene fabrics.

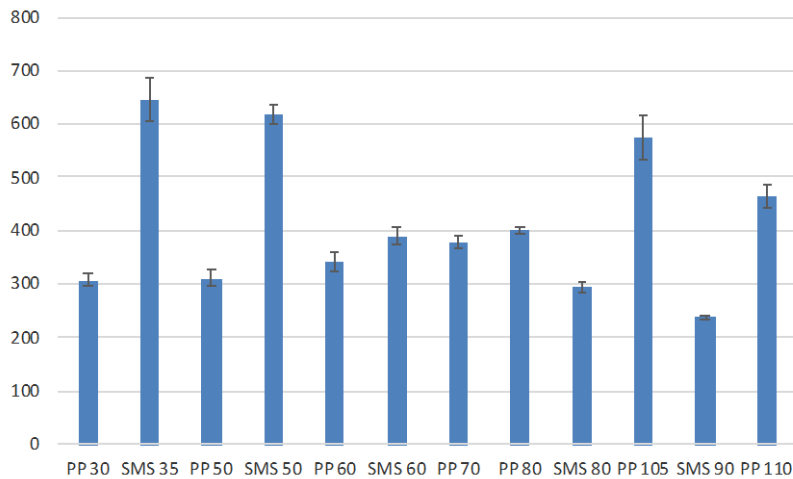
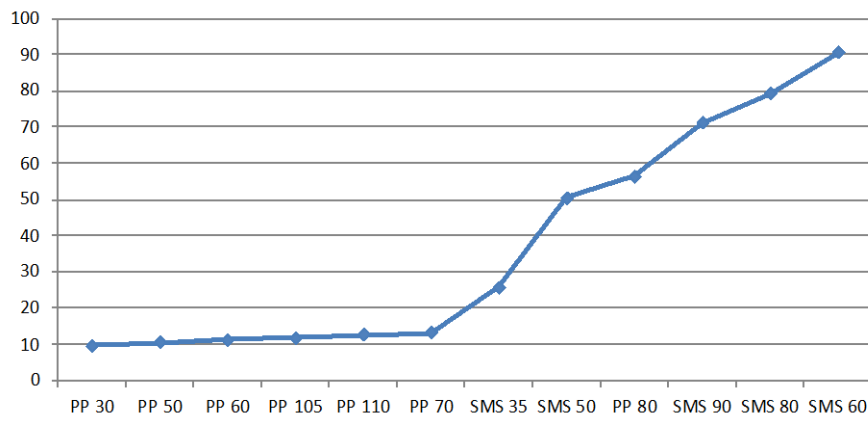
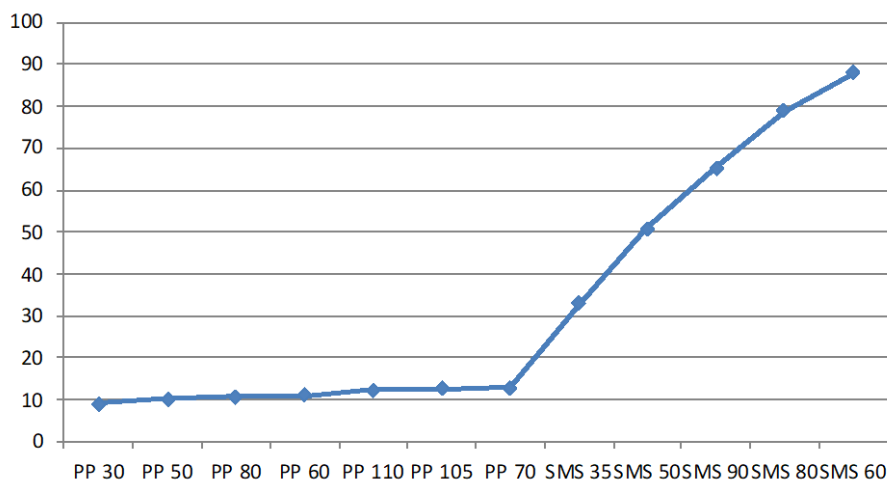


Figure 8. Air permeability test results (L/m²/sec)



**Figure 9.** Water penetration resistance results for front side of SMS and PP samples (Pa)



**Figure 10.** Water penetration resistance results for back side of SMS and PP samples (Pa)

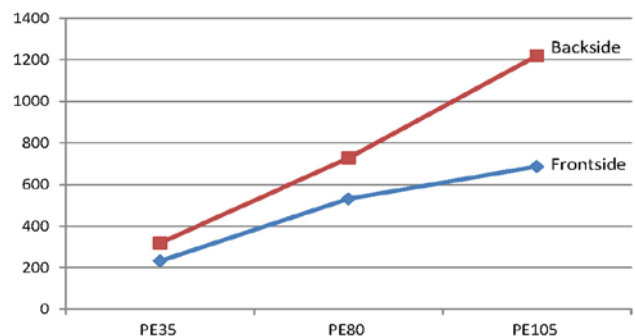
Figure 11 shows the water permeability resistance of the front and back sides of PE-coated fabrics. As can be seen from Figure 11, both front and back sides of PE fabrics have very high water pressure, providing high protection against water penetration.

### 3.6 Statistical analysis

The relationship between variables was tested using IBM SPSS 25 statistics program. As can be seen from Table 5, water vapor permeability and air permeability values are directly related to fabric thickness and fabric unit weight.

As can be seen from one-way anova test results presented in Table 6, there is a significant relationship between fabric type (PP, SMS, PE) on fabric thermal conductivity, thermal resistance, thermal diffusion, thermal absorption, water vapor resistance, water vapor permeability and air permeability.

Paired Sample T-test was used to evaluate whether there is a significant relationship between membrane reinforcement and fabric thermal and water vapour properties. Table 7 indicates that there is a significant relationship between membrane integration and functional properties of fabric.



**Figure 11.** Water penetration resistance results for PE-coated sample

**Table 5.** Correlation values

Variables	N	Pearson Correlation	Sig. (2-tailed)
Fabric unit weight & water vapor permeability	27	0.881	0.000
Fabric unit weight & air permeability	27	-0.650	0.000
Fabric thickness& water vapor permeability	27	0.893	0.000
Fabric thickness& air permeability	27	-0.499	0.008
Fabric thickness & termal absorption	27	0.402	0.038

**Table 6.** One way ANOVA test results

ANOVA						
		Sum of Squares	df	Mean Square	F	Sig.
Thermal conductivity	Between Groups	8693.692	2	4346.846	387.899	.000
	Within Groups	268.947	24	11.206		
	Total	8962.639	26			
Thermal resistance	Between Groups	.037	2	.018	52.605	.000
	Within Groups	.008	24	.000		
	Total	.045	26			
Thermal diffusion	Between Groups	86833.933	2	43416.967	159.576	.000
	Within Groups	6529.852	24	272.077		
	Total	93363.785	26			
Thermal absorption	Between Groups	1413.843	2	706.922	108.414	.000
	Within Groups	156.495	24	6.521		
	Total	1570.338	26			
Water vapor resistance	Between Groups	22.251	2	11.125	5.607	.010
	Within Groups	47.616	24	1.984		
	Total	69.867	26			
Water vapor permeability	Between Groups	13681.575	2	6840.787	70.682	.000
	Within Groups	2322.777	24	96.782		
	Total	16004.352	26			
Air permeability	Between Groups	116740.859	2	58370.430	1.143	.336
	Within Groups	1225446.690	24	51060.279		
	Total	1342187.550	26			

**Table 7.** Paired sample t-test results

Paired Samples Correlations						
			N	Correlation	Sig.	
Pair 1	Thermal conductivity without membrane & Thermal conductivity with membrane		12	.996	.000	
Pair 2	Thermal resistance without membrane & Thermal resistance with membrane		12	.913	.000	
Pair 3	Thermal diffusion without membrane & Thermal diffusion with membrane		12	.979	.000	
Pair 4	Thermal absorption without membrane & Thermal absorption with membrane		12	.997	.000	
Pair 5	Water vapour resistance without membrane & Water vapour resistance with membrane		12	.583	.047	
Pair 6	Water vapour permeability without membrane & Water vapour permeability with membrane		12	.877	.000	

The relative thermal comfort index (RTCI) of the samples were calculated using related formula and given in Table 8 and 9. Based on the RTCI results, it was found that the most comfortable fabrics were 35, 80 and 90 for SMS fabrics whereas 70, 60 and 30 for PP fabrics. It is seen

from the results that integration of membrane to the fabrics reduces the comfort properties of the fabric.

**Table 8.** RTCI indexes of SMS fabrics

Samples	RTCI
SMS 35	0.676
SMS 80	0.675
SMS 90	0.652
SMS 50	0.554
SMS 60	0.526
SMS 35 + Membrane	0.457
SMS 90 + Membrane	0.426
SMS 60 + Membrane	0.396
SMS 80 + Membrane	0.336
SMS 50 + Membrane	0.284

**Table 9.** RTCI indexes of PP fabrics

Samples	RTCI
PP 70	0.474
PP 60	0.452
PP 30	0.433
PP 50	0.422
PP 80	0.392
PP 105	0.348
PP 110	0.336
PP 30 + Membrane	0.257
PP 60 + Membrane	0.248
PP 50 + Membrane	0.244
PP 80 + Membrane	0.218
PP 70 + Membrane	0.187
PP 110 + Membrane	0.169
PP 105 + Membrane	0.146

#### 4. CONCLUSION

In this study, it is aimed to investigate the comfort and protection properties of three different nonwoven fabrics, SMS, PP and PE-coated, and membrane-nonwoven combinations for the production of newly designed functional disposable surgical gown.

Results revealed that tear strength of the SMS fabrics is higher than that of PP and PE fabrics. Tensile strength of the all fabrics along both directions was found to be very close to each other. Samples joined by welding method have higher seam strength than that of ultrasonic one. Hydrostatic pressure test results indicated that water pressure at which the water penetrates into the fabric is higher in SMS fabric than PP fabrics. However, since water penetration is observed over a certain pressure for both fabric types, membrane reinforcement is required for both PP and SMS fabrics, especially in areas that may be exposed to fluid passage. It was found that the air permeability values of SMS fabrics were higher than that of PP fabrics, and the air permeability of PE fabrics was

zero due to PE coating. Considering the comfort performance, the lack of air permeability has a negative effect on the comfort of the wearer. Thermal comfort properties of SMS, PP and PE coated fabrics and SMS + membrane and PP + membrane fabrics were examined. Membrane reinforcement caused an increase in thermal conductivity, thermal resistance, thermal diffusion, thermal absorption and water vapor resistance values. All SMS and PP samples have a RET value lower than  $6.0 \text{ Pa} \cdot \text{m}^2/\text{W}$ , indicating that they are extremely breathable and providing greater comfort to wearers. Based on the RTCI results for membrane reinforced and non-membrane fabric types, RTCI values of SMS and SMS+membrane fabrics were found to be higher than that of PP fabrics, providing higher comfort feeling. The comfort values of 35, 80 and 90 for SMS fabrics and 70, 60 and 30 fabrics for PP fabrics were found to be higher compared to others.

As a result of the statistical evaluations, it was found that the fabric thickness and unit weight had a great effect especially on the water vapor resistance. SMS nonwoven fabrics consist of three thermally or adhesively bonded layers. The lower and upper layers are made of spunbond and the middle layer is made of meltblown material. PP nonwoven fabrics, on the other hand, are single-layer fabrics produced using spunbond, and their comfort and protection properties are lower compared to SMS fabrics. Although PE coated fabrics have great waterproof and impervious performance, their comfort properties are low due to the lack of water vapor and air permeability.

According to findings obtained in this study, it was concluded that the disposable surgical gown produced from SMS nonwoven fabric, and membrane reinforcement in areas where there is a likelihood of exposure to body fluids was the most suitable model that meets the performance and comfort requirements of the wearer. It is expected that this study will provide a better understanding of the effect of fabric selection, sewing method and membrane integration on the wearer's comfort and tensile properties in surgical gown design and contribute to the current literature on medical textiles.

#### ACKNOWLEDGEMENT

This study was supported by Istanbul Technical University Scientific Research Projects (Project Number: MGA-2018-41026).


#### Declaration of interest statement

The authors declare that there is no conflict of interest.

## REFERENCES

1. McBriarty JP, Henry NW. (1992). Performance of Protective Clothing, Fourth Volume, West Conshohocken, PA: ASTM International, DOI: 10.1520/STP1133-EB.
2. Song G, Cao W. (2011). Handbook of medical textiles, Chapter 8: Medical textiles and thermal comfort, Woodhead Publishing Limited, USA.
3. Eryuruk SH, Kayaoglu BK, Kalaoglu F. (2017). A study on ultrasonic welding of nonwovens used for surgical gowns. *International Journal of Clothing Science and Technology*, 29(4), pp. 539-552.
4. Zhong W (2013). An introduction to healthcare and medical textiles, DEStech publications, USA.
5. Prabir J. (2011). Assembling technologies for functional garments—An overview. *Indian Journal of Fibre & Textile Research* 36, pp.380-387.
6. Dammacco G, Turco E, Glogar MI. (2012). Design of Protective Clothing, In S. Bischof Vikusic (Ed.), *Functional Protective Textiles*, Firenze, Italy: Grado Zero Espace, pp. 1-32.
7. Das A, Alagirusamy R. (2010). Science in Clothing Comfort, Woodhead India, New Delhi, India.
8. Saville BP, Institute T. (1999). Physical Testing of Textiles, Woodhead Publishing, Limited.
9. Huang J. (2006). Thermal parameters for assessing thermal properties of clothing. *Journal of Thermal Biology* 31(6): pp. 461-466.
10. Li J, Barker RL, Deaton AS. (2007). Evaluating the Effects of Material Component and Design Feature on Heat Transfer in Firefighter Turnout Clothing by a Sweating Manikin. *Textile Research Journal* 77, pp. 59-66.
11. Onofrei E, Rocha AM, Catarino A. (2012). Investigating the effect of moisture on the thermal comfort properties of functional elastic fabrics. *Journal of Industrial Textiles* 42 (1), pp. 34-51.
12. Celcar D. (2013). Influence of Phase-Change Materials on Thermo-Physiological Comfort in Warm Environment. *Journal of Textiles*, Hindawi Publishing Corporation, Article ID 757319, <http://dx.doi.org/10.1155/2013/757319>.
13. Bartkowiak G, Dabrowska A, Marszałek A. (2013). Analysis of thermoregulation properties of PCM garments on the basis of ergonomic tests. *Textile Research Journal* 83 (2), pp. 148-159.
14. Hatch KL, Markee NL, Maibach HI, Barker RL, Woo SS, Radhakrishnaiah P. (1990). "In Vivo Cutaneous and Perceived Comfort Response to Fabric Part III: Water Content and Blood Flow in Human Skin Under Garments Worn by Exercising Subjects in a Hot, Humid Environment. *Textile Research Journal* 60, pp. 510-519.
15. Shi H, Wang J, Chen X, Luo S, Zhang L. (2016). Research on the seam performance of waterproof clothing based on continuous ultrasonic welding technology. *International Journal of Clothing Science and Technology* 28 (2), pp.171-190.
16. Yoo S, Barker RL. (2005). Comfort Properties of Heat-Resistant Protective Workwear in Varying Conditions of Physical Activity and Environment. Part I: Thermophysical and Sensorial Properties of Fabrics. *Textile Research Journal* 75 (7), pp. 523-530.
17. Rogale SF, Rogale D, Dragecic Z, Nikolic G. (2007). Technical systems in intelligent clothing with active thermal protection. *International Journal of Clothing Science and Technology* 19(3/4), PP. 223-233.
18. Pamuk O, Abreu MJ, Ondogan Z. (2008). An Investigation on The Comfort Properties for Different Disposable Surgical Gowns by Using Thermal Manikin. *Tekstil ve Konfeksiyon* 3, pp. 236-239
19. Woo SS, Shalev I, Barker RL. (1994). Heat and Moisture Transfer Through Nonwoven Fabrics Part I: Heat Transfer. *Textile Research Journal* 64 (3), pp 149-162.
20. Issa M, Abreu MJ, Schacher L, Adolphe D, Silva MEC. (2004). The Influence of The Sterilisation Process on Certain Thermal Properties. *Eur J Appl Phys.* 92, pp. 673-678
21. Bogdan A, Sudol-Szopińska I, Szopiński T. (2011). Assessment of Textiles for Use in Operating Theatres with Respect to the Thermal Comfort of Surgeons. *Fibres & Textiles in Eastern Europe* 192 (85), pp 65-69.
22. Aslan S, Kaplan S, Cetin C. (2013). An Investigation About Comfort and Protection Performances of Disposable and Reusable Surgical Gowns By Objective And Subjective Measurements. *The Journal of The Textile Institute* 104(8), pp. 870-882.
23. Kar J, Fan J, Yu W. (2011). Advances in Knitting Technology. Chapter 10: Women's apparel: knitted underwear. Woodhead Publishing Series in Textiles, pp 235-261. <https://doi.org/10.1533/9780857090621.3.235>
24. Matusiak M, Sikorski K. (2011). Relative Thermal Comfort Index as a Measure of the Usefulness of Fabrics for Winter Clothing Manufacturing. *Fibres & Textiles In Eastern Europe* 89 (6), pp. 94-100.
25. TS EN 13795+A1. (2013). Surgical drapes, gowns and clean air suits, used as medical devices for patients, clinical staff and equipment-General requirements, processors and products, test methods, performance requirements and performance levels.
26. Rubenstein DA, Yin W, Frame MD. (2022). Chapter 4 - Introduction to heat transfer, Editor(s): David A. Rubenstein, Wei Yin, Mary D. Frame, In *Biomedical Engineering, Biofluid Mechanics (Third Edition)*, Academic Press, pp 135-156. <https://doi.org/10.1016/B978-0-12-818034-1.00004-9>.
27. Oğlakcıoğlu N, Marmaralı A. (2010). Thermal comfort properties of cotton knitted fabrics in dry and wet states, *Tekstil ve Konfeksiyon* 3, pp 213-217.
28. Pac MJ, Bueno MA, Renner M. (2001). Warm-Cool Feeling Relative to Tribological Properties of Fabrics", *Textile Research Journal*, 71(9), pp 806-812.

# Use of Natural and Synthetic Materials in Denim Washing Process as an Alternative to Pumice Stone

İsmail İvedi<sup>1</sup>  0000-0002-1259-9554

Ahmet Çay<sup>2</sup>  0000-0002-5370-1463

<sup>1</sup>Roteks Tekstil İhr. San. ve Tic. A.Ş., R&D Department, AOSB, Çiğli, İzmir, Türkiye

<sup>2</sup>Department of Textile Engineering, Faculty of Engineering, Ege University, Bornova, İzmir, Türkiye

**Corresponding Author:** ismailivedi@roteks.com.tr

## ABSTRACT

In this study, the use of synthetic stones and peach kernels in the denim stone washing process instead of pumice stone was investigated. The performance of each alternative was identified with different washing methods, i.e. conventional, low liquor, and spraying methods. The stone washing effects of each alternative were compared. Moreover, energy and water consumption and equivalent carbon dioxide emission of each method were analyzed. The results indicated that although pumice stone led to the best aging effect in the conventional method, synthetic stones and peach kernels showed better performance when the low liquor method was used. Additionally, the energy consumption and carbon dioxide emission of the low liquor method was shown to be lower. Therefore, it was concluded that synthetic stones or peach kernels could be a sustainable alternative to pumice stone and the selection of low liquor method for this application would be advantageous.

## ARTICLE HISTORY

Received: 21.02.2022

Accepted: 16.11.2022

## KEYWORDS

Denim washing, pumice stone, ecological stone washing, sustainability, synthetic stone

## 1. INTRODUCTION

The concepts of sustainability, product life cycle, and ecological production are of great importance considering the environmental impacts of the textile and apparel industry. Therefore, many countries, companies, and organizations around the world have started to implement innovative initiatives and technologies in order to re-evaluate their activities and produce their products both using less water, less energy, and causing low carbon emissions [1]. Within the very complex structure of the textile supply chain that includes a wide variety of raw materials, processes, and therefore products, denim washing emerges as an important production route capable of responding quickly to the needs of the fashion market [2]. However, although denim washing provides added value to the product, it also has the potential to harm the environment [3] due to water and energy consumption and the production of waste emissions and effluents [4, 5].

In order to create a desired aged effect on the denim garments; whiskers, laser, stone wash, spray, bleach, etc. processes are implemented which are called dry and wet processes [6]. The conventional stone washing process is

carried out with pumice stone or similar volcanic stones in order to achieve the desired worn, aging effect on denim products. The desired appearance is obtained by abrading the dyestuffs on the product with the mechanical effect created by rubbing the stones on the clothes in the drum washing machine. The use of pumice stones has problems such as the difficulty of removing the stones from the products, hairiness in the products, decreasing the strength of the fabric and tearing problems, clogging of the machine pipes [7, 8]. In addition, pumice stone is the biggest waste load for waste treatment plants since it decomposes over time after each wash and becomes completely unusable after a certain number of washings [9].

In order to reduce or eliminate the disadvantages of denim washing, some applications such as use of enzymes, use of bleaching agents with pumice, ozone applications, laser treatment, ultrasonic treatment and low temperature plasma have been the subject of denim research [7, 10-16]. In example, to reduce the usage of pumice stone, Telli and Babaarslan [17] combined stone washing with neutral cellulase enzymes in their research. Another application for sustainable denim washing is the total elimination of the

**To cite this article:** İvedi İ, Çay A.. 2023. Use of Natural and Synthetic Materials in Denim Washing Process as an Alternative to Pumice Stone. *Tekstil ve Konfeksiyon* 33(1), 68-76.



pumice stone by the use of a stainless-steel rough drum in the machine [18]. An effective measure for sustainable denim washing against stone washing with pumice might be the investigation of the use of synthetic and natural stones, while only a few studies appeared in the literature on the use of alternative materials for stone washing. Alam et al. [19] used post-used shoe soles for stone washing of denim garments instead of pumice stone. Chattopadhyay and Pachauri [20] produced a series of synthetic stones composed of different amounts of calcium carbonate as filler material and silicon dioxide and aluminum as abrasive materials. Cement and sand were used as bonding agents. It was reported that the use of synthesized stone with certain composition in stone washing was found to be a better substitute for conventional pumice stones in terms of strength, wetting time, and fading of denim garments. In the study of Hoque et al. [21], in which waste wood and wood composite was investigated for the use in acid washing as an alternative to pumice stone, it was reported that pumice stone and wood composite led to higher fading compared to waste wood. Maryan and Montazer [22] investigated the use of organo-montmorillonite in denim washing and indicated that an old-look of fabric could be produced. They concluded that the best concentration is the use of 30% of organo-montmorillonite per 1 kg of denim product. In this study, the potential use of peach kernels and polyethylene-based synthetic materials for stone washing processes alternative to pumice stone was investigated for the first time in the literature.

One of the ways to reduce water and energy consumption in denim washing processes is to make improvements in drum washing machines. The conventional stone washing process is carried out in drum washing machines with a liquor ratio of around 1:10. The denim products are tumbled with pumice stones and auxiliary chemicals at 30-60°C for a certain period of time. A faded look and soft hand is obtained due to the physical abrasion force created by the pumice stones on the denim garments. In the low liquor method, the washing principle is the same; however, the liquor ratio can be reduced to 1:5. In low liquor denim washing machines, the distance between the drum and the wall of the washing machine is lower compared to conventional machines, therefore the desired washing effect can be achieved by using less water and chemicals. There is also a spraying method using an improved version of the classical drum washing machine, which includes spray nozzles as well as a drum. The diameter of the nozzles of the spray nozzles is between 0.1-0.4 mm. In this method, the denim products and pumice stones are loaded into the drum and the liquor including bleaching and auxiliary chemicals is sprayed inside the drum onto the products by the spraying nozzles placed on the drum cover. Therefore, the liquor ratio can be reduced to very low values, such as 1:2, which leads to a very low water consumption. In this study, the comparison of this three types of drum machines

(conventional, low liquor and spray-type machines) was also investigated. The appearance and strength of the resultant materials were examined considering the stones and machines used. Furthermore, energy and water consumption and equivalent CO<sub>2</sub> emissions of each application were identified.

## 2. MATERIAL AND METHOD

### 2.1 Material and Machines

Indigo dyed denim fabric (98/2 CO/EL, 3/1 Z twill weave, 12 oz/yd<sup>2</sup>, 24% elasticity) was purchased from Matesa Denim AŞ., Turkey. The amylase enzyme and dispersing agent for the desizing process were supplied from Dystar, Singapore. Cellulase enzyme obtained from Fourkim San. Tic. A.Ş., Turkey. It was used to provide a chemical stone washing effect to denim garments.

Natural and synthetic materials that can replace pumice stone and aging processes were carried out by conventional drum washing, spraying, and low liquor ratio methods. Synthetic stones were first developed with a 3D printer in different constructions. After creating the mold according to the specified design, it was produced in multiple quantities. As a natural material, peach kernels were used. Figure 1 shows the stones used for the alternative stone washing processes.

Drum-type washing machines (Tolkar, model 3700) were used for pre-washing and stone washing processes both in conventional and low liquor methods. Both drum-type washing machines and spray systems (Method Makine, Turkey) were used for the spraying method.



Figure 1. Synthetic stone and peach kernel used in the study

### 2.2 Method

In all methods, pre-treatments were carried out at 60°C degrees. Stone-washing processes are carried out at 40 °C for both conventional and low liquor methods while room temperature was used for the spraying method.

The general process flow and the energy sources used for each process are shown in Figure 2. Each trial was carried out for 50 pairs of trousers. Fixed recipes for laser pretreatment, rinsing, centrifuging, and drying was applied for each trial (laser pretreatment for 50 min; centrifuging for 20 min for conventional and low-liquor washing and 30 min for spraying, drying at 70 °C for 50 min, rinsing at room temperature). The parametric study plan applied for

different methods and stones in washing processes (shown as Rinse washing, RW; Stone washing, SW) is shown in Table 1. The industrially applied general processing time of stone washing process with a pumice stone in conventional and low-liquor ratio is 30 min, however, in the preliminary trials, it was observed that 30 min process with synthetic stones and peach kernels was found to be inadequate for the desired stone wash effect. Therefore, the processing time of stone washing with synthetic stones and peach kernel was extended to 60 minutes.

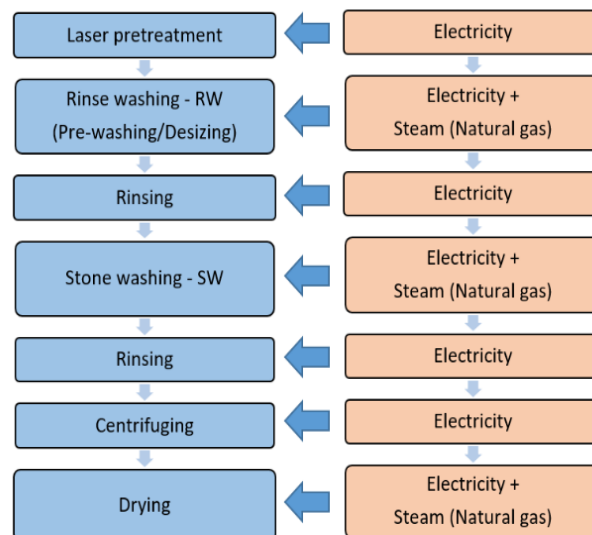


Figure 2. General process flow with energy inputs

Table 1. Washing process parameters

Machine	Stone type	Process	Temperature, °C	Time, min	Stone amount, kg	Water consumption, litres	Notation
Conventional	Pumice	RW	60	5	-	250	C-P
		SW	40	30	50	200	
	Synthetic	RW	60	5	-	250	C-S-50
		SW	40	60	50	200	
	Synthetic	RW	60	5	-	250	C-S-75
		SW	40	60	75	200	
	Peach kernel	RW	60	5	-	250	C-PK-50
		SW	40	60	50	200	
	Peach kernel	RW	60	5	-	250	C-PK-75
		SW	40	60	75	200	
Spray	Pumice	RW	60	5	-	250	S-P
		SW	Room temp.	55	50	18	
	Synthetic	RW	60	5	-	250	S-S-50
		SW	Room temp.	55	50	18	
	Synthetic	RW	60	5	-	250	S-S-100
		SW	Room temp.	55	100	18	
	Peach kernel	RW	60	5	-	250	S-PK-50
		SW	Room temp.	55	50	18	
	Peach kernel	RW	60	5	-	250	S-PK-100
		SW	Room temp.	55	100	18	
Low-liquor	Pumice	RW	60	5	-	125	L-P
		SW	40	30	50	125	
	Synthetic	RW	60	5	-	125	L-S-50
		SW	40	60	50	125	
	Synthetic	RW	60	5	-	125	L-S-75
		SW	40	60	75	125	
	Peach kernel	RW	60	5	-	125	L-PK-50
		SW	40	60	50	125	
	Peach kernel	RW	60	5	-	125	L-PK-75
		SW	40	60	75	125	

In order to evaluate the differences between the application methods, light cabinet analysis to evaluate the aging effect

(according to ISO 3664:2009 standard), elasticity and recovery test (according to ASTM D3107-07 standard), tear

strength test (according to ISO 13937-2:2000 standard) were applied to the resultant products. Physical testing data were analyzed statistically by one-way ANOVA followed by Duncan post-hoc test SPSS 2015 programme. Differences of  $p < 0.05$  were considered statistically significant.

In addition to the effect and quality parameters, energy and water consumption, and greenhouse gas emissions were also examined. For analysis, electricity consumption is calculated using machine data. In wet processes and drying processes, heating is carried out with steam (saturated steam at 6 bar gauge pressure). The amount of steam ( $m_s$ ) required for heating up to the process temperature was calculated by Equation (1). Here,  $m_m$  is the amount of material (water, fabric, and stones),  $T$  is the process temperature,  $T_0$  is the ambient temperature, and  $h_{fg}$  is the enthalpy of evaporation. It is assumed that the steam condenses during heating and turns into saturated water at the same pressure.

$$m_s = \frac{\sum(m_m C)(T - T_0)}{h_{fg}} \quad (1)$$

In order to calculate the amount of steam used due to the heat losses from the machine surfaces, the heat losses from the surface ( $\dot{q}$ , kJ/h) were calculated according to Equation (2), where  $h_c$  and  $h_r$  are the convective and radiative heat transfer coefficient,  $T_s$  machine surface temperature and  $T_0$  ambient temperature, respectively [23].

$$\dot{q} = (h_c + h_r)A(T_s - T_0) \quad (2)$$

$$h_c = 5,22 \sqrt[4]{T_s - T_0} \quad (2a)$$

$$h_r = \frac{20,4 \varepsilon}{T_s - T_0} \left[ \left( \frac{T_s}{100} \right)^4 - \left( \frac{T_0}{100} \right)^4 \right] \quad (2b)$$

The amount of natural gas ( $m_{ng}$ ) required to produce the steam used was calculated using Equation (3), where  $h_s$  is the enthalpy of the steam,  $h_w$  is the enthalpy of the feed water,  $\eta$  is the boiler efficiency and  $LHV$  is the heating value of the fuel.

$$m_{ng} = \frac{m_s(h_s - h_w)}{\eta LHV} \quad (3)$$

As well as energy consumption investigation, equivalent CO<sub>2</sub> emissions (CO<sub>2</sub>e) due to energy use of each process were calculated. CO<sub>2</sub>e emission due to fuels (Scope 1) and purchased electricity (Scope 2) were calculated based on Intergovernmental Panel of Climate Change (IPCC) guidelines using GHG protocol calculation tools [24] with Equation (4), where,  $CE$  is the CO<sub>2</sub>e emission (kg),  $FC$  the activity data (amount of fuel or electricity consumption,

kWh for electricity and m<sup>3</sup> for natural gas) and  $EF$  the CO<sub>2</sub>e emission factor (kgCO<sub>2</sub>e/kWh for electricity, kgCO<sub>2</sub>e/m<sup>3</sup> for natural gas).

$$CE = FC \times EF \quad (4)$$

Specific energy consumption (kWh/piece), specific equivalent carbon dioxide emissions (kgCO<sub>2</sub>e/piece), and specific water consumption values (liter/piece) were calculated by dividing consumption and emission values by the number of trousers processed. Thus, the energy and water used and the equivalent carbon dioxide emissions due to the energy consumption released to nature for the processing of 1 piece of trousers were reported and compared.

### 3. RESULTS AND DISCUSSION

#### 3.1 Light Cabinet Analyses

Stone washing trials were carried out according to three different techniques and compared each other using a pumice stone, synthetic stone and peach kernel and the resultant aging effects were visually investigated. Figure 3 shows the resultant samples after each trial.

In the conventional method (Figure 3-a), it was observed that similar aging effects were obtained in the trials using a pumice stone and peach kernels. For synthetic stones lower aging effects were obtained, however, it was investigated that the aging effect was improved as the number of synthetic stones increased.

In the trials conducted with the low liquor method, it was observed that the use of pumice stone and peach kernels gave similar results, as in the conventional system. On the other hand, it was indicated that better aging effects can be achieved compared to the standard pumice stone application when the amount of peach kernel was increased. A lower aging effect was achieved with synthetic stones, and it was shown that the increase in the number of synthetic stones led to an increase in the aging effect, which was close to those of pumice stones.

In the spraying method, the increase in the amount of material in the experiments with alternative materials provided a better aging effect. However, a paler and greener effect was obtained compared to pumice stone. It could be concluded that peach kernels showed better results compared to synthetic stones possibly due to the rougher surface structure. The low liquor method was found to be appropriate for the use of alternative materials in denim stone washing processes.



(a)



(b)



(c)

**Figure 3.** Stone washed denim trousers with pumice stones, synthetic stones and peach kernels in (a) conventional method, (b) low liquor method and (c) spraying method (Figure sequence for conventional method from left to right; C-P, C-PK-50, C-PK-75, C-S-50, C-S-75; Low liquor method from left to right; L-P, L-PK-50, L-PK-75, L-S-50, L-S-75; Spraying method from left to right; S-P, S-PK-50, S-PK-100, S-S-50, S-S-100)

### 3.2 Physical Analyses

Table 2 shows the tear strength, elasticity and recovery analysis results. When the tear strength values were statistically examined, it was observed that the type of machine used in stone washing process is important in terms of tear strength. Accordingly, it was observed that the tear strength in both weft and warp directions was statistically significantly lower than the others in the spraying method. Since the liquor ratio is lower compared to other methods, there is less water in the drum in this method. Thus, the denim products have a high direct physical contact with both the stones and the machine surfaces. The elasticity analysis results of the processes

were found to be statistically insignificant according to the machine used.

It was investigated that the effect of the stone type (pumice, synthetic and peach kernel) on the tear strength varies according to the machine type. It was seen that the effect of both stone type and amount on the tear strength in the weft and warp direction was insignificant in the spraying and low liquor methods. On the other hand, in the conventional method, it was indicated that the stone type has an effect on the tear strength results. Accordingly, the highest tear strength was provided by the peach kernel, followed by the synthetic stone and the pumice stone, and the difference between them was found to be statistically significant. This

result was attributed to the lower density of the peach kernel compared to the pumice stone and the synthetic stone. On the other hand, the amount of stone was found to be statistically insignificant. Statistical analyses on elasticity values showed that the effect of the stone type and amount was statistically insignificant for both methods.

### 3.3 Energy and Water Consumption and CO<sub>2</sub>e Emissions

In the preliminary studies, it was observed that the processing time should be extended in order to achieve the desired effect when synthetic materials and peach kernels were used as an alternative to pumice stone in the stone washing process. Prolonging the processing time leads to both an increase in energy consumption and an increase in greenhouse gas emissions. For this reason, energy and carbon dioxide emission analysis was carried out to determine to what extent the use of synthetic stone and peach kernel affected the energy consumption and carbon dioxide emission of the total process in different types of machines.

In Figure 4, the energy consumption of each step of the denim washing process by the use of pumice stone, synthetic stone or peach kernels in different devices (conventional, spray and low liquor machines) were illustrated. As can be seen, more than half of the energy consumption of the total process was used for the drying process.

When the conventional system was examined, it was observed that both electricity and natural gas consumption increased with the use of synthetic stones or peach kernels

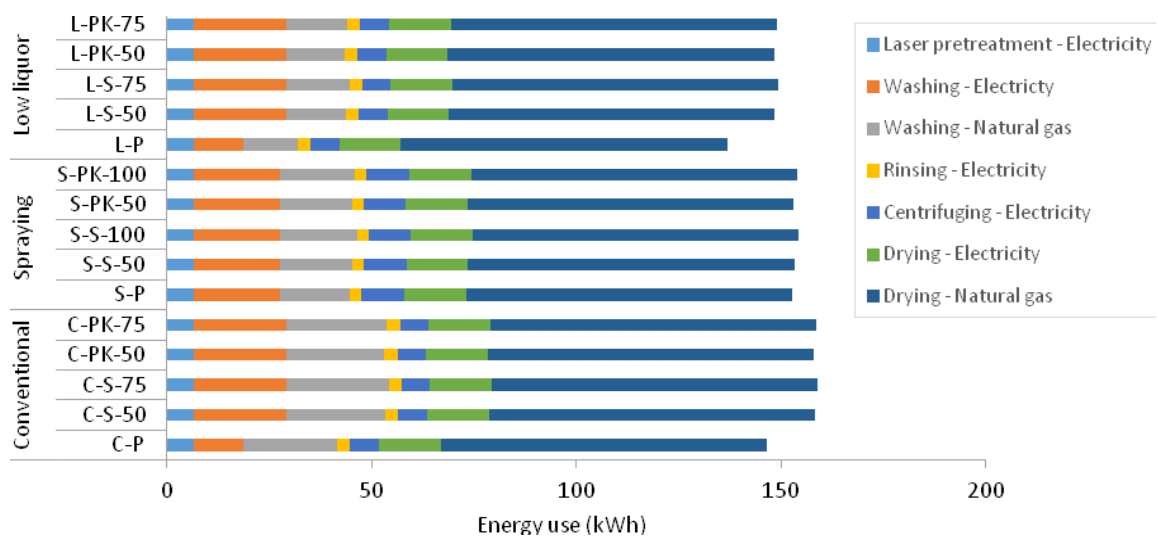
as the processing time increased compared to the use of pumice stone. This increase was at the range of 33-36% when only the washing processes are considered and 7.8-8.6% for the entire process. The energy consumption of using synthetic stone or peach kernel for the conventional system is similar. The increase in the amount of stone increased energy consumption to a certain extent.

In the spraying system in which pumice stone is used, although the processing time is shorter and the natural gas consumption is lower due to the processing at room temperature, the total process energy consumption was found to be higher than the conventional system, due to the higher electricity use. On the other hand, in the case of using synthetic stone or peach kernels in the spraying system, there is no difference in energy consumption compared to the use of pumice stone. Moreover, considering the use of alternative stones, it was observed that the energy consumption in the spraying system was lower than in the conventional application.

The lowest energy consumption was achieved with low liquor device and using pumice stone. When synthetic stones or peach kernels were used, although the processing time is longer, the energy consumption was similar to the conventional system with pumice stone, due to the lower natural gas consumption for heating since less water is used in the low liquor system. Therefore, from the energy consumption point of view, it was shown that spraying or short liquor devices are more suitable for the use of synthetic stones or peach kernels.

**Table 2.** Tear strength, elasticity and recovery of the samples

Method	Process	Tear Strength (N)		Elasticity (%)	Recovery (%)
		Warp	Weft		
Conventional	C-PK-50	19.7	31.1	20.7	4.0
	C-PK-75	22.7	27.9	19.7	4.0
	C-P	8.2	27.2	18.3	4.0
	C-S-50	16.2	22.8	18.5	3.8
	C-S-75	14.8	25.4	18.8	3.8
Low-Liquor	L-PK-50	10.4	28.6	19.6	2.8
	L-PK-75	10.8	26.4	19.4	2.5
	L-P	8.3	30.0	19.5	2.5
	L-S-50	11.6	32.2	19.3	3.3
	L-S-75	12.4	33.0	18.4	2.8
Spraying	S-PK-50	9.8	23.4	21.3	3.8
	S-PK-100	10.9	21.9	19.7	3.5
	S-P	10.3	21.5	19.5	3.5
	S-S-50	8.8	19.0	18.1	4.3
	S-S-100	9.4	22.1	22.9	3.8

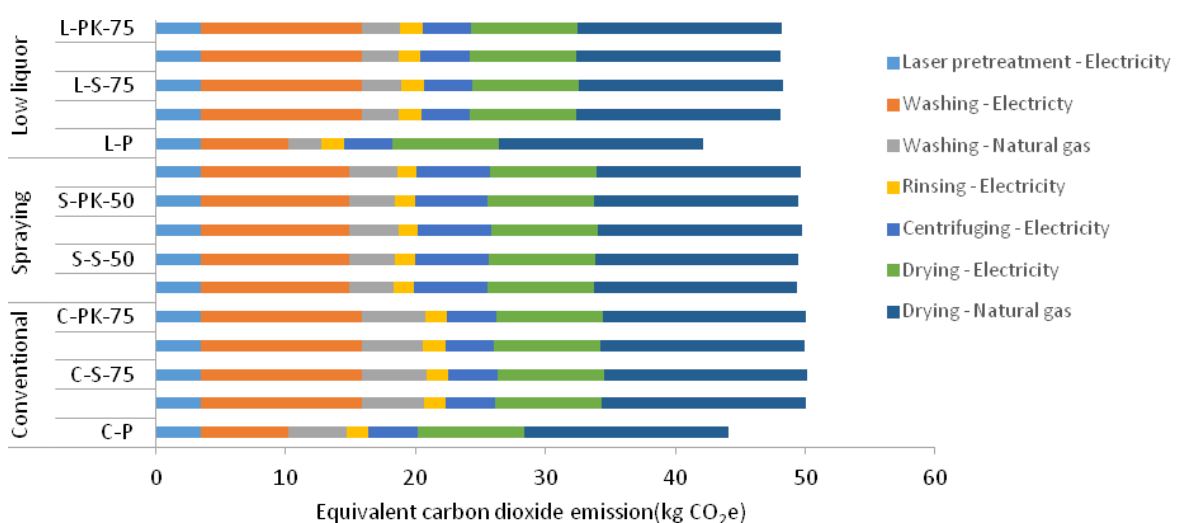


**Figure 4.** Energy use in each step of the denim washing process

Figure 5 shows the equivalent carbon dioxide emissions originating from energy consumption of each step of the denim washing process by the use of using pumice stone, synthetic stone or peach kernels in different devices (conventional, spray and low liquor). Depending on the type of machine and stone used, it has been observed that carbon dioxide emissions are in the range of 44-50 kg CO<sub>2</sub>e. Similar to energy consumption, the highest emission source was the drying step. This was followed by washing processes.

The lowest emission was achieved with the low liquor device and the use of pumice stone. This is followed by the conventional device using pumice stones. The use of alternative stones in these systems led to an increase in carbon dioxide emissions. These increases are about 52-54% in the conventional system and 63-66% in the low

liquor system for washing steps. On the other hand, considering the entire process, it was calculated that the use of alternative stone instead of pumice stone showed an emission increase of approximately 13% in the conventional system and 14% in the low-liquor system. In the spray system, it has been observed that the use of pumice stone or alternative stones was not different in terms of emissions, since the electricity consumption of the system was high. For alternative stones, spraying and low liquor systems were found to result in similar values and lower carbon dioxide emissions than the conventional system. In terms of greenhouse gas emissions caused by energy consumption in the denim washing process, it was revealed that it would be advantageous to choose one of the spraying or low liquor systems when synthetic stones or peach kernels are used as an alternative to pumice stone.



**Figure 5.** Equivalent carbon dioxide emissions in each step of the denim washing process

Specific energy use (kWh/piece) and water use (liter/piece), and specific equivalent carbon dioxide emission (kgCO<sub>2</sub>e/piece) of the entire denim washing process were given in Table 4. Water consumption was not affected by the type of stone used. The specific water consumption of the spraying and low liquor systems (10 liters/piece and 11 liters/piece, respectively) is half the water consumption of the conventional system. Specific energy consumption varies between 2.73-3.17 kWh/piece depending on the process parameters. It was investigated that the low liquor system has lower specific energy consumption compared to other systems for all types of stones. The specific equivalent carbon dioxide emission originating from energy consumption was in the range of 0.84-0.98 kgCO<sub>2</sub>e/unit. Therefore, similar to energy consumption, the selection of a low liquor system will be advantageous for the use of alternative stones in denim washing.

#### 4. CONCLUSION

In this study, the potential of using synthetic stones and peach kernels in the denim washing process alternative to pumice stone was investigated. Additionally, the performance of each material was investigated in three different stone washing methods, which are conventional, spraying and low liquor washing. With the advantage of using less water and chemicals in spraying and low liquor methods, the specific water consumption in the stone-washing process is reduced from 22 liters/piece to 10-11 liters/piece. The pumice stone melts within an average of 2

washes. However, synthetic and natural materials can be used more than 100 times. Therefore, compared to pumice stone in conventional, low liquor and spraying methods, the cost of stone used per unit product was reduced by 45% by the use of natural and synthetic materials.

For the conventional method, the best aging effects were obtained by pumice stone. On the other hand, when the low liquor method was used, synthetic stones and peach kernels showed better effects compared to pumice stone. The reason for this was interpreted as the peach kernel and synthetic stones are less affected by the high rib effect caused by low liquor machine drums. However, the pumice stone was easily broken down by the rib effect. Energy consumption and carbon dioxide emission of the processes were found to be lower in the low liquor method compared to the conventional method. Therefore, the selection of the low liquor method for the use of alternative stones was revealed to be appropriate due to both higher effecting performance, and reduced energy consumption and carbon dioxide emission.

#### Acknowledgment

This work was supported by The Scientific and Technical Research Council of Turkey (TUBITAK) through TEYDEB 1501 project (No:3180537). A limited part of this study was presented in IITAS2021, XV<sup>th</sup> International Izmir Textile and Apparel Symposium, 26-27 October 2021, İzmir, Turkey.

**Table 3.** Specific energy and water consumption and specific carbon dioxide emission in denim washing processes

Machine	Process	Specific energy consumption kWh/piece	Specific water consumption liter/piece	Specific carbon dioxide emission kgCO <sub>2</sub> e/piece
Conventional	C-P	2.93	22	0.88
	C-S-50	3.16	22	1.00
	C-S-75	3.18	22	1.00
	C-PK-50	3.16	22	1.00
	C-PK-75	3.17	22	1.00
Spraying	S-P	3.03	10	0.98
	S-S-50	3.04	10	0.98
	S-S-75	3.06	10	0.98
	S-PK-50	3.04	10	0.98
	S-PK-75	3.06	10	0.98
Low liquor	L-P	2.73	11	0.84
	L-S-50	2.97	11	0.96
	L-S-75	2.99	11	0.97
	L-PK-50	2.96	11	0.96
	L-PK-75	2.98	11	0.96

---


## REFERENCES

1. Pekin M. 2006. Greenhouse gas emissions produced by transportation sector (Master's thesis, in Turkish), Istanbul Technical University, Turkey.
2. Periyasamy AP. 2020. Environmental hazards of denim processing – I. *Asian Dyer* February-March 2020, 56-60.
3. Garcia B. 2015. Reduced water washing of denim garments, in *Denim, Manufacture, Finishing and Applications*, Paul R. (Ed.), UK: Woodhead Publishing, 405-423.
4. Shamsuzzaman M, Kashem MA, Sayem ASM, Khan AM, Shamsuddin SM, Islam MM. 2021. Quantifying environmental sustainability of denim garments washing factories through effluent analysis: A case study in Bangladesh. *Journal of Cleaner Production* 290, 125740.
5. Luo Y, Wu X, Ding X. 2022. Carbon and water footprints assessment of cotton jeans using the method based on modularity: A full life cycle perspective. *Journal of Cleaner Production* 332, 130042.
6. Arjun D, Hiranmayee J, Farheen MN. 2013. Technology of industrial denim washing. *International Journal of Industrial Engineering & Technology* 3(4), 25-34.
7. Ghoranneviss M, Shahidi S, Moazzenchi B, Anvari A, Rashidi A, Hosseini H. 2007. Comparison between decolorization of denim fabrics with oxygen and argon glow discharge. *Surface & Coatings Technology* 201, 4926-4930.
8. Card A, Moore MA, Ankeny M. 2006. Garment washed jeans: impact of launderings on physical properties. *International Journal of Clothing Science and Technology* Vol. 18 No. 1, 2006 pp. 43-52
9. Hooshmand M, Sözen S, Sensoy HA, Orday N, Yagci N, Orhon D. 2020. Color and pumice stone problems in denim processing effluents: removal potential by integrated physical-chemical treatment. *Journal of Chemical Technology and Biotechnology* 95: 142-150
10. Mondal IH, Khan MR, Ahmed F. 2016. Physico-mechanical properties of finished denim garment by stone-enzymatic treatment. *Journal of Textile and Apparel Technology and Management* 10(1), 1-6.
11. Khan MR, Mondal IH. 2013. Physico-mechanical properties of finished denim garment by stone-bleach treatment. *Journal of Chemical Engineering* 28(1), 36-40.
12. Tarhan M, Sarıışık M. 2009. A comparison among performance characteristics of various denim fading processes. *Textile Research Journal* 79(4), 301-309.
13. Hasan Z, Asif AH, Razzaque A, Hasan R, Sur S, Faruque O. 2021. An experimental investigation of different washing processes on various properties of stretch denim fabric. *Journal of Materials Science and Chemical Engineering* 9, 1-15.
14. Mezarıcıöz S, Toksöz M. 2014. Investigation of effect of special washing processes on denim fabrics's properties. *Tekstil ve Konfeksiyon* 24(1), 86-95.
15. Ticha MB, Meksi N. 2021. Exploitation of ultrasonic waves to develop and model a sustainable process for washing denim fabrics. *Journal of Natural Fibers* DOI: 10.1080/15440478.2021.2002758.
16. Fraj AB, Jaouachi B, 2021. Effects of ozone treatment on denim garment properties. *Coloration Technology* 137, 678-688.
17. Telli A, Babaarslan O. 2017. The effect of recycled fibers on the washing performance of denim fabrics. *The Journal of the Textile Institute* 108(5), 812-820.
18. Khan KR, Jintun S. 2021. Sustainability issues of various denim washing methods. *Textile & Leather Review* 4(2):96-110.
19. Alam R, Islam T, Rahman M, Antor AANA, Rahman R, Tamanna TA. 2021. Sustainable denim fabric washing with post-used rubber shoe sole: An eco-friendly alternative of Pumice stone. *Indian Journal of Science and Technology* 13(48), 4723-4731.
20. Chattopadhyay DP, Pachauri RD. 2012. Preparation of synthetic stones for denim washing and analysis of wash effects. *Textiles and Light Industrial Science and Technology* 1(2), 24-28.
21. Hoque S, Hossain J, Imtiaz A, Das S, Rashid MA. 2018. Scope of dry wood & wood composite alternate to stone in case of acid wash on denim fabric. *International Journal of Current Engineering and Technology* 8(2), 382-388.
22. Maryan AS, Montazer M. 2015. One pot denim washing and finishing using organo-montmorillonite: introducing nano mineral washing and finishing. *Textile Research Journal* 85(1), 91-100.
23. EİE, Elektrik İşleri Etüt İdaresi Genel Müdürlüğü. 1997. Sanayiye Enerji Yönetim Esasları, Cilt II.
24. GHG Protocol. The GHG Emissions Calculation Tool. Retrieved from <https://ghgprotocol.org/calculation-tools>



# Investigation of Anti-Pilling Properties of Different Fabrics Applied with Polyvinylcaprolactam

Burcu Büyükkoru<sup>1,2</sup>  0000-0001-2345-6789

Ali Kara<sup>1</sup>  0000-0003-2457-6314

<sup>1</sup>Bursa Uludağ Üniv. / Fen-Ed. Fakültesi Kimya Bölümü / Bursa, Türkiye

<sup>2</sup>Rudolf-Duraner Kimyevi Maddeler San. ve Tic. A.Ş. / R&D Department / Bursa, Türkiye

**Corresponding Author:** Ali Kara, akara@uludag.edu.tr

## ABSTRACT

Pilling is one of the most important problems in the textile industry still not confidently solved. The problem is a kind of mechanically caused fabric defect consisting by a series of roughly spherical masses of entangled fibers called pills. Many studies have been carried out to define this problem in detail, determine the pilling intensity by different methods and improve the pilling grades of fabrics. One of the most beneficial methods to improve values is chemical finishing by applying specific polymers. In this study, a specific synthesized anti-pilling polymer was used for chemical finishing by padding method. A specific polymer based on polyvinylcaprolactam (PVCL) was synthesized and applied on the fabrics. The polymer has been characterized with FT-IR, NMR, DSC, elemental analysis devices also to optimize application-parameters. Especially pilling grades of blended fabrics of natural and synthetic staple fibres are often worse than other non blended fabrics, PVCL polymer was applied on a selection of different polyester cotton blends or polyester viscose blend, which have pilling values between 2-3. PVCL-Polymer applications were carried out by using these 7 different fabrics. As a result, approximately 1.5-2 pilling degree improvement was achieved. Anti-pilling polymers applied on the fabrics used to improve pilling values often decrease hydrophilicity values of the fabrics and worsen touch. However, the specific PVCL-polymer does not lead to a loss of smooth hand neither to a loss of smooth fabric touch. On the contrary, it improves both hydrophilicity and smooth touch not causing fabric yellowing. PVCL is distinguished from other products used for pilling improvement in the textile industry.

## 1. INTRODUCTION

For sustainable textiles, quality must be increased in order to use the garment for a long time without losing its properties. If the clothes used are long-lasting, the user's need for new clothes decreases and the quality increased textiles can be used as second-life clothes by other consumers. In addition, the production of quality products indirectly reduces the product environmental footprint [1]. One of the most important quality problems in the textile industry which shortens the life-time of garments is pilling. Pilling is a crucial parameter for fabric's quality and sustainable textiles. Pilling is a surface defect of textiles caused by intensive wear and care of textiles, like washing and tumble drying. This problem is especially important for fabrics that appeal to the human senses, such as top clothing and upholstery [2]. Mainly, pilling is seen in garment areas near pockets and collars, so pills are mostly found in these areas [3].

A lot of parameters influence pilling in knitted and woven

fabrics, like type of fibres, shape of fibres, fibre staple length, spinning technology used to produce the yarn, fabric construction, finishing technology, etc. All these parameters influence the pilling tendency of a garment [4]. Knitted fabrics tend to pill more readily than woven fabrics. Since knitted constructions are composed of a series of loops, a greater amount of yarn surface area is exposed, making them more susceptible to abrasion in wear. Moreover, knitted fabrics are more often constructed of low-twist yarns made of staple fibres to give a soft, bulky feel and appearance [5].

The pilling mechanism complex and many factors affect pilling during the use of the fabric. Pilling problems may occur in addition as a result of misuse and very often wrong washing of clothes. One of the main reasons that accelerates the formation of pilling is the unnecessarily long and intensive wash cycles which increase mechanical rubbing on the fabric surface creating even more pilling.

**To cite this article:** Büyükkoru B, Kara A. 2023. Investigation of Anti-Pilling Properties of Different Fabrics Applied with Polyvinylcaprolactam. *Tekstil ve Konfeksiyon* 33(1), 77-87.

## ARTICLE HISTORY

Received: 09.12.2021

Accepted: 23.11.2022

## KEYWORDS

Anti-pilling, pilling, hydrophilicity, polyvinylcaprolactam

---

With the increase use of synthetic fibers and their blends in recent decades, the importance of pilling has increased even more [4]. In example polyester fabrics have excellent properties such as high strength, attractive hand, dimensional stability and easy-care properties. Out of these reasons polyester fibers are the most frequently fibres used in the textile industry including outdoor, sports and active wear, as well as protective clothing, medical textiles, automotive parts and in many other technical textile applications. However, the pilling of polyester staple fibre-fabrics and snagging of polyester filament fabrics are still not totally solved problems [7]. As the polyester content increases in e.g. polyester (PES)/cotton (CO) blend fabric, pilling almost increases [8]. Increased pilling occurs on the fabric surface because polyester acts as a kind of anchor fiber for the pill [9]. Because of polyester-fibers do not fracture easily and therefore their pills do not easily wear off [10].

To determine fabric's pilling tendency, various methods have been used and reported in literature [11-15], Martindale is the most common pilling test in textile industry. The PVCL-polymer treated fabrics were exposed to 2000 cycles by using Martindale pilling tester device according to the ISO-12945-2 method.

Some methods used to improve the pilling degrees of fabrics have been reported in the literature [17-19]. One of the most useful of these methods is chemical finish [20, 21]. Endo or exo-cellulases are generally used as an anti-pilling agent in textile finishing [22, 23]. Sufficient pilling improvement in PES/CV, PES/CO, CO/CV blended fabrics could be obtained except viscose (CV) fabrics with these chemicals. The impact of cellulose waste on cellulosic fabrics were studied by Körlü et al. Cellulase enzymes are less effective in viscose fabrics in comparison to cotton fabrics [24]. Anti-pilling compounds, in addition to enzymes, have been utilized. All of today's anti-pilling chemicals have the disadvantage of being pricey or giving fabrics a rough hand. Despite the fact that several different compounds have been claimed to be anti-pilling chemicals [25], the textile industry requires more than only anti-pilling properties. The cloth treated with anti-pilling chemicals should also have other desirable characteristics [26]. It should keep its hydrophilicity, be non-yellowing, and have a nice hand. As a result, an alternate anti-pilling chemical is needed to address the pilling issue. The anti-pilling polymer developed by the researchers in this study differs in that it minimizes the likelihood for pilling while having no negative impact on fabrics' hydrophilicity, hand, or brightness. Polyvinylcaprolactam is the name of the anti-pilling polymer that has been synthesized and studied. PVCL was applied and tested on a variety of fabrics to establish its effectiveness as an anti-pilling agent. PVCL was also tested to see if it had any detrimental effects on the fabrics' hydrophilicity and brightness. PVCL is a functional polymer that has been shown to work as an anti-pilling agent for a variety of fabrics with no negative side effects.

As a result, the pilling problem in fabrics is eradicated, allowing for higher-quality products while also lowering energy, production, and operating expenses [27].

## 2. MATERIAL AND METHOD

### 2.1. Material

#### 2.1.1 Chemicals

Vinylcaprolactam (VCL) (BASF) was used as a monomer and was supplied from BASF. 2M Azobisisobutyronitrile (AIBN) in toluene is the an initiator for polymerization of VCL. These chemicals were supplied from Merck.

#### 2.1.2 Fabrics

In order to demonstrate the improvement of pilling values, it was purposefully worked with fabrics where improvement is hardest to achieve. For this purpose, fabrics are generally chosen from blended fabrics containing polyester and viscose fibers. The pilling value of the fabrics used should be maximum level 3 in Martindale testing to understand whether the specially modified Polyvinylcaprolactam (PVCL) improves pilling values in the fabrics. While selecting fabrics with a maximum pilling value of 3, untreated fabrics were exposed to Martindale test method. Seven fabrics with a pilling degree of 3 or less were used throughout the study, and they are listed in the Table 1 from F-1 to F-7. A microscopic approach was utilized to qualitatively determine which fibers are present in fabrics. The microscope's brand is Olympus, and the model is BX51. Following the microscopic identification of the fibers in the fabrics, their percentages in the fabrics were determined using a chemical method according to ISO-1833-11. Table 1 lists the fibers in the fabrics as well as their percentages. For F-1, PES and CO fibers were found under the light microscope. The percentages of these fibers were determined as 68% PES, 22% CO by chemical method. CV and PES fibers were observed for F-2. The percentages of these fibers were discovered to be 64% PES, 32% CV and 4% EA., F-3 consists of CV and PES fibers. The percentages of these fibers were determined as 77% CV and 23% PES. F-4 is made up of CV and PES fibers, as shown in Table 1. 78 percent CV and 22 percent PES were determined to be the percentages of these fibers. Only CO fibers were found in F-5, indicating that it is totally made up of CO textiles. Under a light microscope, PES and EL fibers were visible in F-6. By using a chemical approach, the percentages of these fibers were discovered to be 66 percent PES, 32 percent CV, and 2 percent EL. F-7 fibers were discovered to be CV, PES, and EL. The percentages of PES, CV, and EA were discovered to be 64 percent, 32 percent, and 4 percent, respectively. Fabric surfaces were photographed at x44 magnification using a digital surface microscope (LEICA brand, DVM6 model). Table 1 contains images.

**Table 1.** Properties of fabrics

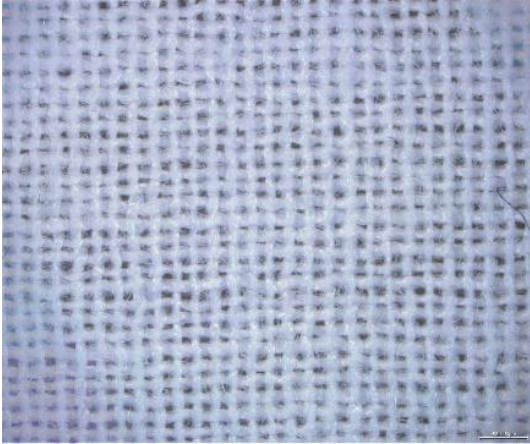






Article	Colour	Fabric type	Fiber composition	Surface image of fabric under digital surface microscope
F-1	White	Woven	68% PES, 32% CO	
F-2	White	Woven	55% CV, 45% PES	
F-3	light pink	Woven	77% CV, 23% PES	
F-4	dark pink	Woven	78% CV, 22% PES	

Table 1. Continued

Article	Colour	Fabric type	Fiber composition	Surface image of fabric under digital surface microscope
F-5	Orange	Knitted	100% CO	
F-6	green plaid pattern	Woven	66% PES, 32% CV, 2% EA	
F-7	Black	Woven	64% PES, 32% CV, 4% EA	

## 2.2 Method

### 2.2.1 Synthesis of PVCL

Vinylcaprolactam (VCL) and the initiator 2 M AIBN in toluene were used for synthesis. PVCL was synthesized by free radical polymerization method [28,29]. 50 ml of VCL (0.37 mmol) and 3.25 g of 2 M AIBN in toluene (0.017 mmol) were added. Reaction was carried out at 65 °C under nitrogen atmosphere. The reaction was completed after 3 hours, PVCL was obtained as slight yellowish liquid. The chemical structure of the VCL monomer (Figure 1) and reaction scheme (Figure 2) are given below.

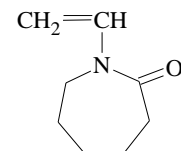


Figure 1. Structure of VCL

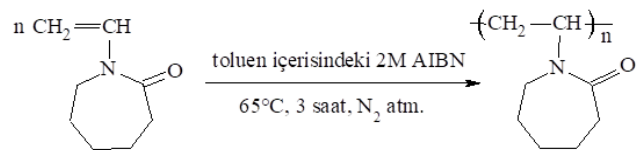


Figure 2. Polymerization reaction of PVCL

### 2.2.2 Polymer Characterization

PVCL was characterized by FT-IR (Shimadzu, IR-Prestige-21), NMR (JEOL-ECZ500R), UV-Visible Spectrophotometer (Shimadzu, UV-1700, PharmaSpec), DSC (Perkin-Elmer DSC 4000 equipment), and elemental analysis (Perkin Elmer 2400 Series II).

### 2.2.3 Finishing process

Continuous impregnation by padding method was used for the application process. PVCL solutions with concentrations of 10, 20, 30, 40 and 50 g/l were prepared by using soft water adjusted to pH value 5.5 by using acetic acid. These solutions applied to fabrics using the padding method. The foulard machine used in the applications is made by Ataç and is type F-350. The fabrics were then dried on the Mathis-stenter frame at 130°C after this process (Mathis brand, PTC 96 model). PVCL was applied on white treated fabric to observe the yellowing impact. Fabric was subjected to 170°C after the application process. By impregnating the seven different reference fabrics at individual squeeze roller pressures of 2-3 bar to obtain a pick-up value on of 70% on all fabrics was achieved. The fabrics were dried at different temperatures on the Mathis-stenter frame. In order to define the optimum temperature for PVCL, the temperature range during drying of the fabrics was studied with different temperature values between 120°C and 170°C. In addition, 170°C was used to understand the yellowing effect of PVCL on white fabrics by Datacolor degree of whiteness detection method. Parallel studies were carried out for all fabrics, first for the touch and hydrophilicity and the second for the pilling test.

### 2.2.4 Measuring pilling values of fabrics treated with PVCL

Martindale pilling tester device was used to determine pilling values of the fabrics. PVCL treated fabrics were exposed to 2000 cycles by this device according to the ISO-12945-2 method.

### 2.2.5 Determination of pilling values of fabrics treated with PVCL

The pilling potential of treated fabrics was predicted using a subjective method. PVCL-treated fabrics achieved a perfect score of 5 out of 5. There will be no piling in the fabric as a result of this. A score of 4 indicates very minimal pilling, whereas a score of 3 indicates moderate pilling. Pilling is plainly noticeable in a fabric with a pilling score of 2. Fabrics with a lot of pilling get a score of 1.

### 2.2.6 Determination of hydrophilicity values of fabrics treated with PVCL

The water absorption capacity of the fabrics is examined when obtaining their hydrophilicity values. The AATC 79 standard procedure is utilized for this. A stopwatch is used to

measure time in this method. The stopwatch begins when water is sprayed onto the fabric with a pipette and ends when the fabric absorbs the water drop. The fabric's hydrophilicity value is calculated using the elapsed time. This method was used to measure the hydrophilicity of all treated textiles. As a result, the influence of anti-pilling chemicals on the fabric's water absorbency values was evaluated.

### 2.2.7 Evaluation of hand of fabrics treated with PVCL

The hand of PVCL-treated fabrics was compared to that of untreated materials. As a result, the impact of anti-pilling polymer on fabric hand was explored. The hand is assessed based on the sensation it gives the user as they take the fabric between their fingertips. The cloth might be described as silky, slippery, thick, or thin as a result of this sensation. The favored hand is usually the same, despite the fact that the hand is relative and varies from person to person from time to time. When the treated fabrics' hand was compared to their untreated counterparts, the hand effect of PVCL was found to be identical.

### 2.2.8 Evaluation of whiteness values of fabrics treated with PVCL

The whiteness test was carried out with the Datacolor 600TM equipment. White cloth was treated with 50 g/l PVCL to evaluate the yellowing effect of PVCL on treated fabrics. In a Mathis-stenter frame, the fabric was exposed to 170°C for 1 minute after application. Using a Datacolor equipment, the whiteness value of this cloth was measured in Berger units. In the Berger unit, the whiteness value of the untreated fabric was also assessed. Untreated cloth and fabric treated with 50 g/l PVCL had their whiteness values compared.

## 3. RESULTS AND DISCUSSION

N-vinylcaprolactam was polymerized by free radical polymerization. 2 M AIBN in toluene was used as a catalyst and VCL was used as a monomer. Therefore, PVCL was synthesized successfully.

### 3.1 Determination of polymerization with FT-IR analysis

The FT-IR spectra of VCL and PVCL are given in Figure 3 and Figure 4. Their spectrums are compared in Figure 5. Also, the peak assignments are tabulated in Table 2. Firstly, FT-IR spectrum of VCL is observed and it is shown in the following figure.

In the FT-IR spectrum of VCL, the characteristic carbonyl peak (C=O) is at 1622  $\text{cm}^{-1}$ . The peaks for the C=C were observed at 1661  $\text{cm}^{-1}$  and at 943  $\text{cm}^{-1}$ . The peaks in the 2932 and 2851  $\text{cm}^{-1}$  correspond to the aliphatic C-H stretching. The -CH<sub>2</sub>- peaks are at 1439–1305  $\text{cm}^{-1}$ . C-N stretching vibrations are at 1266–1046  $\text{cm}^{-1}$ .

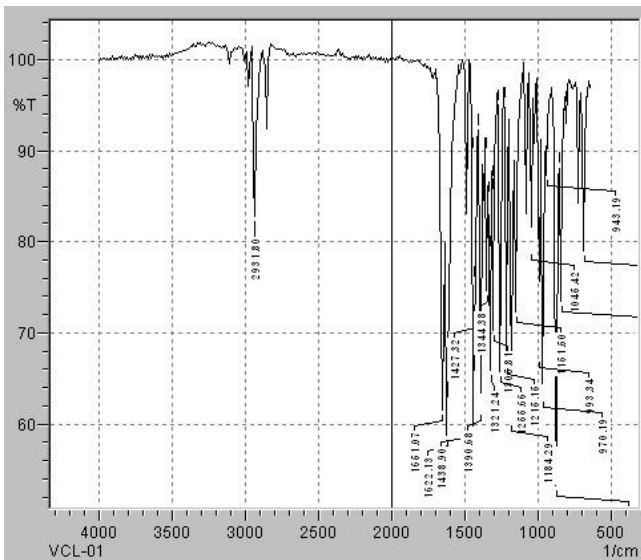


Figure 3. FT-IR spectrum for VCL

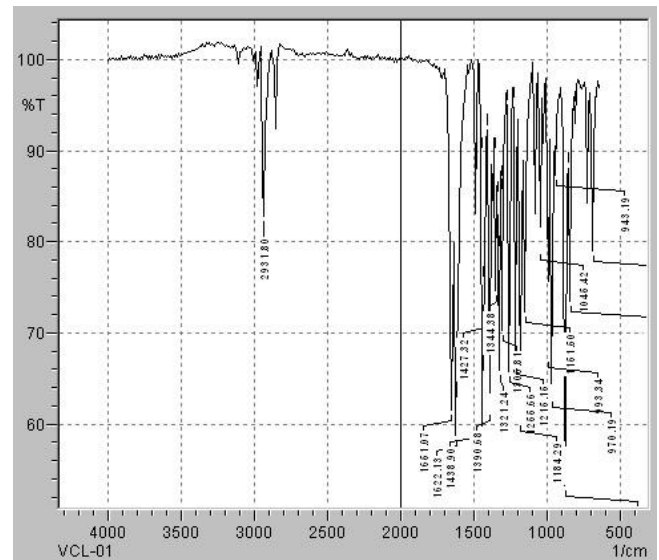


Figure 5. FT-IR spectrum for VCL and PVCL samples

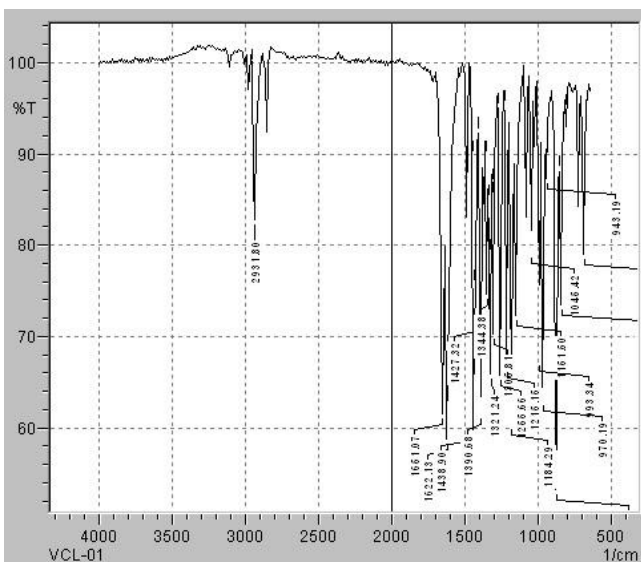


Figure 4. FT-IR spectrum for PVCL

In the spectrum of PVCL, C=O bond stretching at  $1622\text{ cm}^{-1}$  becomes broader and peak of double bond ( $\text{C}=\text{C}$ ) near  $\text{C}=\text{O}$  peak disappeared. The aliphatic C-H stretching was observed at  $2924$  and  $2865\text{ cm}^{-1}$ . The vinyl,  $\text{CH}_2=\text{CH}$ - peak in the spectrum of monomer at  $943\text{ cm}^{-1}$  is not observed in the spectrum of PVCL. The other vinyl peak at  $1622\text{ cm}^{-1}$  is replaced with shifted C=O peak. The  $\text{CH}_2$  peaks are at about  $1440\text{ cm}^{-1}$ . Peaks belong to double bond disappeared completely. The peaks of C-N stretching vibration at  $1261$ – $1161\text{ cm}^{-1}$  in the monomer spectrum showed changes in intensity and position in the spectrum of polymer. This might be due to changes in conformation of side group and resonance structures. This can also be observed in the range of  $3700$ – $3150\text{ cm}^{-1}$  where new peaks corresponding to the OH and N-H are observed in the spectrum of polymer. The sharpness of the peaks in polymer spectrum showed regularity in polymer molecular chain.

FT-IR spectra of monomer and polymer is compared and it is proved that polymer was successfully obtained and the polymerization proceeds by carbon-carbon double bond opening. Shift values of monomer and polymer are given below.

Table 2. Shift values of VCL and PVCL

Functional group	VCL, shift ( $\text{cm}^{-1}$ )	PVCL shift ( $\text{cm}^{-1}$ )
N-H	3150	3150
Aliphatic C-H	2924, 2864	2924, 2864
C=O	1622	1622
C-N	1477	1477
- $\text{CH}_2$	1440	1440
C=C	1661	-
=CH and $\text{CH}_2$	2924, 943	-
O-H	-	3450

These results are very similar to those reported in the literature [30]. The FT-IR spectrum of PVCL, with results consistent with the literature, clearly showed that the polymer was successfully synthesized.

### 3.2 Determination of polymerization with NMR analysis

H atoms in PVCL structure are numbered and illustrated in Figure 6. In the  $^1\text{H}$ -NMR spectrum of PVCL, four different peaks were observed.

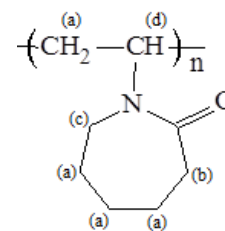


Figure 6. Numbered representation of H atoms in PVCL structure

The  $^1\text{H}$  NMR spectrum of the polymer is provided in Figure 7.  $^1\text{H}$ -NMR spectrum of PVCL taken in DMSO- $d_6$  is examined, peaks are obtained as below. In the  $^1\text{H}$ -NMR spectrum, the protons ( $\text{H}_a$ ) for methylene group, (6 H,  $-\text{CH}_2-$  of the caprolactam ring and 2H,  $-\text{CH}_2-$  of the backbone) appear at 1.524 ppm. The peaks for  $\text{CH}_2$  groups close to  $\text{C}=\text{O}$  (2H,  $-\text{COCH}_2-$ ), ( $\text{H}_b$ ) are observed at 2.293 ppm and the peaks for  $-\text{CH}_2$  groups close to N (2H,  $-\text{NCH}_2-$ ), ( $\text{H}_c$ ) are seen at 3.040 ppm. The peaks for CH group ( $^1\text{H}$ ,  $-\text{NCH}-$  of the  $\alpha$  position), ( $\text{H}_d$ ) are exhibited at 4.341 ppm.

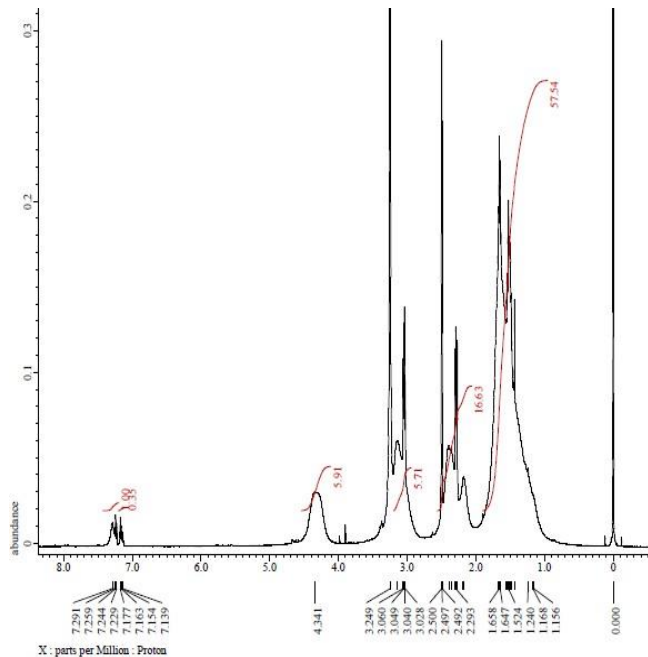


Figure 7. NMR spectrum for PVCL

These characteristic peaks are similar to articles reported in the literature [31]. Thus, it has been proved that homopolymerization takes place and PVCL is successfully synthesized.

### 3.3 Determination of polymerization with differential scanning calorimetry (DSC) analysis

By using Perkin-Elmer DSC 4000 equipment, differential scanning calorimetry was performed. Measurements were taken by using 3 mg PVCL sample. The DSC thermogram of the polymer are given in Figure 8. In the thermogram of the polymer, there is a broad peak at about  $67^\circ\text{C}$  and a less probable peak at about  $137^\circ\text{C}$ , which can be the glass transition temperature ( $T_g$ ) value.

Values are similar to results reported in the literature [30]. Hence, it is proven that PVCL was synthesized in success.

### 3.4 Determination of polymerization with elemental analysis

Elemental analysis results of PVCL are given in Table 3.

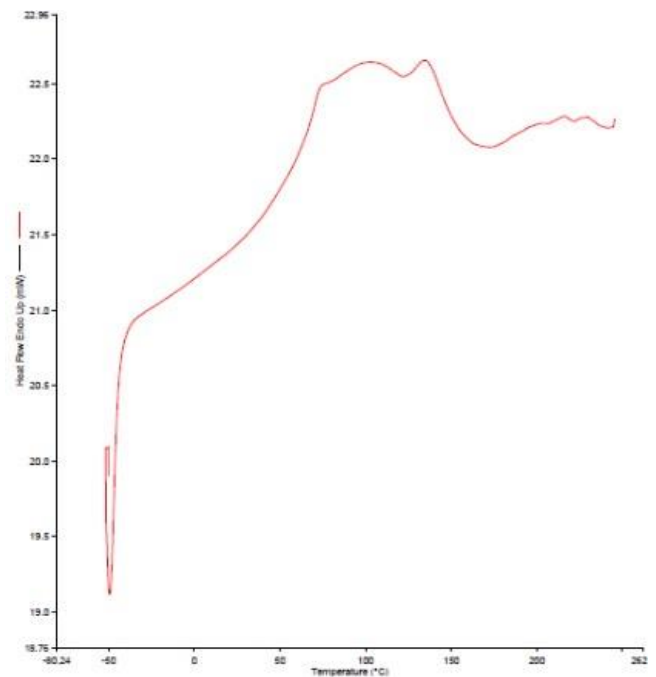


Figure 8. DSC results for PVCL

Table 3. Elemental analysis results of PVCL

Composition of the initial reaction mixture (mol%)		Elemental analysis (%)		
VCL	2 M AIBN in toluene	Carbon	Hydrogen	Nitrogen
95.61	4.39	65.39	9.37	10.09

### 3.5 The impact of the polymer on pilling efficiency

Foulard process was applied to fabrics (F1 to F7) with PCVL polymer synthesized and characterized. Pilling performance of treated fabrics which dried in the stenter machine and rested in condition was tested with the Martindale pilling device. Pilling values of the fabrics were determined with the subjective method and pillgrade machine. The data obtained are given in the Table 4. As can be seen from table, when the pilling values of untreated fabrics are between 2 and 3, treated fabrics have better pilling values. Also improvement of the values are higher when application quantity of PVCL increases.

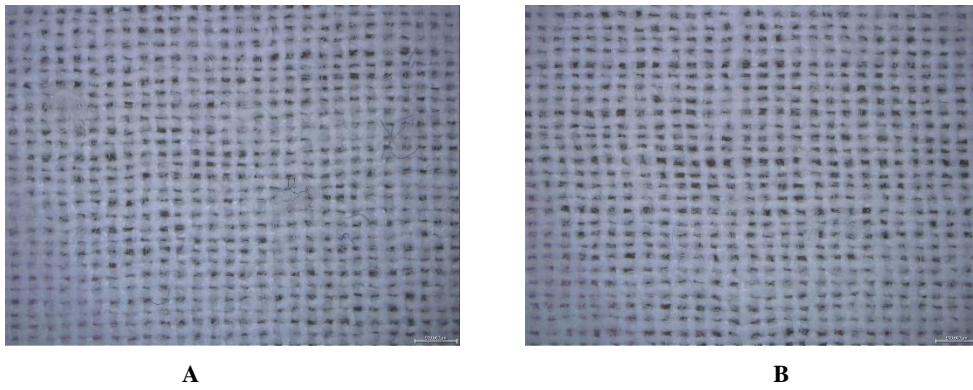
It is clearly demonstrated that PVCL contributes anti-pilling properties of fabrics. 40 g/l PVCL application is enough for all fabrics in order to achieve acceptable pilling degrees. It is observed that nearly 1.5 pilling grades of improvement was achieved after 40 g/l PCVL application.

Surface images of PVCL treated (40 g/l) and untreated fabrics after the pilling test were also compared to demonstrate PVCL decreases pilling tendency of the fabrics. Photographs including the surface images of the fabrics are shown in Figure: 9-15. There are almost no pills on the surface of all treated fabrics with 40 g/l PVCL when a lot of pills are seen on the surface of untreated ones.

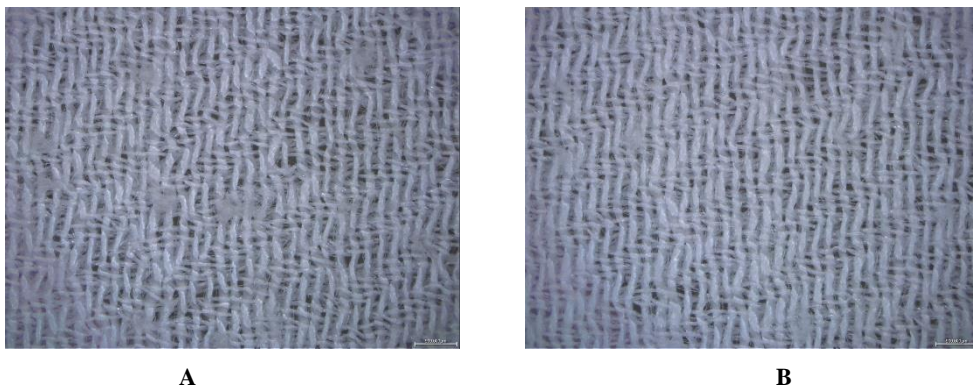
**Table 4.** Pilling results of fabrics treated with different concentrations of PVCL

Artical	Pilling degrees of untreated fabric	Pilling degrees of treated fabric with 20 g/l PVCL	Pilling degrees of treated fabric with 30 g/l PVCL	Pilling degrees of treated fabric with 40 g/l PVCL	Pilling degrees of treated fabric with 50 g/l PVCL
F-1	3	4	4-4.5	4-5	4.5-5
F-2	3	3.5-4	3.5-4	4	4
F-3	2	2.5-3	2.5-3	3	3-3.5
F-4	2-3	3	3	3-4	3.5-4
F-5	2-3	3	3	3.5	3.5
F-6	3	4-4.5	4.5	4.5-5	4.5-5
F-7	2-3	3.5	4	4.5-5	4.5-5

\*Degree of pilling 5: means no pilling; 1 means very severe pilling



**Figure 9.** Surface images of F-1 **A)** Untreated **B)** 40 g/l PVCL treated



**Figure 10.** Surface images of F-2 **A)** Untreated **B)** 40 g/l PVCL treated



**Figure 11.** Surface images of F-3 **A)** Untreated **B)** 40 g/l PVCL treated





**A**



**B**

**Figure 12.** Surface images of F-4 **A)** Untreated **B)** 40 g/l PVCL treated



**A**



**B**

**Figure 13.** Surface images of F-5 **A)** Untreated **B)** 40 g/l PVCL treated



**A**

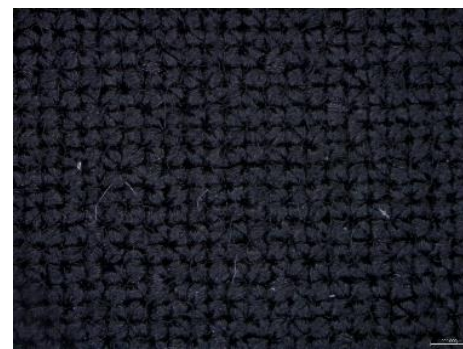


**B**

**Figure 14.** Surface images of F-6 **A)** Untreated **B)** 40 g/l PVCL treated



**A**



**B**

**Figure 15.** Surface images of F-7 **A)** Untreated **B)** 40 g/l PVCL treated

### 3.6 The impact of polymer on fabric hydrophilicity

Hydrophilicity values of untreated and PVCL-treated fabrics were demonstrated in Table 5. Hydrophilicity of F-1 and F-7 untreated fabrics was not good enough and their values were recorded as 10 and 50 second. When PVCL applied to these fabrics their hydrophilicity values were measured as 1 second, means they absorbs water immediately. For other treated fabrics, hydrophilicity values were recorded better than untreated ones or remains same if they absorbs water in 1 second. In short, it is clearly demonstrated that PVCL contributes hydrophilicity.

### 3.7 The impact of polymer on fabrics hand

A hand with a rating of 5 out of 5 is very soft, while one with a value of 1 is quite hard. Fabrics that have not been treated have a hand of 2-3.5, whereas fabrics that have been treated with PVCL have a hand of 3-4. This is proof that PVCL has no negative effects on the hand. Hand is preferable to untreated materials for some treated fabrics. Some treated fabrics, on the other hand, aren't soft enough and are too slippery. Softener can be added to the solution in this scenario. Combinations of polymer and softener were developed and applied to the fabrics. As a result, the hand value of these textiles was 4-5, and the softener had no effect on the materials' pilling values. It can be said that using appropriate softeners as additives to improve the hand of the applied fabrics has no disadvantages.

### 3.8 The impact of polymer on fabric whiteness values

White fabrics (F1 and F2) were treated with 50 g/l PVCL and subjected to 130°C and 170°C for 1 minute in a Mathis-stenter frame to study the yellowing effect of

PVCL. The Daticolor 600TM equipment was used to determine the whiteness value of these fabrics and results (in Berger unit) are shown in Table 6. The whiteness degree for untreated F-1 is a Berger value of 54.8. At 130°C fabric's whiteness value was likewise assessed and recorded as 55.6 Berger. However, it is clearly demonstrated that F-1 turn yellow at 170°C and the whiteness value is measured as 59.8 Berger, means F-1 is negatively affected at this temperature. The results are similar for F-2 fabric. When the findings were examined, it was evident that there was no significant change, indicating that PVCL has no influence on fabric whiteness at 130°C.

## 4. CONCLUSION

- PVCL was synthesized and characterized successfully. Fabrics (F1-F7) were treated with different concentrations of PVCL. Pilling values of treated fabrics were measured and it is proved that PVCL is beneficial in increasing the pilling values of fabrics with approximately 1.5 degrees of pilling.
- Pilling values of treated fabrics with 40 g/l PVCL were recorded as 4.5-5, means almost no pills on the fabric surface.
- The hydrophilicity values of treated fabrics and untreated fabrics were also compared. It was found that PVCL improves hydrophilicity of the fabrics.
- PVCL gives good handle to fabrics and do not cause yellowing on fabrics at 130°C.
- The PVCL functional polymer was named as "RUCO-PLAST EPG 19041" to market it as an anti-pilling chemical on Rudolf-Duraner's product list.

**Table 5.** Hydrophilicity values of fabrics treated with different concentrations of PVCL

Artical	Hydrophilicity values of untreated fabrics	Hydrophilicity values of treated fabrics with 20 g/l PVCL	Hydrophilicity values of treated fabric with 30 g/l PVCL	Hydrophilicity values of treated fabric with 40 g/l PVCL	Hydrophilicity values of treated fabric with 50 g/l PVCL
F-1	10 s	3 s	2 s	1 s	1 s
F-2	6 s	3 s	3 s	2 s	2 s
F-3	1 s	1 s	1 s	1 s	1 s
F-4	1 s	1 s	1 s	1 s	1 s
F-5	1 s	1 s	1 s	1 s	1 s
F-6	4 min	1.5 min	40 s	8 s	6 s
F-7	50 s	7 s	4 s.	1 s	1 s

**Table 6.** Comparing the degree of whiteness of the white fabrics treated with different temperatures and untreated ones

Artical	Whiteness degree of untreated fabric	Whiteness degree of treated fabric at 130°C	Whiteness degree of treated fabric at 170°C
F1	54.8	55.6	59.8
F2	52.7	53.2	60.4

## Acknowledgement

This work was supported by the [TUBITAK-TEYDEB] under Grant [number 3170840] and by the [Bursa Uludag University under Grant [number FGA-2021-656]. It was carried out in cooperation with Uludağ University-Rudolf Duraner. The authors would like to express their gratitude

## REFERENCES

- Oğlakçioğlu N, Marmaralı A. 2007. Thermal comfort properties of some knitted structures. *Fibres&Textiles in Eastern Europe* 15(5-6), 94-96.
- Türker E, Dönmez ET, Turan NY. Measurement of pilling occurred on textile surfaces by image process. *İleri Teknoloji Bilimleri Dergisi* 6(1).
- Tomasino C. 1992. *Chemistry-Technology of Fabric Preparation & Finishing*. Department of Textile Engineering, Chemistry & Science College of Textiles, North Carolina State University.
- Telli A. 2019. An image processing research consistent with standard photographs to determine pilling grade of woven fabrics. *Tekstil ve Konfeksiyon* 29(1), 268-276.
- Ukponmwan JO, Mukhopadhyay A, Chatterjee KN. 1998. Pilling. *Text. Prog.* 28, 40.
- Man L, Raymand W. 2009. Mechanisms of pilling formation and reduction by attrition methods. The Hong Kong Polytechnic University Institute of Textiles & Clothing, Hong Kong.
- Başığit ZO. 2018. Effects of chemical and surface modification on mechanical and chemical properties of polyester fabrics. *Düzce University Journal of Science & Technology* 6, 1344-1353.
- Sivakumar VR, Pillay KPR. 1981. Study of pilling in polyester/cotton blended fabrics. *Ind. J. Text. Res.* 6, 22.
- Li L, Jia G, Zhou W. 2009. Effect of yarn properties on the pilling of cashmere treated fabric. *Fibres & Textiles in Eastern Europe* 17, 76-79.
- Yahya C, Akaydın M. 2013. Effects on laundering process on pilling characteristic of cotton plain fabric. *Pamukkale University Journal of Engineering Sciences* 19, 4.
- Zhang J, Wang X. 2008. Objective pilling evaluation of wool fabrics. *Textile Research Journal* 77(12), 929-936. <https://doi.org/10.1177/0040517507083522>
- Wang XY, Gong RH, Dong Z, Porat I. 2007. Abrasion resistance of thermally bonded 3D nonwoven fabrics. *Science Direct, Wear* 262, 424-431.
- Dalbaşı ES, Kayseri GÖ. 2015. Research about the effect of the anti-pilling treatments on different structured cotton knitted fabrics. *Tekstil ve Konfeksiyon* 25, 54-60.
- Nihat C, Değirmenci Z, Kaynak HK. 2010. Effect of nano-silicone softener on abrasion and pilling resistance and color fastness of knitted fabrics. *Tekstil ve Konfeksiyon* 20(1), 41-47.
- Tusief MQ, Mahmood N, Saleem M. 2012. Effect of different anti-pilling agents to reduce pilling on polyester/cotton fabric. *Journal Of The Chemical Society Of Pakistan* 34(1), 53-57.
- Abril HC, Millan MS, Torres Y. 1998. Automatic Method Based on Image Analysis for Pilling Evaluation in Fabrics. *Opt. Eng* 37(11), 2937-2947.
- Kowalczyk D, Brzezinski S, Kaminska I. 2015. Multifunctional bioactive and improving the performance durability nanocoatings for finishing PET/CO woven fabrics by the solgel method. *Journal of Alloys and Compounds* 649, 387-393.
- Hashemikia S, Montazer M. 2012. Sodium hypophosphite and nano TiO<sub>2</sub> inorganic catalysts along with citric acid on textile producing multi-functional properties. *Applied Catalysis A: General* 417-418, 200-208.
- Kulyk I, Scapinello M, Stefan M. 2012. Generation of nano roughness on fibrous materials by atmospheric plasma. 12th High-Tech Plasma Processes Conference (HTPP-12), *Journal of Physics*. <https://doi.org/10.1088/1742-6596/406/1/012015>
- Tusief MQ, Mahmood N, Amin N. 2012. Fabric tensile strength as affected by different anti-pilling agents at various concentration and pH levels. *Journal of The Chemical Society of Pakistan* 34(1), 53-57.
- Montazer M, Mazaheri F, Khosravian SH, Azimi M, Bameni M, Sadeghi AH. 2011. Application of resins and crosslinking agents on fiber blend fabric to reduce pilling performance. Optimized by Response Surface Methodology. Society of Plastics Engineers, *Journal of Vinyl&Additive Technology*. <https://doi.org/10.1002/vnl.20274>
- Mavruz S, Oğulata R. 2009. Biyoparlatma uygulanmış örme kumaşlara tekrarlı (çoklu) yıkamaların etkisinin incelenmesi. *Tekstil ve Konfeksiyon* 3, 224-230.
- Bahtiyari MI, Duran K, Körlü AE. 2010. Usage of commercial cellulases in biopolishing of viscose fabrics. *Tekstil ve Konfeksiyon* 20(1), 57-54.
- Körlü AE., Duran K, Bahtiyari Mİ, Perinçek S. 2008. The Effects of Cellulase Enzymes on Cellulosic Fabrics. *Tekstil ve Konfeksiyon* 18(1), 35-41.
- Ming Yu M, Wang Z, Lv M, Hao R, Zhao R, Qi L, Liu S, Yu C, Zhang B, Fan C, Li J. 2016. Antisuperbug Cotton Fabric with Excellent Laundering Durability. *ACS Appl. Mater. Interfaces* 8, 19866-19871.
- Bui HM, Enhrhardt A, Bechtold T. 2008. Pilling in cellulosic fabrics, part 2: A study on kinetics of pilling in alkali-treated lyocell fabrics. *Journal of Applied Polymer Science* 109, 3696-3703.
- Kertmen M, Marmaralı A. 2019. Örme Kumaşlarda Sürdürülebilirlik için Boncuklanma ve Patlama Mukavemet Özelliklerinin Değerlendirilmesi. 17th International The Recent Progress Symposium On Textile Technology And Chemistry, Bursa.
- Büyükkoru B, Kara A. 2021. Investigation of antipilling properties of different fabrics applied with polyvinylimidazole. *Textile and Apparel*, 31(4), 274-283.
- Büyükkoru B, Kara A. 2022. Investigation of the pilling properties of polyvinyl phosphonic acid treated fabrics. *Journal of the Faculty of Engineering and Architecture of Gazi University* 37(2), 697-709.
- Usanmaz A, Özdemir T, Polat O. 2009. Solid state polymerization of N-vinylcaprolactam via gamma irradiation and characterization. *Journal of Macromolecular Science, Part A* 46(6), 597-606.
- Kozanoğlu S, Özdemir T, Usanmaz A. 2011. Polymerization of N-Vinylcaprolactam and Characterization of Poly(N-Vinylcaprolactam). *Journal of Macromolecular Science, Part A, Pure and Applied Chemistry* 48, 467-477.

to the Rudolf-Duraner for providing the necessary textiles and supplies for the project, as well as a wide range of options and devices for textile applications of the synthesized polymers. This research has been the subject of a patent application. The study has successfully completed a pre-evaluation phase (with the patent number: PT2019-03389).

# Linear Model Equation for Prediction and Evaluation of Surface Roughness of Plain-Woven Fabric

Kura Alemayehu Beyene  0000-0002-2293-5048

Nuredin Muhammed  0000-0001-9335-3064

Ethiopian Institute of Textile and Fashion Technology, Bahir Dar University, Bahir Dar, 1037, Ethiopia

**Corresponding Author:** Kura Alemayehu Beyene, kuraalemayehu@gmail.com

## ABSTRACT

Nowadays, evaluating fabric touch can be a great interest of industries to match the quality needs of consumers and parameters for the manufacturing process. Modeling helps to determine how structural parameters of fabric affect the surface of a fabric and also identify the way they influence fabric properties. Moreover, it helps estimate and evaluates without the complexity and time-consuming experimental procedures. In this research paper, the linear regression model was developed that was utilized for the prediction and evaluation of surface roughness of plain-woven fabric. The model was developed based on nine different half-bleached plain-woven fabrics with three weft Yarn counts 42 tex, 29.5 tex & 14.76 tex, and three weft thread densities (18 picks per cm, 21 picks per cm & 24 picks per cm) and then the surface roughness of plain-woven fabric was tested by using Kawabata (KES-FB4) testing instrument. The findings reveal that the effects of count and density on the roughness of plain-woven fabric were found statistically significant at the confidence interval of 95%. The weft yarn count has a positive correlation with surface roughness values of plain-woven fabrics. On the other hand, pick density has a negative correlation with the surface roughness values of plain-woven fabrics. The correlation between measured surface roughness by KES-FB4 and calculated surface roughness by the model equation show how they are strongly correlated at 95% ( $R^2$  of 0.97).

## 1. INTRODUCTION

The properties of fabrics depend on their physical, chemical, and structural characteristics. Fiber type, yarn type, yarn smoothness, fabric structure, fabric thickness, and the presence of additional materials like membranes influence the comfort of clothing. In addition, the dyeing, finishing, and coating processes can also influence a material's properties [1,5].

Nowadays, consumers demand fabrics and clothing which not only look good but also feel comfortable and follow easy care. Consumers choose comfort as the most important attribute that they seek apparel products, which is followed by easy care and durability. As comfort is an individualistic sense it is very difficult to define, design, or determine it [2, 3]. Measuring and evaluating fabric surface properties can be of great interest in the industry nowadays to match the quality requirements for the consumer and the parameters for the manufacturing process purpose [3]. The most

important properties of the fabrics which affect the sensorial comfort properties of fabric and cloth are the constructional parameters during manufacturing. The most effective parameters that can be counted on the surface properties of fabrics and cloths are such as thickness, weight per square meter, the pattern of weave, thread density, crimp%, yarn count, etc. [3, 5].

The surface of the textile fabrics is not absolutely flat and smooth. Its geometrical roughness to certain extents is considerable. The roughness was defined as irregularities in the surface that can be described geometrically as the size of roughness elements or mechanically by the friction coefficients. Roughness is a descriptive term for a fabric surface that has the feel of sandpaper as per ASTM-D123-09. Smoothness and roughness of fabric and cloth materials are important sensorial properties for the design of many textile fabrics including plain bed-sheet, medical textiles, hygiene and healthcare products, sportswear, underwear,

**To cite this article:** Beyene KA, Muhammed N. 2023. Linear Model Equation for Prediction and Evaluation of Surface Roughness of Plain-Woven Fabric. *Tekstil ve Konfeksiyon* 33(1), 88-94.

## ARTICLE HISTORY

Received: 23.11.2021

Accepted: 13.12.2022

## KEYWORDS

Surface Roughness, Linear Regression Modeling, Prediction, Plain-Woven Fabric, and Structural Parameters

---

lingerie, and other consumer products that needs to have special sensitive surface tactile properties [6, 7]. The surface roughness influences the fabric hand and it plays a significant role in the end use of the fabric. A factor having an important role in the configuration of the surface characteristics of the fabric is the crimp of the yarns, under the consideration that the yarn densities of warp and weft are of the same class. If the crimp values of the weft and warp yarns are close to each other, the fabric produced is balanced in terms of appearance. The geometrical roughness characteristics of the fabrics provide information on their structural characteristics. The surface of the textile fabrics is not absolutely flat and smooth. Its geometrical roughness to certain extents is considerable. The surface roughness influences the fabric hand and it plays a significant role in the end-use of the fabric. A factor having an important role in the configuration of the surface characteristics of the fabric is the crimp of the yarns, under the consideration that the yarn densities of warp and weft are of the same class. If the crimp values of the weft and warp yarns are close to each other, the fabric produced is more or less balanced in terms of appearance [8-11]

Modeling is the process of perception of textiles by the skin fills the gap between two contemporary existing solutions: objective and subjective assessment of handling properties of fabrics [12-16]. The different number of mathematical models concerning the human body, clothing, and environment offer useful equations and tools. This is used in identifying important parameters in material design and for predicting fabrics and clothing performance under some environmental conditions [4, 16].

The measurement and evaluation of fabric surface roughness are assessed by using either contact or non-contact methods. In this regard, many devices and techniques have been developed and employed. The Kawabata Evaluation System for Fabrics (KESF), Fabrics Analysis by Simple Tests (FAST), and Fabric Touch Tester (FTT) systems are available for measuring the fabric handle-related characteristics under the contact methods. But, as far as the tactile responses are concerned, all the low-stress mechanical characteristics directly or indirectly stimulate the touch pressure roughness and other mechanoreceptors of human skin [10-16].

The measurement, quantification, and analysis of surface roughness have been the subject of many kinds of research works, due to the difficult part of these parameters in the selection of suitable fabric for diverse technical and clothing end-uses fabrics. Many types of research have focused on the measurement of fabric surface properties by objective and subjective methods. In recent years, there is technological advancement in the realism, accuracy, and predictive capabilities of equations and tools for the theory and simulation of materials or products. Predictive modeling has now become a powerful tool that can also

deliver real value through application and innovation to different industries. It forms an essential part of the research and development effort of many of the world's leading organizations and can be incredibly valuable for businesses. Using modeling, it is possible to identify the effective aspects of plain-woven fabric structure on surface roughness and also discover the way that they influence the property of surface roughness of plain-woven fabrics. Used in a combination of good analysis and experimentation, materials modeling can drive progress, saving time, cost, effort, and resources. The results obtained from the model are tangible, available quickly, and have project relevance.

Most of the researchers were focused on experimental methods for characterizing the surface roughness of fabrics but, their focus on modeling the roughness of a commonly used plain-woven fabric is limited, and hence most industries are suffering from knowing the level of surface roughness of their product. In this research, a linear regression model was developed based on the geometrical parameter of fabrics. Thereby the designers in the weaving looms can design plain-woven and various types of woven fabrics with specific surface roughness; simply by applying changes in fabric structural parameters "(such as weft yarn density and weft yarn linear density)" and laboratory personnel can simply calculate the surface roughness of given fabrics by identifying structural parameter and using the regression model equations. The model is a guide to selecting a suitable fabric for various end uses and a way to test and predict the surface roughness of any kind of woven fabric.

## 2. MATERIAL AND METHOD

### 2.1 Material

#### A. Fiber

The fiber which was used in this research work was 100% cotton and the fiber-specific characteristics properties from USTER HVI 1000 were mentioned in tabular form as shown in Table 1.

#### B. Fabrics

Plain-woven fabrics, nine 100% cotton, were produced with different yarn and fabric structural parameters by Picanol air-jet loom. As indicated in Table 2, the fabric properties were modified by using three different weft densities (PPC) and three different weft yarn linear densities (weft count), while the other factors such as warp density, warp count, tension, speed, and relative humidity (RH%) percent remained constant. The warp tension force is 1.58KN and the speed of the loom is 550 RPM. The fabrics were then

**Table 1.** Properties of cotton fiber

Fiber source	SCI	Mst [%]	Mic	Mat	UHML [mm]	SF [%]	Str [g/tex]	Elg [%]
Metema	102	8.0	4.65	0.86	28.8	10.5	23.8	7.3
Awash	110	8.9	4.72	0.87	28.65	8.0	23.1	6.4
Metema	93	8.8	4.21	0.85	28.76	8.9	21.9	6.6
Awash	110	8.7	4.49	0.86	28.59	8.2	22.2	7.0
Metema	88	7.8	4.60	0.86	28.57	11.1	20.5	6.9
Awash	105	7.8	4.50	0.86	27.33	7.4	22.8	7.0
	102	8.4	4.53	0.86	28.45	9.0	22.4	6.9

**Table 2.** Constructional parameters of plain-woven fabric

Fabric code	Weave type	Warp density (Ends/cm)	Warp count (tex)	Weft density (Picks/cm)	Weft count (tex)
<i>FK<sub>1</sub></i>	Plain	24	29.5	18	14.76
<i>FK<sub>2</sub></i>	Plain	24	29.5	21	14.76
<i>FK<sub>3</sub></i>	Plain	24	29.5	24	14.76
<i>FK<sub>4</sub></i>	Plain	24	29.5	18	29.5
<i>FK<sub>5</sub></i>	Plain	24	29.5	21	29.5
<i>FK<sub>6</sub></i>	Plain	24	29.5	24	29.5
<i>FK<sub>7</sub></i>	Plain	24	29.5	18	42
<i>FK<sub>8</sub></i>	Plain	24	29.5	21	42
<i>FK<sub>9</sub></i>	Plain	24	29.5	24	42

subjected to a combination pretreatment process. The chemicals used were sodium hydroxide 3%, hydrogen peroxide 4%, sodium silicate 2%, wetting agent 0.5%, EDTA 0.5 (% owf), and 10:1 liquor ratio. The fabric is treated at 90 °C temperature for 1:30 hr. at a machine speed of 40 m/min jigger machine (Mesdan-Lab model) was used.

## 2.2 Experimental design

Central composite design (CCD) is an efficient technique for experimentally exploring relationships between investigated factors and system response. Central composite design experiments need a minimum number of trials for estimating the main effect, require a smaller number of runs, and allow sequential experimentation, which provides

flexibility and time-saving in running the experiment and analysis [17, 18]. The experiment has 8 non-center and 5 center points and the total run is 13 with five replications as shown in Table. 3.

## 2.3 Experimental procedure

Five test specimens 20.0 × 20.0 cm are prepared for measuring surface roughness by Kawabata Evaluation System (KES-FB4) from each produced sample and conditioned at 65 ± 2% relative humidity and 20 ± 2°C for a minimum of 24 hr. before testing according to ASTM-D1776 practice for conditioning and testing textile materials. The data were statistically analyzed and evaluated using the Design-Expert software analysis of variance (ANOVA) was done.

**Table 3.** The experimental design with two factors and three levels.

Code	Run	Factor 1	Factor 2	Response 1
		Count (tex)	Density (Picks/cm)	SMD
<i>FK<sub>2</sub></i>	1	14.76	21	1.315
<i>FK<sub>5</sub></i>	2	29.5	21	1.906
<i>FK<sub>8</sub></i>	3	42	21	2.321
<i>FK<sub>1</sub></i>	4	14.76	18	1.389
<i>FK<sub>5</sub></i>	5	29.5	21	1.906
<i>FK<sub>5</sub></i>	6	29.5	21	1.906
<i>FK<sub>9</sub></i>	7	42	24	2.321
<i>FK<sub>5</sub></i>	8	29.5	21	1.906
<i>FK<sub>4</sub></i>	9	29.5	18	2.137
<i>FK<sub>5</sub></i>	10	29.5	21	1.906
<i>FK<sub>3</sub></i>	11	14.76	24	1.113
<i>FK<sub>6</sub></i>	12	29.5	24	1.520
<i>FK<sub>7</sub></i>	13	42	18	2.566

## 2.4 Developing an empirical model

There are several statistical approaches available nowadays to researchers to analyze multiple outcomes or informants. With multiple informants, researchers can jointly model the associations between factors (count and density) and response (surface roughness) using a linear regression modeling approach available in standard software packages [18, 19]. The actual equations are derived from the coded equations after the coded equations have been determined. The coded equations are determined first, and the actual equations are derived from the coded equations. The actual equation for each term (factors) was obtained from the coded equation by being replaced with its coding formula as shown in Equation (1) [17-19].

$$X_{coded} = \frac{X_{actual} - \bar{X}}{\frac{X_{High} - X_{Low}}{2}} \quad (1)$$

Where  $X_{coded}$  coded values of Surface Roughness,  $X_{actual}$  is the actual value of Surface Roughness,  $\bar{X}$  the mean values of Surface Roughness,  $X_{High}$  the maximum values of Surface Roughness, and  $X_{Low}$  the minimum value of Surface Roughness.

There should be some assumptions made in order to obtain a valid and trustworthy model for the prediction and evaluation of the surface roughness of plain-woven fabrics, even though various parameters affect the surface roughness of woven fabrics.

### Assumptions

The characteristics of all fibers are the same.

The fabric is produced with a constant tension force.

The fabric is produced with the same warp count and density.

The experimental results of surface roughness from the forming trials performed according to the matrix by central composite are tabulated in Table 3 by Response 1. These values are fed to the Design-Expert software for developing the surface roughness of the fabric by only considering the count and density of the plain-woven fabric as shown in Equation (2).

$$SMD = \beta_0 + \beta_1 A(\text{Count}) + \beta_2 B(\text{Density}) \dots\dots\dots(2)$$

### 2.5 Model validity test

It is necessary to check the fitness of the linear regression model to ensure that it gives an acceptable approximation to the true values and verifies that none of the least-squares regression assumptions are violated. Proceeding with the exploration and optimization of a fitted response surface

will likely give poor or misleading results unless the model provides an adequate fit [17, 18].

### 2.6 Model test

A plain fabric consisting of different structural parameter which has different weft densities and weft counts were used for the model test against surface roughness measured values by KES-FB4. Structural parameter analysis (density and count) was done for the fabrics which are used for model validation purposes. The count of weft yarn from the fabric is measured according to ISO 7211-5; the density of weft yarn will be measured by using ISO 7211-2 standard. Finally, the average value of each measurement was used for calculating the surface roughness of the fabrics by developing the SMD model equation by Equation (2). The surface roughness of the fabrics was also measured by the Kawabata KES-FB4 instrument. Finally, the calculated and the measured value were checked for their correlations by plotting graphs.

## 3. RESULTS AND DISCUSSION

### 3.1 Effects of count and density on the surface roughness

Surface roughness data sets are normally distributed, as illustrated in Figure 1, and were obtained from the KES-fb4 in Table 2 under the response column. From the box plot in Figure 2, it is observed that the collected data have no out layers either an upper limit or lower limit. This implies that the collected data are normal and can be used for further statistical analysis.

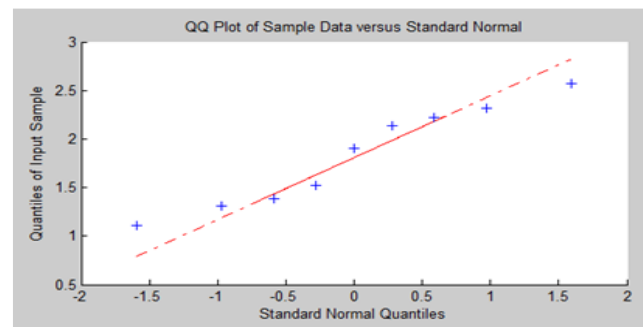


Figure 1. The quantile-quantile plot of the input data Vs. standard normal

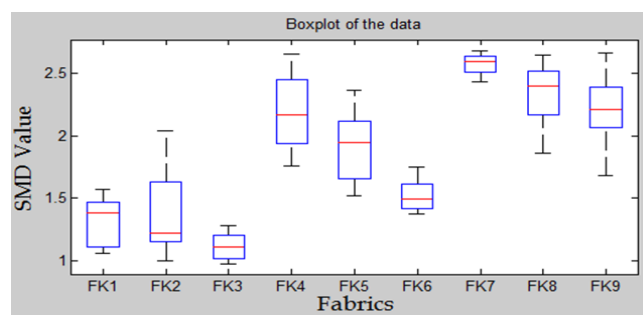
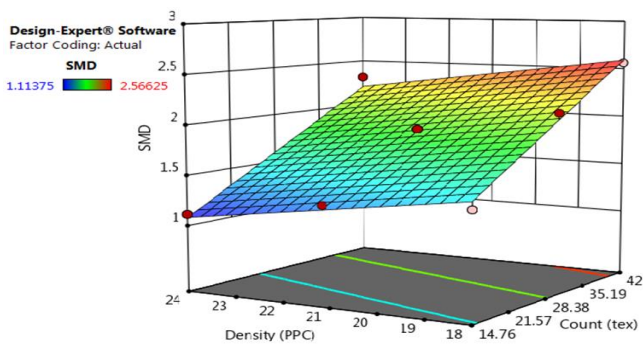


Figure 2. The box plot of the collected data set

ANOVA results of the linear models presented in Table 4 indicate that the model can adequately be used to describe the surface roughness of the fabrics based on the fabric parameters such as count and density of weft yarn. The F-value is 166.83 ( $P < 0.0001$ ) which implies that the model is significant for surface roughness. An F-value this large could occur due to noise only 0.01 percent of the time. A P-value is a measure of the test's significance [19, 20]. If the P-value is less than 0.05 ( $P < 0.05$ ), the model terms in the linear model equation are significant. Both the model terms weft count and weft density and their interactions (count X density) are statistically significant at 95% of the confidence interval since they have a P-value of 0.0001, 0.0002, and 0.0331 respectively. The Predicted  $R^2$  of 0.9407 is in reasonable agreement with the Adjusted  $R^2$  of 0.9651; i.e., the difference is less than 0.2, which ensures a satisfactory adjustment of the model to the experimental data.

A smooth fabric surface provides a bigger contact area with the human body, while a rougher fabric surface has less contact area when it gets in contact with the human body [4, 16]. The effect of weft yarn count on surface roughness values of fabrics was observed in that surface roughness values increase with weft yarn count (coarser), while it decreases as the weft yarn gets finer and finer as shown in Figure 3. Also, the surface smoothness of the fabrics increases as the pick density of the fabrics increases, and the surface roughness of the fabric increases as the weft thread density decreases as shown in Figure 3. This was because as the thread density of weft yarn increases the pick and valley on the fabric surface decreased which resulted in the interlacement of warp and weft yarns [10, 22, 23].



**Figure 3.** The effects of both density and count on the surface roughness of the fabric

### 3.2 Model equation for surface roughness

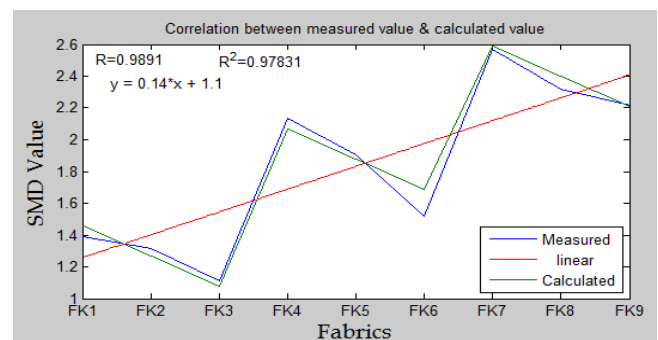
The actual model equation was developed by using surface roughness values of the nine samples which were measured by the KES-FB4 instrument. The equation in terms of actual factors (count and density) can be used to make predictions about the response (surface roughness) for given levels of each factor. Here, the levels of each factor should be stated in the original units for each factor in the linear model equations. This equation can be used to determine the relative impact of each factor because the coefficients are scaled to accommodate the units of each

factor and the intercept is at the center of the design space as shown in Equation (3).

$$SMD = +1.98837 + 0.041492 * \text{Count} - 0.063241 * \text{Density}. \quad (3)$$

### 3.3 Model validity test

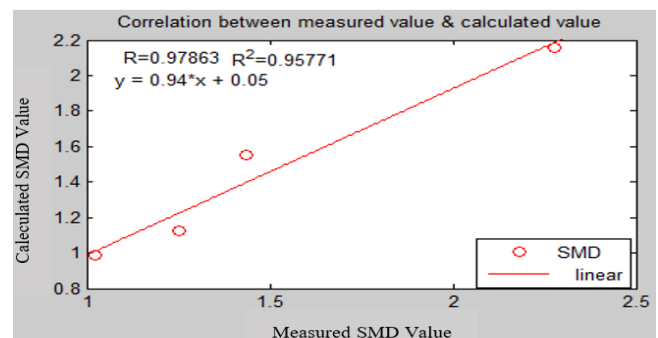
The model validation test was done by checking the correlation between the measured data obtained from the experimental method (KES-FB4) and the calculated (estimated) data obtained from the developed actual model equations SMD as shown in Equation (3). As it is shown in Figure 4, the proposed model equation can properly correlate the experimentally measured data from (KES-FB4) at the confidence interval of 95% ( $R^2$  of 0.97). The model efficiency was tested by using three different fabrics which are not used for the model equation extraction. The fabric's properties were studied and identified the weft density and count by using the ISO 7211-5 and ISO 7211-2 standard.



**Figure 4.** The correlation between the measured SMD values by KES-FB4 and the calculated SMD value by the model equation

### 3.4 Model test

The fabric properties which were used for the model test which was 100% cotton half-bleached and the parameter of construction were shown in Table 5. The correlation between the surface roughness values from KES-FB4 and the surface roughness values from the developed model equation were found to strongly correlate at the 95% degree of freedom as shown in Figure 5. The model can be used for the prediction and evaluation of plain-woven and other woven fabrics which are hundred percent cotton fabrics.



**Figure 5.** The correlation between the measured SMD values by KES-FB4 in X-direction and calculated SMD value by model equation in Y-direction for model testing



**Table 4.** ANOVA table for the linear model

Source	Sum of Squares	df	Mean Square	F-value	p-value	Decision
Model	2.14	3	1.07	166.83	P < 0.0001	Significant
Count	1.92	1	1.92	299.98	P < 0.0001	Significant
Density	0.2160	1	0.2160	33.69	P < 0.0002	Significant
Count*Density	0.0004	1	0.0004	6.35	P < 0.0331	Significant
Residual	0.0641	10	0.0064			
Lack of Fit	0.0641	6	0.0107			Not-significant
Pure Error	0.0000	4	0.0000			
Cor Total	2.20	12				

**Table 5.** Fabrics parameters for model test

Fabric code	Weave type	Warp Density (Ends/cm)	Warp count (tex)	Weft density (Picks/cm)	Weft count (tex)	Measured (SMD)	Calculated (SMD)
<i>MT<sub>1</sub></i>	Plain	32	28	32	28	1.25	1.1264
<i>MT<sub>2</sub></i>	Plain	20	20	20	20	1.437	1.5533
<i>MT<sub>3</sub></i>	Plain	21	36	21	36	2.277	2.1540
<i>MT<sub>4</sub></i>	Plain	28	18.5	28	18.5	1.023	0.9859

#### 4. CONCLUSION

Even though different structural parameters affect the surface properties of the fabrics, it is possible to control the surface behavior of the fabric with the developed model equations. The surface roughness of plain-woven fabric was mainly affected by weave type, thread density, weft, and warp linear density. The weft count and density were used for the model equation which can be used for the prediction and evaluation of the surface roughness of plain-woven fabric. The model is statistically significant and can adequately be used to describe the surface roughness of the fabrics. The surface roughness increases with count increases and the surface roughness decrease as the density

of the weft thread increases. To produce fabrics with smooth surface qualities, both yarn density and weft yarn fineness should be increased. The model was validated and tested the correlation between measured by KES-FB4 and calculated by the developed model equation revealed that the model was strongly correlated with the confidence interval of 95% ( $R^2$  of 0.95). This study needs further research and investigation since it does not only count and density affect the surface properties of woven fabrics there are many factors even in both the warp and weft direction of the woven fabrics.

#### REFERENCES

1. K. A. Beyene, E. K. Gebeyehu and B. F. Adamu, "The effects of pretreatment on the surface roughness of plain-woven fabric by the Kawabata Evaluation System," *Textile Research Journal*, 2022, pp. 1-9, 00405175221139322.
2. Ashdown, S., *Improving body movement comfort in apparel, in Improving comfort in clothing*. 2011, Elsevier. p. 278-302.
3. Roy Choudhury, A.K., P.K. Majumdar, and C. Datta, 1 - Factors affecting comfort: human physiology and the role of clothing, in *Improving Comfort in Clothing*, G. Song, Editor. 2011, Woodhead Publishing. p. 3-60.
4. Pense-Lheritier, A.-M., et al., Sensory evaluation of the touch of a great number of fabrics. *Food quality and preference*, 2006. 17(6): p. 482-488.
5. Atalie, D. and G.K. Rotich, Impact of cotton parameters on sensorial comfort of woven fabrics. *Research Journal of Textile and Apparel*, 2020. 24(3): p. 281-302.
6. Akgun, M., The effect of fabric balance and fabric cover on surface roughness of polyester fabrics. *Fibers and Polymers*, 2013. 14(8): p. 1372-1377.
7. Mao, N., Y. Wang, and J. Qu. Smoothness and roughness: Characteristics of fabric-to-fabric self-friction properties. in *The Proceedings of 90th Textile Institute World Conference*. 2016. The Textile Institute.
8. Akgun, M., B. Becerir, and H.R. Alpay, The effect of fabric constructional parameters on percentage reflectance and surface roughness of polyester fabrics. *Textile Research Journal*, 2012. 82(7): p. 700-707.
9. Classen, E., 3 - Comfort testing of textiles, in *Advanced Characterization and Testing of Textiles*, P. Dolez, O. Vermeersch, and V. Izquierdo, Editors. 2018, Woodhead Publishing. p. 59-69.
10. Beyene, K.A. and S. Gebeyaw, The effects of yarn and fabric structural parameters on surface friction of plain-woven fabrics. *Research Journal of Textile and Apparel*, 2021. 25(4): p. 210-218.
11. Beyene, K.A. and V. Sampath, Modeling Surface Roughness for prediction and evaluation of Bed-Sheet woven Fabric. *CTA-2019*, 2019: p. 42.
12. Beyene, K. A., Mengie, W., & Korra, C. G., Effects of weft count and weft density on the surface roughness of 3/1 (Z) twill woven

- 
- fabric. *Research Journal of Textile and Apparel*, ahead-of-print(ahead-of-print). <https://doi.org/10.1108/RJTA-08-2021-0104>
13. Beyene, K. A., & Kumelachew, D. M., An investigation of the effects of weave types on surface roughness of woven fabric. *Textile Research Journal*, 2022. 92(14-15).
  14. Beyene KA. Comparative study of linear and quadratic model equations for prediction and evaluation of surface roughness of a plain-woven fabric. *Research Journal of Textile and Apparel*. 2022 Feb 22.
  15. Beyene KA, Korra CG. Modeling for the Prediction and Evaluation of the Crimp Percentage of Plain Woven Fabric Based on Yarn Count and Thread Density. *Tekstilec*. 2022 Jan 1;65(1).
  16. Kawabata, S. and M. Niwa, Objective Measurement of Fabric Mechanical Property And Quality. *International Journal of Clothing Science and Technology*, 1991. 3(1): p. 7-18.
  17. Myers, R.H., et al., Response surface methodology: a retrospective and literature survey. *Journal of quality technology*, 2004. 36(1): p. 53-77.
  18. Raissi, S. and R.-E. Farsani, Statistical process optimization through multi-response surface methodology. *World Academy of Science, Engineering and Technology*, 2009. 51(46): p. 267-271.
  19. Normand, S.-L.T., Some old and some new statistical tools for outcomes research. *Circulation*, 2008. 118(8): p. 872-884.
  20. Chihara, L., Introduction to Linear Regression Analysis. *The American Mathematical Monthly*, 2002. 109(7): p. 681.
  21. Greenland, S., Valid p-values behave exactly as they should: Some misleading criticisms of p-values and their resolution with s-values. *The American Statistician*, 2019. 73(sup1): p. 106-114.
  22. Becerir, B., M. Akgun, and H.R. Alpay, Effect of some yarn properties on surface roughness and friction behavior of woven structures. *Textile Research Journal*, 2016. 86(9): p. 975-989.
  23. Kayseri, G.Ö., N. Özdil, and G.S. Mengüç, Sensorial comfort of textile materials. *Woven fabrics*, 2012: p. 235-66.

# The Effect of Various Textile Wastes (Human Hair, Denim and Pantyhose) on the Mechanical Properties of Composite Materials

Hande Sezgin  0000-0002-2671-2175

Istanbul Technical University, Faculty of Textile Technologies and Design, Textile Engineering Department, Istanbul, Türkiye

**Corresponding Author:** Hande SEZGİN, sezginh@itu.edu.tr

## ABSTRACT

As technology advances and people's needs rise, the amount of waste produced rises in tandem with increased productivity in every industry. Aside from the fact that clothing is one of the most basic human necessities, the unstoppable growth of the fast fashion trend in recent years has boosted both the textile industry's production and waste. The goal of this research is to recycle these textile industry wastes and use them in a different sector. In this context, the mechanical properties (Charpy impact strength, drop-weight impact strength, tensile strength, and flexural strength) of hybrid composite structures composed of recycled textile wastes (denim waste, human hair waste, and pantyhose waste) and E-glass plain woven fabric are compared to those of E-glass plain woven fabric reinforced composite structures. While the vacuum assisted resin transfer method is used for production, epoxy resin is employed as the matrix material. The mechanical results reveal that, aside from tensile strength, the mechanical properties of the textile waste (denim, human hair, and pantyhose) and E-glass fabric reinforced hybrid composite constructions can compete with those of the pure E-glass fabric reinforced sample. In both impact strength tests, the hybrid samples reinforced with human hair outperform the other samples, whereas the denim waste hybridized samples get the highest flexural strength values. Besides that, the statistical significance of all results is evidenced by a 2-sample t-test.

## ARTICLE HISTORY

Received: 06.04.2022

Accepted: 23.11.2022

## KEYWORDS

Denim waste, E-glass fabric, human hair, pantyhose waste, recycling

## 1. INTRODUCTION

The need of recycling waste materials is becoming more widely recognized in light of climate change and gradual depletion of natural resources [1]. The textile industry is the world's second most polluting industry, accounting for 10% of total global carbon emissions [2]. The spread of the concept of fast fashion caused a large number of textile materials to go to landfills [3, 4]. While the amount of textile waste produced is increasing on a daily basis, a study found that in 2030, an individual will generate approximately 17.5 kg of textile waste per year [3]. This demonstrates how crucial the recycling of textile materials with varied life cycles (short-life textiles - disposable textiles, etc., medium-life textiles - garments, carpets, etc., long-lasting textiles - construction textiles, etc.) is as an

environmental concern. The textile wastes are divided into three main categories as; production waste, preconsumer waste, and postconsumer waste. Production waste includes waste from various textile manufacturing procedures, while preconsumer waste covers unsold/damaged products in retailers, and postconsumer waste comprises products that the owners no longer desire to use. These waste groups can be recycled using mechanical, chemical, or thermal processes. The most popular process is mechanical recycling, which is based on a technique that converts textile materials to smaller pieces such as yarns or fibers [1].

Textile materials are manufactured from both synthetic and natural materials. Non-renewable petroleum-based polymers are the raw material source for synthetic-based

**To cite this article:** Sezgin H. 2023. The Effect of Various Textile Wastes (Human Hair, Denim and Pantyhose) on the Mechanical Properties of Composite Materials. *Tekstil ve Konfeksiyon* 33(1), 95-103.

---

fibers, which account for the vast bulk of textile fibers. Fibers made from these polymers by industrial chemical synthesis procedures withstand environmental degradation and require many years to disappear in nature due to their hydrophobic and extremely crystalline characteristics [5, 6]. Natural fibers, which appear more innocent than synthetics and are supposed to be harmless to nature, require a huge amount of fertilizers and pesticides that can harm the environment and human health, as well as a large amount of energy and water to manufacture [5, 7]. Given the environmental damage caused by both natural and synthetic fibers, the need of recycling these materials is obvious. Textile materials are recycled for reuse in the textile industry as well as in other sectors. Recycled textile materials can be utilized to produce garments, filler materials, insulation materials, and as reinforcement materials in composite structures [8-10]. Waste textile materials can be used in a variety of ways in composite materials. Fabric, yarn, fiber, and nano/micro particle fillers are examples of these forms [3]. Textile materials are preferred as reinforcement materials in composite structures because they offer excellent strength, stiffness, and fatigue resistance [11].

The primary goal of producing textile-based composite materials is to achieve good performance qualities while reducing material weight and cost [12]. Glass fiber, which has one of the best combinations of these three qualities, accounts for more than 87% of the reinforcement material in textile-reinforced composite constructions [13]. There are various types of glass fibers, and E-glass fibers are most commonly employed in composite structures due to their moderate modulus, low cost, and high strength values [14]. E-glass fiber-reinforced composites are commonly used in automobiles, boats, pipes, water tanks, and aircraft [15]. Despite its great performance, glass fiber is now being substituted with natural and/or recycled materials due to a decline in raw material resources and an increase in sustainability awareness [13].

Three distinct textile wastes (denim, pantyhose, and human hair) are applied as reinforcement material in composite structures in the scope of this investigation. The first waste category is discarded denim fabrics. Denim manufacture is one of the most environmentally destructive textile processes. For denim finishing operations such as sandblasting and aging, several toxic chemicals are employed, and these chemicals are intermingled with water resources [16]. Furthermore, considering the environmental damage caused by the manufacture of cotton fiber utilized in denim production, the relevance of recycling this waste group is widely understood. Cotton is the most common natural fiber in the textile industry, with denim being the most popular application [17-19]. The textile sector is growing at a rapid pace, and demand is rising. Many cotton-producing countries, however, have had to restrict their cotton planting areas due to dwindling water resources

[17]. While cotton cultivation is estimated to use 1-6% of the world's total fresh water, producing 1 kg of cotton lint requires 10000-17000 L of water [20]. In many countries, recycling cotton waste is one of the key options to address this issue and ensure cotton self-sufficiency [17]. Cotton fiber's elastic recovery property, high strength, elongation at break in the dry condition, and resistance to thermal deterioration all contribute to its use as a reinforcement material in composites. These composites are commonly utilized in the interior panels of automobiles [21].

Waste pantyhose is the second type of waste. It is a waste product of the textile industry, having a short lifespan and a thin and flexible construction that renders it unsuitable for reuse. As pantyhose slip away after a few wears, consumption and waste are fairly considerable. According to a 2016 UK survey, a woman spent £3,000 on pantyhose throughout her lifetime [22]. Because they contain coal and petroleum-based raw materials, these polyamide-based textile products, which may contain elastane at particular ratios, disintegrate in nature for a long period [22]. Due to its elastic modulus, abrasion resistance, hardness, tensile strength, low friction coefficient, impact absorption capacity, thermal stability, and low density, polyamide fibers are favoured as a reinforcing material in composite materials, notably for use in armors [23-26]. Polyamide fibers with hydrophilic features offer high toughness and very good elastic properties due to the crystalline region composition of 65-85% [2].

Human hair is the final waste group examined in this study. It is not used in the manufacture of textiles but it is an animal fiber. It is regarded as a useless material nearly everywhere in the world and is disposed of in municipal landfills [27]. Many harmful gases, such as ammonia, sulfur dioxide, and hydrogen sulphides, are generated when attempting to eliminate this waste group by burning [28]. Although plant fibers are the most commonly utilized reinforcement material in composite structures, animal fibers, including human hair, are also used [29]. Superior tensile strength, moderate degradation rate, hydrophilic qualities, low cost, unique chemical composition, and elastic recovery properties are some of the properties of human hair fiber that make it a promising reinforcement material [13, 29-31].

Looking through the literature, it is obvious that there are studies that investigate the use of denim wastes [32-41] in polymer composite constructions. There are, however, only a few investigations on polymer composites reinforced with human hair [42-47], and none on waste pantyhose-reinforced composite structures. In one of these studies, Zonatti et al. (2015) produced various composites using different thermoset resins (epoxy, polyester orthophthalic, and polyurethane) and recycled denim wastes. The fiber ratios of the composites were kept constant at 30%. The obtained results showed that the tenacity and Young's

modulus values of denim waste-reinforced epoxy-based composites increased by two times when compared to pure epoxy resin, whereas the tenacity and Young's modulus values of denim waste-reinforced orthophthalic polyester resin-based composites increased by two and three times, respectively, when compared to pure orthophthalic polyester resin. There were no substantial changes in these parameters in polyurethane resin composites [40]. In the study conducted by Baccouch et al. (2022), cotton, polyester, and cotton/polyester wastes were brought into nonwoven surface form and composite panels were produced by vacuum infusion technique. The mechanical, thermal, and acoustic properties of nonwovens and composite samples were investigated in this study, which utilized cotton wastes obtained from discarded denim fabrics. The results showed that nonwoven samples produced with 100% denim waste had the highest specific Young's modulus, specific tensile strength, and elongation values, whereas 100% denim waste reinforced composite structures had the highest specific Young's modulus, specific tensile strength, and impact strength values [41]. Senthilnathan et al. (2014) constructed hybrid composite structures employing several reinforcement materials (coconut fiber, human hair fiber, and glass fiber) in an epoxy resin matrix. Six different composite designs were produced by hand lay-up method, including glass fiber reinforced plastic (GFRP), coconut coir reinforced plastic (CCRP), human hair reinforced plastic (HHRP), glass - coconut coir - human hair- glass hybrid composite (GCHGRP), coconut coir-glass-human hair-coconut coir hybrid composite (CGHCRP), and human hair-coconut coir-glass-human hair hybrid composite (HCGHRP). The results showed that, whereas CCRP had the highest tensile load capacity, HCGHRP had the best flexural strength. Furthermore, when compared to other composites, HCGHRP exhibited significant impact strength values [46]. In another study, Selvan et al. used the hand lay-up technique to produce five different composite designs reinforced with jute fiber and human hair fiber with varying ratios. As a matrix material, epoxy resin was used. The mechanical properties were investigated, and the results showed that increasing the human hair content enhanced

the tensile, flexural, double shear, and impact properties [47].

As a consequence of reviewing the literature on these investigations, the goal of this research is to develop hybrid composite materials reinforced with waste textile materials that can be used in substitute of the most commonly used E-glass reinforced composite materials. When considering the used waste groups, the fact that a study in which polyamide-based pantyhose waste was evaluated as a reinforcement material had not been done before reveals the study's originality, while utilizing cotton, a fiber that consumes a high amount of chemicals, water, and energy during its production, and the use of human hair which is sent from barber shops to landfills in almost every country, despite having very high mechanical properties, shows the contribution of the study to sustainability.

## 2. MATERIAL AND METHOD

### 2.1 Material

In this study, four diverse textile materials (E-glass fabric, waste denim, waste pantyhose and human hair) are used as reinforcement materials. E-glass (supplied by Omnis Kompozit) is in the form of plain-woven fabric and technical properties are given in Table 1. Preconsumer waste denim fabric (supplied by Calik Denim) and postconsumer waste pantyhose (supplied by consumers) are used in fiber form. Undyed human hair obtained from a male barber is cut into 10-30 mm lengths and used. A microscope (Zeiss, Primo Star) is used to measure the diameter and length of the waste fibers used. The average diameters of waste cotton, polyamide, and human hair are  $18.7 \pm 1 \mu\text{m}$ ,  $19.7 \pm 0.7 \mu\text{m}$ , and  $70 \pm 5 \mu\text{m}$ , respectively, while the average lengths of cotton and polyamide fibers are 20-40 mm and 30-50 mm, respectively. Denim is comprised entirely of cotton fibers, whereas pantyhose is made up of 85% polyamide and 15% elastane. The matrix system consists of an epoxy resin (F-1564, Fibermak) and a hardener (F-3486, Fibermak). The technical properties of the resin system are given in Table 2. They are mixed in a ratio of 3:1.

**Table 1.** Technical properties of E-glass fabric

Basis Weight (g/m <sup>2</sup> )	Warp x Weft Densities (epc x ppc)*	Thickness (mm)	Warp Yarn Count (Tex)	Weft Yarn Count (Tex)
300	4 x 3	0.37	600	850

\* epc: ends per cm and ppc: picks per cm

**Table 2.** Technical properties of resin system.

	Density (25 °C) [g/cm <sup>3</sup> ]	Viscosity (25 °C) [cps]	Epoxide value [Eq/kg]	Amine value [Eq/kg]
Epoxy resin	1.1-1.2	1250-1450	5.80 - 6.05	-
Hardener	1.0	10-20	-	8.55 - 9.30



**Figure 1.** (a) Feeding and (b) output unit of rag pulling machine, (c) feeding and (d) output unit of carding machine

## 2.2 Method

### Preparation of waste reinforcement materials

Waste denim fabrics and waste polyamide pantyhose are turned into fiber form by going through a rag pulling machine (Balkan Machine – Type: DT 10) (Figure 1(a) - (b)) separately before composite material production. After that, these fiberized materials are put into the carding machine (Mesdan – Type: 337A) (Figure 1(c) - (d)), which produces an aligned web form. In addition, the other waste reinforcement material human hair is washed, dried and after that cut into lengths of 1 to 3 cm and then fed to the carding machine to form an oriented web form.

### Production of composite materials

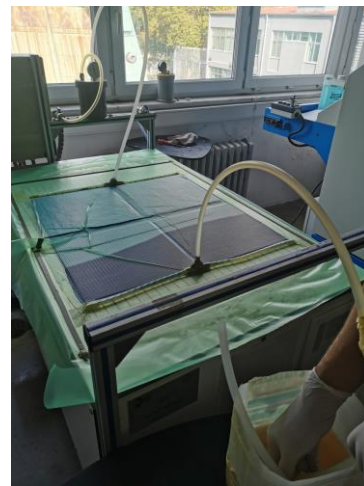
Composite fabrication is realized by vacuum-assisted resin transfer method (Figure 2) at 90°C and structures are cured for 3 hours under 1 atm pressure. Following the application of a PVA-based releasing agent to the vacuum table, the reinforcing materials are spread onto the table and covered with peel-ply fabric, a resin-flow mesh, and a vacuum bag. The vacuum pump is used to remove surplus air before production. The produced resin is then infused into the reinforcement material, and the surplus resin is vacuumed out with the help of a vacuum pump.

Three layers of reinforcement material are used to create the composite structures. While the E-glass reinforced structure has three layers of E-glass woven fabric, the same weight of denim waste, pantyhose waste, or human hair waste is placed between two layers of E-glass fabric in hybrid composite structures (Figure 3). Table 3 shows sample codes and reinforcement types.

### Physical analysis

The weights of the samples cut in specified sizes are measured with a precision balance to calculate the fiber

weight ratios of the composite samples. The weights of the reinforcement materials in those dimensions are computed using the areal densities of the reinforcement materials, and the fiber weight ratio for each sample group is determined. A caliper is used to measure the thickness of the samples. By dividing the weights by the volumes of test samples whose dimensions and weights have been measured, density values are calculated.



**Figure 2.** Production of the composite sample by vacuum-assisted resin transfer method



**Figure 3.** Produced samples

**Table 3.** Sample codes and reinforcement types

Sample Code	Reinforcement layer I	Reinforcement layer II	Reinforcement layer III
GGG	E-glass fabric	E-glass fabric	E-glass fabric
GDG	E-glass fabric	Denim waste	E-glass fabric
GPG	E-glass fabric	Pantyhose waste	E-glass fabric
GHG	E-glass fabric	Human hair waste	E-glass fabric

## Mechanical Analysis

### Charpy impact resistance

The Charpy impact test is carried out using the Devotrans impact tester (Model: DVT CD OK) in compliance with BS EN ISO 179: 1997 (Sample dimensions: 127×12.7 mm). The samples have a notch cut out in the center, and 12 joule impact energy is applied to the notched samples. Three specimens in the 0° direction and three specimens in the 90° direction are tested from each sample group, and the mean values are presented along with standard deviation values.

### Drop-weight impact resistance

The drop-weight impact test performed with the BESMAK impact tester (custom-made) is carried out following the ASTM D7136 standard (sample dimensions: 89×55 mm). According to the potential energy law, the impact is adjusted to 20 joules by altering the height of the striker (diameter: 16 mm, weight: 41 kg). Each sample group is given five measurements, and the mean results are given by standard deviation values.

### Flexural strength

The ASTM D790-10 standard (sample dimensions: 136x20 mm) is used to conduct the flexural strength test with the Shimadzu universal testing machine (AG-IS Series). The crosshead speed is set at 6 mm/min. Three specimens in the 0° direction and three specimens in the 90° direction are tested from each sample group, and the mean values are presented along with standard deviation values.

### Tensile strength

Tensile testing is carried out with the use of a Shimadzu universal testing machine (AG-IS Series), in accordance with the ASTM D638 standard (sample overall length: 115 mm, the width of narrow section: 6mm). Six measurements are taken for each sample group (3 specimens at 0° direction and 3 specimens at 90° direction), with the crosshead speed set to 3 mm/min. The standard deviation values are included alongside the tensile strength mean values.

## Statistical Analysis

The statistical significance of the physical and mechanical test results comparisons is investigated using the Minitab 16 software program and the 2-sample t-test method at a 95% confidence interval. The results are evaluated according to the p-value and those below 0.05 are expressed as statistically significant.

## 3. RESULTS AND DISCUSSION

### 3.1 Physical Analysis

Table 4 shows the thickness, density, and fiber weight ratios of composite samples. The fiber weight ratios of the waste-reinforced samples are comparable (38-44%), while the fiber weight ratio of the 3-ply E-glass fabric-reinforced sample (65%) is significantly higher than the others. When the fiber weight ratios of the GGG sample are compared to those of the GDG, GPG, and GHG hybrid samples statistically, it is discovered that the differences are all statistically significant (p values are 0.014, 0.000, and 0.017, respectively), whereas the differences in the fiber weight ratios of the hybrid samples (except for the GDG-GHG comparison) are not. This scenario is hypothesized to be caused by two factors. E-glass has a hydrophobic surface and this reduces its liquid affinity [48]. In addition, since the middle layer is a fiber layer in waste-reinforced sandwich structures, it has much more gaps than the E-glass woven fabric reinforced sample. These gaps allow the material to absorb more resin and reduce the fiber weight ratio. When the waste-reinforced samples are compared, it is discovered that the fiber weight ratio of the structure with the human hair inter layer (GHG) is greater than the others. The reason is that, whereas the inside section of human hair is hydrophilic, the surface is hydrophobic [49].

The GGG sample has a much lower thickness (p values of GGG-GDG, GGG-GPG and GGG-GHG thickness comparisons are 0.034, 0.017 and 0.001, respectively) than the others because the E-glass fiber absorbs less resin than the reinforcement materials in the other samples. Furthermore, the high density of the E-glass fiber (2.56 g/cm<sup>3</sup>) and the higher fiber weight ratio in the GGG sample compared to the other samples resulted in a higher density.

**Table 4.** Physical properties of composite samples

Sample Code	Thickness ± SD (mm)	Density ± SD (g/cm <sup>3</sup> )	Fiber Weight Ratio ± SD (%)
GGG	0.93 ± 0.06	1.47 ± 0.08	0.65 ± 0.03
GDG	1.95 ± 0.19	1.21 ± 0.08	0.39 ± 0.03
GPG	1.69 ± 0.14	1.24 ± 0.05	0.40 ± 0.02
GHG	1.70 ± 0.08	1.16 ± 0.09	0.44 ± 0.02

### 3.2 Mechanical Analysis

#### Charpy impact resistance

Figure 4 shows the Charpy impact resistance values of composite samples taken at 0° and 90° directions. The excellent impact resistance of the E-glass fiber is one of its most distinguishing characteristics [50]. The impact resistance of the composite sample with a human hair layer between two E-glass fabrics (GHG) is higher than that of the E-glass fabric reinforced sample (GGG), according to the results. It has been observed in several research in the literature that hybridizing glass fiber with natural fibers at particular rates increases the material's impact resistance. The high elongation value of the additional natural fiber was cited as the cause of this condition [21, 51]. The high impact resistance obtained in the hybrid sample with the human hair interlayer can be explained by the high elongation value of human hair (dry: 20-30%, wet: up to 50%) [52], which is a form of wool. Additionally, in a study conducted by Saiman et al. (2013), the mechanical properties of composites reinforced with yarns of varying yarn counts were investigated, and it was revealed that increasing yarn diameter resulted in a significant increase in the impact strength of the composite material. One of the reasons for the high impact resistance obtained from the GHG sample may be that the diameter of the human hair used in this study is approximately three times that of the other waste fibers [53].

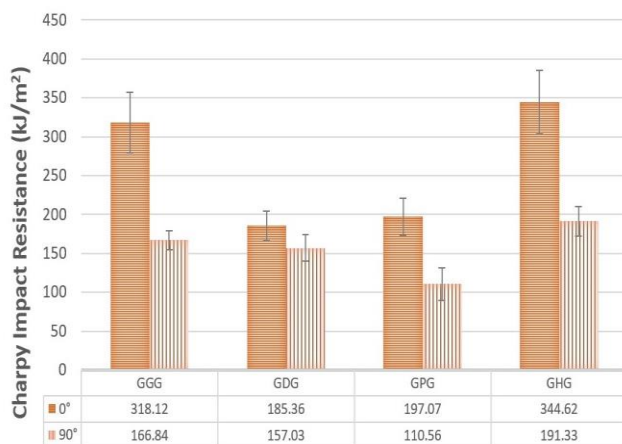


Figure 4. Charpy impact resistance results

Waste denim (GDG) and waste pantyhose (GPG) reinforced composite samples have fairly similar and lowest impact resistance values at 0° direction (p-value for 0° and 90° directions are 0.085 > 0.05 and 0.015, respectively). Furthermore, the impact resistance values of samples collected from 0° direction are higher than those of samples taken from 90° direction. The 0° direction corresponds to the plain-woven E-glass fabric's warp direction and the oriented directions of the waste fiber webs, therefore this is an expected result. The statistical significance of this situation is also investigated using the 2-sample t test, and the results obtained from the 0° and 90° directions of each of the GGG, GDG, GPG, and GHG samples are compared with each other, yielding p values of 0.005, 0.025, 0.009, and 0.012, respectively.

#### Drop-weight impact resistance

Structures having stiff surfaces in their outer layers and more hollow and shock-absorbing layers in their inner layers are known to withstand mechanical loads better [54, 55]. In the drop-weight impact test, the load is applied to the fabric layer first, then to the fiber layer in between, resulting in an increase in the amount of energy absorbed. Consistent with this information, the samples containing waste textile fiber webs absorb more energy than the GGG sample, as shown in Table 5.

The acquired results are similar to the Charpy impact test results and show that the GHG sample absorbs more energy than the others. This is thought to be due to the fact that the elongation value of human hair is quite high compared to other fibers [52]. It has also been statistically proven by a 2-sample t test, except for the GDG sample. The p-value in the analysis examining the differences in the absorbed energies of the GHG and GDG samples is found as 0.106, indicating that there is no statistically significant difference between them and the p values of other comparisons (GHG-GGG and GHG-GPG) are found as 0.014 and 0.049, respectively. Furthermore, in a study examining the mechanical properties of hybrid composite structures made of coconut fiber, human hair fiber, and glass fiber, it was discovered that the impact resistance of the hybrid composite structure made up of a high percentage of human hair fiber was greater than the others, supporting the result [46].

Table 5. The drop-weight impact strength test results

Sample Code	Maximum load ± SD (kN)	Absorbed energy ± SD (J)	Maximum load ± SD (kN)
GGG	2.54 ± 0.08	9.88 ± 0.62	11.73 ± 1.07
GDG	2.64 ± 0.09	13.67 ± 1.01	17.00 ± 1.73
GPG	2.38 ± 0.08	12.61 ± 1.83	14.93 ± 1.28
GHG	2.46 ± 0.11	15.52 ± 1.79	22.17 ± 2.01



## Flexural strength

Figure 5 shows the flexural strength of the samples taken in the 0° and 90° directions. Higher values are obtained with samples taken from the 0° direction, as is the case with impact strength. The statistical significance of this situation is also reviewed using the 2-sample t test, and the results from the 0° and 90° directions of each of the GGG, GDG, GPG, and GHG samples are compared, achieving p values of 0.001, 0.020, 0.000, and 0.000, respectively. When the strength values are examined, it is discovered that the three layers of E-glass fabric reinforced sample (GGG) has the lowest value, while the denim waste (GDG) and pantyhose waste (GPG) reinforced structures have the greatest values.

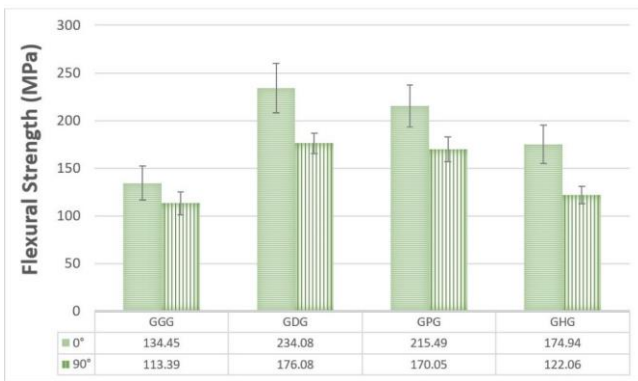


Figure 5. Flexural strength test results

The fiber weight ratio of the GGG sample is much higher than that of the other samples, as shown in Table 3, indicating that the epoxy resin ratios of the hybrid composite samples are higher than that of the GGG sample. Brittle materials have greater flexural strength [53]. As it is known that increasing the cured epoxy ratio increases the brittleness of the material, higher flexural strength values of hybrid composites are expected. Besides this, Shibata et al. (2015) noted that increasing the length of the fiber used in fiber-reinforced polymer composites enhanced the flexural strength of the composite material. The fibers obtained from the denim and pantyhose wastes used in this study are known to be longer than the length of human hair. This is assumed to be the reason the GDG and GPG samples have higher bending strength values than the GHG sample [56].

## Tensile strength

Figure 6 shows the tensile strength values of composite samples. The samples reinforced with three layers of E-glass fabric (GGG) show the highest tensile strength values in both directions when compared to the hybrid samples reinforced with waste materials. This circumstance is also statistically analyzed, and it is demonstrated that there is a significant difference ( $p: 0.000 < 0.05$ ) between the tensile strength values of the GGG samples and the tensile strength values of the hybrid samples obtained from both directions. The GGG sample's middle layer is made of E-glass plain-woven fabric, whereas the other three samples are in the

shape of fiber webs. The tensile strength of woven constructions is increased because the intersection of the yarns generates a stable situation in the structure [55]. Plain woven textiles, which have the most warp/weft interlaces per unit area, are more resistant to in-plane shear movements, making them good reinforcing materials [57].

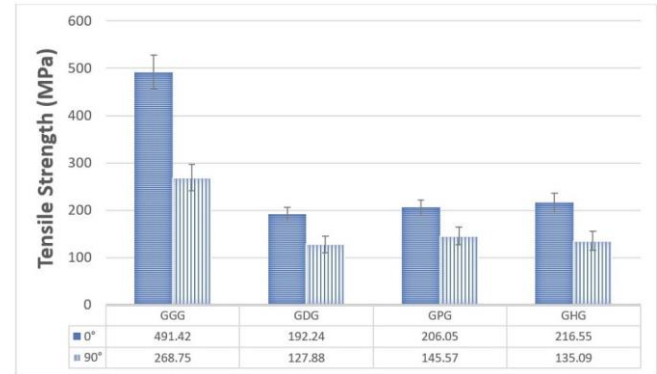


Figure 6. Tensile strength test results

According to the literature, the tensile strength of composite materials is mostly related to the tensile strength of the fiber utilized and increases as the number of glass layers increases [50]. This could explain why the GGG sample has such a high tensile strength value. Besides that, in a study comparing the mechanical properties of coconut, human hair, and glass fiber-reinforced hybrid composite structures with those of glass fiber-reinforced composite structures, it was discovered that glass fiber-reinforced composite has the highest tensile strength [46]. This information from the literature corroborates the outcome.

## 4. CONCLUSION

Textile-reinforced composite materials hybridized with various textile wastes (denim, pantyhose, and human hair) are produced in this study, and their mechanical properties are compared to those of E-glass fabric-reinforced composite. Because E-glass is the most commonly used fiber in composite production, it is chosen as the control sample. Pantyhose, which has a very short lifespan and cannot be given to someone else for reuse, denim, which has a large environmental impact both during cotton cultivation and fabric production, and human hair, which is sent to landfills every day by hairdressers and barbers, are chosen as textile wastes to be evaluated for this purpose. The key findings are listed below.

- Textile waste-reinforced hybrid composite samples have much lower densities than E-glass fabric-reinforced sample.
- The impact (Charpy and drop-weight) strength values of the hybrid composite samples reinforced with human hair are higher than those of the other samples, which could be attributed to the larger diameter of human hair compared to other waste fibers.

- The flexural strength values of the textile waste-reinforced hybrid composite samples are significantly greater than those of the E-glass fabric-reinforced samples; additionally, the highest strength values are obtained with the samples reinforced with denim and pantyhose wastes, which could be credited to the longer length of these fibers.
- The strength of samples taken from the 0° direction is higher in all mechanical tests.
- However, the tensile strength values of textile waste-reinforced hybrid composites are significantly lower than those of the E-glass reinforced sample.

These findings indicate that waste textile-reinforced hybrid composite materials can be used as an alternative to E-glass reinforced composites when tensile strength is not required and bending and impact strength are important. The significance of various waste groups is revealed by assessing the waste of pantyhose, which has never been used as a reinforcement material in the literature, as well as human hair, which is not commonly used in polymer-based composites. In our world of diminishing natural resources, it is expected that the findings of this study will serve as a guide for future research and shed light on the recycling studies of many waste groups that are currently not recycled.

## REFERENCES

1. Yalcin-Enis I., Kucukali-Ozturk M., Sezgin H. 2019. Risks and management of textile waste. In: Gothandam K., Ranjan S., Dasgupta N., Lichtfouse E. (eds) *Nanoscience and Biotechnology for Environmental Applications*. Environmental Chemistry for a Sustainable World, vol 22. Springer, Cham.
2. Echeverria CA, Handoko W, Pahlevani F, Sahajwalla V. 2019. Cascading use of textile waste for the advancement of fibre reinforced composites for building applications. *Journal of Cleaner Production* 208, 1524-1536.
3. Kamble Z, Behera BK. 2021. Sustainable hybrid composites reinforced with textile waste for construction and building applications. *Construction and Building Materials* 284, 122800.
4. Lu JJ, Hamouda H. 2014. Current status of fiber waste recycling and its future. *Advanced Materials Research* 878, 122-131.
5. Wang Y. 2010. Fiber and Textile Waste Utilization. *Waste and Biomass Valorization* 1, 135-143.
6. Egan J, Salmon S. 2022. Strategies and progress in synthetic textile fiber biodegradability. *SN Applied Sciences* 4(22). <https://doi.org/10.1007/s42452-021-04851-7>.
7. Zhang Y, Liu X, Xiao R, Yuan Z. 2015. Life cycle assessment of cotton T-shirts in China. *The International Journal of Life Cycle Assessment* 20, 994-1004.
8. Hawley JM. Textile recycling: a system perspective. In: Wang, Y. (ed.) *Recycling in Textiles*, pp. 7-24. Woodhead Publishing, 2016, Cambridge
9. Kotliar A. 199. Wood-like properties from carpet and textile fibrous waste: mitigating the coming landfill crisis. *Polymer-Plastics Technology and Engineering* 38(3), 513-531.
10. Briga-Sá A, Nascimento D, Teixeira N, Pinto J, Caldeira F, Varum H, Paiva A. 2013. Textile waste as an alternative thermal insulation building material solution. *Construction and Building Materials* 38, 155-160.
11. Mishra R, Behera B, Militky J. 2014. Recycling of textile waste into green composites: Performance characterization. *Polymer Composites* 35(10), 1960-1967.
12. Hasan KMF, Horváth PG, Alpár T. 2021. Potential fabric-reinforced composites: a comprehensive review. *Journal of Materials Science* 56, 14381-14415.
13. Masood Z, Ahmad S, Umair M, Shaker K, Nawab Y, Karahan M. 2018. Mechanical behaviour of hybrid composites developed from textile waste. *Fibres and Textiles in Eastern Europe* 26, 46-52.
14. Hameed N, Sreekumar PA, Francis B, Yang W, Thomas S. 2007. Morphology, dynamic mechanical and thermal studies on poly (styrene-co-acrylonitrile) modified epoxy resin/glass fibre composites. *Composites Part A: Applied Science and Manufacturing* 38(12), 2422-2432.
15. Elanchezian C, Ramnath BV, Hemalatha J. 2014. Mechanical Behaviour of Glass and Carbon Fibre Reinforced Composites at Varying Strain Rates and Temperatures. *Procedia Materials Science* 6, 1405-1418.
16. Radhakrishnan, S. 2017. Denim Recycling. In: Muthu, S. (eds) *Textiles and Clothing Sustainability*. Textile Science and Clothing Technology. Springer, Singapore. [https://doi.org/10.1007/978-981-10-2146-6\\_3](https://doi.org/10.1007/978-981-10-2146-6_3)
17. Yousef S, Tatariants S, Tichonovas M, Sarwar Z, Jonušienė I, Kliucininkas L. 2019. A new strategy for using textile waste as a sustainable source of recovered cotton. *Resources Conservation & Recycling* 145, 359-369.
18. Pensupa N, Leu SY, Hu Y, Du C, Liu H, Jing H, Wang H, Lin CSK. 2017. Recent Trends in Sustainable Textile Waste Recycling Methods: Current Situation and Future Prospects, In: Lin C. (eds) *Chemistry and Chemical Technologies in Waste Valorization*. Topics in Current Chemistry Collections. Springer, Cham.
19. Yousef S, Tatariants M, Tichonovas M, Kliucininkas L, Lukosiute SI, Yan L. 2020. Sustainable green technology for recovery of cotton fibers and polyester from textile waste. *Journal of Cleaner Production* 254, 120078.
20. Baydar G, Ciliz N, Mammadov A. 2015. Life cycle assessment of cotton textile products in Turkey. *Resources, Conservation and Recycling* 104, 213-223.
21. Giridharan R, Jenarathanan MP. 2019. Preparation and characterisation of glass and cotton fibers reinforced epoxy hybrid composites. *Pigment & Resin Technology* 48(4), 272-276.
22. Hasret F, Agac S. 2021. A sustainable design example: Evaluation of pantyhose with bricolage and deconstruction method. *Global Journal of Arts Education* 11(1), 71-88.
23. Guler S. 2018. The effect of polyamide fibers on the strength and toughness properties of structural lightweight aggregate concrete. *Construction and Building Materials* 173, 394-402.
24. Jeon JK, Kim W, Jeon CK, Kim JC. 2014. Processing and mechanical properties of macro polyamide fiber reinforced concrete. *Materials* 7, 7634-7652.
25. Jeon JK, Kim W, Kim GY, Jeon CK. 2016. Polyamide fiber reinforced shotcrete for tunnel application. *Materials* 9(3), 163.
26. Nieto SPR, Giraldo ES, Pedrao D, Calderon G, Valbuena GCC. 2014. Influence of nylon on the tensile strength of a polymer matrix composite material. *Tecciencia* 9(16), 78-84.
27. Gupta A. 2014. Human Hair "Waste" and Its Utilization: Gaps and Possibilities. *Journal of Waste Management* 2014, 498018.
28. Nanda BP, Satapathy A. 2020. Processing and thermal characteristics of human hair fiber-reinforced polymer composites. *Polymers and Polymer Composites* 28(4), 252-264.

29. Butt WA, Mir BA, Jha JN. 2016. Strength behavior of clayey soil reinforced with human hair as a natural fibre. *Geotechnical and Geological Engineering* 34, 411-417.
30. Jain D, Kothari A. 2012. Hair fibre reinforced concrete. *Research Journal of Recent. Sciences* 1, 128-133.
31. Vengatesan KJ, Prasanth T, Swagath Kumar VKS, Suresh K, Chokkalingam P. 2017. Study on mechanical properties and structural analysis of human hair fiber reinforced epoxy polymer. *International Journal of Advanced Research in Basic Engineering Science and Technology* 3, 754-759.
32. Temmink R, Baghaei B, Skrifvars M. 2018. Development of biocomposites from denim waste and thermoset bio-resins for structural applications. *Composites Part A: Applied Science and Manufacturing* 106, 59-69.
33. Hassani P, Soltani P, Ghane M, Zarrebini M. 2021. Porous resin-bonded recycled denim composite as an efficient sound-absorbing material. *Applied Acoustics* 173, 107710.
34. Oztemur J, Sezgin H, Yalcin-Enis I. 2021. Design of an impact absorbing composite panel from denim wastes and acrylated epoxidized soybean oil based epoxy resin. *Tekstil ve Konfeksiyon* 31(3), 229 – 234.
35. Meng X, Fan W, Mahari WAW, Ge S, Xia C, Wu F, Han L, Wang S, Zhang M, Hu Z, Ma NL, Le QV, Lam SS. 2021. Production of three-dimensional fiber needle-punching composites from denim waste for utilization as furniture materials. *Journal of Cleaner Production* 281, 125321.
36. Sezgin H, Kucukali-Ozturk M, Berkalp OB, Yalcin-Enis I. Design of composite insulation panels containing 100% recycled cotton fibers and polyethylene/polypropylene packaging wastes. *Journal of Cleaner Production* 304, 127132.
37. Meng X, Fan W, Ma Y, Wei T, Dou H, Yang X, Tian H, Yu Y, Zhang T, Gao T. 2020. Recycling of denim fabric wastes into high-performance composites using the needle-punching nonwoven fabrication route. *Textile Research Journal* 90(5-6), 695-709.
38. Islam S, Messiry ME, Sikdar PP, Seylar J, Bhat G. 2020. Microstructure and performance characteristics of acoustic insulation materials from post-consumer recycled denim fabrics. *Journal of Industrial Textiles*, <https://doi.org/10.1177/1528083720940746>.
39. Lu L, Fan W, Meng X, Liu T, Han L, Zhang T, Dong J, Yuan L, Tian H. 2021. Modal analysis of 3D needled waste cotton fiber/epoxy composites with experimental and numerical methods. *Textile Research Journal* 91(3-4), 358-372.
40. Zonatti WF, Guimaraes BMG, Duleba W, Ramos JB. 2015. Thermoset composites reinforced with recycled cotton textile residues. *Textiles and Clothing Sustainability* 1, <https://doi.org/10.1186/s40689-014-0001-7>.
41. Baccouch W, Ghith A, Yalcin-Enis I, Sezgin H, Miled W, Legrand X, Faten F. 2022. Investigation of the mechanical, thermal, and acoustical behaviors of cotton, polyester, and cotton/polyester nonwoven wastes reinforced epoxy composites. *Journal of Industrial Textiles* 51(6), 876–899.
42. Verma A, Singh V. 2019. Mechanical, microstructural and thermal characterization of epoxy-based human hair-reinforced composites. *Journal of Testing and Evaluation* 47(2), 1193-1215.
43. Selvakumar K, Meenakshisundaram O. 2019. Mechanical and dynamic mechanical analysis of jute and human hair-reinforced polymer composites. *Polymer Composites* 40(3), 1132-1141.
44. Ansari AA, Dhakad SK, Agarwal P. 2020. Investigation of mechanical properties of sisal fibre and human hair reinforced with epoxy resin hybrid polymer composite. *Materials Today: Proceedings* 26(2), 2400-2404.
45. Balachandar M, Ramnath BV, Kumar SA, Sankara GS. 2019. Experimental evaluation on mechanical properties of natural fiber polymer composites with human hair. *Materials Today: Proceedings* 16(2), 1304-1311.
46. Senthilnathan D, Gnanavel Babu A, Bhaskar GB, Gopinath KGS. 2014. Characterization of glass fibre – coconut coir– human hair hybrid composites. *International Journal of Engineering and Technology* 6(1), 75-82.
47. Panneer Selvan S, Jaiganesh V, Selvakumar K. 2014. Investigation of mechanical properties and optimization in drilling of jute and human hair hybrid composite. *International Conference on Advances in Design and Manufacturing*, 631-636.
48. Khan RA, Khan MA, Zaman HU, Pervin S, Khan N, Sultana S, Saha M, Mustafa AI. 2010. Comparative studies of mechanical and interfacial properties between jute and E-glass fiber-reinforced polypropylene composites. *Journal of Reinforced Plastics and Composites* 29(7), 1078-1088.
49. Popescu C, Höcker H. 2007. Hair—the most sophisticated biological composite material. *Chemical Society Reviews* 36, 1282-1291.
50. Portella EH, Romanzini D, Angrizani CC, Amico SC, Zattera AJ. 2016. Influence of stacking sequence on the mechanical and dynamic mechanical properties of cotton/glass fiber reinforced polyester composites. *Materials Research* 19(3), 542-547.
51. Zeeshan M, Ali M, Anjum AS, Nawab Y. 2019. Optimization of mechanical/thermal properties of glass/flax/waste cotton hybrid composite. *Journal of Industrial Textiles*. <https://doi.org/10.1177/1528083719891420>.
52. Velasco MVR, Dias TCDS, Freitas AZD, Júnior NDV, Pinto CASDO, Kaneko TM, Baby AR. 2009. Hair fiber characteristics and methods to evaluate hair physical and mechanical properties. *Brazilian Journal of Pharmaceutical Sciences* 45(1), 153-162.
53. Saiman MPB, Wahab MSB, Wahit MUB. 2013. The effect of yarn linear density on mechanical properties of plain woven kenaf reinforced unsaturated polyester composite. *Applied Mechanics and Materials* 465-466, 962-966.
54. Skrifvars M, Dhakal H, Zhang Z, Gentilcore J, Åkesson D. 2019. Study on the mechanical properties of unsaturated polyester sandwich biocomposites composed of uniaxial warp-knitted and non-woven viscose fabrics. *Composites Part A: Applied Science and Manufacturing* 121, 196-206.
55. Haery HA, Zahari R, Kuntjoro W, et al. 2014. Tensile strength of notched woven fabric hybrid glass, carbon/epoxy composite laminates. *Journal of Industrial Textiles* 43, 383-395.
56. Shibata S, Cao Y, Fukumoto I. 2005. Press forming of short natural fiber-reinforced biodegradable resin: Effects of fiber volume and length on flexural properties. *Polymer Testing* 24(8), 1005-1011.
57. Campbell FC. 2010. *Structural Composite Materials*. ASM International.

